University of Alberta

DESIGN, SYNTHESIS AND EVALUATION OF CANCER TARGETING α-PEPTIDES AND NOVEL PEPTIDOMIMETIC β-PEPTIDES

By

SAHAR AHMED

A thesis submitted to the Faculty of Graduate Studies and Research

in partial fulfillment of the requirements for the degree of

DOCTOR OF PHILOSOPHY

in

Pharmaceutical Sciences

Faculty of Pharmacy and Pharmaceutical Sciences

Fall 2010

Edmonton, Alberta

Examining Committee

Dr. Kamaljit Kaur, Faculty of Pharmacy and Pharmaceutical Sciences

Dr. Edward Knaus, Faculty of Pharmacy and Pharmaceutical Sciences

Dr. Franco Pasutto, Faculty of Pharmacy and Pharmaceutical Sciences

Dr. Carlos Velázquez, Faculty of Pharmacy and Pharmaceutical Sciences

Dr. Dennis Hall, Chemistry, Faculty of Science

Dr. Mohsen Daneshtalab, Pharmacy, Memorial University of Newfoundland

Dedications

I would like to dedicate this thesis to

my dear husband, Yasser and my sweet kind children, Mohamed and Amar, who helped and supported me with all love and patience during the whole time. Without their help, support and passion I would not have been able to complete my advanced studies.

The spirit of my MOM (AMENA), peace on her, she was always there supporting me and encouraging me. I hope she was here so she can enjoy all her hard work with me.

My dear DAD (Mahmoud) and my dear brothers and sisters, for all their love, encouragement and support throughout my whole life.

My father and mother- in- law for their support and encouragement all the time.

ABSTRACT

Current cancer therapies have low specificity for tumor cells and have serious toxic side effects. Targeting drugs to the cancer cells can help improve the outcome of existing cancer therapies. In recent years, a number of peptides have been identified by peptide phage display for targeting different tumor types. Peptides identified from the phage display for targeting cancer cells can be further improved for specific binding and metabolic stability by chemical manipulation of their structures.

The aims of this work were: (i) to develop a peptide array-whole cell binding assay for screening peptides with specific binding affinity for cancer cells (ii) design of novel peptidomimetics to improve their properties as drug candidates. First, peptide arrays based on the lead peptide sequences NGR and p160 were designed and synthesized. A direct peptide-cell binding assay using CyQUANT dye allowed identification of several new peptides with higher affinity for MDA-MB-435 and MCF-7 cancer cells compared to the wild type p160. These peptides did not recognize the normal endothelial HUVEC cells. Three p160 peptide analogues, namely, **11 (**RGDPAYQGRFL), **18 (**WXEAAYQRFL), and **40 (**WXEPAYQRKL), that displayed highest affinity for the cancer cells were manually synthesized and labelled with FITC. The binding ability of these peptides was confirmed using fluorescence imaging and flow cytometry. The results confirmed the high and specific affinity of peptides **11** and **18** for the cancer cells.

The peptide array-cell binding assay established in this study is not only useful for the identification of cancer targeting peptides. It can also be used for the generation of diagnostic tools for cancer. Secondly, two new classes of β-peptides, β^3- and β^2-peptides derived from L-Asp and L-Dap monomers, respectively, were synthesized. The methodology allowed independent buildup of the β-peptide backbone and the introduction of sequential side chain substitutions. It is shown that α/β mixed peptide increases target recognition and retains the proteolytic stability. Moreover, β-peptides impart no cytotoxicity, which will expand their potential application in the design of biologically active peptides. As a result, these compounds represent good candidates for new drugs and as tools to gain further insight into protein folding and molecular recognition processes.

ACKNOWLEDGEMENTS

I would like to express my deepest gratitude to all of the following people.

- My advisor Dr. Kamaljit Kaur for her guidance and encouragement during my research project. Her professional leadership, excellent scientific methods, and critical thinking have been, and will still be, a great benefit to my scientific career. Her patience and support was the most encouraging for me, I doubt that I will ever be able to express my gratitude fully, but I devote to her all the success I had or will have in my upcoming career.
- My committee members, Dr. Edward Knaus, Dr. Franco Pasutto for their tremendous help, useful discussions and continuous support during my graduate studies. I would like to express my appreciation to Dr. Afsaneh Lavasanifar and her laboratory for providing me with the opportunity to start tissue culture work in her laboratory and their suggestions and help throughout the research.
- My supervisory committee and examination committee members for their advice and positive feedback which helped me and improved the overall out come.
- Dr. Randy Whittal (Department of Chemistry, University of Alberta) for providing exceptional assistance and advice with the mass spectrometry.
- Dr. Tara Sprules (McGill University, Montreal) who helped us with the NMR experiments and interpretation of the data.

- Dr. Samar Hamdy, Dr. Zengshaun Ma, Dr. Azita Haddadi, Dr. Anu Stella Mathews, Zahra Ghotbi and Mostafa Shahin for their sincere help in teaching me the tissue culture, FACS, and ELISpot techniques.
- My previous and current lab mates (Reem Beleid, Wael Soliman, Gagandeep Kharaud, Rania Soudy, and Krishna Bodapati) for the great support they have given me throughout the program.
- Dr. Vishwa Somayaji for his help with the mass spectrometry.
- Mr. Wayne Moffat for teaching me how to use the CD spectrophotometer.
- Mr. Jeff Turchinsky for helping me place the orders and figure out a lot of stuff that cannot be done without him.
- Mrs. Joyce Johnson for her help and support for the whole period of my program.

Finally, I would also like to thank the following agencies/institutes for the financial support.

- Egyptian Government for the financial support during my program.
- Antoine Noujaim Graduate Scholarship.
- NSERC and the Faculty of Pharmacy and Pharmaceutical Sciences, University of Alberta, Canada.

TABLE OF CONTENTS

LIST OF TABLES

LIST OF FIGURES

LIST OF SCHEMES

LIST OF ABBREVIATIONS

BOP	Benzotriazol-1-yloxy-tris(dimethylamino)-phosphonium hexafluorophosphate
CYANA	Combined assignment and dYnamics Algorithms for NMR Application
d	Doublet
DCM	Dichloromethane
dd	Doublet of doublet
ddH_2O	Double distilled water
DIC	1,3-diisopropylcarbodiimide
DMEM	Dulbecco's modified eagle medium
DMF	*N*,*N*-dimethylformamide
DMSO	Dimethyl sulfoxide
DNA	Deoxyribonucleic acid
DPC	Dodecyl phospho choline
EC	Endothelial cell
ECM	Extra cellular matrix
EDTA	Ethylene diamine tetraacetic acid
ELISA	Enzyme-linked immunosorbent assay
EPR	Enhanced permeation and retention
FACS	Fluorescence activated cell sorter
FCS	Fetal calf serum
FDA	Food and Drug Administration
FITC	Fluorescein isothiocyanate
FAK	Focal adhesion kinase
Fmoc	9-Fluorenylmethyloxycarbonyl
GM-CSF	Granulocyte-macrophage colony stimulating factor
h	Hour
HBTU	*O*-Benzotriazole-*N*,*N*,*N*̀,*N*̀-tetramethyl-uronium hexafluorophosphate

HIV	Human Immunodeficiency Virus
HOBt	N-Hydroxybenzotriazole
HPLC	High Performance Liquid Chromatography
IFN-γ	Interferon gamma
IL	Interleukin
L	Liter
M	Molar
m	Multiplet
mAbs	Monoclonal antibodies
MALDI	Matrix-assisted laser desorption/ionization
MBHA	Methylbenzhydramine
mg	Milligram
MFI	Mean fluorescence intensity
min	Minute
mL	Milliliter
mRNA	Messenger ribonucleic acid
MS	Mass spectrometry
ng	Nanogram
NGR	Asparagine Glycine Arginine
nm	Nanometer
NMM	N-Methylmorpholine
NMP	1-Methyl-2-pyrrolidinone
NMR	Nuclear magnetic resonance
NOESY	Nuclear overhauser effect spectroscopy
NPs	Nanoparticles
OBOC	One bead one compound
OD	Optical density
P13K	Phosphatidylinositol-3-kinase
PBC	Phosphate Borate Citrate buffer
Pbf	2,2,4,6,7-Pentamethyldihydrobenzofuran-5-sulfonyl
PBS	Phosphate buffer saline

PDB	Protein data bank
PEG	Polyethylene Glycol
RGD	Arginine Glycine Aspartic acid
RNA	Ribonucleic acid
ROS	Reactive oxygen species
RP	Reversed Phase
s	Singlet
scFv	single-chain variable fragment
siRNA	short interfering RNA
S/N	Signal-to-noise
SPPS	Solid phase peptide synthesis
t	Triplet
TFA	Trifluoroacetic acid
TFE	2,2,2-Trifluroethanol
THF	Tetrahydrofuran
TIPS	Triisopropylsilane
TNF-α	Tumor necrosis factor alpha
TOCSY	Total Correlated Spectroscopy
TOF	Time of flight
UV	Ultraviolet
V	Volt
VEGF	Vascular endothelial growth factor
Vis	Visible

Amino acids Abbreviations

Ala (A)	Alanine
Arg (R)	Arginine
Asn (N)	Asparagine
Asp (D)	Aspartic acid
Cys (C)	Cysteine
Gln (Q)	Glutamine
Glu (E)	Glutamic acid
Gly (G)	Glycine
His (H)	Histidine
Leu (L)	Leucine
Lys (K)	Lysine
Phe (F)	Phenylalanine
Pro (P)	Proline
Tyr (Y)	Tyrosine
Val (V)	Valine
Trp (W)	Tryptophan
Nle(X)	Norleucine
β-Ala (Z)	β-Alanine

CHAPTER 1 Introduction

1.1 Targeting Cancer Cells

1.1.1 Cancer (an overview)

The term 'cancer' – Latin for crab – was coined by Hippocrates the father of medicine in 460 BC because of its similarity to the swollen veins radiating from breast tumors. Since then, our understanding of cancer has increased significantly, especially with the development of technology to map genes and determine their role in human disease.[1] Despite this stream in knowledge, finding effective treatments has proved to be difficult and remains a major challenge. Different theories tried to explain what cancer is. "Cancer" is, in fact, a general term that refers to over 100 distinct diseases affecting many different tissues and cell types. Hanahan and Weinberg have argued that in order for a cell to become cancerous, it must acquire six unique traits as a result of altered cell physiology.[2,3] These defining characters of cancer cells are: 1) the ability to generate their own growth signals or respond to weak growth signals that are ignored by healthy cells, 2) insensitivity to antiproliferative signals, 3) resistance to cellular suicide mechanisms that normally cause abnormal cells to die by apoptosis, 4) the capacity for limitless replication, 5) the ability to stimulate new blood vessel development (angiogenesis), and 6) tumor invasion and metastasis.[2] Hanahan and Weinberg have also suggested that these characteristic are shared by most, if not all, human tumors.[2]

Why and how does cancer spread?

There are two different mechanisms by which cancer can spread, namely local and remote. Healthy tissues and organs are seized together by a group of fibrous molecules in which individual cells are ordered and rooted. Local spread of tumor occurs because tumors often release substances that dissolve these fibrous molecules and allow cancerous cells to invade healthy tissue. As a tumor enlarges, it develops its own blood supply and lymph vessels in which detached cells can be carried around the body at remote parts.[4] This is called metastasis or secondary tumor.[5] The lymph nodes nearest to the primary tumor are very frequent sites for metastasis (**Figure 1.1)**.

How common is cancer?

Cancer is a major worldwide problem. Despite recent advances in treatment modalities, cancer remains a major source of morbidity and mortality throughout the world. The World Health Organization (WHO) estimates that in 2002 there were 10.9 million new cases of cancer globally, with 6.7 million deaths, and 24.6 million persons living with cancer.[6] Over the last 20 years, increasing life expectancy has become a major determent of increasing cancer incidences. The WHO has estimated that with this ageing of populations there could be, by 2020, 16 million new cases per year and around 10 million deaths.[7a] Based on 2009 Canadian statistics, current incidence rates, 40% of Canadian women and 45% of men will develop cancer during their lifetimes.[7b] Further,

based on current mortality rates, 24% of women and 29% of men, or approximately 1 out of every 4 Canadian, will die from cancer.

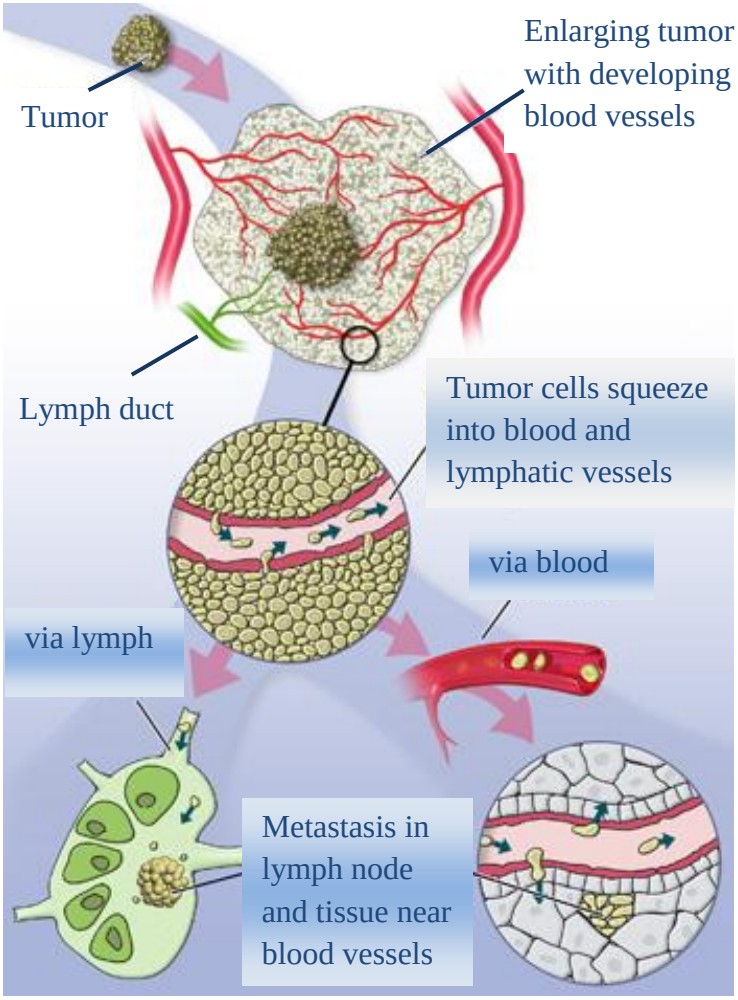

Figure 1.1. Diagram showing the mechanisms of tumor spreading. (adapted from http://www.thinkquest.org)

Obstacles and promises in cancer

A major hurdle in cancer therapy is the unrestrained delivery of the administrated anticancer agents all over the body. This means that both cancer and normal cells are exposed to the antiproliferative effects of anticancer agents.[8]

Most of the chemotherapeutics are delivered in such a way. The sensitivity of cancer cells might be the only way that chemotherapeutic agents will get more to the cancer tissue compared to normal ones due to their high metabolic rate. If this will be the case, more concentration of the drug is required which will result in dose limiting toxicity. The inability to deliver sufficient amount of the anticancer agents to the right place where the cancer is located results in failure of the treatment and increases the drug resistance.[9] For example, radiation therapy and surgery, which generally are localized treatments, can cause substantial damage to normal tissue in the treatment field, resulting in scarring and, in severe cases, loss of function of the normal tissue. Chemotherapy, in comparison, which generally is administered systemically, can cause substantial damage to organs, such as bone marrow, mucosa, skin and the small intestine, which undergo rapid cell turnover and continuous cell division. As a result, undesirable side effects such as nausea, loss of hair and drop in blood cell count occur during systemic treatment of a cancer patient with chemotherapeutic agents. Such undesirable side effects often limit the amount of a drug that can be administered. Thus, cancer remains a leading cause of patient morbidity and death.[10]

Different classes of chemotherapeutic agents produce different specific toxicity (**Figure 1.2** and **Table 1.1**).[11] For example, anthracyclines such as doxorubicin (DOX), epirubicin, and daunorubicin (DNR) remain among the most active anticancer agents for treatment of a wide variety of solid tumors and hematological malignancies. Unfortunately, their cardiac toxicity, like cardiomyopathy and congestive heart failure, still limits their usefulness.[11]

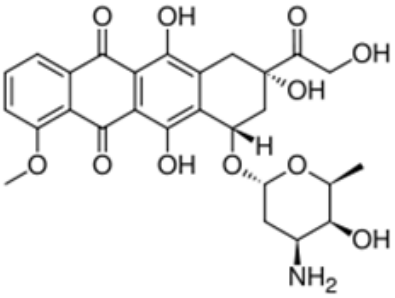

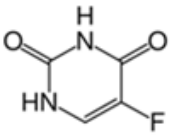

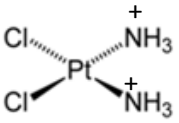

Doxorubicin **5-Fluorouracil** **Cisplatin**

Figure 1.2. Structures of some representative chemotherapeutic agents.

For such toxicity characters, developing strategies that will help cancer treatment agents to restrict their action only to cancer cells, and sparing normal ones, will result in decrease of systemic side effects, systemic toxicity, and increasing their efficiency. Such specific mode of treatment will also reduce drug resistance.

Table 1.1: Cardiovascular toxicity associated with anticancer agents.[11]

Drug class (Example)	Therapeutic use	Mechanism(s)	Other toxicities
Anthracyclines (Doxorubicin, Epirubicin)	Leukemia and solid tumors	Oxidative stress (ROS), iron chelation	Gastrointestinal toxicity
Alkylating agents (Cisplatin)	Various neoplastics	Electrolyte imbalance (hypomagnesaemia) Coronary artery fibrosis	Myelotoxicity, nephrotoxicity, and ototoxicity
Antimetabolites (5-Fluorouracil)	Various solid tumor	Vasospasm	Myelotoxicity, skin toxicity, and gastrointestinal toxicity

1.1.2 Tumor Specific Targeting Strategies

Efforts have been made to target various drugs specifically to tumor sites.[12] Different strategies are used to enhance the specific delivery of anticancer agents. Targeting can be either to the cell surface or to the new blood vessels receptors by which the effective concentration of the drug will be higher at the cancer site. These strategies include, (i) the use of drug carriers, such as, micelles or liposomes, which will help in accumulating the drug at the tumor site due to their physical properties, (ii) use of prodrug that will be activated preferentially at the cancer cell to give the toxic form, and (iii) binding drug to a ligand such as, antibodies, peptides, and aptamers, that has the ability to home to overexpressed tumor-associated antigens.

1.1.2.1 Selective Cancer Targeting using Drug Carriers

Drug carriers, such as liposomes, polymers and other nanoparticles, have been shown to extravasate and localize to areas of increased vascular permeability, such as those found in angiogenic tumor, in a process referred to as passive targeting. Of these drug delivery systems, liposome-based formulations of the anthracycline drugs have had a great impact on the treatment of cancer patients to date.[12-14] Tumor vessels have an increased permeability to macromolecules owing to a lack of tight junctions that are normally present between adjacent vasculature endothelial cells of other vessels. The size of the gaps between the cells in tumor vessels is sufficiently large to allow the extravasation of most targeted therapeutics from vessels into the tumor interstitial

space.[12-14] The therapeutic agents retained in these carriers while in circulation are not freely available, thus minimizing the uptake by normal tissues. Liposomes eventually become subject to enzymatic degradation and/or phagocytic attack, leading to release of drug for subsequent diffusion to tumor cells. Surface modification of carriers with polyethylene glycol (PEG), commonly referred to as the pegylation process, to produce sterically hindered or STEALTH liposomes, has been shown to protect carriers from reticuloendothelial system uptake.[12] This allows extended circulation time, which in turn maximizes carrier uptake by tumor. The limited lymphatic drainage helps the carrier-bound drug to accumulate in tumor tissue. The phenomenon of the combined effect of these factors is termed the enhanced permeation and retention (EPR) effect. The pegylated liposomal doxorubicin is in the market and currently being used for cancer treatment.[15] Examples of few such delivery systems are shown in **Table 1.2.**[16]

Recent developments in this field have generated systems that deliver the therapeutic directly to cancer cells through active tumor targeting. This has been achieved by linking therapeutic moieties to high-affinity ligands directed against cancer-associated targets. Some of the actively targeting ligands, such as antibodies and peptides, are described below in Sections 1.1.2.3 and 1.1.2.4. Linking such ligands to the surface of liposomes or nanoparticles can dramatically increase the targeting efficiency of these systems. [12-14]

Table 1.2: Examples of colloidal delivery system-based drugs available for cancer treatment.[16]

Drug name	Delivery system	Mode of action	Trade name and company
Daunorubicin citrate	Liposome	Anthracyclin, DNA intercalator	DaunoXome®–Gilead Sciences, Myocet™–Zeneus Pharma
Doxorubicin HCl	Liposome	Anthracyclin, DNA intercalator	Liposome encapsulated doxorubicin–Neopharm
Doxorubicin HCl	Pegylated Liposome*	Anthracyclin, DNA intercalator	Doxil®–Tibotec Therapeutics, Caelyx®–Schering-Plough
Carmustine (BCNU)	Polymer conjugate	Alkylating agents	Gliadel®–Guilford Pharmaceuticals

* Polyethylene glycol-coated liposome

1.1.2.2 Selective Cancer Targeting using Prodrug Activation

In order to lessen severe side effects of systemic chemotherapeutic treatment, several prodrug strategies have been developed.[17] Selective delivery of cancer therapeutics is done by administering a less toxic prodrug form that can be converted into an active drug at the cancer site. Some employ unique aspects of tumor physiology (such as selective enzyme expression or hypoxia), whereas others are based on tumor antigen-specific delivery techniques.[17]

Following the above approach, a group of researchers at the 'Cancer Research Campaign's Centre for Cancer Therapeutics' are investigating virus-directed enzyme-prodrug therapy (VDEPT).[18] Here the virus carrier passes a gene to the cancer cells to make it produce an enzyme (**Figure 1.3**). The enzyme is chosen because it is able to convert non active drug (a prodrug) into an active drug. As the cells die, the toxic molecule will be released to kill adjacent cells as well.

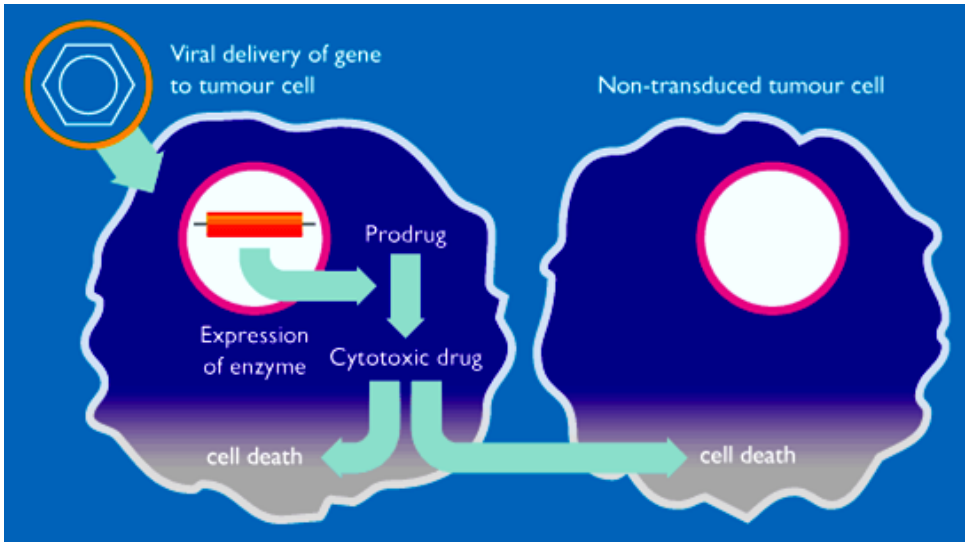

Figure 1.3. Gene therapy used to activate a non-toxic pro-drug into a cytotoxic drug within a cancer cell. (Adapted from http://www.abpi.org.uk)

1.1.2.3 Selective Cancer Targeting using Antibodies

Overexpression of unique molecular cancer cell surface markers can be used to design new molecules that bind to these markers with high affinity. As a result these agents can efficiently and selectively target therapeutic agents to cancer cells. For example, ~2,000,000 HER-2 receptors are present on an overexpressing cancer cell surface, whereas, a non-overexpressing normal cell has

10,000- 20,000 molecules on its surface.[19] This suggests that a 100-fold higher drug concentration can reach the cancer cell compared to normal ones. Furthermore, a more conservative approach is to generate specific monoclonal antibodies (mAbs), where an antibody can be raised against the unique marker and a drug can be linked to the antibody. Upon administration of the drug/antibody complex to the patient, the binding of the antibody to the marker results in the delivery of a relatively high concentration of the drug to the tumor. In this respect, several studies have shown that antibodies and antibody fragments can improve tumor targeting.[20, 21]

The clinical success of mAb was shown by the FDA approval of Rituxan (an anti-CD20 mAb against B-cell lymphoma), Herceptin (an anti-Her2/neu mAb against breast cancer), and Mylotarg (an anti-CD33 mAb against acute myeloid leukemia). The clinical use of mAbs has further validated the cell surface targeting approach for cancer therapy (**Figure 1.4**). Examples of approved monoclonal antibodies for cancer treatment are listed in **Table 1.3**. Several mAbs that target cell surface receptors are now in clinical trials. Some of these antibodies are unconjugated, and they bind to and inhibit tumor growth by inhibiting the promitogenic function of these receptors, e.g., IMC-C225 cetuximab,[22-24] an anti-EGFR (epidermal growth factor receptor) chimerized mAb.[25] Unfortunately, several factors are limiting the use of mAbs to target cancer. First of all, the large molecular weight of the antibody's which is ~160,000.

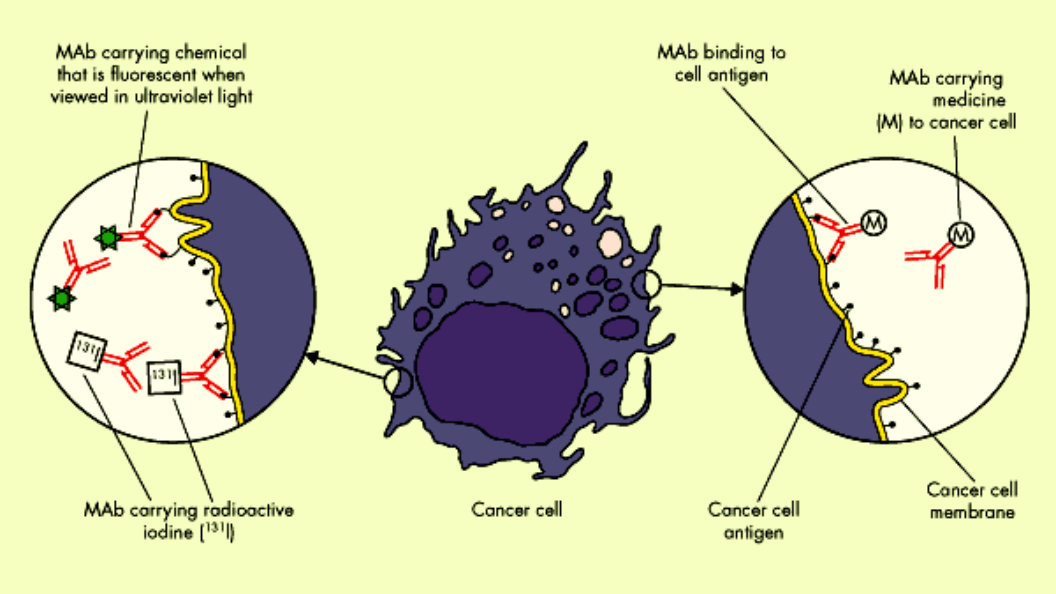

Figure 1.4. Different uses of monoclonal antibody in targeting cancer. (Adapted from http://www.abpi.org.uk)

Table 1.3: A list of the approved monoclonal antibodies for cancer treatment.[16]

mAb name (Approval year)	Target	Treatment	Naked/conjugate	Trade name
Gemtuzumab ozogamicin (2000)	CD33	Acute myelogenous leukaemia	Calicheamicin, Cytotoxic antibiotic	Mylotarg
Rituximab (1997)	CD20	Non-Hodgkin's lymphoma	Naked*	Rituxan®
Trastuzumab (1998)	HER-2	Breast cancer	Naked*	Herceptin®
Cetuximab (2004)	EGFR	Colorectal cancer	Naked*	Erbitux™
Bevacizumab (2004)	VEGF	Colorectal cancer	Naked*	Avastin™

* Antibodies that are approved for cancer treatment and have potential to be used in the future as vehicles for selective delivery of therapeutics in cancer diagnosis and treatment.
** VEGF: Vascular endothelial growth factor.

Secondly, this molecule has difficulty reaching into the interior of large tumor mass where the blood supply is inadequate. Also, the poor stability and non specific uptake by the liver and the reticuloendothelial system are limiting factors. These could result in poor tumor penetration of the antibody and also cause dose-limiting toxicity to the normal organs.[26] Recent advances in antibody technology has resulted in the production of antibody fragments, such as scFv, which has been helpful to resolve certain size-related issues.[27]

1.1.2.4 Selective Cancer Targeting using Peptides

The use of synthetic peptides emerged ~20 years ago, when somatostatin analogues were demonstrated to specifically recognize endocrine –related tumors and were developed as specific diagnostic or therapeutic tool.[28] In these regard, peptides are excellent alternatives to mAbs as they alleviate some of the problems associated with mABs such as they are smaller in size, generally do not bind to the reticuloendothelial cells, are chemically more stable, less immunogenic, and can be easily synthesized and conjugated to functional units, giving homogenous molecules unlike mAb.[8,29,30] In recent years, several studies have demonstrated effective tumor targeting using peptide ligands.[31-33] Some of the promising cancer targeting peptides are discussed in **Table 1.5**.

1.1.3 Cancer Targeting Peptides

1.1.3.1 Screening Cancer Targeting Peptides

As mentioned before, peptides represent a good alternative to mAbs as targeting agents. However, the major challenge is to select peptides that have high affinity and are specific for cancer cells. Different avenues have been pursued to achieve this goal, as illustrated in **Table 1.4,** and the most common ones are discussed below.

Table 1.4: Peptides library approaches to discover tumor targeting peptides.[8]

Method	Type
Biological peptide library methods	1. Phage-display peptide library either panning with cell surface receptor or intact cells.[34] 2. Bacterial-display peptide library either panning with cell surface receptor or intact cells.[35]
One-bead one-compound combinatorial library (OBOC)	On bead screening with purified cell surface receptor or intact cell.[36]
Spatially addressable peptide library methods	1. Multipin technology[37] 2. Spot synthesis [38]
Iterative synthesis and deconvolution methods	Positional scanning method [39]

Phage-display library as a tool for screening cancer targeting peptides

Phage–display library methods have been employed to identify peptide-protein or peptide-intact cell interaction. The phage-display peptide library

approch was first developed by Parmley and Smith in 1988.[40] In this method, a stretch of random double-stranded DNA (dsDNA) is inserted in the gene that encodes pIII protein. The encoded peptides are expressed or "displayed" on the phage surface as a fusion product with one of the phage coat proteins pIII.[8] The phage-display peptide library is screened against immobilized target proteins, intact cells or *in vivo* selection by intravenous injection in mouse tail. The bound phages are eluted with weak acid, amplified in *Escherichia coli*, and then re-panned a second time for better selection. The amino acid sequence of the peptide presented on the phage surface is determined by DNA sequencing. The process of phage-display is shown in **Figure 1.5.**

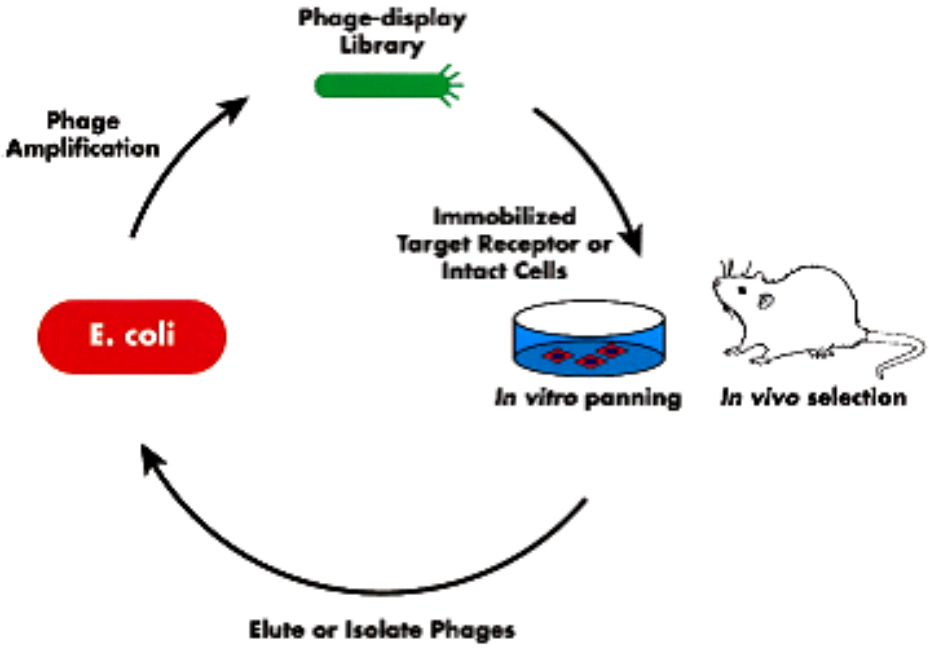

Figure 1.5. The use of phage-display peptide library method to discover cancer targeting peptides.[8] (Adapted from reference 8).

Biopanning or successive screening of phage-display library against known cell surface proteins, human sera and tumor cells have resulted in identification of numerous specific binding peptides. Some of the tumor cell surface or vasculature targeting peptides identified by phage display libraries are summarized in **Table 1.5.**

Table 1.5: Target-specific peptides identified by phage-display library.[30]

Peptide Ligand	**Cellular Target**
Tumor cell surface	
TSPLNIHNGQKL	Human head and neck squamous cell cancer
CVFXXXYXXC CVAYCXXXXCYVC	Prostate-specific antigen (PSA)
LTVXPWX	Human multiple myeloma M-protein
Tumor vasculature	
CDCRGDCFC (RGD-4C), ACDCRGDCFCG	αvβ3, αvβ5
CNGRCVSGCAGRC, CVLNGRMEC, NGRAHA	Aminopeptidase N
CGSLVRC, CGLSDSC	Vasculature of various tumors
TAASGVRSMH, LTLRWVGLMS	NG2 proteoglycan
RRKRRR	VEGF
Surface immunoglobulin	
FXDXRL, XIHYIF, FHEPENSISVNQLDC, ETLPAPLAPQVQYDA	Human multiple myeloma M-protein
LVRSTGQFV, LVSPSGSWT, ALRPSGEWL, AIMASGQWL	Human chronic lymphocytic leukaemia (CLL) surface idiotypes

The first study where a human patient was used to screen phage-display peptides for tissue targeting against interleukin-11 was reported by Pasqualini et al.[41] Phages were recovered from different tissues after only one round of selection and a peptide that mimicked interleukin-11 and bound to the interleukin-11 receptor in the prostate was isolated. Despite the great advances and the huge number of peptides that have been identified through the use of phage display technique, the nature of biological system i.e. the phage-display, bacterial-display, or other recombinant peptide library methods make it restricted to the development of L-amino acid peptides only. In contrast, the other library methods (**Table 1.4**) used in the discovery of cancer targeting peptides are synthetic-based and can be applied to peptide libraries with D-amino acids, unnatural amino acids, or even non amino acid building blocks.[42]

One bead one-compound libraries as tool for screening cancer targeting peptides

In one bead one compound (OBOC) method, peptide libraries are prepared by split and mix method and each bead displays only one peptide. **Figure 1.6** shows an example of OBOC method where 27 different tripeptides are synthesized on the beads. The OBOC library is then screened against different biological targets with a number of different assays.[36,43] Beads that interact with the specific target are then physically isolated for structural determination. Some of the peptides identified using the OBOC methods are summarized in **Table 1.6.**

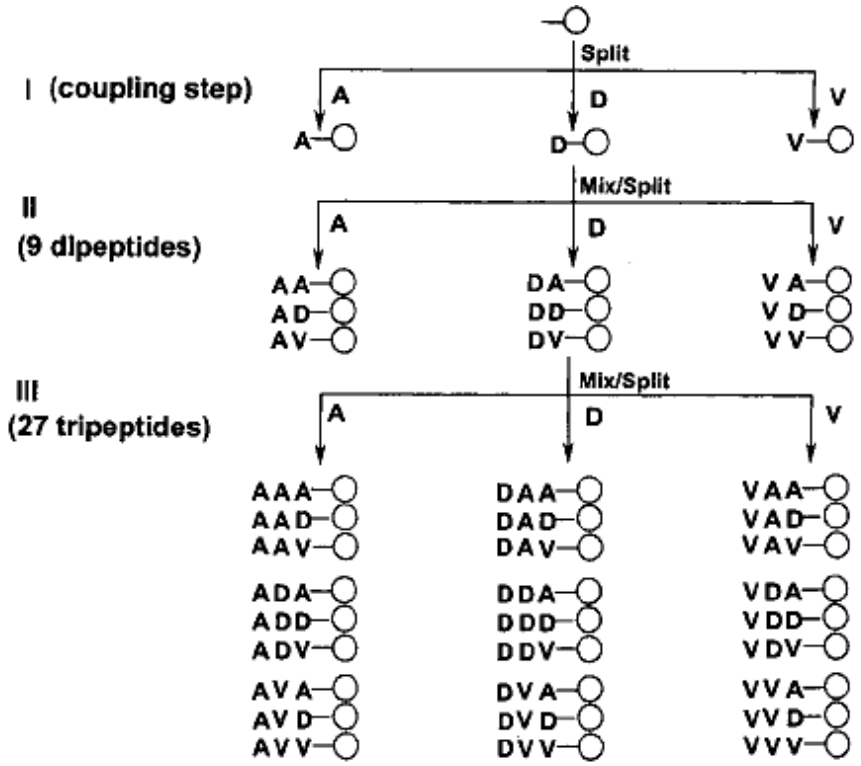

Figure 1.6. Synthetic scheme of the split-mix synthesis method. A = alanine, D = aspartic acid, V = Valine.[43] (Adapted from reference 43)

Table 1.6: Peptide ligands identified from OBOC combinatorial library.[8]

Peptide Ligand	**Cellular Target**
LNNIVSVNGRHX, DNRIRLQAKX	$\alpha_6\beta_1$integrin of DU145 prostate cancer cell line
RWID, RWFD, xtxGmxkx, xGrfxswx	idiotype of WEHI-279 murine lymphoma cell line
kmviywkaG, kGGrhykfG, yiknrkhhG, kikmviswkG	$\alpha_6\beta_1$integrin of DU145 prostate cancer cell line
cNGRGEQc	$\alpha_3\beta_1$ integrin of A549 non-small cell lung cancer cell line

Lowercase letters represent D-amino acids. Peptides with D-cysteines at the amino and carboxy terminus were cyclized by disulfide formation.

Some of the limitations that OBOC method faces are: First, this method is limited to the screening of soluble targets. Second, even though in principle it is possible to screen for the interaction of bead-immobilized ligands with insoluble ligates (such as bacteria and living cells), there are practical limitations to the effective implantation of such approach, including non-specific binding as well as quantitative determination of the relative binding.

SPOT libraries as tool for screening cancer targeting peptides

The spot-synthesis method developed by Ronald Frank, opened up countless opportunities to synthesize and subsequently screen large arrays of synthetic peptides on planar cellulose derivatized membranes.[38] In addition to that, the cost per peptide is less than 1% of peptides synthesized conventionally on resin. The SPOT method follows standard fluorenylmethoxycarbonyl (Fmoc) chemistry on conventional cellulose sheets, and can utilize different building blocks, natural or unnatural ones. The procedure involves three phases: preparation of the cellulose membrane, which is currently available through different companies, stepwise coupling of the amino acids, and cleavage of the side-chain protection groups. If necessary, peptides can be cleaved from the membrane for assays performed using soluble peptides. These features make this method an excellent tool for screening large numbers of peptides for many different purposes. The potential applications range from simple binding assays, to more sophisticated enzyme assays and studies with living microbes or cells. The time required to complete the protocol depends on the number and length of the peptides. Spot membrane was used to screen the interaction between peptides

based on the amino acid sequence of fibronectin type III domain 8–11 (FN-III 8–11) and human mesenchymal stem cell, which revealed some sequences that could be used for biomaterial purposes.[44]

1.1.3.2 Use of Peptides as Cancer Targeting Agents

Approaches similar to that used for mAb, that have been identified for cancer targeting, can be applied to peptides. As mentioned before, mAb can be used as cancer targeting agents in different ways, such as naked antibody alone, radiolabeled antibody, antibody–chemotherapeutic agent conjugate, antibody–small molecule toxin, antibody–protein toxin, and drug-loaded liposomes decorated with mAb. Similar approaches can also be applied to cancer targeting peptides. **Figure 1.7** illustrates the various peptide-targeting approaches to cancer.

1.1.3.3 Well known and Promising Cancer Targeting Agents

In recent years, a number of peptides have been identified using the methods discussed above for targeting different tumors and cell types.[8,45-47] Among these, tumor homing peptides RGD,[48-50] and NGR,[51-54] sequences have received particular attention. These peptides target the αvβ3 integrin and aminopeptidase N receptors, respectively, in the tumor cells and vasculature.[48, 50] A dodecapeptide GE11 has also been reported that binds to the epidermal growth receptor (EGFR) over-expressed by tumors.[45,55] Another 12-mer peptide p160,

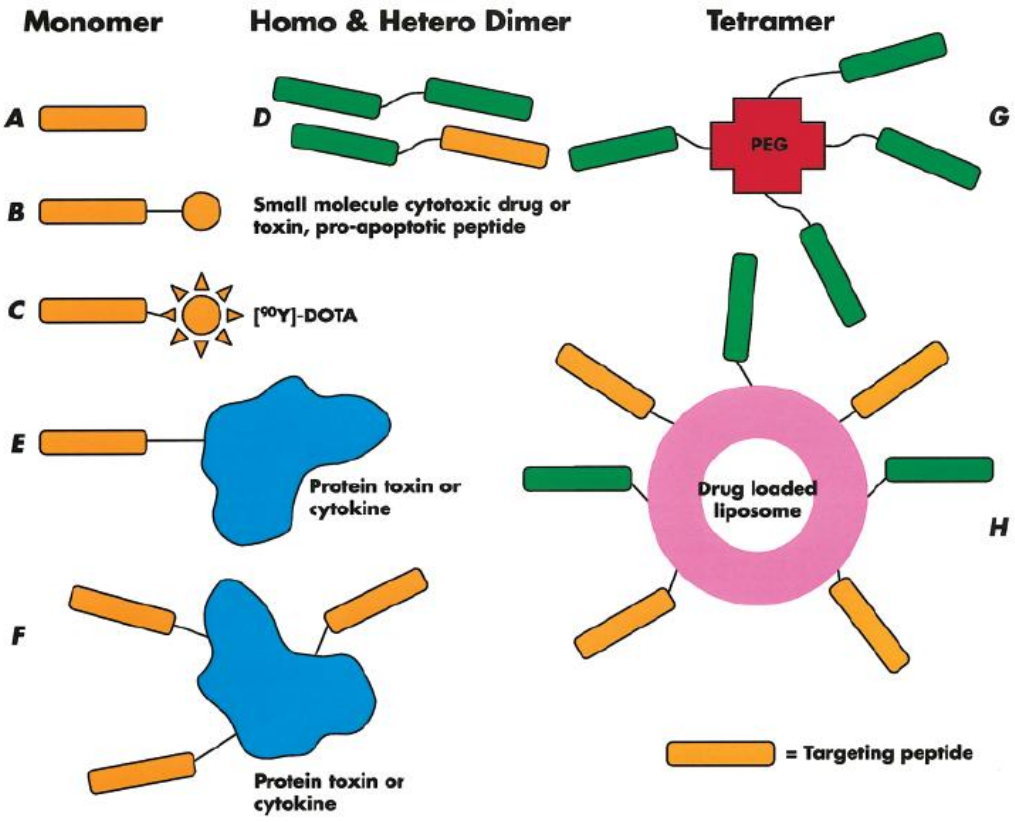

Figure 1.7. Various peptide-targeting approaches: (A) naked peptide monomer, (B) monomeric peptides conjugated to small molecule cytotoxic drug, toxin, or pro-apoptotic peptides, (C) [90Y]-DOTA labeled peptides, (D) homo- and heterodimeric peptides, (E) one peptide conjugated to protein toxins or cytokines, (F) multiple peptides conjugated to protein toxins or cytokines, (G) tetrameric peptides with a polyethylene glycol scaffold, and (H) drug loaded liposome decorated with two different targeting peptides.[8] (Adapted from reference 8)

with a yet unidentified receptor, has been shown to bind MDA-MB-435, MCF-7, and WAC-2 human cancer cells strongly and specifically.[56,57] In the coming section some of these peptides (**Table 1.7**) will be discussed in details highlighting their potential use in cancer targeting.

Table 1.7: Examples of popular cancer targeting peptide sequences.

Cancer Targeting Sequences	Receptor/Target Cell
RGD (Arg-Gly-Asp)	αvβ3 integrin
NGR (Asn-Gly-Arg)	Aminopeptidase N (CD13)
P160 (VPWMEPAYQRFL)	Breast and neuroblastoma cancer cells

RGD containing peptides

A 9-mer peptide RGD-4C (CDCRGDCFC) was identified through *in-vivo* phage selection approach and has the ability to home to tumor vasculature.[58,59] RGD containing peptides were found to bind integrins receptors selectively. Integrins are a family of glycosylated transmembrane receptors, named for their ability to integrate extracellular and intracellular activities. They are heterodimeric composed of non-covalently paired alpha and beta chains that regulate tumor angiogenesis, invasion and migration by cell-cell and cell-ECM interactions (**Figure 1.8**). There are 24 distinct *αβ* heterodimers most of which interact with specific ECM. The RGD sequence has been identified as an essential binding motif for seven out of the 24 integrin receptors. For example, integrins such as αvβ3 and αvβ5 recognize the RGD part of the extra cellular ligands, fibronectin and vitronectin.[58,59] Upon ligand binding, integrins which lack intrinsic kinase activity will aggregate to form cell membrane focal adhesions. Focal adhesion kinase (FAK) is recruited and auto-phosphorylated which in turn activate signaling through phosphatidylinositol-3-kinase (P13K) and extra cellular

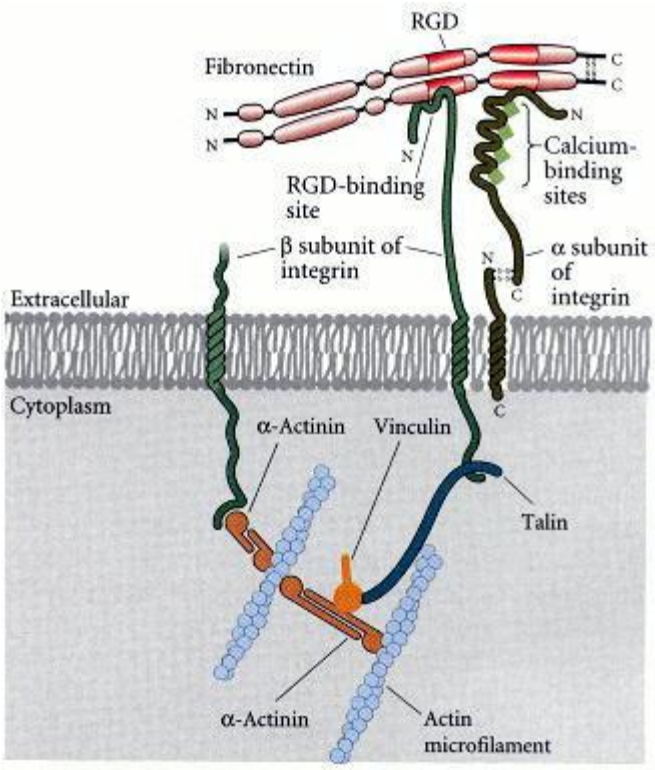

Figure 1.8. Schematic showing binding of cytoskeleton to the extracellular matrix through the integrin molecule.[58] (Adapted from reference 58)

signal regulate kinase (EPK)/MAPK. αvβ3 Integrin was found to be upregulated during metastasis of malignant melanoma cells, so inhibition of the interaction between this integrin and the extracellular matrix induces apoptosis and inhibit metastasis.[60] In fact, peptides containing RGD motif efficiently block these integrin–ligand interactions (**Figure 1.9**).

Since the RGD-sequence is conserved in all natural and new developed ligands, the relative affinity and specificity of the peptides and proteins are determined by other amino acid residues flanking the RGD-motif, especially at the two positions following the aspartic acid. Besides direct interactions between these residues and the integrin, flanking groups influence the folding of the

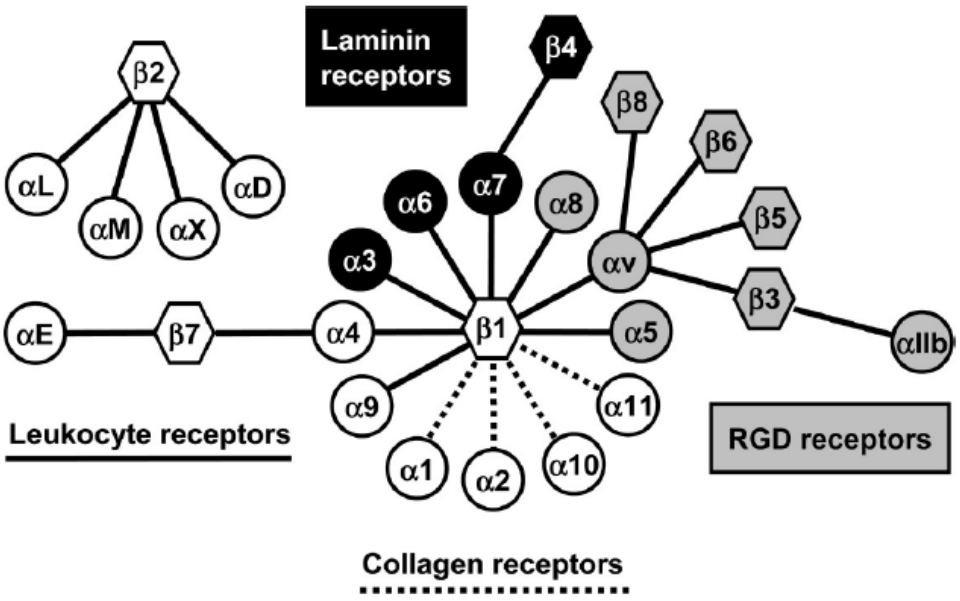

Figure 1.9. The integrin family: RGD receptors, laminin receptors, leukocyte receptors, and collagen receptors.[59] (Adapted from reference 59)

peptide (**Figure 1.10**) and thereby the conformational features of the RGD-motif. Cyclization is commonly employed to improve the binding properties of RGD-peptides. Since cyclization confers rigidity to structure, it greatly improves the selectivity of the promiscuous RGD-sequence for a specific integrin subtype. As shown in **Figure 1.10**, specificity and affinity for αvβ3-integrin is introduced in peptide ligands by ring closure and flanking amino acids, which force the arginine and aspartic acid side-chains into the proper conformation. Furthermore, cyclic peptides are also found to be more stable, and non-natural peptide modifications, such as the introduction of D-amino acids as well as replacement with

peptidomimetic structures yield RGD-peptide ligands with increased specificity and nanomolar or higher affinity.[61]

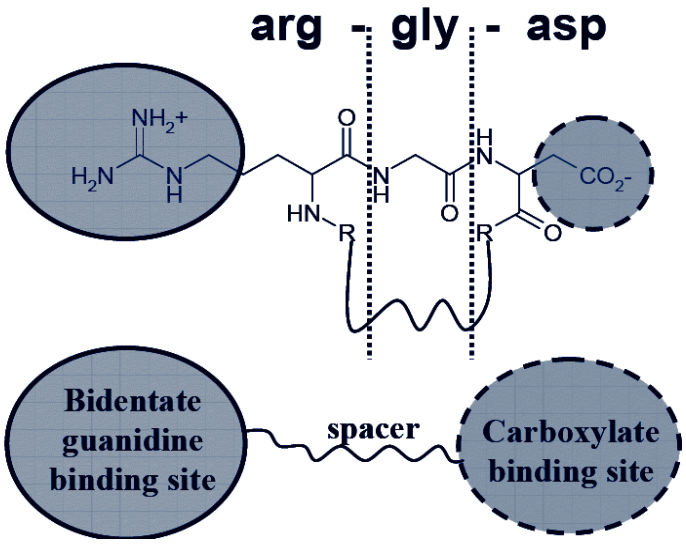

Figure 1.10. Schematic representation of the RGD binding motif.

One of the best studied RGD-peptide ligands for $\alpha_V\beta_3$-integrin is c(RGDf-N(Me)-V), which is also known as Cilengitide. Cilengitide is in phase III clinical trials for the treatment of malignancies including melanoma, glioblastoma and prostate cancer.[62] The first approach in which the RGD motif was used for drug targeting purposes, rather than as a single antiangiogenic entity, focused on the delivery of doxorubicin to angiogenic endothelial cells. A doxorubicin-RGD4C conjugate (doxo-RGD4C) proved to be equally effective as free doxorubicin *in vitro* and, more importantly, demonstrated improved inhibition of tumor growth and spreading of metastases in mice. In addition to an improved efficacy, doxo-RGD4C also displayed reduced toxicity to liver and heart.[48] Different studies are

now under investigation for the use of radiolabeled cilengitide to quantify integrin expression for evaluation during and after antiangiogenic therapy.[63]

NGR containing peptides

Another popular sequence that shows enhanced binding to tumor cells is NGR containing peptides. Various cyclic and linear peptides containing the Asn-Gly-Arg (NGR) motif have been identified using *in vivo* panning of peptide-phage libraries in tumor-bearing animal models.[48] The NGR motif resembles RGD, and NGR peptides can bind to integrins, but the affinity of NGR peptides to integrins is lower than the affinity of RGD-integrin binding.[64] Despite the integrin-NGR interaction, the RGD-4C peptide does not effectively compete with the tumor homing of a phage displaying the NGR motif,[48] indicating that the receptor for NGR is different from the receptors for the RGD-4C peptide, the αv integrins.

Studies designed at elucidating the molecular basis behind NGR tumor-homing properties showed that this motif can specifically bind to cells expressing aminopeptidase N (CD13),[54] a membrane-bound metallopeptidase that plays multiple functions as a regulator of various hormones and cytokines, protein degradation, antigen presentation, cell proliferation, cell migration, and angiogenesis.[65-67] CD13 is hardly expressed by the endothelium of normal blood vessels but it is up-regulated in angiogenic blood vessels.[54,68] It has been shown that NGR-containing peptides can target activated endothelial cells not only in tumors, but also in other physiologic or pathologic conditions, such as inflammation and retinal disorders. Consistently, Buehler *et al.* recently demonstrated that endothelial CD13 is up-regulated in a murine model of cardiac

angiogenesis and that a fluorophore-tagged CNGRC conjugate co-localizes with CD13 and with the endothelial marker CD31 on blood vessels only in angiogenic areas.[69] Recent work has also shown that proliferating retinal blood vessels express CD13 and that CNGRC-phage can home to angiogenic retina.[70] This peptidase is also expressed by many cells of normal tissues, including myeloid cells, antigen-presenting cells, keratinocytes, mast cells, epithelial cells from renal proximal tubules, small intestine, prostate and bile duct canaliculi.[66] Although CD13 receptor is expressed in some normal tissues, the isoform that is expressed in cancer tissue was found to be different as proved by immunohistochemical analysis. For instance, the immunoreactivities of two anti-CD13 monoclonal antibodies (WM15 and 13C03) with CD13 expressed by tumor endothelia and normal epithelia, respectively, in renal cell carcinoma sections are markedly different. WM15 can stain tumor blood vessels and little or not normal kidney epithelia, whereas, 13C03 can strongly stain the apical part of epithelial cells of proximal tubules and much less tumor blood vessels.[68]

CD13 is synthesized as an intracellular precursor of 967 amino acid residues and posttranslationally modified in the Golgi to produce a 150 to 240 kDa mature cell surface molecules comprising a short cytoplasmatic N-terminal domain, a single transmembrane part, and an extracellular domain containing the active site (**Figure 1.11**).[71, 72] Within the mature glycosylated protein, 25% to 30% of the molecular weight is composed of carbohydrates. Differential glycosylation results in at least 5 isoforms that are differentially available. In endothelial cells CD13 specifically interacts with galectin-3, a proangiogenic

protein, in a carbohydrate recognition-dependent manner.[73] It is possible that the selectivity of NGR peptides for endothelial CD13 is related to different glycosylation ratio or due to conformational changes caused by complex formation with this or other unknown compounds.

Immunogenic studies of NGR have shown that this motif is scantily, or not at all, immunogenic when studied in various conjugates.[74] Further NGR sequences have been found to be part of fibronectin. Fibronectin is one of the major ECM proteins that play an important role in wound repairing, cell adhesion, spreading, migration, and angiogenesis. Using SWISS-PROT search it was found that fibronectin contains two conserved GNGRG motives. NGR sequence therefore became popular choice for targeting. These peptides have been exploited for ligand-directed delivery of various drugs and particles to tumor vessels, in the attempt to increase their antitumor activity. NGR-containing peptides have been successfully used to deliver cytotoxic drugs such as DOX, apoptotic peptides, and cytokines such as tumor necrosis factor (TNF), to the tumor or tumor vasculature, and enhance the antitumor activity of the cargo.[48, 68] For instance, it has been shown that peptides containing cyclic CNGRC and linear GNGRG motives can be used to deliver tumor necrosis factor alpha (TNF-α),[53,75] interferon gamma,[76,77] and liposomal doxorubicin[78,79] to tumor neovasculature for improving their therapeutic properties.

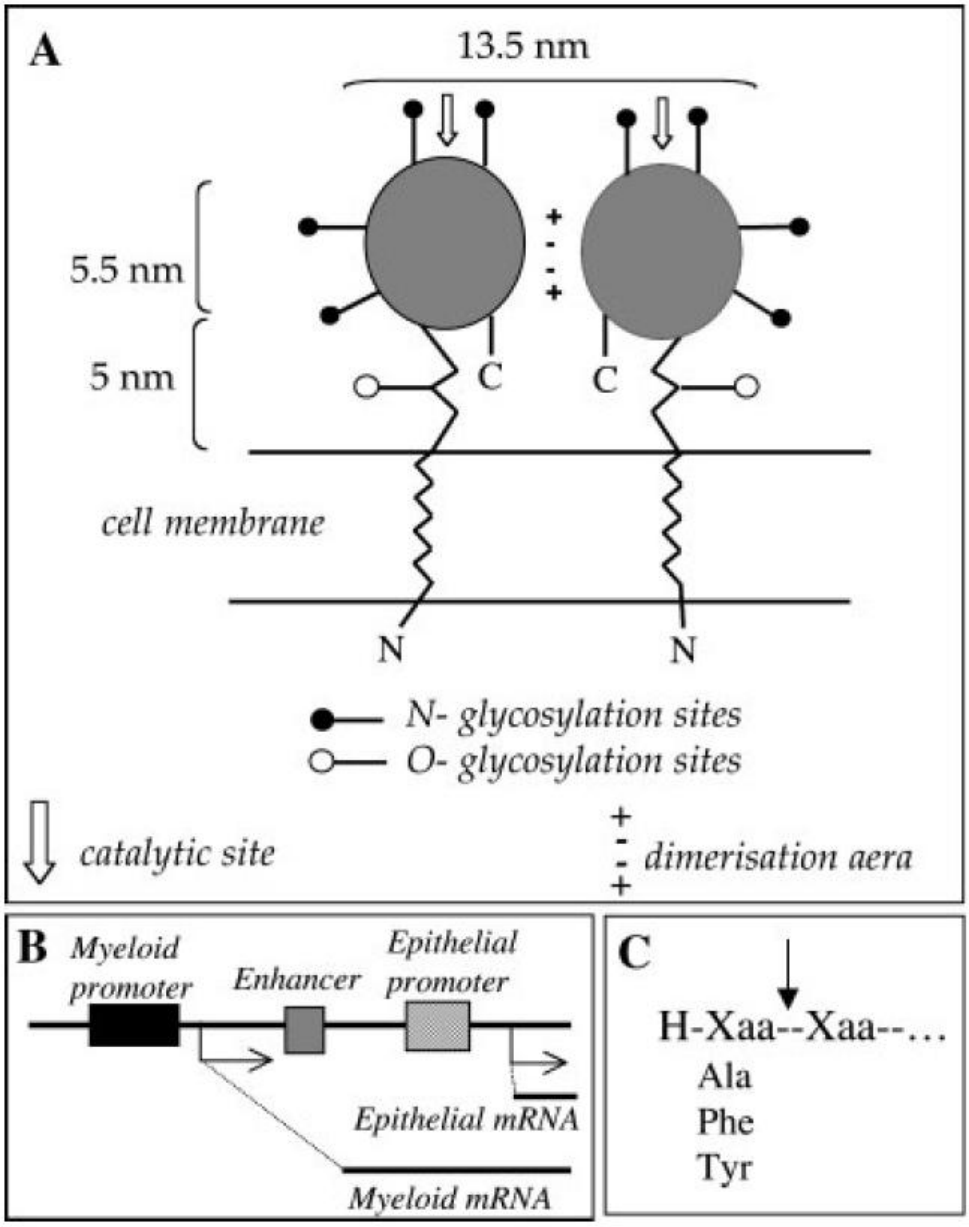

Figure 1.11. Schematic diagrams showing APN/CD13 protein (A) and promoter (B). The enzyme is a dimer of two non covalently associated monomers. The genes are controlled by two promoters, an epithelial and amyeloid promoter (in the hematopoiet system). (C) Substrate specificity where the arrow indicates the bond cleaved.[71] (Adapted from reference 71)

The CNGRC-TNF conjugate, called NGR-TNF, is currently in phase II clinical studies.[80] Other investigators have used the NGR motif embedded in

similar or different molecular scaffolds for delivering drugs, antiangiogenic drugs, tissue factor, viruses and other compounds to tumor vessels.[81,82] Recently, a CNGRC peptide with an acetylated N-terminal α-amino group and labeled with paramagnetic quantum dots has been successfully exploited for quantitative molecular magnetic resonance imaging (MRI) of tumor angiogenesis.[83] More recently, nanoparticles coated with NGR motif were used to deliver c-myc siRNA (c-myc is an oncogene overexpressed and activated in various human tumors) and doxorubicin for anticancer therapy.[84]

A number of studies were conducted to investigate the effect of cyclization of NGR peptide on receptor binding.[51, 74] It was found that both linear GNGRG and cyclized CNGRC fused with the N-terminus of TNF-α (by genetic engineering) can target the tumor.[75] However, the antitumor activity of CNGRC-TNF-α was found to be >10-fold higher than that of GNGRG-TNF-α, suggesting the importance of cysteine flanking NGR residue (**Figure 1.12**).[51, 74] It was proven that both GR residues are required for the loop formation, which is stabilized by the hydrogen bond interaction between the CO of the terminal Gly5 and the NH group of Asn2. Based on these studies, cyclized NGR became more popular; however, due to the implication of disulfide bond formation between adjacent peptide when used to decorate liposomes, another way for cyclization was introduced. An amide bond formation instead of the disulfide bond was proposed and developed by Negussie et al.[85] The authors synthesized c-NGR in the form of c-KNGRE and found the peptide to have sufficient binding affinity for biological applications.

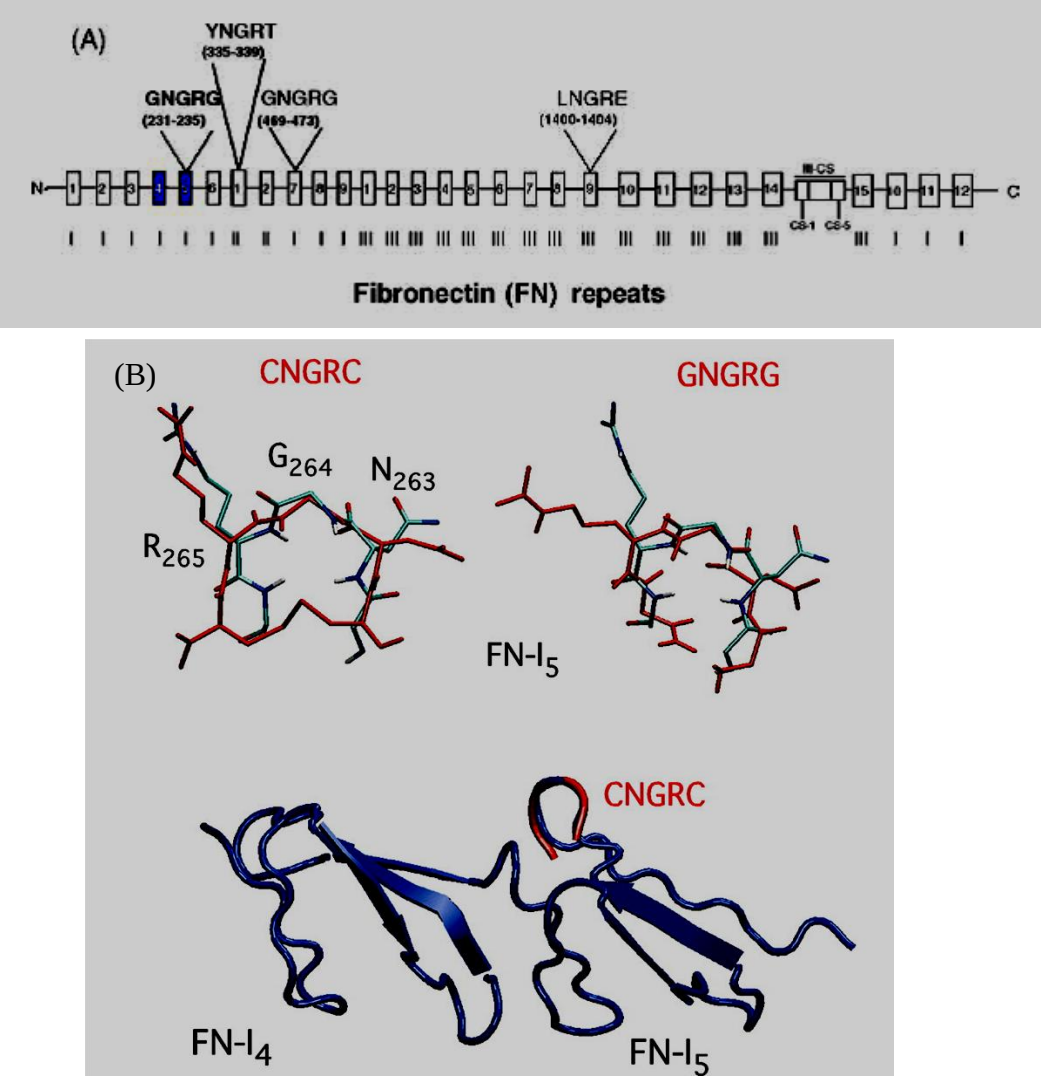

Figure 1.12. (A) Schematic representation of human fibronectin repeats; (B) Superposition of NGR most populated structures in 4th to 5th fibronectin type I (FN-I4-5) with CNGRC/G peptide.[73, 84] (Adapted from references 73 and 84)

The highest level of overexpression of CD13 receptors was identified on primary human umbilical vein endothelial cells (HUVECs) and human tumor cell lines UC-3, HT-1080, H1299, Hey and PC3-MM2. These cell lines are most

commonly used when using NGR containing peptides for targeting.[86]

Recent studies have revealed that compounds containing NGR motif can rapidly deamidate and generate isoaspartate-glycine-arginine (isoDGR), which is a ligand of αvβ3-integrin (**Figure 1.13**).[52] NGR is easily transformed to a succinimide intermediate that undergoes hydrolysis to form *iso*DGR and DGR mixtures. Isoaspartate formation can occur, in principle, also at DGR sites in proteins.

isoDGR motif can also be exploited for drug targeting to tumors. Corti et al showed that peptide degradation of c-CNGRC lead to the deamidation of NGR to isoDGR and at the same time lead to switching in CD13 to integrin binding, whereas, linear peptides mainly undergo degradation reactions which produce non-functional six/seven-membered ring compounds, unable to bind αvβ3, and small amount of isoDGR.[52] Structure-activity studies showed that the cyclic isoDGR could bind αvβ3 with an affinity >100-fold higher than that of linear isoDGR which result in inhibition of endothelial cell adhesion and tumor growth more efficiently. Cyclic isoDGR could also bind other integrins, although with 10-100-fold lower affinity. These results highlight the fact that enhanced binding of the cyclic form of NGR peptide compared to linear is due to the nonspecific interaction with integrins.[52]

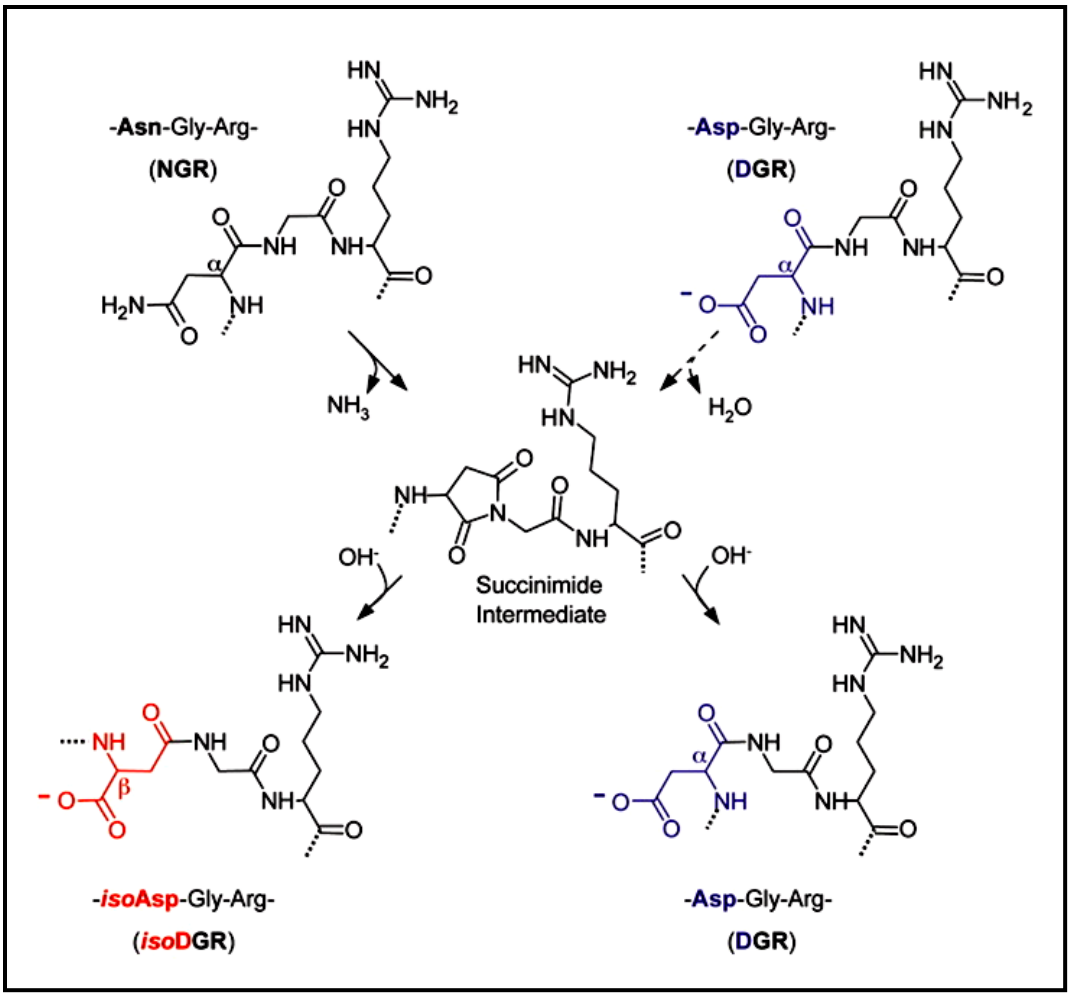

Figure 1.13. NGR transition to isoDGR in conjugates leading to the formation of *iso*DGR and DGR via a succinimide intermediate.[52]

P160 peptides

P160, a 12-mer peptide with sequence VPWMEPAYQRFL, was identified through random peptide phage display against neuroblastoma cell line WAC2.[47] Neuroblastoma is the most frequent solid tumor developing in children. The prognosis of this cancer remains poor, especially in children with advanced-disease stage.[87] Eight peptides were identified that showed affinity for WAC2 cells using phage display (**Figure 1.14**). Three promising phages, named t36,

t147 and t160 were chosen for further study. Binding of t147 and t160 to WAC2 cells was inhibited by pretreatment with the peptide p147 and p160, respectively, which supported that cellular binding of both phages took place through the displayed peptides. Further analysis using confocal microscopy indicates that the majority of t160 was internalized by the cells while t147 binds to the surface. Phage t147 was found to bind to a range of tumor cell as well as erythrocytes, lymphocytes and epithelial cells to lesser extent. On the other hand, phage t160 bound to a range of neuroblastoma cell lines and breast cancer with no binding to any of the normal tested cells. These finding provided the basis that p160 peptide could be used to target drugs to cancer tissue without targeting the normal one.[47]

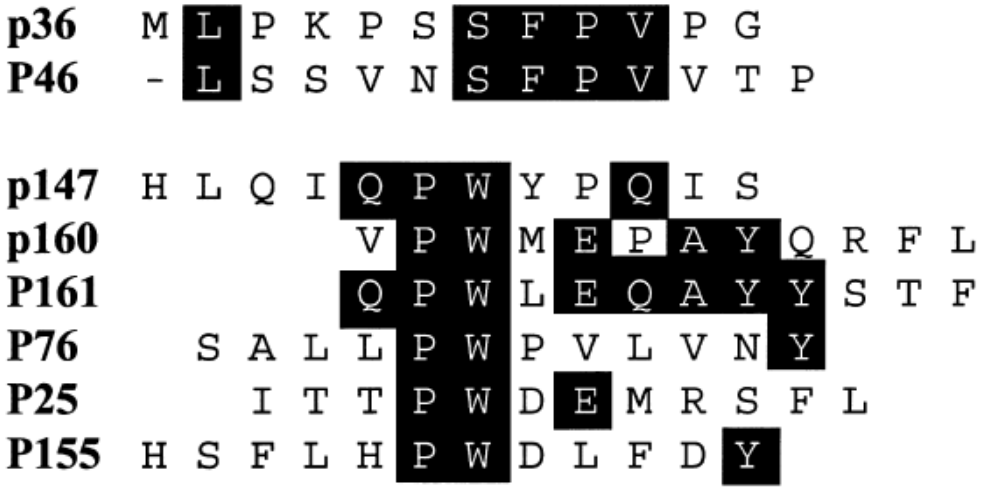

Figure 1.14. Sequence of peptides displayed on 8 candidates phages bound to neuroblastoma cell line WAC2.[47] (Adapted from reference 47)

Neuroblastoma are diagnosed as metastatic disease and, even with intensive therapy, are usually associated with poor survival, which has not improved in the past decade. Delivery of cytotoxic drugs or radionuclides into the tumor and metastases could facilitate a targeted therapy with increased drug

concentration in the tumor and fewer side effects on vital organs, as is so important for small children. Further investigation by Askoxylakis and coworker showed that the p160 peptide binds to different cancer cells, such as MCF-7 breast carcinoma cells, MDA-MB 435 and WAC2, and the binding capacity of p160 to these cells was found to be 7%, 1.6%, and 1.6% of the applied dose per 10^6 cells, respectively.[47] This binding was found to be inhibited by the addition of unlabelled peptide and not with other negative control such as D-p160 or Octreotide. These results confirmed that the binding of p160 peptide takes place through specific receptor.

Time kinetics of p160 binding with these different cells was similar, with an initial high and fast uptake and a decrease in signal over time with maximum uptake around 20 min.[56,57] This decrease in radioactivity signal was explained by the authors as degradation of the peptide itself by cell-surface peptidases and degradation of the internalized peptide in the lysosomal compartment. The decrease could also be due to a deiodination process resulting in the loss of labeled peptide. Binding experiment to HUVEC cells revealed only small binding of less than 0.4% of the applied dose/10^6 cell. Through a binding competition at different concentrations, the maximum number of binding sites was found to be 1.03×10^{-11} μmol/cell. Further studies indicated that p160 was internalized inside the cells.[56] The internalization was studied at two different temperatures, 37 and 4 °C, and the internalization of the peptide at 4 °C was inhibited which, further confirmed that internalization of p160 peptide occurs through receptor mediated endocytosis.

Organ distribution studies of radiolabeled p160 showed a higher uptake in tumor than in most other organs.[57] Only in blood and kidneys the uptake was almost the same as in tumor. The high uptake by the kidneys may be due to renal excretion of the peptide. A possible explanation for the elevated blood values, according to the authors is an interaction of p160 with serum proteins such as albumin. Furthermore, a rapid degradation of the peptide by serum proteases might also be a reason for the high blood radioactivity values, because such degradation might lead to ^{131}I-labeled fragments that cannot bind to the tumor and thereafter circulate in the bloodstream before being excreted. In addition, deiodination of the labeled peptide can result in high concentrations of free ^{131}I that might circulate in the bloodstream and be responsible for the high radioactivity values in blood. Perfusion of the tissue with 0.9% NaCl lead to reduction of the uptake in all organs except tumor. Comparative study of radiolabeled p160 and radiolabeled RGD-4C revealed similar uptake by the tumor while lower accumulation in kidney and liver in the case of p160 compared to RGD peptide. Investigation of the metabolic properties of p160 revealed that the peptide is not stable in human serum. P160 is rapidly degraded by serum proteases. The cleavable sites were identified between the amino acids ^{10}Arg-^{11}Phe, ^{9}Gln-^{10}Arg, and ^{4}Met-^{5}Glu. The degradation products of p160 start to be detected only after 5 min of incubation with serum. Further investigation of some of the fragments of p160 and p160 analogues revealed similar or better binding compared to the native p160 peptide as shown in **Table 1.8**.[56, 57]

Table 1.8: Binding of p160 peptide and peptide fragments to neuroblastoma WAC 2 cells.[57]

Fragment Name	Sequence	Ratio (binding relative to p160)
p160	VPWMEPAYQRFL	1
p160-8-1	EPAYQRFL	1.20
p160-8-2	WMEPAYQRFL	1.04
p160-8-3	VPWMEPAY	0.12
Nle-p160-8-2	WXEPAYQR	1.73
ßAla-p160-8-2	WMEPβAYQR	2.56

1.1.4 Proteolytic Stability of Cancer Targeting Peptides

In the last decade, a large number of cell-binding peptides with the potential of targeting ability have been identified (**Table 1.7**). However, the use of peptides in pharmaceutical applications is limited due to their susceptibility to proteolytic degradation and their poor absorption from the gut, rapid excretion through the kidneys and therefore low bioavailability. Moreover, the highly flexible conformation of short and medium linear peptide sequences decreases the activity and selectivity.[56,57,88] Therefore, modifications of the peptide structure with reference to the peptide backbone and/or the amino acid side chains can improve the pharmacological properties of peptides. For instance, **Figure 1.15** shows some of the commonly used peptide modifications to increase proteolytic stability, such as the introduction of D-amino acids, unnatural amino acids to give peptoids and aza peptides, as well as peptide cyclization.[89]

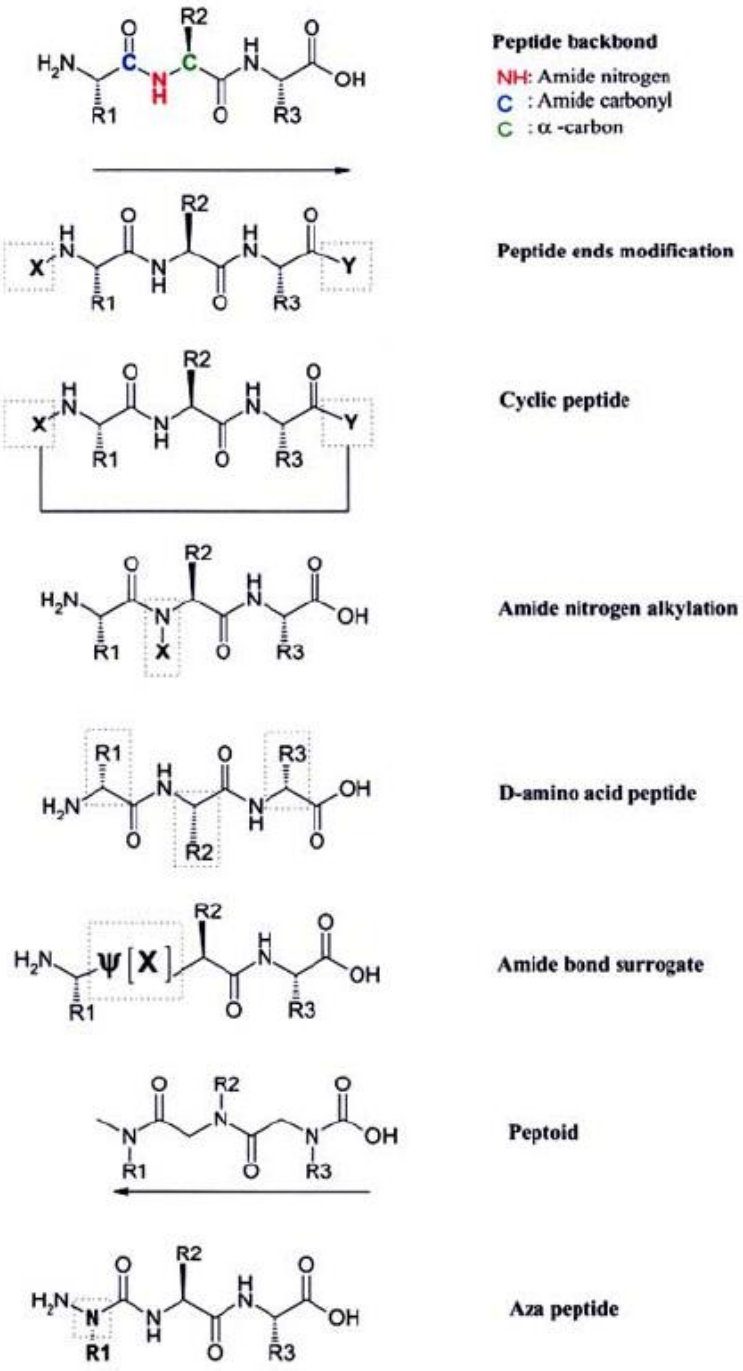

Figure 1.15. Peptide modifications to increase proteolytic stability. The figure illustrates the place where modifications are introduced, and the type of alterations. X and Y represent any chemical group or atom. R correspond to the side chain of any of the 20 natural amino acids.[89] (Adapted from reference 89)

1.2 Peptidomimetic β-Peptides

1.2.1 Peptidomimetics

Over the years, numerous efforts have been made to develop synthetic mimetics of biologically active α-peptides that maintain a significant activity of the parent compound as well as produce improved pharmacological properties, such as, metabolic stability and bioavailability. Peptidomimetics has emerged as an avenue to overcome these problems as well as identify drug-like molecules. Peptidomimetics should maintain a secondary structure as well as other structural features analogous to that of the original peptide and at the same time mimic peptide function and improve their bioavailability.

Different classes of peptidomimetics have been developed through the structural modification of the α-peptide backbone, such as, introduction of one extra methylene group in the backbone to give either β^2 or β^3–peptides, or two methylene groups to give γ-peptides. Others include, peptoids where the side chain of the amino acid is attached to the NH of the backbone to give N-substituted glycines,[90] as well as the introduction of different structural constraints, such as *trans*-2-aminocyclopentyl carboxylic acid (*trans*-ACPC), and *trans*-2-aminocyclohexyl carboxylic acid (*trans*-ACHC),[91] the use of peusodopeptide backbone of repeating N-(2-aminoethyl)-glycine units linked by peptide bonds, with nucleobase to produce peptide nucleic acids (**Figure 1.16**). [92]

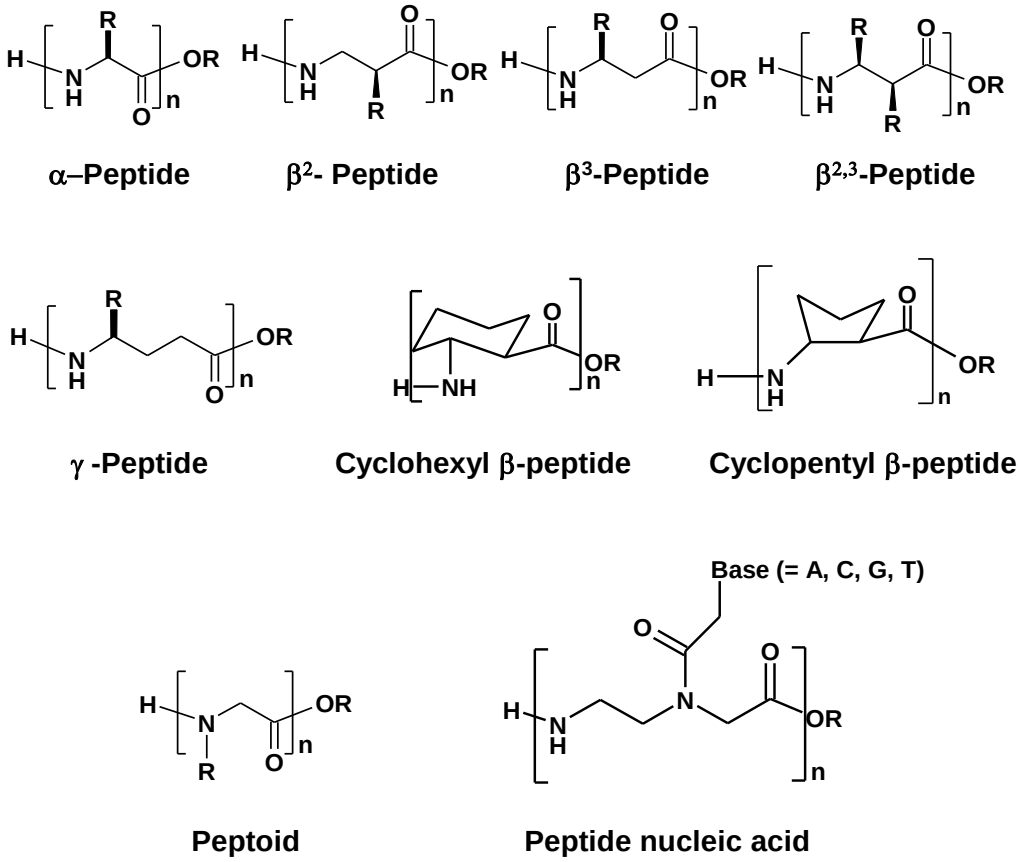

Figure 1.16. Examples of different peptidomimetics.

Among the peptidomimetics reported, β-peptides are becoming increasingly popular from biological and pharmaceutical standpoint.[93] Although they can display similar biological activity as α-peptides, for instance, somatostatin receptor agonist β-peptide, they are considerably more resilient to proteolysis and metabolism.[94,95] Furthermore, these molecules exhibit well-defined secondary structures such as helices, sheets, and turns in solution.[96,97]

β-peptides are composed of β-amino acids, which contain one additional methylene group in the backbone compared to α-amino acids (**Figure 1.16**). β-amino acids can have side chains present at C_α, C_β, or both $C_{\alpha,\beta}$ positions giving

β^2-, β^3-, or $\beta^{2,3}$-peptides, respectively. The field of β-peptides has evolved by the work of mainly three groups, D. Seebach,[93] S. Gellman,[98] and recently A. Schepartz.[99]

1.2.2 Synthesis of β-peptides

β-peptides are accessible by solid-phase peptide synthesis (SPPS). Parallel syntheses of these molecules have made it possible to study their structure-activity relationships in a systematic manner.[93] Generally, β-peptides are synthesized using N-Fmoc-protected β-amino acid monomers.[93] These β-amino acids are usually made from corresponding α-amino acids employing different methods. However, most methods are not practical enough to give the corresponding amino acid with the correct side chain and the special protection of the side chain needed for SPPS. The most modified and recent method used for the synthesis of β^2-amino acid was developed by Seebach and colleagues (**Scheme 1.1**). By adopting the Evans method, aminomethyl compounds are coupled with a chiral *N*-acyl-benzyloxazolidinone. The *N*-methoxymethylbenzyl carbamate ($ZNHCH_2OMe$) shows enhanced reactivity under Ti-enolate conditions, permitting the isolation of alkylated products in 60–90% yields, making this method suitable of a wide variety of β^2-amino acids.[100,101]

Scheme 1.1. Preparation of β^2-amino acids by amidomethylation.

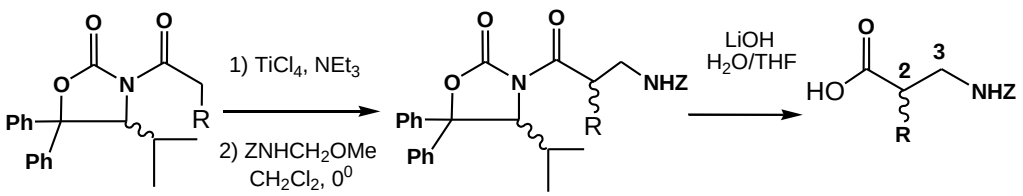

R=Me, ^{t}Pr, ^{i}Bu, Bn, $Br(CH_2)_2$, $Br(CH_2)_4$,$Br(CH_2)_3$
(60-90% yields)

A second method was developed by Gellman and co-workers where they treated chiral amines with achiral acrylate derivatives at high temperature (**Scheme 1.2**).[102] This resulted in 1:1 mixtures of diastereoisomers which were separated by crystallization and chromatography. Subsequently, cleavage of the chiral director afforded the enantiopure β^2-amino acids.

For the preparation of β^3-peptides, Seebach *et al* were the first to report the syntheses of β^3-amino acid residues with proteinogenic side chains.[103] Their method is still the most popular method for the preparation of Fmoc protected β^3-amino acids. In their method, β^3-homoamino acids were synthesized via Arndt-Eistert homologation of the α-amino acids (**Scheme 1.3**). The α-amino acid was converted to the corresponding diazoketones by reaction of the mixed anhydrides (formed with i-BuOCOCl/N-methyl morpholine) with CH_2N_2. It was reported that the partial hydrolysis of the mixed anhydride (due to moisture in ethereal CH_2N_2 solution) lead to the formation of the methyl ester and was found to be the major side product of this reaction (up to 15%).

Scheme 1.2. Preparation of β^2-amino acid by Michael-type reaction of chiral amines with achiral acrylate.

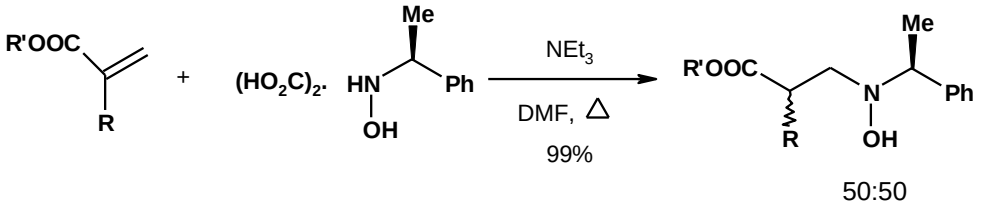

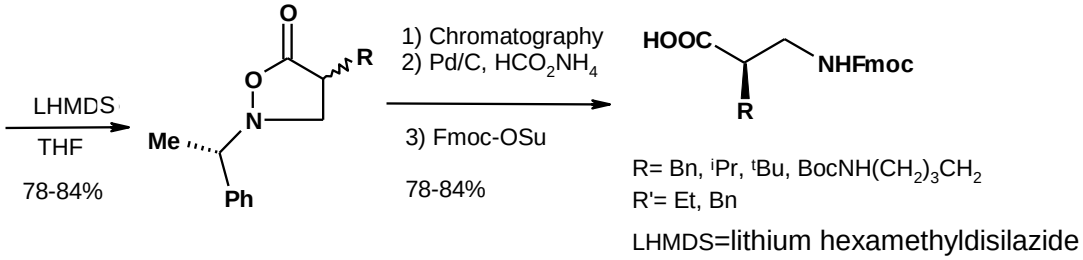

The diazoketone was decomposed in THF containing 10% H_2O (nucleophilic attack) with catalytic amounts of CF_3COOAg added as a homogeneous solution in Et_3N. Significant loss of the Fmoc protecting group was also observed under these conditions (**Scheme 1.3**). In addition, this procedure requires the use of diazomethane gas, which is a highly toxic and explosive gas, making the synthetic procedure non trivial. This methodology is based on the direct conversion of α-amino acid to the corresponding β^3-amino acid, making the synthesis limited to the natural α-amino acids only. Novel methods for easy access of these oligomers with a wide variety of side chains are therefore sought for.

Scheme 1.3. Arndt-Eistert homologation to afford β^3-substituted amino acid.

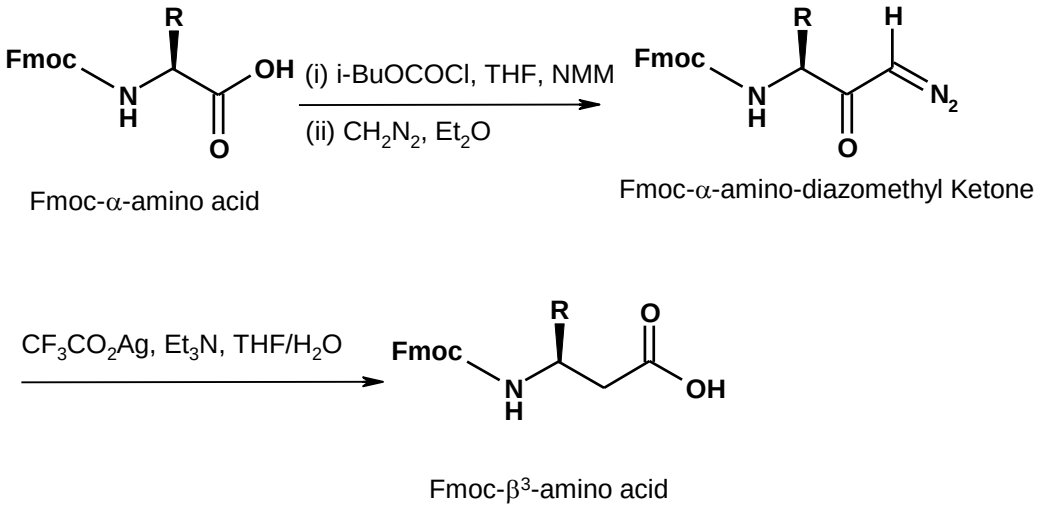

Fmoc-α-amino acid

Fmoc-α-amino-diazomethyl Ketone

Fmoc-β^3-amino acid

1.2.3 Structural Conformation of β-Peptides

β-Peptides adopt different secondary structures in solution. In general, the substitution pattern dictates the solution conformation of these peptidomimetics. Monosubstituted β^3- or β^2-peptides form 14-helical structures and alternating β^2/β^3-peptides prefer 10/12 helices (**Figure 1.17**).[91,99,104,105,106] The helical secondary structure is enhanced in the presence of organic solvents, such as methanol and 2,2,2-trifluoroethanol (TFE), and efforts have been made to stabilize this conformation in aqueous solutions. [96,107, 108-110]

The folding of the peptides in solution is very important as the biological activity of peptides is dependent on their conformation. Most often, the conformation dictates the specific binding to the receptor and as a result their biological response. In this regard, β-peptides that fold into 14-helix have received special attention.[99,111] The structural and conformational differences

between the 3.6_{13} helix (α-helix) of an α-peptide, and 14-helices of β^3- and β^2-peptides are summarized in **Figure 1.18**.[93]

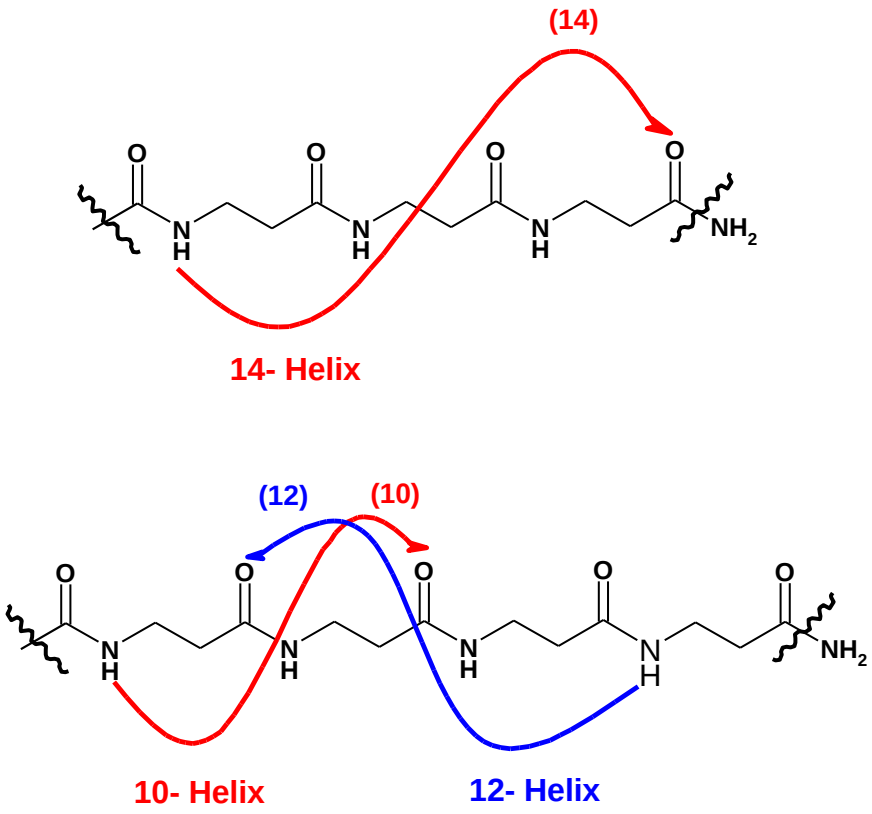

Figure 1.17. Nomenclature for β-peptide helices, 14-helix and 10/12-helix, based on hydrogen-bonding patterns.

Strategies to control conformation of β-peptides

The 14-helix of β-peptide is formed due to the stable hydrogen bond between the proton at NH position *i* and the carbonyl group at *i*+2 (**Figure 1.17**). Top view examination of the helix indicates that the side chains of residues i and i+3 are located nearly on the top of each other (**Figure 1.18**) and suggests that hydrophobic interactions between overlapping aliphatic side chains could play

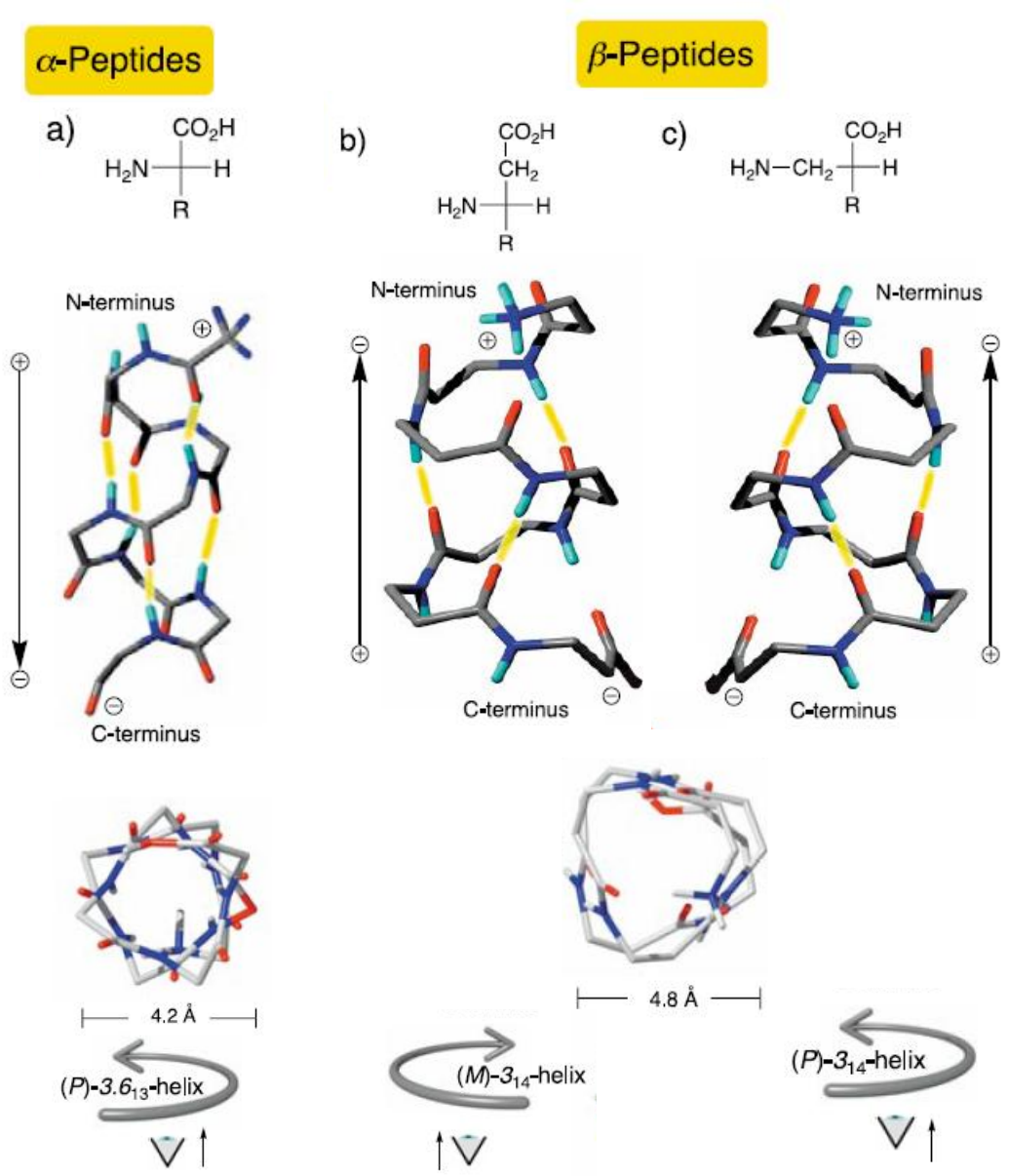

Figure 1.18. Comparison of α and β-peptidic helix structures derived from NMR analysis. Natural α-peptides form 3.6_{13} helix (a), whereas, the β^3- (b) and β^2- (c) peptides form 3_{14}-helix. Homologation of the natural α-amino acids (right handed or P helix) to β^3- or β^2-amino acids with retention of configuration results in (left handed or M)- or (P)-3_{14}-helices with inversion of the macrodipole.[93]

significant role in stabilizing the overall structure. The distance between residues at positions i and i+3 is approximately 5 Å. The helix is compact with a diameter

of ~4.8 Å slightly larger than that of the α-helix (4.2 Å). Stabilization of the helical structure of β-peptides has been achieved by increasing the level of pre-organization of β-peptides. Though, the rules used for α-peptides do not essentially apply, for example, C(α)- or C(β)- tetrasubstitution of β-amino acid residues is not compatible with β-peptides 14-helix formation.[112-114] Gellman and coworker, found that homo-oligomers constituting of *trans*-2-aminocyclohexyl carboxylic acid (*trans*-ACHC) form ideal 3_{14} left hand helix.[91] The nature of the solvent can influence the stability of the helical structure. As mentioned before, β-peptides form stable 14-helix in different organic solvents, whereas folding in an aqueous environment is highly relevant to applications in biology. Although helicity in water is essentially weaker in the absence of strong backbone pre-organization, principles guiding the design of β-peptides with high level of 14-helix in aqueous solution have recently been studied by several groups.[96,110,115] Some of these strategies are (i) salt bridge or lactam formation between complementary charged i/i+3 side chains (e.g β^3-HOrn/β^3-HGlu; β^3-HOrn/β^3-HAsp), (ii) the use of electrostatic interaction to maximize the interaction with macrodipole (e.g. by free charged termini, and appropriate orientation of the salt bridge), and (iii) introduction of β^3-amino acids with high intrinsic 14-helix propensity, such as *trans*-ACHC.

For non-charged β^3-amino acids, 14-helix propensities have been found to differ from α-helix of corresponding α-amino acids. Branched side chains of Ile, Thr, and Val which are known to be destabilizing in α-helix, are strong 14-helix stabilizers. In contrast, Ala which is the most α-helix–stabilizing α-amino acid,

the methyl side chain is one of the most 14-helical destabilizing. Helix bundle in β^3-peptides has been revealed to increase 14-helicity in aqueous solution.[92] It has been postulated that, a large macrodipole may build up, especially in peptides with longer chains, and may act destabilizing, an effect that can be weakened by inclusion of negatively charged side chains close to the (+)-pole and positively charged side chains close to the (-)-pole. The macrodipole can also be stabilized by capping the N- and C-terminal groups thereby removing the charge.[93]

1.2.4 Proteolytic Stability of β-Peptides

Peptidomimetic β-peptides display remarkable stability against degradation by proteolytic enzymes.[108,111,116,117] Hence, β-peptides with a wide variety of potential applications in medicinal chemistry have been synthesized, such as antibacterial and virus entry inhibitors agents, and inhibitors of protein–protein interactions.[94,118] The pharmacokinetics of β-peptides are equally remarkable, with elimination half lives of 3-10 hr, compared with less than 15 min for α-peptides following intravenous injection in rats. β-peptides can also cross cell membranes and localize to the cell nuclei by the attachment of β-peptide segments derived from HIV-1 Tat proteins, which could permit the design of β-peptides that can affect biological targets in the nucleus.[119] Such properties of β-peptides as medicinal agents stem from their ability to fold into stable secondary structures without the need for tertiary interactions in a relatively short oligomer.

The proteolytic stability of β-peptides arises because of lack of any interaction between them and the *in vivo* enzymes. However, to be an ideal drug candidate, correct balance between the stability and the affinity for the biological receptor is often desired. Several strategies have been used to obtain appropriate balance between proteolytic stability, bioavailability and biological activity, such as design of mixed peptides containing α- and β-amino acid residues or design of peptides where the backbone and the side chains together mimic the natural α-peptide.[118,120,121]

1.2.5 Biologically Active β-Peptides

Different approaches are available for developing bioactive peptides, such as, direct sequence conversion, and distribution of the physiochemical properties. Peptides designed using direct sequencing were applied to different peptide analogues, for instance, somatostatin receptor binding β-peptide was designed based on the natural α-peptide somatostatin through the use of β^2/β^3 motif of Lysine/Tryptophan, respectively. This oligomer binds to one of the somatostatin receptor subtype (hsst4) with Kd of 83 nM.[94] Another example of this strategy was the conversion of a piece of the RNA-binding protein Tat to the β-peptide sequence. This β^3-peptide analogue of the Tat protein was able to bind TAR RNA with nanomolar affinity.[122]

The activity of many biologically active antimicrobial peptides is based on their physicochemical properties.[123] Several antibacterial β-peptides have been designed by incorporating the amphipathic helix with appropriate side chains.

Gellman's group has reported a 17-residue β-peptide (β-17) with 12-helix that possess potent antibacterial activity against a variety of Gram-positive and Gram-negative bacteria.[120,124] In this study Gellman et al. show that there is no relationship between 14-helical stability and antimicrobial potency, however, the ability of the β-peptide to form an amphiphilic helix was crucial for the antimicrobial activity.[120,124] β^3-nonapeptide, H-(β^3hAla-β^3hLys-β^3hPhe)$_3$-OH, inhibits cholesterol transport and uptake in the lumen of the small intestine by blocking the SRB-class B. This effect was based on the ability of these peptides to form an amphipathic helix.[125] Such studies highlight the potential of peptidomimetic β-peptides in the design of pharmaceutical agents.

1.3 Thesis Proposal

1.3.1 Thesis Rational

Current cancer therapies have low specificity for tumor cells and have serious toxic side effects. Targeting drugs to the cancer cells can help improve the outcome of existing cancer therapies. Antibodies are commonly used as targeting ligand, but there are some limitations for their use as discussed above (**Section 1.1.2.3**). In the recent years, cancer targeting peptides have emerged as ideal agents to target cancer cells. Several peptides have been identified by *in vivo* screening of peptide-phage libraries that target tumor vasculature, such as peptide containing RGD and NGR, or targeting the tumor cell surface, such as p160 peptide. Peptides identified from the phage display for targeting cancer cells can be further improved for specific binding and metabolic stability by

chemical manipulation of their structures. Developing new methods to screen peptides for specific recognition by cancer cells will provide a reliable method to profile fresh cancer cells derived from patients. Such binding profile may one day enable the physician to choose appropriate targeting peptides to treat a specific cancer. At the same time, strategies can be developed to increase the stability of peptides through the use of peptidomimetic β-peptides.

1.3.2 Thesis Objective

The objective of this thesis is to develop a peptide array-whole cell binding assay for screening peptides with specific binding affinity for cancer cells. This method will provide a rapid way for screening large number of peptides for cancer cell targeting and could provide a new tool for cancer diagnosis. The second part of the thesis deals with the design of novel peptidomimetics as an avenue to stabilize peptides and improve their properties as drug candidates.

Specific Objectives

In the first part of the thesis (Chapter 2) attempts were made to synthesize peptide arrays (up to 140 peptides) on functionalized cellulose membranes using covalent conjugation. Peptide libraries were designed based on the sequences of two lead peptides, namely, NGR and p160. These peptides arrays were used to study the interaction between peptides and cancer cells, such as HT-1080, MDA-MB-435, and MCF-7. Binding with normal cells, such as HUVEC cells, was also conducted to screen peptides that specifically bind to cancer cells. A fluorescence

imaging based method (peptide array-whole cell binding assay) was developed to screen peptides with specific and high affinity for cancer cells.

The second part of the thesis (Chapter 3) addresses the design and synthesis of two families of β-peptides, β^2- and β^3- peptides using a new synthetic approach. Representative β-hexapeptides were synthesized starting from *β*-amino-L-alanine and L-Aspartic acid monomers. The solution conformation of these peptides was studied using circular dichroism and NMR spectroscopy. The proteolytic stability and cytotoxicity was also evaluated. Finally, a mixed α/β-peptide was synthesized and evaluated for proteolytic stability compared to an α-peptide.

1.4 References

(1) Waterston, R. H., Lander, E. S., Sulston, J. E. *Proc Natl Acad Sci U S A* **2002**, *99*, 3712-6.

(2) Hanahan, D., Weinberg, R. A. *Cell* **2000**, *100*, 57-70.

(3) Renan, M. J. *Mol Carcinog* **1993**, *7*, 139-46.

(4) Opdenakker, G., Van Damme, J. *Int J Dev Biol* **2004**, *48*, 519-27.

(5) Koopman, G., Heider, K. H., Horst, E., Adolf, G. R., van den Berg, F., Ponta, H., Herrlich, P., Pals, S. T. *J Exp Med* **1993**, *177*, 897-904.

(6) Parkin, D., Bary, F., Ferlay, J., Pisani, P. *CA Cancer J Clin;* **2005**, *55*, 74-108.

(7) (a) Quinn, M. J. *J Natl Cancer Inst* **2003**, *95*, 1258-61, (b) http://www.statcan.gc.ca.

(8) Aina, O. H., Sroka, T.C., Chen, M.L., Lam, K.S. *Biopolymers* **2002**, *66*, 184-99.

(9) Kirsner, K. *AANA J* **2003**, *71*, 55-62.

(10) Garattini, S., La Vecchia,C. *Eur J Cancer* **2001**, *37*, S128–S147.

(11) Raschi, E., Vasina, V., Ursino, M. G., Boriani, G., Martoni, A., De Ponti, F. *Pharmacol Ther* **2010**, *125*, 196-218.

(12) Ferrari, M. *Nat. Rev. Cancer* **2005**, *5*, 161-71.

(13) Kim, C., Lim, S. *J Arch. Pharm. Res* **2002**, *25*, 229-39.

(14) Gao, X., Cui, Y., Levenson, R.M., Chung, L.W., Nie, S. *Nat. Biotechnol.* **2004**, *22*, 969-76.

(15) Sengupta, S., Eavarone, D., Capila, L. *Nature* **2005**, *436*, 568-72.

(16) Shukla, G. S., Krag, D. N. *Expert Opin Biol Ther* **2006**, *6*, 39-54.

(17) Dachs, G., Tupper, J., Tozer, GM. *Anticance Drugs* **2005**, *16*, 349-59.

(18) Hingorani, M., White, C. L., Agrawal, V. K., Vidal, L., Melcher, A., Harrington, K. J. *Curr Cancer Drug Targets* **2007**, *7*, 389-409.

(19) Roskoski, J. R. *Biochem. Biophy Res Commun.* **2004**, *319*, 1-11.

(20) Nielsen, U. B., Marks, J.D., *Pharm Sci Technol Today* **2000**, *3*, 282-91.

(21) Denardo, S., O'Grady, LF., Richman, CM., Goldstein, DS., O'Donnell, RT., Denardo, DA., Kroger, LA., Lamborn, KR., Hellström, KE., Hellström, I., Denardo, GL. *Anticancer Res* **1997**, *17*, 1745-51.

(22) Dearden, C. *BioDrugs* **2002**, *16*, 283-301.

(23) Macdonald, G., Glover, N. *Curr. Opin Drug Disc. Dev.* **2005**, *8*, 177-183.

(24) Bodey, B. *Expert Opin Biol Ther* **2001**, *1*, 603-617.

(25) Kim, E., Khuri, FR., Herbst, RS. *Curr Opin Oncol.* **2001**, *13*, 506-13.

(26) Dvorak, H. F., Nagy, J.A., Dvorak, A.M. *Cancer Cells* **1991**, *3*, 77-85.

(27) Suzuki, M., Takayanagi. A., Shimizu, N., *Cancer Sci* **2004**, *95*, 424-29.

(28) Krenning, E., Bakker, WH., Breeman, WA., Koper, JW., Kooij, PP., Ausema, L., Lameris, JS., Reubi, JC., Lamberts, SW. *Lancet* **1989**, *1*, 242-4.

(29) Mori, T. *Curr Pharm Des* **2004**, *10*, 2335-43.

(30) Shadidi, M., Sioud, M. *Drug Resist Updat* **2003**, *6*, 363-71.

(31) Lee, T., Lin, CT., Kuo, SY., Chang, DK., Wu, HC. *Cancer Res* **2007**, *67*, 10958-65.

(32) Chang, D. K., Lin, C.T., Wu, C.H., Wu, H.C. *PLoS One* **2009**, *4*, 4171.

(33) Lee, T., Wu, HC., Tseng, YL., Lin, CT. *Cancer Res* **2004**, *64*, 8002-8.

(34) Scott, J. K., Smith, G. P. *Science* **1990**, *249*, 386-90.

(35) Brown, C. K., Modzelewski, R. A., Johnson, C. S., Wong, M. K. *Ann Surg Oncol* **2000**, *7*, 743-9.

(36) Lam, K. S., Lebl, M., Krchnak, V. *Chem Rev* **1997**, *97*, 411-448.

(37) Maeji, N. J., Bray, A. M., Geysen, H. M. *J Immunol Methods* **1990**, *134*, 23-33.

(38) Frank, R. *Tetrahedron* **1992**, *48*, 9217-32.

(39) Songyang, Z., Margolis, B., Chaudhuri, M., Shoelson, S. E., Cantley, L. C. *J Biol Chem* **1995**, *270*, 14863-6.

(40) Parmley, S. F., Smith, G. P. *Gene* **1988**, *73*, 305-18.

(41) Arap, W., Kolonin, M. G., Trepel, M., Lahdenranta, J., Cardo-Vila, M., Giordano, R. J., Mintz, P. J., Ardelt, P. U., Yao, V. J., Vidal, C. I.; Chen, L., Flamm, A., Valtanen, H., Weavind, L. M., Hicks, M. E., Pollock, R. E., Botz, G. H., Bucana, C. D., Koivunen, E., Cahill, D., Troncoso, P.; Baggerly, K. A., Pentz, R. D., Do, K. A., Logothetis, C. J.,Pasqualini, R. *Nat Med* **2002**, *8*, 121-7.

(42) Thompson, L. A., Ellman, J. A. *Chem Rev* **1996**, *96*, 555-600.

(43) Lam, K. S., Salmon, S. E., Hersh, E. M., Hruby, V. J., Kazmierski, W. M., Knapp, R. J. *Nature* **1991**, *354*, 82-4.

(44) Okochi, M., Nomura, S., Kaga, C., Honda, H. *Biochem Biophys Res Commun* **2008**, *371*, 85-9.

(45) Li, Z., Zhao, R., Wu, X., Sun, Y., Yao, M., Li, J., Xu, Y., Gu, J. *Faseb J* **2005**, *19*, 1978-85.

(46) Wong, S. C.; Wakefield, D.; Klein, J.; Monahan, S. D.; Rozema, D. B.; Lewis, D. L.; Higgs, L.; Ludtke, J.; Sokoloff, A. V.; Wolff, J. A. *Mol Pharm* **2006**, *3*, 386-97.

(47) Zhang, J., Spring, H., Schwab, M. *Cancer Lett* **2001**, *171*, 153-64.

(48) Arap, W., Pasqualini, R., Ruoslahti, E. *Science* **1998**, *279*, 377–80

(49) Pierschbacher, M. D., Ruoslahti, E. *Nature* **1984**, *309*, 30-3.

(50) Zitzmann, S., Ehemann, V., Schwab, M. *Cancer Res* **2002**, *62*, 5 139-43.

(51) Colombo, G., Curnis, F., De Mori, G. M., Gasparri, A., Longoni, C., Sacchi, A., Longhi, R., Corti, A. *J Biol Chem* **2002**, *277*, 47891-7.

(52) Corti, A., Curnis, F., Arap, W., Pasqualini, R. *Blood* **2008**, *112*, 2628-35.

(53) Curnis, F., Sacchi, A., Corti, A. *J Clin Invest* **2002**, *110*, 475-82.

(54) Pasqualini, R., Koivunen, E., Kain, R., *Cancer Res* **2000**, *60*, 722–27.

(55) Song, S., Liu, D., Peng, J., Sun, Y., Li, Z., Gu, J. R., Xu, Y. *Int J Pharm* **2008**, *363*, 155-61.

(56) Askoxylakis, V., Mier, W., Zitzmann, S., Ehemann, V., Zhang, J., Kramer, S., Beck, C., Schwab, M., Eisenhut, M., Haberkorn, U. *J Nucl Med* **2006**, *47*, 981-8.

(57) Askoxylakis, V., Zitzmann, S., Mier, W., Graham, K., Kramer, S., von Wegner, F., Fink, R. H., Schwab, M., Eisenhut, M., Haberkorn, U. *Clin Cancer Res* **2005**, *11*, 6705-12.

(58) Luna, E. J., Hitt, A.L. *Science* **1992**, *258*, 955–64.

(59) Giancotti, F. G., Ruoslahti, E. *Science* **1999**, *285*, 1028-32.

(60) Albelda, S. M., Mette, S. A., Elder, D. E., Stewart, R., Damjanovich, L., Herlyn, M., Buck, C. A. *Cancer Res* **1990**, *50*, 6757-64.

(61) Goodman, S. L., Holzemann, G., Sulyok, G. A., Kessler, H. *J Med Chem* **2002**, *45*, 1045-51.

(62) Reardon, D. A., Nabors, L. B., Stupp, R., Mikkelsen, T. *Expert Opin Investig Drugs* **2008**, *17*, 1225-35.

(63) Schottelius, M., Laufer, B., Kessler, H., Wester, H. J. *Acc Chem Res* **2009**, *42*, 969-80.

(64) Healy, J. M., Murayama, O., Maeda, T., Yoshino, K., Sekiguchi, K., Kikuchi, M. *Biochemistry* **1995**, *34*, 3948-55.

(65) Luan, Y., Xu, W. *Curr Med Chem* **2007**, *14*, 639-47.

(66) Riemann D, K. A., Langner *J. Immunol Today* **1999**, *20*, 83-8.

(67) Razak K, N. A. *Blood Rev* **1992**, *6*, 243–50.

(68) Curnis, F., Arrigoni, G., Sacchi, A. *Cancer Res* **2002**, *62*, 867-74.

(69) Buehler, A., van Zandvoort, MA., Stelt, BJ. *Arterioscler Thromb Vasc Biol* **2006**, *26*, 2681–7.

(70) Lahdenranta, J., Sidman, RL., Pasqualini, R., Arap, W. *FASEB J* **2007**, *21*, 3272–8.

(71) Bauvois, B., Dauzonne, D. *Med Res Rev* **2006**, *26*, 88-130.

(72) Razak, K., Newland, A.C. *Blood Rev* **1992**, *6*, 243–50.

(73) Yang, E., Shim, JS., Woo, HJ., Kim, KW., Kwon, HJ. *Biochem Biophys Res Commun* **2007**, *363*, 336–41.

(74) Di Matteo, P., Curnis, F., Longhi, R., *Mol Immunol* **2006**, *43*, 1509–18.

(75) Curnis, F., Sacchi, A., Borgna, L., Magni, F., Gasparri, A., Corti, A. *Nat Biotechnol* **2000**, *18*, 1185-90.

(76) Curnis, F., Gasparri, A., Sacchi, A., Cattaneo, A., Magni, F., Corti, A. *Cancer Res* **2005**, *65*, 2906-13.

(77) Sacchi, A., Gasparri, A., Curnis, F., Bellone, M., Corti, A. *Cancer Res* **2004**, *64*, 7150-5.

(78) Pastorino, F., Brignole, C., Marimpietri, D., Cilli, M., Gambini, C., Ribatti, D., Longhi, R., Allen, T. M., Corti, A., Ponzoni, M. *Cancer Res* **2003**, *63*, 7400-9.

(79) Pastorino, F., Brignole, C., Di Paolo, D., Nico, B., Pezzolo, A., Marimpietri, D., Pagnan, G., Piccardi, F., Cilli, M., Longhi, R., Ribatti, D., Corti, A., Allen, T. M., Ponzoni, M. *Cancer Res* **2006**, *66*, 10073-82.

(80) Gregorc, V., Citterio, G., Vitali, G., Spreafico, A., Scifo, P., Borri, A., Donadoni, G., Rossoni, G., Corti, A., Caligaris-Cappio, F., Del Maschio, A., Esposito, A., De Cobelli, F., Dell'Acqua, F., Troysi, A., Bruzzi, P., Lambiase, A., Bordignon, C. *Eur J Cancer* **2010**, *46*, 198-206.

(81) Ellerby, H. M., Arap, W., Ellerby, L. M., Kain, R., Andrusiak, R., Rio, G. D., Krajewski, S., Lombardo, C. R., Rao, R., Ruoslahti, E., Bredesen, D. E., Pasqualini, R. *Nat Med* **1999**, *5*, 1032-8.

(82) Zhang, Z., Harada, H., Tanabe, K., Hatta, H., Hiraoka, M., Nishimoto, S. *Peptides* **2005**, *26*, 2182-7.

(83) Oostendorp, M., Douma, K., Hackeng, T. M., Dirksen, A., Post, M. J., van Zandvoort, M. A., Backes, W. H. *Cancer Res* **2008**, *68*, 7676-83.

(84) Chen, Y., Wu, J.J., Huang, L. *Mol Ther* **2010**, *18*, 828-34.

(85) Negussie, A. H., Miller, J. L., Reddy, G., Drake, S. K., Wood, B. J., Dreher, M. R. *J Control Release* **2010,** 143, 265-273**.**

(86) Moffatt, S., Wiehle, S., Cristiano, R. J. *Hum Gene Ther* **2005**, *16*, 57-67.

(87) Schwab, M. *Bioessays* **1998**, *20*, 473-9.

(88) Yamamoto, Y., Tsutsumi, Y., Mayumi, T. *Curr Drug Targets* **2002**, *3*, 123-30.

(89) Adessi, C., Soto, C. *Curr Med Chem* **2002**, *9*, 963-78.

(90) Ronald, N., Zuckermann, Janice M. Kerr, Stephen B. H. Kent, Walter H. Moos *J Am Chem Soc* **1991**, *114*, 10646–47.

(91) Daniel, A., Laurie, C., Isabella, K., Douglas, P., and Gellman,S. *Am Chem Soc* **1999**, *121*, 6206–12.

(92) McMahon, B. M., Mays, D., Lipsky, J., Stewart, J. A., Fauq, A., Richelson, E. *Antisense Nucleic Acid Drug Dev* **2002**, *12*, 65-70.

(93) Seebach, D., Beck, A. K., Bierbaum, D. J. *Chem Biodivers* **2004**, *1*, 1111-239.

(94) Gademann, K., Kimmerlin, T., Hoyer, D., Seebach, D. *J Med Chem* **2001**, *44*, 2460-8.

(95) Hook, D. F., Bindschadler, P., Mahajan, Y. R., Sebesta, R., Kast, P., Seebach, D. *Chem Biodivers* **2005**, *2*, 591-632.

(96) Cheng, R. P., Gellman, S. H., DeGrado, W. F. *Chem Rev* **2001**, *101*, 3219-32.

(97) Gademann, K., Hintermann, T., Schreiber, J. V. *Curr Med Chem* **1999**, *6*, 905-25.

(98) Raguse, T., Lai, J. R., LePlae, P. R., Gellman, S. H. *Org Lett* **2001**, *3*, 3963-6.

(99) Kritzer, J. A., Tirado-Rives, J., Hart, S. A., Lear, J. D., Jorgensen, W. L., Schepartz, A. *J Am Chem Soc* **2005**, *127*, 167-78.

(100) Hintermann, T., Seebach, D. *Helv Chim Acta* **1998**, *81*, 2093-126.

(101) Seebach, D. S., L., Gessier, F., Bindscha¨dler, P., Ja¨ger, C., Josien, D., Kopp, S., Lelais, G., Mahayan,, Y. R., Micuch, P. S., R., Schweizer, B. W. , *Helv Chim Acta* **2003**, *86*, 1852-61.

(102) Lee, H. S., Park, J. S., Kim, B. M., Gellman, S. H. *J Org Chem* **2003**, *68*, 1575-8.

(103) Seebach, D., Overhand, M., Kuhnle, M., Martinoni, B., Oberer, L. *Helv Chim Acta* **1996**, *79*, 913-41.

(104) Epand, R. F., Raguse, T. L., Gellman, S. H., Epand, R. M. *Biochemistry* **2004**, *43*, 9527-35.

(105) Lee, M. R., Raguse, T. L., Schinnerl, M., Pomerantz, W. C., Wang, X., Wipf, P., Gellman, S. H. *Org Lett* **2007**, *9*, 1801-4.

(106) Seebach, D., Ciceri, P.E., Overhand, M., Jaun, B., Rigo, D., Oberer, L.,Hommel, U., Amstutz, R., Widmer,H., *Helv Chim Acta* **1996**, *79*, 2043-51.

(107) Rueping, M., Mahajan, Y. R., Jaun, B., Seebach, D. *Chemistry* **2004**, *10*, 1607-15.

(108) Frackenpohl, J., Arvidsson, P. I., Schreiber, J. V.,Seebach, D. *Chembiochem* **2001**, *2*, 445-55.

(109) Guarracino, D. A., Chiang, H. R., Banks, T. N., Lear, J. D., Hodsdon, M. E., Schepartz, A. *Org Lett* **2006**, *8*, 807-10.

(110) Raguse, T. L., Lai, J. R., Gellman, S. H. *J Am Chem Soc* **2003**, *125*, 5592-3.

(111) Wiegand, H., Wirz, B., Schweitzer, A., Camenisch, G. P., Rodriguez Perez, M. I., Gross, G., Woessner, R., Voges, R., Arvidsson, P. I., Frackenpohl, J., Seebach, D. *Biopharm Drug Dispos* **2002**, *23*, 251-62.

(112) Marqusee, S., Baldwin, R. L. *Proc Natl Acad Sci U S A* **1987**, *84*, 8898-902.

(113) Chakrabartty, A., Baldwin, R. L. *Adv Protein Chem* **1995**, *46*, 141-76.

(114) Glattli, A., Daura, X., Seebach, D., van Gunsteren, W. F. *J Am Chem Soc* **2002**, *124*, 12972-8.

(115) Hart, S. A., Bahadoor, A. B., Matthews, E. E., Qiu, X. J., Schepartz, A. *J Am Chem Soc* **2003**, *125*, 4022-3.

(116) Horne, W. S., Gellman, S. H. *Acc Chem Res* **2008**, *41*, 1399-408.

(117) Seebach, D., Gardiner, J. *Acc Chem Res* **2008**, *41*, 1366-75.

(118) Kritzer, J. A., Lear, J. D., Hodsdon, M. E., Schepartz, A. *J Am Chem Soc* **2004**, *126*, 9468-9.

(119) Umezawa, N., Gelman, M. A., Haigis, M. C., Raines, R. T., Gellman, S. H. *J Am Chem Soc* **2002**, *124*, 368-9.

(120) LePlae, P. R., Fisk, J. D., Porter, E. A., Weisblum, B., Gellman, S. H. *J Am Chem Soc* **2002**, *124*, 6820-1.

(121) Aguilar, M. I., Purcell, A. W., Devi, R., Lew, R., Rossjohn, J., Smith, A. I., Perlmutter, P. *Org Biomol Chem* **2007**, *5*, 2884-90.

(122) Gelman, M. A., Richter, S., Cao, H., Umezawa, N., Gellman, S. H., Rana, T. M. *Org Lett* **2003**, *5*, 3563-5.

(123) Tossi, A., Sandri, L., Giangaspero, A. *Biopolymers* **2000**, *55*, 4-30.

(124) Porter, E. A., Weisblum, B., Gellman, S. H. *J Am Chem Soc* **2005**, *127*, 11516-29.

(125) Werder, M., Hauser. H., Abele, S., Seebach D. *Helv Chim Acta* **1999**, *82*, 1774-83.

CHAPTER 2 Screening Cancer Targeting Peptides using Peptide Arrays

2.1 Introduction

A number of peptides have been recently identified by peptide phage display for targeting different tumors and cell types.[1-4] Among these, tumor homing RGD containing peptides, which are known to home to $\alpha_v\beta_3$ and $\alpha_v\beta_5$ integrins, have been studied extensively.[5-7] A second peptide motif, that accumulated in tumors, was derived from a phage display library with the general structure $CX_3CX_3CX_3C$ (X = variable residue, C = cysteine). This peptide, CNGRCVSGCAGRC, contained the sequence Asn-Gly-Arg (NGR) which has been identified as a cell adhesion motif and is found to bind Aminopeptidase N (CD13) in tumors.[8-11] NGR peptides can bind a specific aminopeptidase isoform that is expressed in tumor vessels and not other isoforms expressed in normal epithelia.[11]

NGR peptides have proven to be useful for delivering various antitumor compounds to tumors with specificity.[12,13] A peptide containing the NGR motif has been coupled to different anticancer compounds, such as doxorubicin, proapoptotic peptides, and TNF by coupling its C terminus to the N terminus of the anticancer drug, and shown to enable targeted delivery of these drugs to tumor vessels.[5,12,14] Besides CNGRC, other tumor vasculature targeting peptides have been identified, such as linear NGRAHA and cyclic CVLNGRMEC.[10] Cyclized NGR containing peptides are found to be more efficient than the linear ones. This is because the disulfide bridge constrain is critical for stabilizing the bent conformation required for better binding to the receptor.[8]

Another 12-mer peptide p160, with a yet unidentified receptor, has been shown to bind breast cancer cells strongly and specifically.[15,16] *In vivo* biodistribution experiments in tumor-bearing mice showed that the uptake of peptide p160 was mainly by the tumor compared to normal organs.[15] P160 has been used recently to decorate the exterior surface of virus capsid to target tumor *in vivo*.[17]

Peptide p160 therefore shows great promise in the development of targeted drug delivery systems. The prerequisites for the use of an agent as targeting vehicle are its selective binding to the tissue of interest and its limited uptake by healthy tissues. In this context, our hypothesis is that peptides identified from the phage display for targeting cancer cells can be further improved for better and selective binding by chemical manipulation of their structures.[18] For instance, peptide arrays can be used for screening a library of designed peptides to complement random phage display screening. The recent growing demands for the high-throughput screening of peptide libraries require the synthesis of large number of peptides in small amounts and test them concurrently. This can be achieved by synthesizing peptide arrays on solid surfaces, such as on cellulose membrane using AutoSpot. Short peptides covalently bound to a solid surface display specific binding affinity to the cells and such peptide/protein arrays are being used for several applications in the biomedical and biotechnology fields.[11, 19-25]

The general objective of this study was to design NGR and p160 peptides based libraries on cellulose membrane and develop a method to screen peptides with high and specific affinity for cancer cells. In the future, these peptides will be conjugated to the surface of drug-loaded-micelles for targeted anti-cancer drug delivery.

The above objective was achieved by performing the following specific aims which are described in this chapter:

(i) Synthesis of a test peptide array on cellulose membrane, followed by cleavage from the solid support and characterization of the peptides,

(ii) Design and synthesis of NGR-based peptide library on cellulose membrane,

(iii) Development of peptide array-whole cell binding assay using MTT assay,

(iv) Development of peptide array-whole cell binding assay using fluorescence imaging,

(v) Design, synthesis and screening of p160-based peptide arrays using newly developed peptide array-whole cell binding assay (fluorescence based), and

(vi) Synthesis of high affinity p160 analogues identified from (v) and evaluation of their uptake by cancer cells using confocal microscopy and flow cytometry.

2.2 Results and Discussion

2.2.1 Cleavable (Soluble) NGR Peptide Array

Peptide array synthesis on cellulose membrane allows the synthesis of large number of peptides at the same time in small concentrations. A small control peptide library was synthesized on a β-alanine cellulose membrane with a cleavable linker to characterize the peptides after cleavage from the membrane.

NGR Library Design

Six peptides, **1**-**6**, based on the sequence of CVL**NGR**MEC peptide were designed with variations in the amino acid sequence (**Table 2.1**). In all sequences, methionine 7 (Met7) was replaced by norleucine (Nle) to avoid oxidation of Met during the synthesis and handling of the peptide. The N-terminal hydrophobic residues Val and Leu were replaced with other hydrophobic residues, such as Ala, Phe, or Leu. Furthermore, the two cysteines at the N- and C-terminal were kept in all sequences to cyclize the peptides and evaluate the ability to obtain cyclized peptides through the disulfide bond formation on the membrane. Amino acid β-ala was added as a spacer at the C-terminal of all the peptides. This was in addition to the β-ala linker which was already present on the β-ala cellulose membrane. Peptides can be linked to the cellulose membranes using a variety of linkers. These linkers allow synthesis of cleavable peptides to obtain different C-terminally modified peptides as shown in **Table 2.2**.

Table 2.1: Amino acid sequence of soluble NGR based peptide library.

Peptide #	Peptide Sequence
1	CVLNGRXECZ
2	CALNGRXECZ
3	CLLNGRXECZ
4	CLANGRXECZ
5	CFLNGRXECZ
6	CVANGRXECZ

Where X is Nle and Z is β-ala.

We chose a membrane with a β-ala linker that is linked to the membrane through an ester bond. The linker allows the cleavage of the peptides from the membrane for additional characterization.

Table 2.2: Linkers and cleavage conditions for synthesis of soluble peptides on cellulose membrane.

Linker	Cleavage condition	C-terminal peptide modification
Rink linker	TFA	Carboxamide
Photo linker	UV light at 365 nm	Carboxamide
Diketopiprazine-forming linker	1. TFA 2. pH 7.5	Peptide-Lys-Pro
Esterification of the first amino acid (e.g. β-ala)	Aqueous NMe_3 Aqueous NH_3	Carboxylic Acid Carboxamide

Synthesis on Cleavable Membrane

A library of six peptide sequences (**Table 2.1**) was synthesized in duplicate in an array format on a β-ala cellulose membrane using AutoSpot. The membrane provided by Intavis (Germany) is derivatized on the surface with Fmoc

protected β-ala which is conjugated to the membrane by a labile ester bond (**Figure 2.1**).

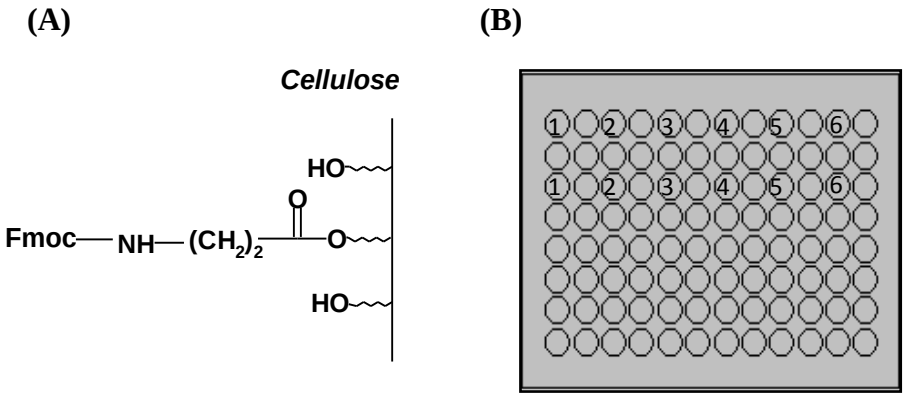

Figure 2.1. Schematic representation of β-ala cellulose membrane. (A) Membrane functionalization with Fmoc-β-ala for spot synthesis. The surface has a loading capacity of 400 nmol/cm^2 delivering peptide concentration of 64 nmol/spot (25 mm^2). (B) A schematic representation of the NGR peptide array showing six peptides in duplicates.

The peptides were synthesized on the membrane following the Spot synthesis method,[26] as depicted in **Figure 2.2**. Briefly, the Fmoc protection of the β-ala was removed from the entire membrane by treatment with piperidine. Another activated Fmoc β-ala (as a spacer) was spotted at defined regions (12 spots for six peptides in duplicates) on the membrane to identify the area for peptide array synthesis as shown in **Figure 2.1**. The rest of the membrane was then capped using acetic anhydride to allow peptides to grow on the specified positions. Fmoc removal of the β-ala yielded free amino group which was subsequently coupled to the activated carboxyl of the following amino acid. Amino acid coupling was continued following repetitive Fmoc removal and coupling till the required length of the peptide is reached. The final Fmoc

removal as well as the side chain deprotection using TFA gave the desired peptide at each spot.

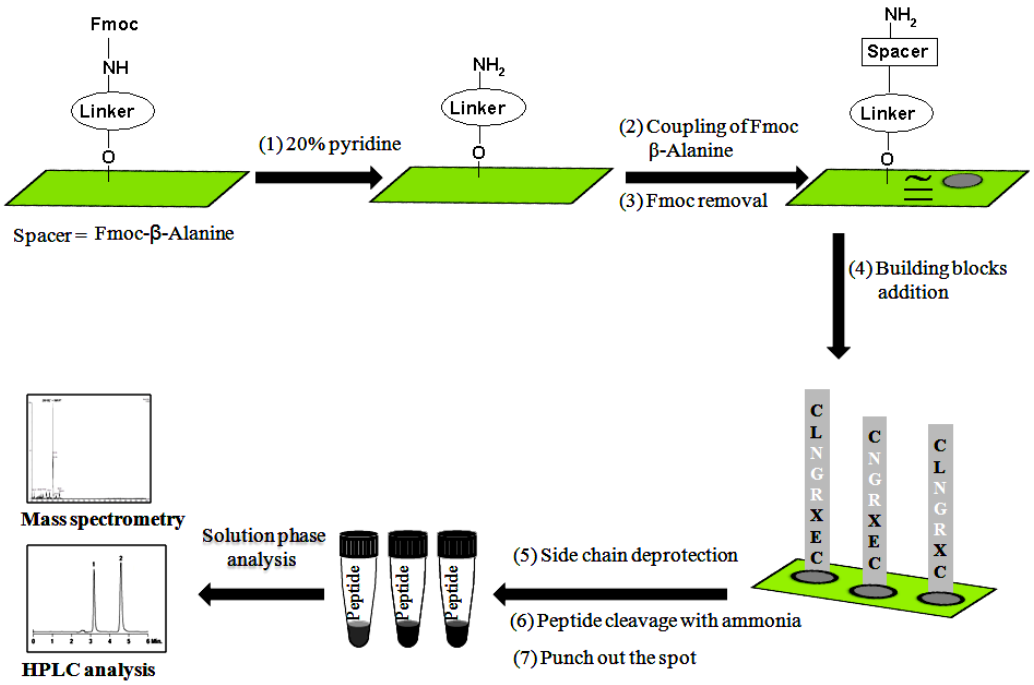

Figure 2.2. Schematic representation of the synthesis and characterization of soluble peptide array prepared on β-ala cellulose membrane.

Ammonolysis of Peptides

Peptides were cleaved from the membrane using ammonia gas and were eluted from the membrane after punching the spots in ELISA plate wells using acetonitrile-water as elution solvent. Ammonolysis of the ester bond between the peptide and the cellulose membrane allowed the cleavage of the peptide-β-Ala-β-Ala into solution for further analysis.[27] At this point, the cysteine of the peptides were also cyclized (oxidized) by exposure to the air.

Peptides **1-6** were analyzed using MALDI-TOF spectrometry. Each peptide showed a single peak representing the $[M+H]^+$ and no truncated peptides were detected as shown in **Figure 2.3 B**. All side chain protections of the amino acids were completely removed, indicating that the acid cocktail used and the length of incubation time (3 h) were sufficient. Difficult side chain protections, such as, 2,2,4,6,7-pentamethyldihydrobenzofuran-5-sulfonyl (Pbf) of Arg which is generally known to take longer deprotection time (as stated in the Intavis manual) was also removed. Finally, a representative peptide, peptide **2**, was also analyzed by analytical RP-HPLC (**Figure 2.3 C**) showing that in general peptides were >95% pure. The results suggest that small peptides can be easily synthesized in an array format on cellulose membrane using AutoSpot with high purity.

2.2.2 Non-Cleavable NGR Peptide Array

Peptides were synthesized on non-cleavable cellulose membrane (amino-PEG500), where the C-terminal of the peptide was anchored to the surface of the amino-PEG500 cellulose membrane through β-ala spacer, to be used for peptide–cell binding studies. The non-cleavable membrane assures that the peptides will not be cleaved during washing steps of the binding experiments, such as, washing of non-specifically bound cells or regeneration of the peptide array.

(A)

Peptide #	Peptide sequence	Mass[M+H]$^+$ Found (Calcd.)
1	CVLNGRXECZZ	1188.53 (1188.42)
2	CALNGRXECZZ	1159.65 (1160.42)
3	CLLNGRXECZZ	1201.80 (1202.40)
4	CLANGRXECZZ	1159.74 (1160.56)
5	CFLNGRXECZZ	1236.78 (1236.56)
6	CVANGRXECZZ	1146.65 (1146.51)

All peptides are N-terminal acetylated and C-terminal as carboxamide.

(B)

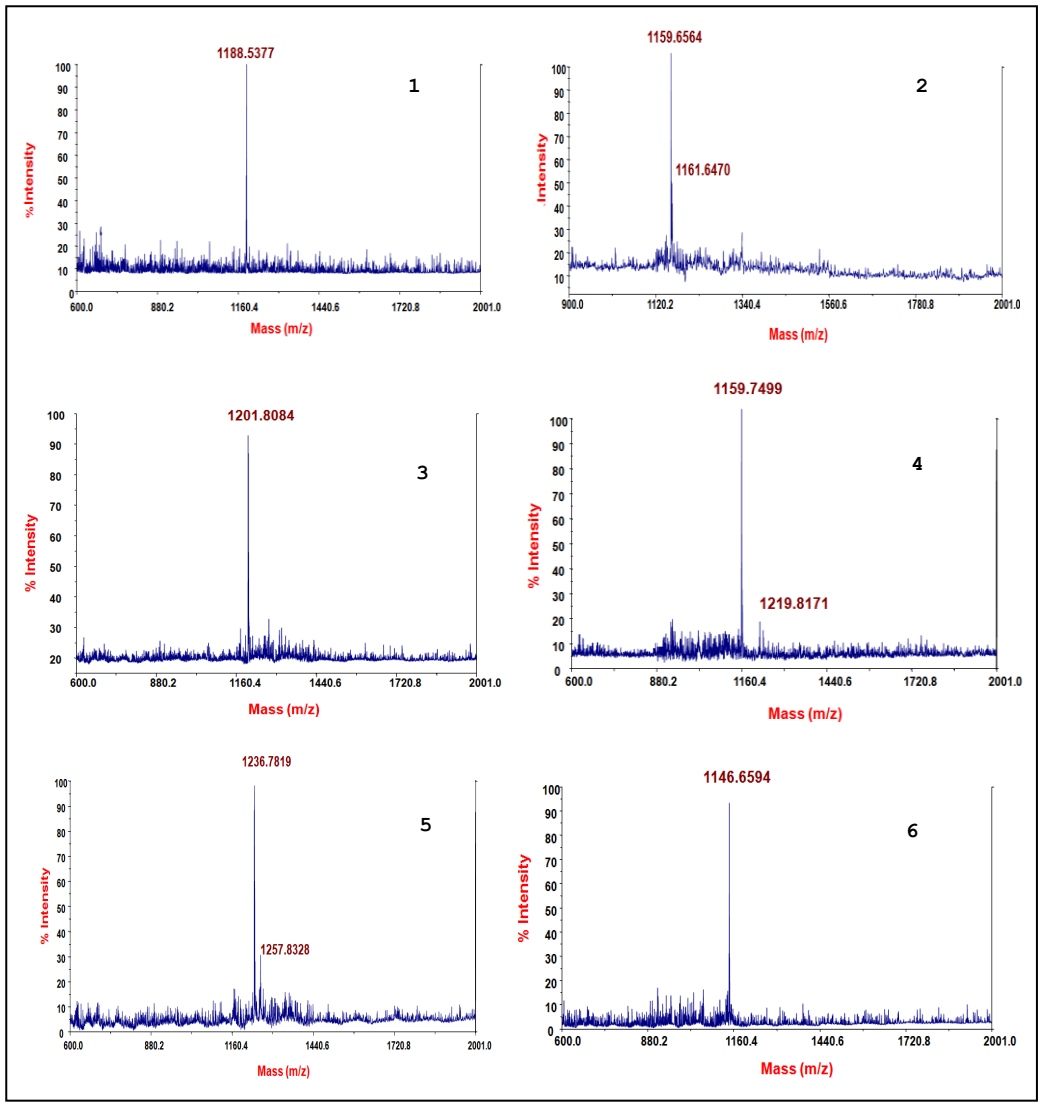

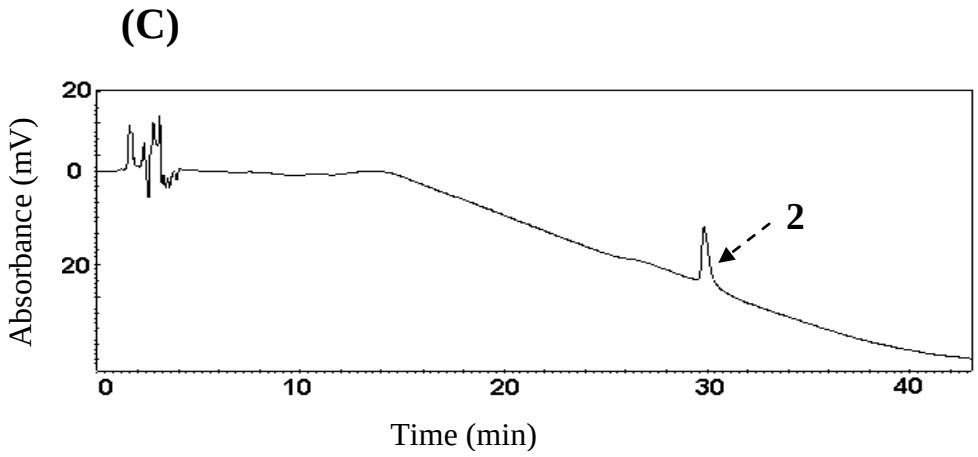

Figure 2.3. Characterization of the control library peptides **1-6**. (A) Amino acid sequences, (B) MALDI-TOF mass spectra, and (C) RP-HPLC chromatogram of one of the control library peptides, peptide **2**.

Peptide library design

Thirty peptides based on the NGR sequence CVLNGRMEC were designed to study the selective binding of peptides to CD13 expressing cancer cell lines, such as, HT-1080 and Hey cell lines (**Table 2.3)**. Peptide **1** (9-mer) represents the lead peptide, and in peptide **2,** the Met was replaced with Nle to overcome problem associated with Met oxidation. In all the designed sequences, Met was replaced with Nle for the same reason. Angelo Corti and coworkers showed that NGR part is essential for binding CD13 receptor expressed by cancer cells.[10] This motif was therefore kept in all peptides and removed only from the negative control peptides **26**-**30**. Peptides **3**-**7** represent ala scan of peptide **2**. Ala scan was performed to determine the importance of each residue in binding. Peptides **8-14** containing NGR motif range from 6-mer to 9-mer peptides. In these sequences, some of the N or C terminal amino acids have been removed. Peptide **15** has Asp8 instead of Glu8, whereas, **16** and **20** have β-ala instead of

Val2 or Leu3, respectively. For peptides **24** and **25**, NGR has been replaced with QGR. The remaining peptides are essentially scrambled sequences with varying length.

Synthesis on Non-cleavable Membrane

The library of 30 peptide sequences (**Table 2.3)** was synthesized in duplicates in an array format on a cellulose membrane using AutoSpot, following the same procedure as described for cleavable membranes. The surface of the membrane used for the synthesis of non-cleavable peptide array is derivatized with a polyethylene (PEG-10) linker and a free amino terminal group. [19-24,28] The cellulose membranes used in this study (provided by Intavis) are acid hardened

Table 2.3: Amino acid sequence of the NGR based peptide array library used for MTT.

Peptide #	Sequence	Peptide #	Sequence
1	CVLNGRMECZ	**16**	C**Z**LNGRXECZ
2	CVLNGR**X**ECZ	**17**	CNGR**G**ECZ
3	C**A**LNGRXECZ	**18**	CNGR**GX**CZ
4	CV**A**NGRXECZ	**19**	CVLNGR**G**ECZ
5	CVLNGR**A**ECZ	**20**	CV**Z**NGRXECZ
6	CVLNGRX**A**CZ	**21**	CLNGRXCZ
7	CVLNGRXE**A**Z	**22**	CNGRGEQCZ
8	CVLNGRXCZ	**23**	CNGRGENCZ
9	CVLNGRCZ	**24**	C**Q**GRGEQCZ
10	CVLNGRECZ	**25**	CVL**Q**GRXECZ
11	CLNGRXECZ	**26**	CVLARAXECZ
12	CVNGRXECZ	**27**	CARACZ
13	CNGRXECZ	**28**	AVLXGXEAZ
14	CNGRCZ	**29**	VLGXEZ
15	CVLNGRX**D**CZ	**30**	CVLGXECZ

for improved stability (pH 1-14), have greater distance to cellulose carrier, and there is a hydrophilic spacer (PEG) which reduces the background. These properties of the membrane make the peptide arrays synthesized on them suitable for direct cell binding assays.

Each peptide was synthesized at a concentration of about 64 nmoles which is spread on the membrane as a spot with a diameter of 4 mm as shown in **Figure 2.4**. Each spot was separated from the next peptide (spot) by 8 mm. The 60 peptide spots were spread on the membrane surface in 5 rows with 12 spots (6 peptides in duplicates) in each row.

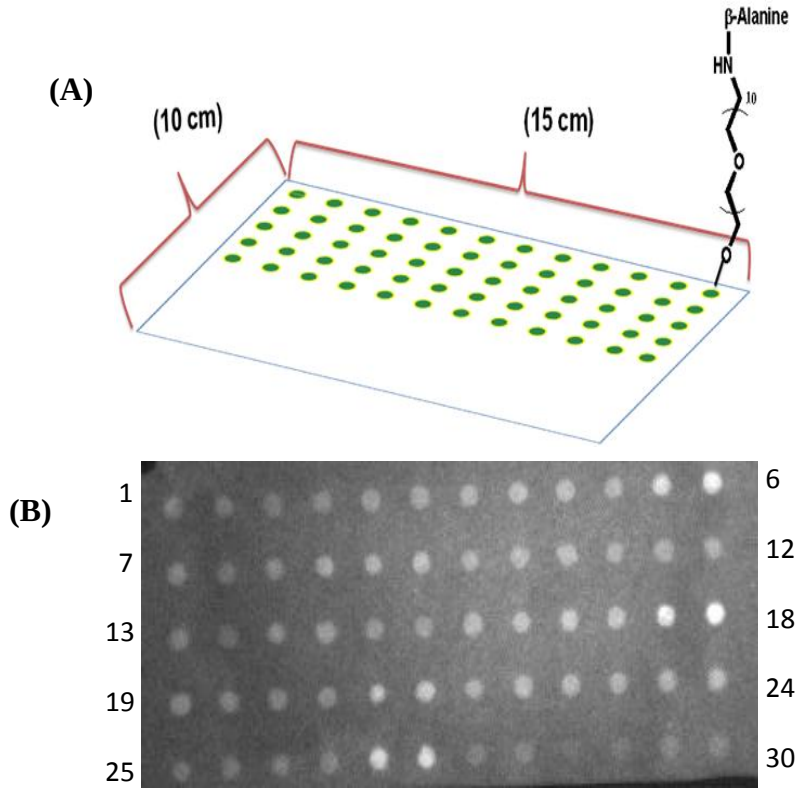

Figure 2.4. (A) Schematic of a cellulose membrane (amino-PEG500-UC540) showing the functionalization on the surface. The surface has a loading capacity of 400 nmol/cm^2 delivering peptide concentration of 64 nmol/spot (25 mm^2). (B) An image of the peptide array at λex= 465 nm and λem= 535 nm showing 30 peptide spots in duplicates.

2.2.3 Level of APN/CD13 Expression in Cancer Cell Lines

APN/CD13 expression level was examined in HT-1080 human fibrosarcoma cell line,[29] and MDA-MB-231 breast cancer cell line. The CD13 expression level was judged by the fluorescence of the cells after incubation with FITC-labeled antihuman CD13 antibody (CD13mAb) (WM15). The binding to the cell surface receptor was quantified by measuring the intensity of the fluorescence using FACS analysis as shown in **Figure 2.5**. The results show that HT-1080 cells express high level of CD13, whereas, MDA-MB-231 do not express this receptor.

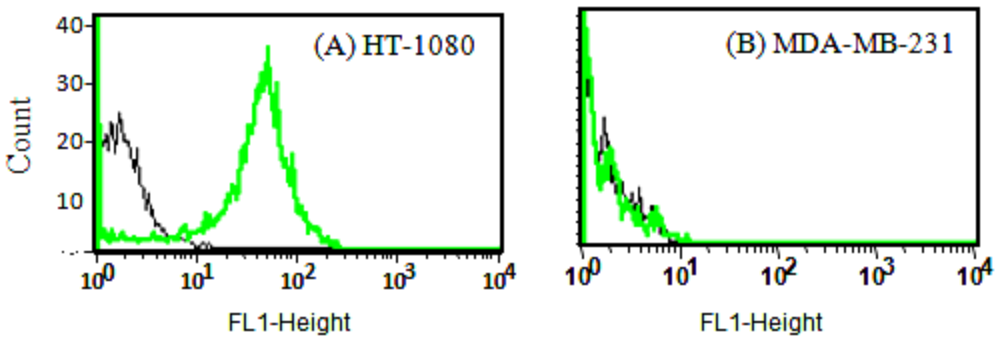

Figure 2.5. FACS analysis showing presence or absence of CD13 in (A) HT-1080 and (B) MDA-MB-231 cells. Cells were incubated with media alone (autofluorescence, black) or with FITC antihuman CD13 antibody (grey).

2.2.4 MTT Assay for Peptide-Cell Binding

NGR peptide library was screened for selective binding to cancer cells using two cancer cell lines, namely, HT-1080 and Hey cells (Epithelial ovarian carcinoma). Hey cell lines are known to be CD13 positive.[30] MDA-MB-231 breast cancer cell line that does not express APN/CD13 receptors, as shown above, was used as a negative control for screening peptide for cell binding. The

cells were allowed to bind directly to the peptides and the bound cells were labeled with the MTT reagent. In the assay, the yellow color of MTT (3-(4,5-Dimethylthiazol-2-yl)-2,5-diphenyltetrazolium bromide) is reduced to purple formazan by living cells by the action of mitochondrial reductase as shown in **Figure 2.6**.[31]

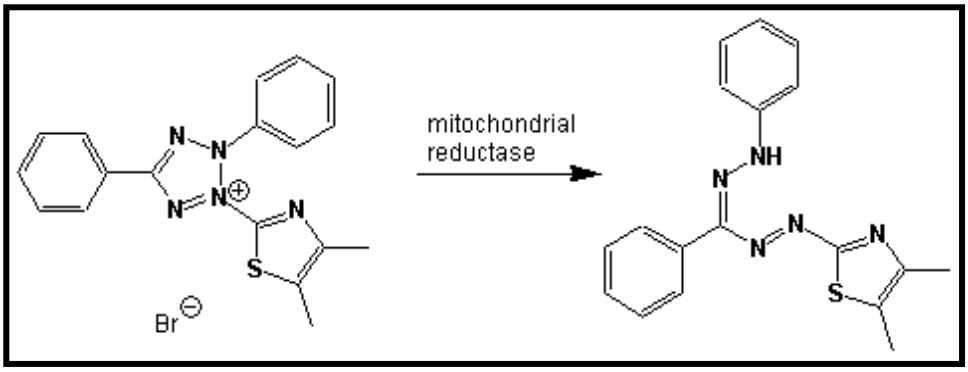

Figure 2.6. MTT reaction in living cells.

Screening peptides using Kodak Imager

Kodak imager was used to image the membrane to detect the violet color produced by MTT. Scanning the membrane at 465 nm was done using Kodak Imager to visualize the purple colour of MTT which absorbs in that wavelength range. The relative cell binding of the peptides was estimated based on the intensity of the dark violet color produced by the bound cells. An image of the membrane after binding of HT-1080 cells to the peptide array is shown in **Figure 2.7.** The binding experiment was repeated after membrane regeneration. Also, the experiment was repeated with the other two cells lines, Hey cells and MDA-MB-231 breast cancer cells.

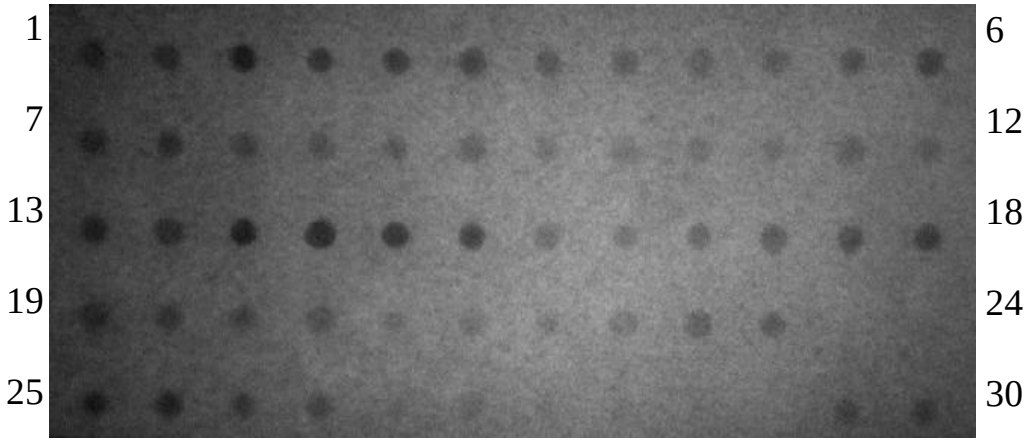

Figure 2.7. NGR peptide library screen: Membrane image of peptide library after incubation with HT-1080 (75 x 10^3 cell /ml) for 36 h at 37 °C, followed by staining the cells with MTT reagent. (each peptide in duplicates)

The relative cell binding was calculated based on the absorption of each spot on the membrane as region of interest (**Figure 2.8**). All the peptides were compared to the wild type NGR peptide **1.** The affinity of the peptides for the two +ve CD13 expressing cell lines HT-1080 and Hey cells followed similar trend (**Figure 2.8 A** and **B**), whereas, the -ve CD13 expressing MDA-MB-231 cells showed relatively low binding (**Figure 2.8 C**). Several peptides showed binding to the HT-1080 cells, however, only peptides **14** and **15** displayed enhanced binding compared to the leads **1** and **2**. Peptide **2** showed better binding than **1** most likely due to the Met to Nle mutation which provides peptide stabilization. From the ala scan of peptide **2,** only peptide **3** where Val was replaced with Ala was able to keep the same binding as peptide **2** which coincides with the results reported by Honda and coworker.[32] The authors showed that Val to Ala replacement gives high cell adhesion effect and induced cell-specific

interaction. Deletion of amino acids from either the C or N-terminal resulted in reduction in the binding affinity compared to peptide **2.** Interestingly, peptides **14** and **15** show higher binding compared to peptide **2.** This high binding capability of peptide **14** might result from the constrained structure which fits well with the similar sequence (GNGRG) found in the fibronectin sequence.[8,29] Peptide **15,** where Glu was replaced with Asp shows higher binding. However, replacement of Asn with Gln completely abolishes the binding as in peptide 24.

The NGR based peptide array also showed significant binding to the Hey cells (**Figure 2.8 B**). In general, the difference in the binding affinity of the peptides (**1-28**) for Hey cells was much less and only negative control peptides **29-30** showed weak affinity. This may be due to the presence of different integrins on the surface of Hey cells such as α_2, and α_6.[33] NGR peptides are known to have some affinity for the intergrin receptors. Most notably, peptide **15** displayed highest affinity for the Hey cells, as also observed for HT-1080 cells. Further, despite the absence of CD13 receptor in MDA-MB-231 cancer cell lines, some affinity between these cells and peptides was also detected (**Figure 2.8 C**). Again, the affinity may be due to the fact that MDA-MB-231 cell line expresses high levels of β_1, α_2, α_3, α_5, and α_6 integrin subunits along with moderate levels of the $\alpha_v\alpha_3$ integrin.[34]

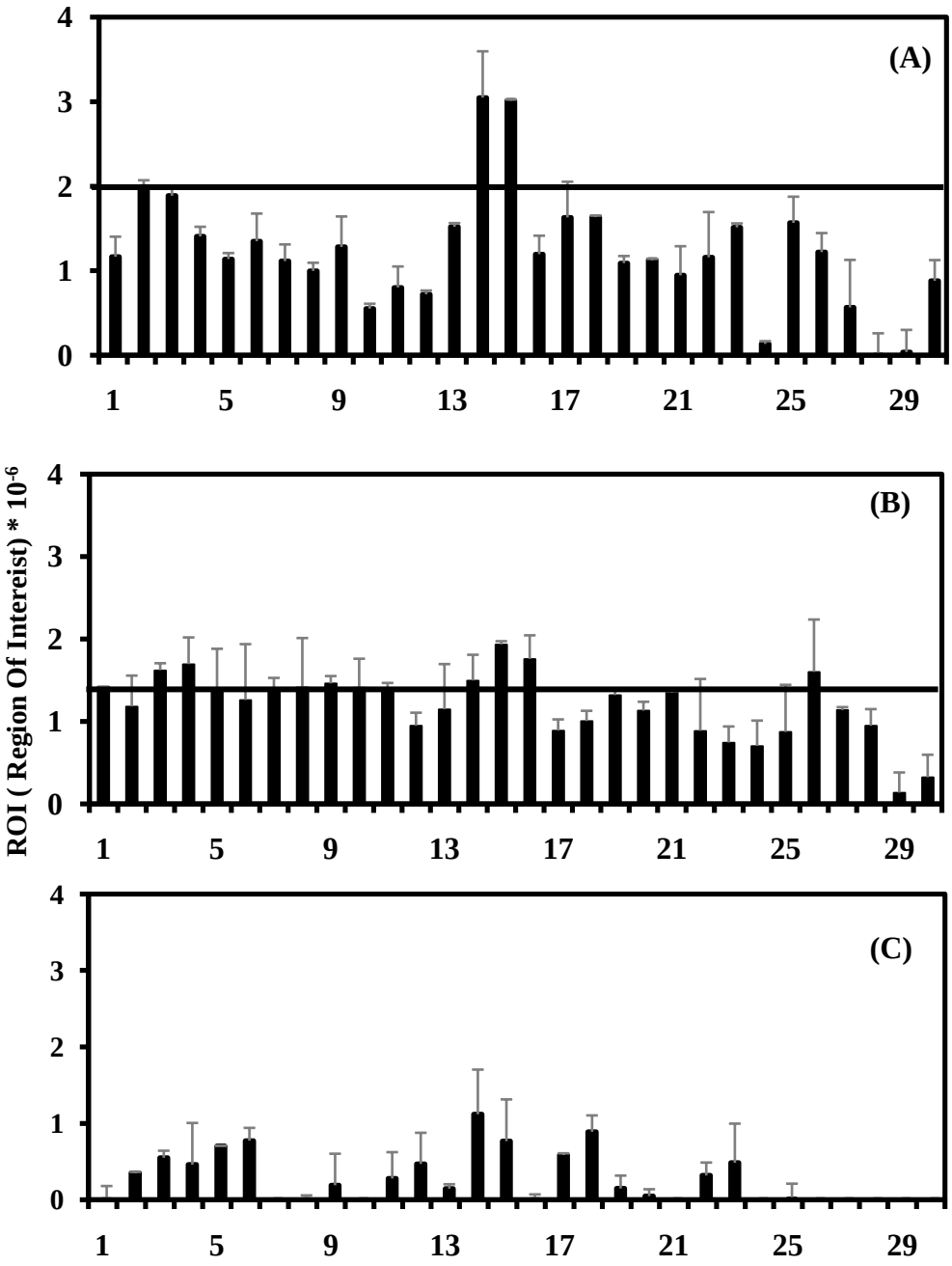

Figure 2.8. Average intensity (absorbance) of each peptide-bound cell as obtained from the Kodak Imager. HT-1080 (A), Hey (B), and MDA-MB-231 (C) cells (75 x 10^3 cell /mL) were incubated with the peptide array for 36 h (A and C) or 18 h (B) at 37 °C, followed by cell staining with MTT reagent. The results are presented as mean intensity ± S.D.

Screening peptides using ELISpot Bioreader

An attempt was also made to visualize the insoluble violet colour of MTT using an ELISpot Bioreader 3000. NGR peptide library was incubated with Hey cells and after treatment with MTT reagent, the membrane was scanned using ELISpot. The instrument images all the spots one after another and saves them together at the end of the scan as shown in **Figure 2.9**.[35,36] The image shows the relative intensity of colour for each spot. The trend for the binding affinity was

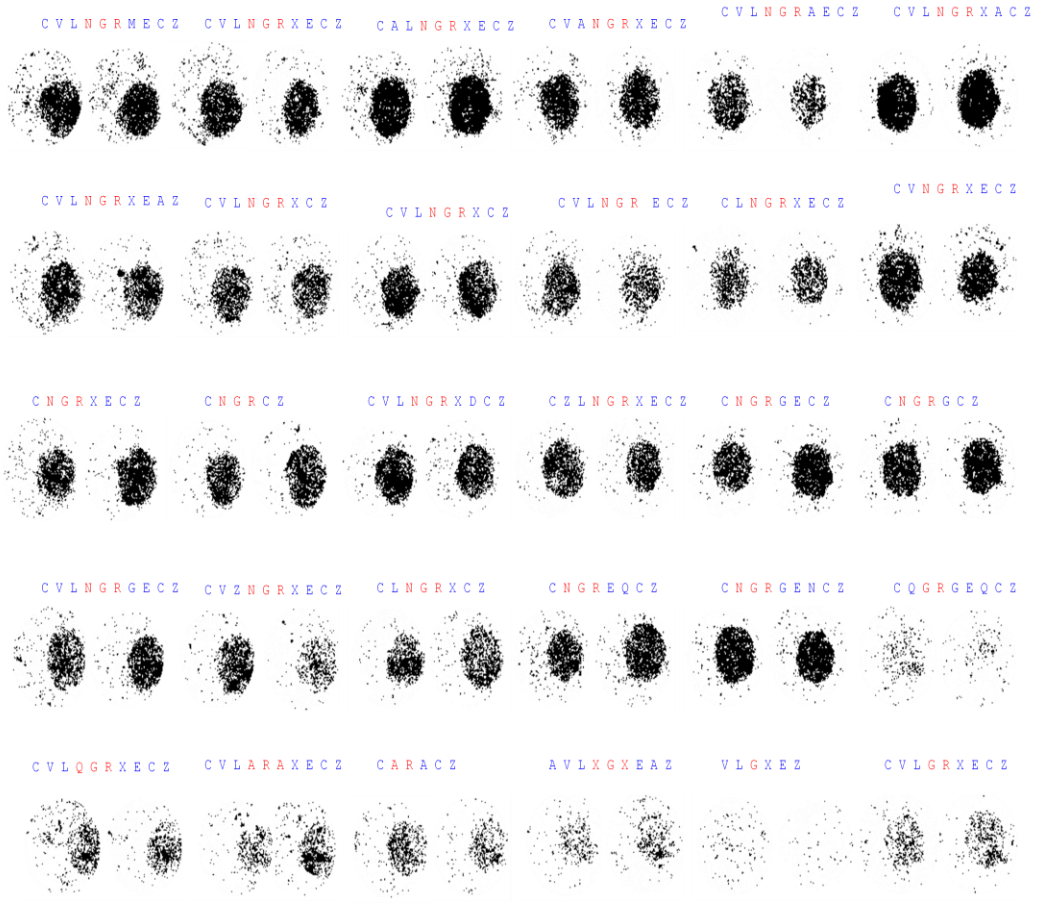

Figure 2.9. ELISpot scan of NGR peptide library after incubation with Hey cells (75 x 10^3 cell/mL) for 18 h at 37 °C, followed by cell staining with MTT reagent. The peptide-bound cells on the membrane were dried and spots were scanned using BioReader 3000 (BioSys, Karben, Germany).

similar to that observed using Kodak imager (**Figure 2.8 B**). However, the software for ELISpot did not allow quantitative analysis of the binding affinity.

2.2.5 Peptide-Cell Binding using Fluorescence

At this point, we decided to use fluorescence to enhance the signal from the peptide-bound cells on the membrane. Another NGR based test library (**Figure 2.10 A**) of 4 peptides (in duplicates) was synthesized to develop the screening method. Two peptides (10-mer and 6-mer) with NGR and two with no NGR (negative control) in the sequence were used in the test library.

The first problem that we faced was the autofluorescence of the peptide spots. As shown in **Figure 2.10 B**, the four test peptides showed high background fluorescence at λ_{ex}= 465nm, λ_{em}= 535nm. However, no fluorescence from the peptides was observed at λ_{ex}= 385 nm, λ_{em}= 460 nm. Therefore, we needed to select a dye with wavelengths where there will be minimal background fluorescence of the peptides.

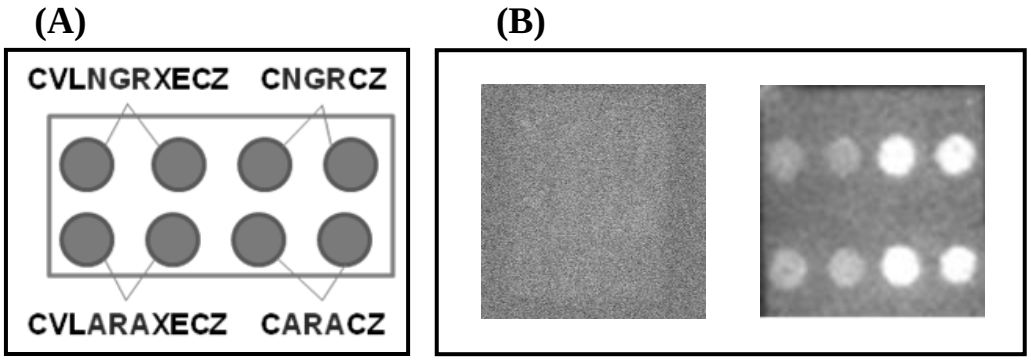

Figure 2.10. (A) A small NGR based peptide library of four different sequences. (B) Images of the peptide library at two different excitation and emission wavelengths, λ_{ex}= 385 nm, λ_{em}= 460 nm (left) and λ_{ex}= 465 nm, λ_{em}= 535 nm (right) using Kodak imager.

Three dyes, namely, DAPI, CFSE, and CyQUANT were chosen for labeling membrane bound cells. The first dye, DAPI or 4̀,6-diamidino-2-phenylindole (**Figure 2.11 A**) is a fluorescent stain that binds strongly to DNA. It is used extensively in fluorescence microscopy to stain both live and fixed cells. We were interested in DAPI because the test peptide array did not show peptide background fluorescence at the wavelengths where DAPI absorbs (λ_{ex}= 385 nm) and emits (λ_{em}= 460 nm). DAPI labeled cells (2,000-20,000 cells) were spotted on the cellulose membrane to observe the fluorescence of the cells and determine the minimum number of cells required for signal using Kodak imager. As shown in **Figure 2.11 B**, the fluorescence signal was low for 2000-6000 cells. Minimum of 8000 cells were needed in order to quantify fluorescence which was rather high as some peptides may have limited affinity for the cells.

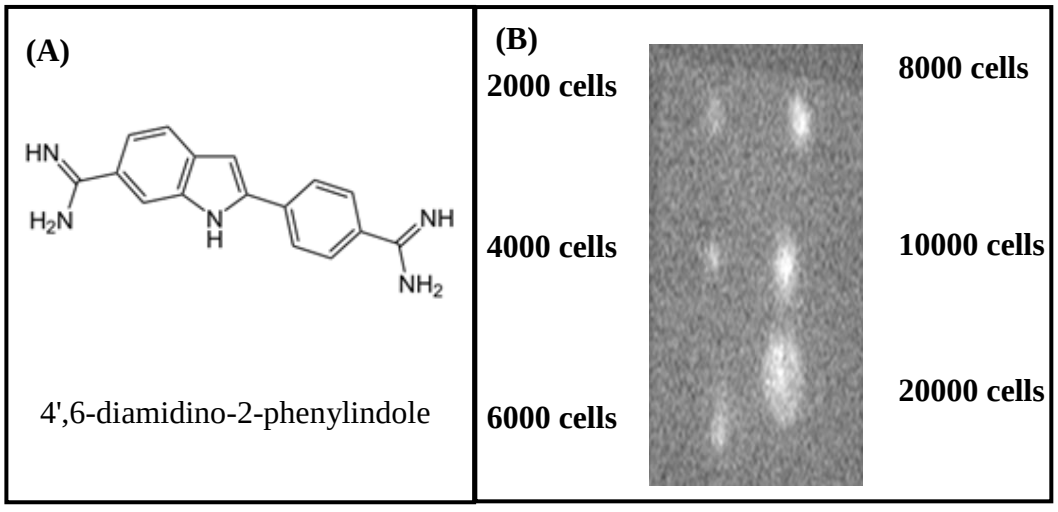

Figure 2.11. Chemical structure of (A) DAPI (λex 385 nm & λem 460 nm), and (B) Fluorescence of different count of DAPI labeled HT-1080 cells spotted on cellulose membrane. The image was taken using Kodak imager with excitation filter 385 nm and emission filter 460 nm.

The second dye used was CFSE or carboxyfluorescein diacetate, succinimidyl ester that absorbs and emits at 465 nm and 535 nm, respectively. CFSE is known to passively diffuse into cells. It is colorless and nonfluorescent until the acetate groups are cleaved by intracellular esterase to yield highly fluorescent carboxyfluorescein succinimidyl ester. The succinimidyl ester group reacts with intracellular amines, forming fluorescent conjugates that are well retained. Excess unconjugated reagent and by-products passively diffuse to the extracellular medium, where they can be washed away. Finally, CyQUANT dye was used that stains the nucleic acid and has the capability of cell permeability. CyQUANT absorbs and emits at same wavelengths as CFSE. Despite the fact that peptides show autofluorescence at this wavelength range these dyes were tried. These dyes have high quantum yield compared to DAPI and may be able to overcome the background peptide fluorescence.

In order to compare the fluorescence of CyQuant, CFSE, and DAPI, 1000 HT-1080 cells were spotted on the membrane and labelled with the dyes. Also, the cells were spotted on a representative 9-mer peptide (spot). We found that CyQUANT allowed detection of as low as 1000 cells when imaged using the Kodak imager. Whereas the other dyes, such as CFSE and DAPI, were not able to detect cells bound in this range or enhanced the autofluorescence of the peptide upon cell binding (**Figure 2.12**). In comparison, the CyQUANT dye showed minimal enhancement of the autofluorescence of the peptides upon cell binding. DAPI showed the same fluorescence intensity in the presence and absence of peptide, however, the signal was low in intensity. CyQUANT dye was chosen for

further cell binding experiments as it allowed detection of less than 1000 cells. Finally, the use of CyQUANT dye will make the peptide-cell binding assay extremely sensitive as this dye has very low intrinsic fluorescence and shows large fluorescence enhancement and high quantum yield upon nucleic acid binding.[37]

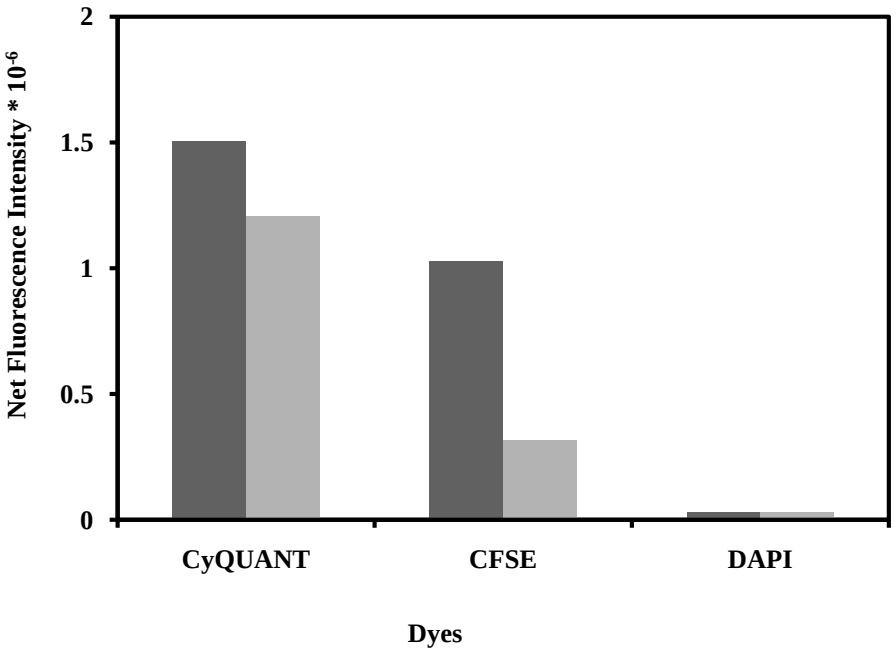

Figure 2.12. Net fluorescence intensity of HT-1080 cells labeled with different dyes. Cells (10^3) were loaded directly to the cellulose membrane (light grey) or to the peptide (CVLNGRXEC) spot on the cellulose membrane (dark grey). Membrane was imaged using Kodak Imager at λ_{ex}= 465 nm, λ_{em}= 535 nm for CyQUANT and CFSE, and at λ_{ex}= 385 nm, λ_{em}= 460 nm for DAPI.

Peptide array membrane regeneration after cell binding assay

One of the advantages of the covalently bound peptide arrays on the cellulose membrane is that the membrane can be regenerated after the binding experiment. Membrane is typically regenerated by washing with ethanol (3 x 25

mL, 5 min), followed by treatment with 0.1 N HCl (2 x 25 mL, 20 min). Finally, the peptide array membrane is washed with DMF (4 x 25 mL, 20 min), ethanol (3 x 25 mL, 3 min), and dried in air. In order to determine if membrane gives reproducible results, peptide-cell binding assay using fluorescence was done three times on the same peptide membrane. The average fluorescence intensity for the four peptides (in duplicates) over three experiments is shown in **Figure 2.13**. The relative binding of the peptides to the cell was essentially maintained even after three times of regeneration of the membrane with small reduction in signal each time. After first regeneration, a maximum of 8% reduction in the fluoresence intensity was observed, while after second regeneration the reduction in fluoresence intensity reached ~14%. These results suggest that for the peptide-cell binding assay the membrane could be reused up to 3 times with good and comparable results.

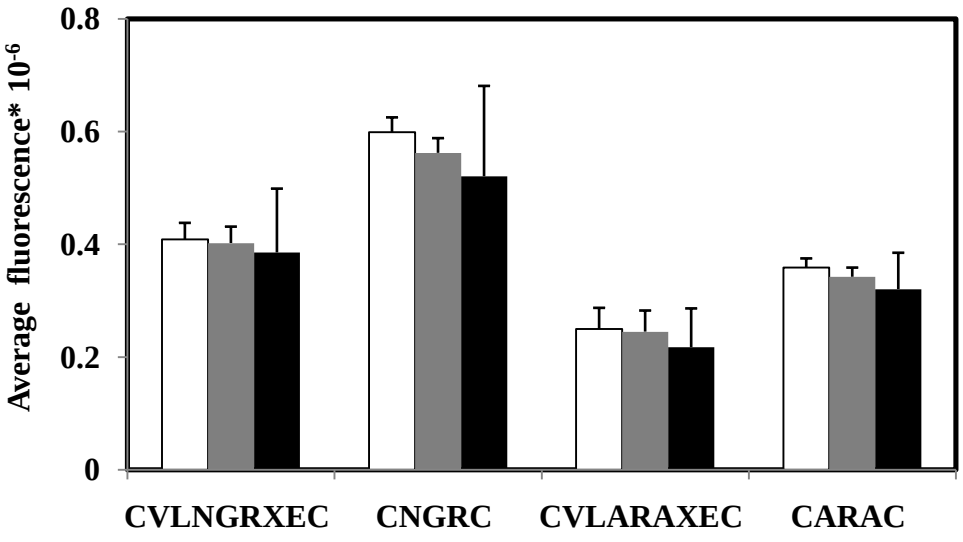

Figure 2.13. Fluorescence intensity of the peptide-bound cells before and after regeneration. After cell binding and CyQUANT labeling, NGR peptide array membrane was imaged, and the cell binding assay was repeated after regeneration once (grey) or twice (black).

Blocking membrane outside the peptide spot

It was observed that the cells show minimal binding outside the peptide spot. We decided to check if blocking the membrane before cell binding could help remove this minimal fluorescence signal. Different methods have been used for blocking cellulose membrane in order to prevent the non-specific interactions, such as between the antibodies and the surface of the cellulose membrane. The most common method used is blocking with Tris Buffered Saline (TBS) with 2% skim milk powder.[38] Cell binding experiments were performed with and without blocking using TBS as blocking agent. First, a cell binding experiment with the test library was performed without blocking. The membrane was washed and regenerated, and the experiment was repeated. This time membrane was blocked with TBS with 2% skim milk powder (0.2% v/v Tween 20) for 2 h prior to cell binding. The cell binding with blocked membrane was repeated once more. The membrane was scanned after each experiment and the results are shown in **Figure 2.14**. It is observed that blocking the membrane once, decreased the fluorescence signal slightly, however, blocking it twice eliminated most of the signal. Blocking the membrane removed the fluorescence from outside the peptide spot but also decreased fluorescence of the peptide-bound cells. This may be due to the blocking of the peptide spot by the blocking agent. Therefore, we decided not to block the membrane before the cell binding experiment. This was not needed especially because minimal cell binding outside the peptide spot was observed and any such background signal was subtracted from the final reading.

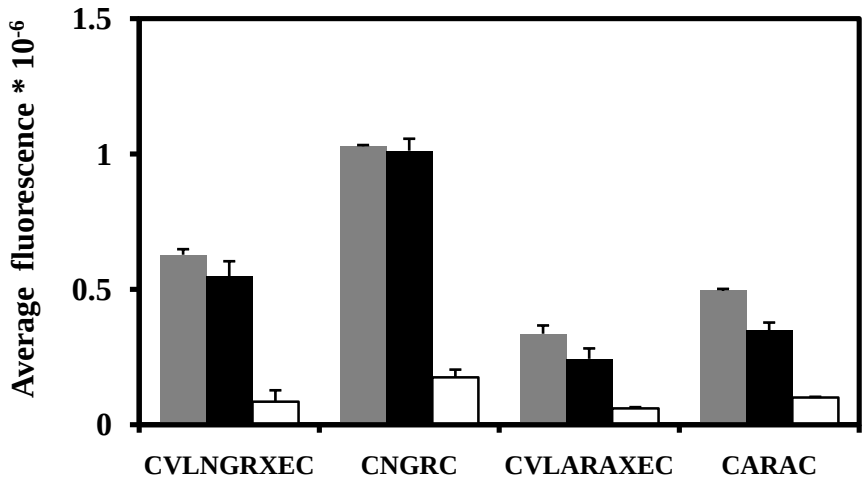

Figure 2.14. Effect of blocking peptide array membrane on cell binding. Non blocked (grey) or blocked once (black) or twice (white). The average fluorescent intensity was measured with the Kodak imager at λex= 465 nm and λem= 535 nm.

2.2.6 P160 Peptide Array and Screening Cancer Specific Peptides

Based on the results presented above, we decided to develop a peptide array-whole cell binding assay for screening p160-derived peptides that bind specifically to the cancer cells. Two cancer cell lines, MDA-MB-435 and MCF-7 as well as a normal endothelial HUVEC cell line were chosen for screening peptide array library.

Peptide array synthesis

A library of seventy peptides was synthesized in an array format on a cellulose membrane using SPOT synthesis.[38] The surface of the cellulose membrane derivatized with a polyethylene (PEG-10) linker and a free amino terminal group (**Figure 2.15 A**) allowed an easy synthesis of peptide arrays.

Peptides were synthesized in duplicates by covalent conjugation to the free amino functional group using a stepwise Fmoc-SPPS procedure. Each peptide was synthesized at a concentration of 64 nmoles which was spread on the membrane in a spot with a diameter of 4 mm. Each spot was separated from the next peptide (spot) by 8 mm evenly distributing 140 peptide spots on the membrane surface as shown in **Figure 2.15 B**. The sequence for the peptide library is shown in **Table 2.4**.

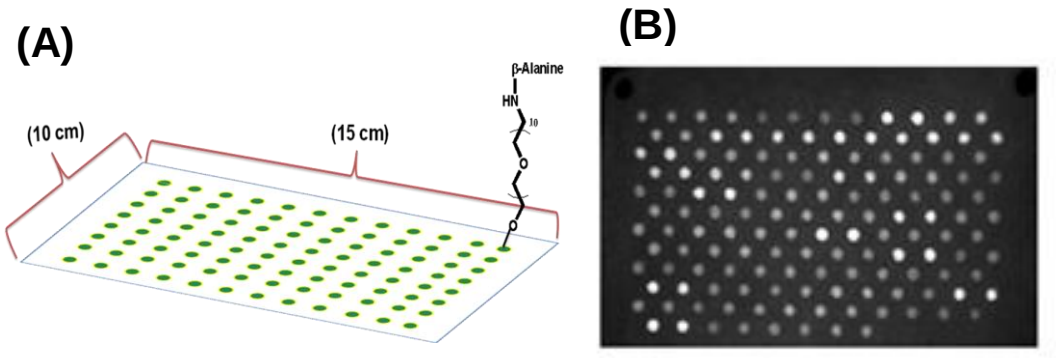

Figure 2.15. (A) Schematic of a cellulose membrane (amino-PEG_{500}-UC540) showing the functionalization on the surface for spot synthesis. The surface has a loading capacity of 400 nmol/cm^2 delivering peptide concentration of 50 nmol/spot (12.56 mm^2). (B) An image of the peptide array at λ_{ex}= 465 nm and λ_{em}= 535 nm showing 70 peptide spots in duplicates.

Peptide library design

Peptide p160 (**1**) is a linear 12-mer peptide carrying a net charge of zero. Peptide sequences based on p160 sequence were designed for selective binding to cancer cells (**Table 2.4**). The designed peptide sequences ranged from 9-mer to 12-mer where the first two N-terminal amino acids (Val-Pro) of p160 sequence

were deleted. Askoxylakis and coworkers have shown that the N-terminal Val and Pro residues do not contribute toward cancer cell binding, in particular, neuroblastoma WAC2 cell binding.[15]

The first set of peptides, **1**-**5** in the library was the control peptides where peptide **1** is p160, **2** is p160 with Nle substituted for Met4, and **5** is the peptide with tumor homing RGD motif. Peptides **3** and **4** are the negative controls where four important C-terminal residues from p160 have been deleted. The second set of peptides, **6-13**, is the fusion sequences containing RGD and/or NGR incorporated into the p160 sequence. The rationale behind this design strategy was to make the peptide more specific for the cancer cells by targeting multiple receptors overexpressed on the surface of the cancer cells such as integrins and p160 receptors. Peptides **6** and **7** have an RGD(E) in the N-terminal region, whereas, **8** and **9** have Q(N)GR motif introduced toward the C-terminal. Peptides **10**-**13** have both the RGD(E) and the Q(N)GR motifs present in the sequence. The third set of peptides were 10-mers and represent Ala scan (**14**-**23**), where **14** is essentially p160 with the first two amino acids deleted and Met replaced with Nle. Ala scan was performed to determine the importance of each residue in binding. The next set of peptides, **24**-**50**, involves replacement of the N- (Trp1 or Nle2) or C-terminal (Phe9 or Leu10) residues with different amino acids. For instance, Trp1 was substituted with conservative mutations such as Leu, Gln, Tyr, Phe, 4-chloro-Phe, and D-Phe or orthogonal amino acids like acidic Glu or basic Lys residues. Likewise, Nle2 was substituted with Leu, D-Leu, Gln, Thr, Glu or Lys. The C-terminal Phe9 and Leu10 were similarly replaced to give peptides **38**-**50**.

Table 2.4: Amino acid sequence and the cell adhesion capacity of the p160 based peptide array library.

Peptide #	**Amino Acid Sequence**	*Relative Cell Adhesion*		*Peptide #*	**Amino Acid Sequence**	**Relative Cell Adhesion**	
		MB-435	MCF-7			*MB-435*	*MCF-7*
1	VPWMEPAYQRFL	1.0	1.0	**38**	WXEPAYQR**E**L	1.2	2.1
2	VPWXEPAYQRFL	1.3	1.4	**39**	WXEPAYQR**L**L	1.3	1.4
3	VPWMEPAY	0.5	0.4	**40**	WXEPAYQR**K**L	2.7	2.7
4	VPWXEPAY	0.7	0.8	**41**	WXEPAYQR**Q**	1.4	1.5
5	GRGDS	1.1	1.1	**42**	WXEPAYQR**Y**L	1.6	1.8
6	**RG**EPAYQRFL	1.7	1.5	**43**	WXEPAYQR**F*** L	0.7	1.7
7	**RGD**PAYQRFL	1.5	1.9	**44**	WXEPAYQR**f**L	1.1	1.9
8	WXEPAYQ**G**RFL	1.0	1.6	**45**	WXEPAYQRF**E**	1.6	1.5
9	WXEPAY**NG**RFL	1.0	1.8	**46**	WXEPAYQRF**l**	1.7	2.0
10	**RG**EPAYQ**G**RFL	1.7	1.9	**47**	WXEPAYQRF**K**	2.2	2.8
11	**RGD**PAYQ**G**RFL	1.7	1.8	**48**	WXEPAYQRF**Q**	1.2	1.5
12	**RG**EPAY**NG**RFL	1.4	1.7	**49**	WXEPAYQRF**T**	0.8	1.5
13	**RGD**PAY**NG**RFL	1.0	2.1	**50**	WXEPAYQRF**F**	1.1	1.8
14	WXEPAYQRFL	1.0	1.7	**51**	XEPAYQRFL	1.1	1.2
15	**A**XEPAYQRFL	1.1	1.2	**52**	**E**EPAYQRFL	1.1	1.2
16	W**A**EPAYQRFL	0.9	1.3	**53**	**L**EPAYQRFL	1.2	1.2
17	WX**A**PAYQRFL	1.6	1.9	**54**	**l**EPAYQRFL	1.0	0.9
18	WXE**A**AYQRFL	2.2	2.7	**55**	**K**EPAYQRFL	0.9	1.6
19	WXEPA**A**QRFL	0.9	1.7	**56**	**Q**EPAYQRYL	0.8	1.0
20	WXEPAY**A**RFL	1.1	1.8	**57**	**T**EPAYQRYL	0.8	1.0
21	WXEPAYQ**A**FL	1.1	1.5	**58**	XEPAYQR**E**L	1.0	1.1
22	WXEPAYQR**A**L	1.0	1.2	**59**	XEPAYQR**L**L	0.9	1.0
23	WXEPAYQRF**A**	1.3	1.6	**60**	XEPAYQR**K**L	1.6	1.7
24	**E**XEPAYQRFL	1.6	1.1	**61**	XEPAYQR**Q**L	0.2	0.95
25	**L**XEPAYQRFL	0.6	1.2	**62**	XEPAYQR**Y**L	0.6	1.0
26	**K**XEPAYQRFL	1.2	1.9	**63**	XEPAYQR**F***L	0.9	1.4
27	**Q**XEPAYQRFL	0.9	1.2	**64**	XEPAYQR**f**L	0.8	1.1
28	**Y**XEPAYQRFL	1.5	1.8	**65**	XEPAYQRF**E**	0.9	1.4
29	**F**XEPAYQRFL	1.2	1.3	**66**	XEPAYQRF**l**	0.9	0.9
30	**F***XEPAYQRFL	1.0	1.3	**67**	XEPAYQRF**K**	1.2	2.0
31	**f**XEPAYQRFL	0.7	1.8	**68**	XEPAYQRF**Q**	0.5	1.0
32	W**E**EPAYQRFL	1.5	2.1	**69**	XEPAYQRF**T**	0.6	0.7
33	W**L**EPAYQRFL	1.6	1.8	**70**	XEPAYQRF**F**	0.8	1.2
34	W**l**EPAYQRFL	1.4	1.5				
35	W**K**EPAYQRFL	1.6	1.8				
36	W**Q**EPAYQRFL	1.5	1.4				
37	W**T**EPAYQRFL	0.7	1.6				

F* (4-chlorophenylalanine), and lower case letter denotes D-amino acid.

Finally, peptides **51-70** were the 9-mers where three N-terminal residues from p160 sequence were deleted. It has been shown previously that an 8-mer peptide (p160-8-1) with four N-terminal residues deleted from the p160 sequence shows better affinity than p160 for the cancer cells.[15] Therefore, up to four N-terminal residues in p160 are not critical for binding and can be safely removed. Peptides **52-70** are the same as **32-50** with the N-terminal Trp deleted.

Peptide array-whole cell binding assay

The cellulose membrane used in this study is the amino-PEG500. As mentioned before this membrane is acid hardened for improved stability (pH 1-14), have greater distance to cellulose carrier, and there is a hydrophilic spacer (PEG) which reduces the background, making it suitable for direct cell binding assay. The peptide arrays on cellulose membranes show remarkable affinity toward different binding moieties and have been used mainly for studying peptide-protein and peptide-antibody interactions.[39-42] Okochi et al. studied the direct interaction of peptides on cellulose membrane with cells.[32] However, the authors punched individual peptide spots into the 96-well plates followed by cell adhesion and cell labeling. Therefore, peptide array–whole cell binding assay described here provides a new method for screening a library of peptides for binding to different cell types.

The peptides were screened for specific binding to cancer cells using two cancer cell lines MDA-MB-435 and MCF-7, and a normal cell line, HUVEC cells. MDA-MB-435 is a melanoma cell line that was considered as a model

breast cancer cell line for several years,[43] whereas, MCF-7 is an adenocarcinoma human breast cell line.[44] The cells were allowed to bind directly to the peptides and the bound cells were labeled with the CyQUANT dye.

The relative cell adhesion of the peptides was estimated based on the fluorescence of the bound cancer or normal cells as shown in **Figure 2.16.** All the peptides were compared to the wild type p160 and the relative cell adhesion ratio for each peptide binding to cancer or normal cells was determined. The relative adhesion ratio for the cancer cells is listed in **Table 2.4**. The affinity of the peptides for the two cancer cell lines followed similar trend (**Figure** 2.16 **A and B**), whereas, the HUVEC cells showed very little binding to all the peptides (**Figure 2.16 C**). Based on the cell adhesion ratio, several peptides were identified that displayed better cell binding compared to the p160. Five peptides that displayed highest affinity (1.7 – 2.7 fold compared to p160) for the cancer cells were **10**, **11**, **18**, **40**, and **47**. Among the fusion peptides (**6-13**), **6**, **7**, **10**, and **11** showed superior binding to MDA-MB-435 cells. For the MCF-7 cells, most of the fusion peptides (**7-13**) showed high cell adhesion. Peptide **11** was chosen for further investigation as it showed low affinity for the HUVEC cells (relative cell adhesion ratio 0.7).

From the alanine scan peptides (**14-23**), peptide **18** displayed highest affinity for the cancer cells relative to p160. The relative cell adhesion ratio was 2.2 and 2.7 for MBA-MB-435 and MCF-7 cells, respectively. In this peptide, Pro has been substituted with Ala. Perhaps, the Pro residue can also be replaced with other amino acids delivering a peptide with better binding spectrum compared to

p160. Zhang *et al.* found, using phage display, that peptides p161 and p25 with a sequence similar to p160, but, with Pro substituted with Gln or Met bound to a variety of tumor cells, and showed no binding to normal cells.[4]

From the peptides that have mutations in the N- or C-terminal residues (**24-70**) with respect to p160, several peptides displayed enhanced binding to cancer cells. Two peptides that showed highest affinity (up to 2.2 - 2.8 fold) for cancer cells compared to p160 in this category were **40** and **47**. In these peptides a C-terminal hydrophobic Phe or Leu was replaced with a basic Lys residue making these analogues positively charged (net charge +1). Peptides **32-36,** where the N-terminal Nle was substituted, also showed relatively better binding (1.4 - 2.1 fold) compared to p160. The 9-mer peptides **52-70,** in general, showed either same or less binding to cancer cells compared to p160 suggesting the importance of the N-terminal Trp residue. Only two 9-mer peptides, **60** and **67**, showed higher binding (range 1.2-2.0 fold) than p160. The results showed that the increase in the net positive charge of the peptides in the C-terminus increases cell adhesion. This may be due to the electrostatic interactions between the peptides and the cancer cells. However, introducing a positive charge (basic residue) in the N-terminal region, such as peptides 26 and 35, does not increase binding affinity to the same extent as observed for **40** and **47**. Peptide **40** was chosen for further investigation.

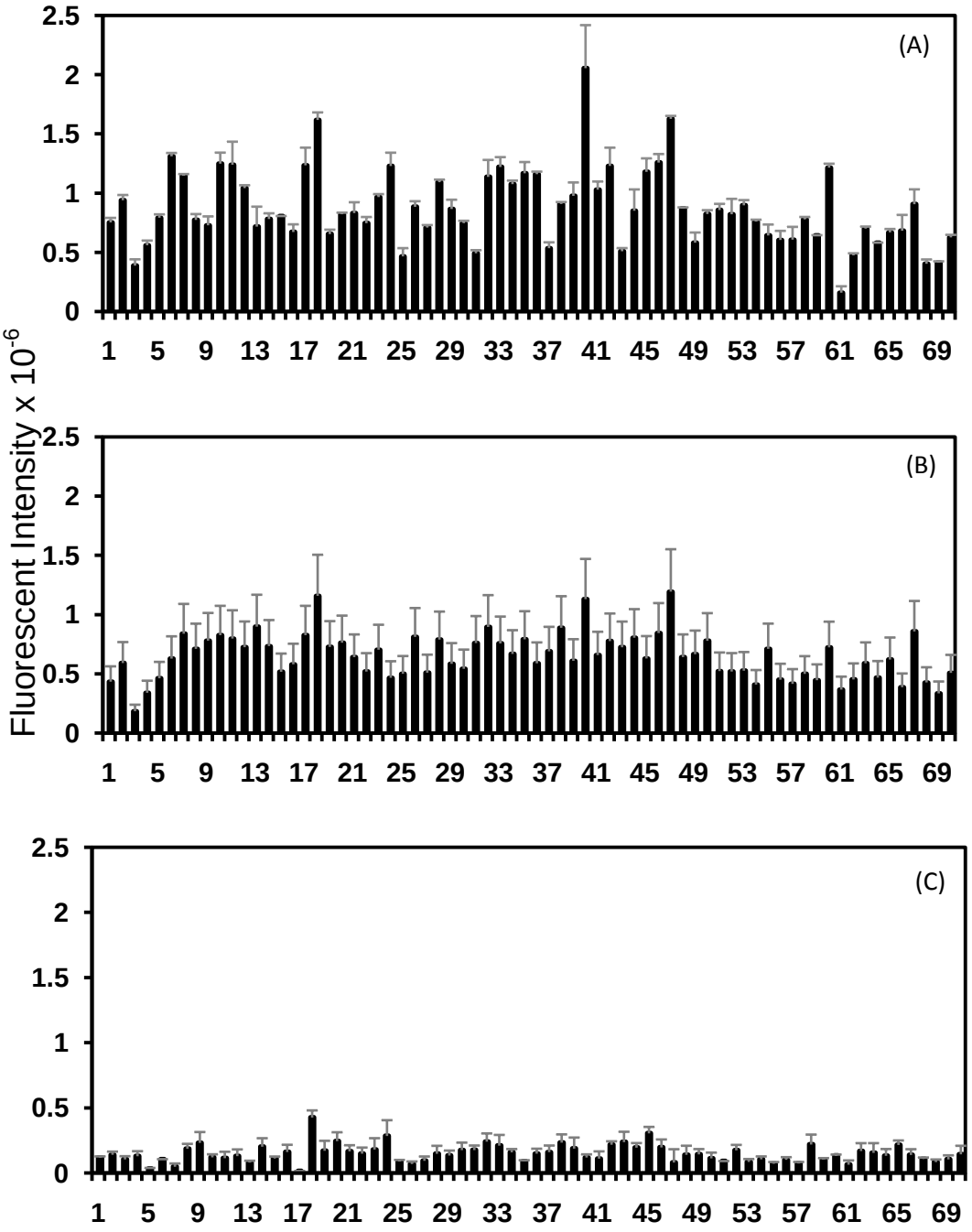

Figure 2.16. Average fluorescence intensity of the peptide bound cells. MDA-MB-435 (A), MCF-7 (B), and HUVEC (C) cells (75 x 10^3 cells/mL) were incubated with the peptide array for 4 h at 37 °C, followed by labeling the cells with the CyQuant dye. The fluorescence intensity was measured using Kodak imager at 465 nm excitation and 535 nm emission.

2.2.7 Affinity and Specificity of Novel p160 based Cancer Targeting Peptides

Five peptides with high binding affinity for cancer cells were identified from the peptide array-cell binding screening (**Table 2.5**). Three peptides, **11**, **18**, and **40**, with high relative cell adhesion ratio were selected for further investigation. Peptide **47** was not chosen for further investigation due to high auto-fluorescence and **60** was skipped as it is same as peptide **40** without N-terminal Trp. Fluorescence based experiments, such as, flow cytometry and confocal microscopy were used to monitor the affinity and specificity of the selected peptides during *in vitro* cell binding experiments.

Synthesis of FITC-labeled peptides

Peptides (p160, **11**, **18**, and **40**) were synthesized manually using SPPS and then fluorescently labeled with 5-FITC in the N-terminus via a β-alanine spacer (**Scheme 2.1**, **page 110**). The identity of the synthesized peptides was confirmed by MALDI–TOF using linear ion mode to avoid meta degradation using the reflected ion mode, and the purity was confirmed using analytical HPLC (**Figure 2.17**).

Table 2.5 Amino acid sequences of the peptide analogues with better binding profile for the cancer cells identified from the peptide array.

Peptide analogue #	Amino acid sequence
1 (p160)*	VPWMEPAYQRFL
11	**RGD**PAY**QGR**FL
18	WXE**A**AYQRFL
40	WXEPAYQR**K**L
47	WXEPAYQRF**K**
60	XEPAYQR**K**L

* Sequence of p160 is shown for comparison.

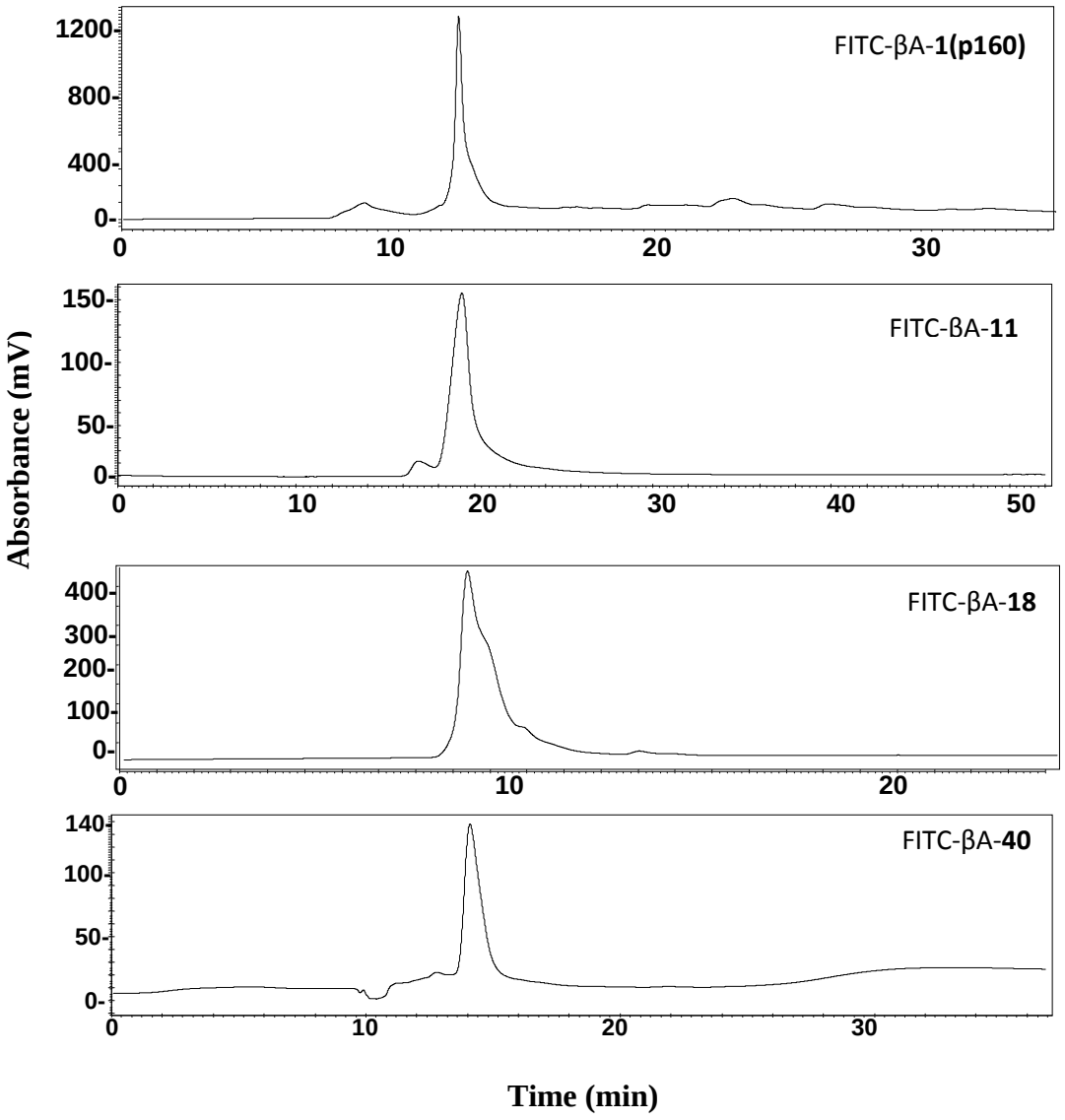

Figure 2.17. RP-HPLC chromatogram of FITC-βA-**1** (p160), FITC-βA-**11,** FITC-βA-**18,** FITC-βA-**40** using isocratic 32% IPA/water using flow rate 1.2 mL/min in 50 min**.**

Fluorescence imaging using FITC-labeled peptides

FITC-labeled peptides were incubated with the MDA-MB-435 cancer cells or the normal HUVEC cells (as negative controls) for 30 min at 37 ºC to characterize the peptide-cell binding. Peptide-cell binding was characterized by

both fluorescence microscopy as well as confocal microscopy of the MDA-MB-435 cells and showed that the peptide analogues uniformly surrounded the nuclei of the cells (**Figure 2.18**). The FITC-labeled peptides, FITC-**11**, FITC-**18**, and FITC-**40**, bound to the surface of the cells, as well as, were present in the cytoplasm. Interestingly FITC-**18** was found to be present in the nucleus as well (**Figure 2.18 C**).

Flow Cytometry using FITC-labeled peptides

The binding of the peptides to the cells was further confirmed using flow cytometry. **Figure 2.19** shows the fluorescence for the different peptides bound to MDA-MB-435 and HUVEC cells, respectively. FITC-labeled p160 was used as a positive control. In general, MDA-MB-435 cells showed significantly higher FITC-fluorescence than the HUVEC cells when bound to FITC-labeled peptides. This shows selective binding of the peptides to cancer cells. MDA-MB-435 cells showed highest FITC-fluorescence when bound to peptide **18**, followed by **11**, p160, and the lowest for **40**. These results indicate that peptide **18** and **11** have higher affinity for MDA-MB-435 cells compared to p160. Peptide **40** showed weak binding compared to p160, in contrast to what was observed in the peptide array-cell binding assay (relative cell adhesion ratio 2.7). This is most likely due to the high auto-fluorescence of peptide **40** (**Figure 2.15 B**) which was enhanced after cell binding.

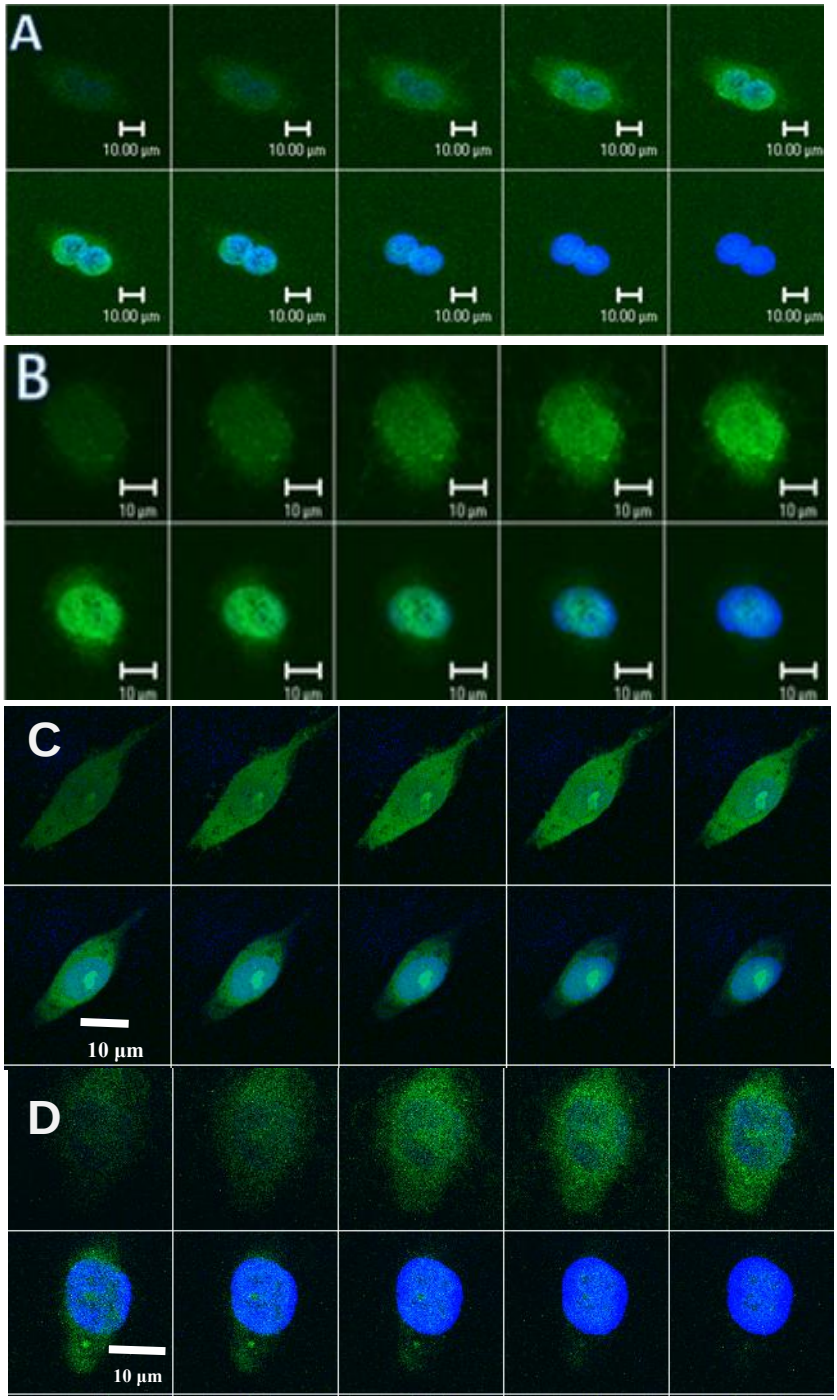

Figure 2.18. Confocal laser scanning microscopy of peptide bound MDA-MB-435 cells. Cells were incubated for 30 minutes with (A) FITC-p160 (10^{-5} mol/L), (B) FITC-11 (10^{-5} mol/L), (C) FITC-18 (10^{-5} mol/L), and (D) FITC-40 (10^{-5} mol/L). Cell nuclei were stained with DAPI (blue). Fluorescence images of the ten slices from the top to the middle of the cells were shown using the Z-stack scan mode of confocal fluorescence microscope.

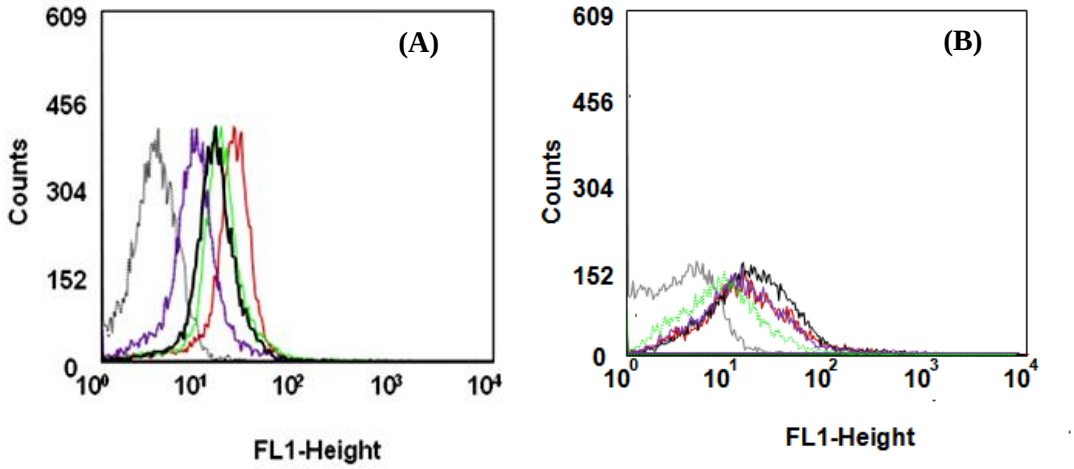

Figure 2.19. FACS analysis of MDA-MB-435 cells (A) or HUVEC cells (B) after incubation with the peptides (10^{-5} mol/L), FITC-βA-1 (p160, black), FITC-βA-11 (green), FITC-βA-18, and FITC-βA-40 (purple) were incubated with the cells for 30 min at 37 °C. Auto- fluorescence of the cells is shown in grey.

Competitive binding

To determine the affinity of new p160 analogues, competition binding assays with MDA-435 cell lines were done. The affinity was evaluated through competition studies using the unlabeled **18, 11** and determined by both FACS and confocal microscopy. In competition experiment, 100-fold excess of unlabeled **18** caused up to 85% decrease in the FITC-fluorescence of the FITC-**18** bound cells (**Figure 2.20**).

Similar competitive experiments for peptide **11** showed very different results. As shown in **Figure 2.21**, only a slight decrease (3%) in the fluorescence was observed when the cells were incubated with FITC-**11** in the presence of 100-fold excess unlabeled **11**. However, a substantial (48%) decrease in FITC-fluorescence was observed when FITC-**11** was incubated in the presence of

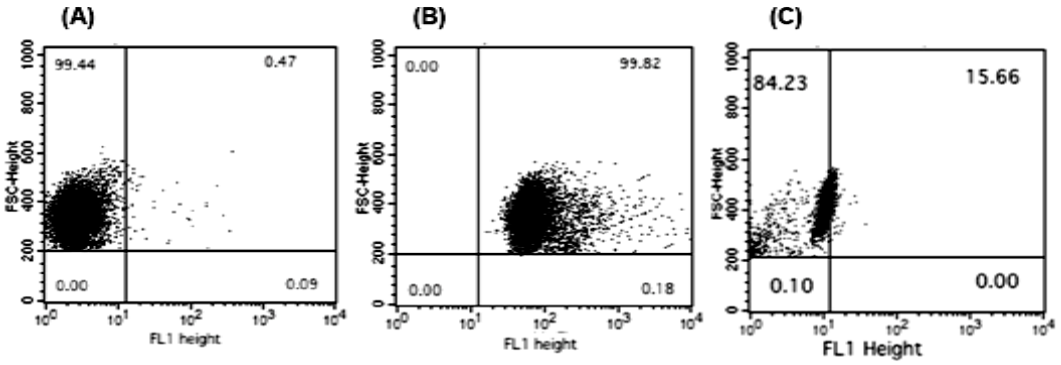

Figure 2.20. FACS analysis for the competitive binding of the peptide **18**, showing (A) autofluorescence of MDA-MB-435 cells, (B) fluorescence of cells after incubation with FITC-**18** (10^{-5} mol/L), and (C) fluorescence of cells after incubation with FITC-18 (10^{-5} mol/L) in the presence of 100-fold excess **18**.

unlabeled c-RGDfK (100 folds). The fluorescence was not completely wiped out in the presence of either excess **11** or c-RGDfK suggesting multiple binding sites for **11** on the cancer cells. As peptide **11** is a fusion peptide with RGD and QGR sequences inserted in the p160 sequence, it can therefore bind to the αvβ3 integrin, aminopeptidase N (CD13), and the putative p160 receptor on the cancer cells. MDA-MB-435 and MCF-7 cancer cells are known to express $\alpha v\beta_3$ integrin, however expression of APN (CD13) by these cells is minimal.

Confocal microscopy shows similar results for FITC-**11** bound to cells in the absence and presence of excess (10-fold) unlabeled p160 **(Figure 2.22)**. A decrease in fluorescence is observed when p160 is present as a competitor. This decrease in fluorescence is about the same order as observed with unlabeled **11** as a competitor using flow cytometry (**Figure 2.21**). These results, along with the FACS experiments, confirm that peptide **11** binds to multiple receptor sites. Thus, targeting multiple receptors with a fusion peptide such as **11** can lead to peptides with higher affinity.

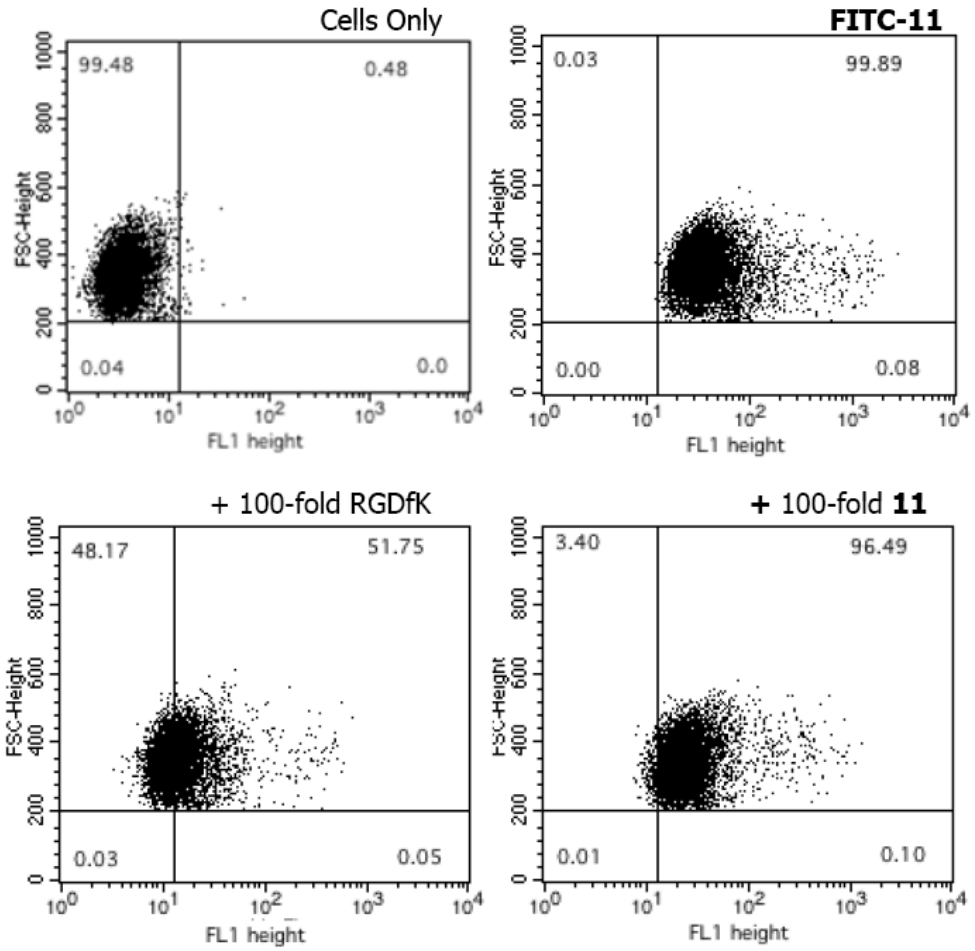

Figure 2.21. FACS analysis for the competitive binding of the peptides, showing autofluorescence of MDA-MB-435 cells (Top left), fluorescence of cells after incubation with 10^{-5} mol/L FITC-11 (Top right), fluorescence of cells after incubation with FITC-11 (10^{-5} mol) in the presence of 100-fold excess **11** (middle left) or c-RGDfK (middle right).

The binding of **18** to cancer cells is presumed to be very similar to that of p160 peptide, as there is a single mutation in **18** compared to p160. Peptide **18**, like p160, showed almost complete removal of fluorescence due to cell bound FITC-**18** in the presence of unlabeled **18** (**Figure 2.20 C**). The receptor mediated specific binding of p160 by the MDA-MB-435 and MCF-7 cancer cells was

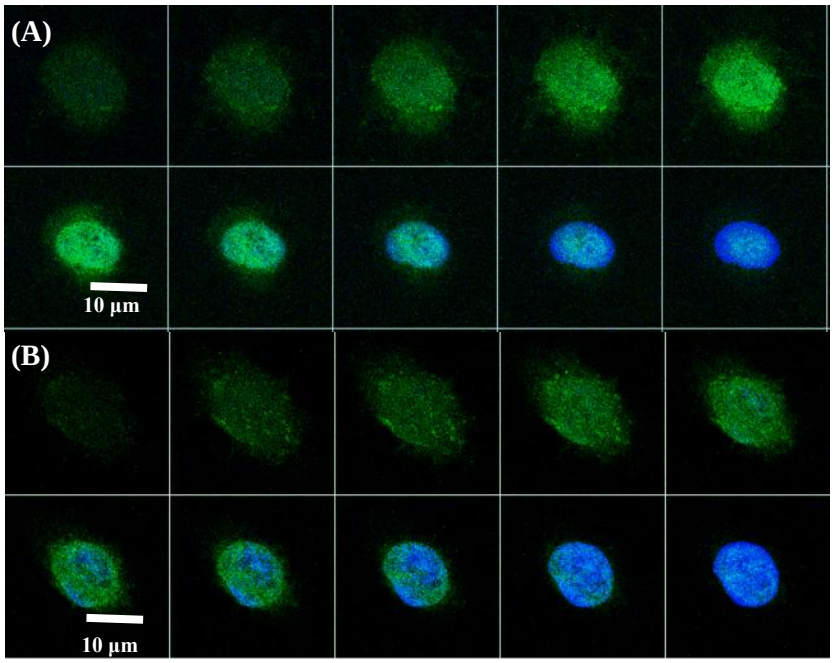

Figure 2.22. Confocal laser scanning microscopy of peptide bound MDA-MB-435 cells. Cells were incubated for 30 minutes with (A) FITC-11 (10^{-5} mol/L) (B) FITC-**11** (10^{-5} mol/L) in the presence of unlabelled p160 (10^{-6} mol/L). Cell nuclei were stained with DAPI (blue). Fluorescence images of the ten slices from the top to the middle of the cells were shown using the Z-stack scan mode of confocal fluorescence microscope. Scale bar is 10 µm.

demonstrated by Askoxylakis et al.[15] A large decrease in cell binding was observed when ^{125}I-labeled p160 (10^{-6} mol/L) was allowed to bind cancer cells in the presence of unlabeled p160 as a competitor. The authors also show internalization of the radio-labeled and FITC-labeled p160, which was inhibited in the presence of unlabeled p160. Furthermore, peptide **18** shows about 3-fold better affinity compared to p160 (**Figure 2.19**) and, in general, peptides like **18** bind to cancer cells in the low micromolar range. This may seem to be a high concentration range in comparison to the other targeting moieties recently reported.[45,46] The HER-2 and EGFR specific affibodies and the cancer-specific aptamers bind to the cells in the nanomolar range. However, it is important to note

that our peptides are very small (10-mers) compared to affibodies (58 amino acids) and aptamers (39-85 nucleotides).[47] These peptides can behave like small molecule drugs and present less *in vivo* problems related to large molecules such as immunogenicity and toxicity.

The peptide array cell screening method described here has allowed the identification of two peptides **11** and **18** for targeting cancer cells without the knowledge of a biomarker or receptor on the cell surfaces. Our studies suggest that peptides such as **11** and **18** can be used for the diagnosis and targeting of disease without the complete understanding of the molecular processes involved in the disease.

2.3 Conclusions

In conclusion, a new method to screen peptides for specific recognition by MDA-MB-435 and MCF-7 cancer cells using peptide array-whole cell interactions has been developed. Peptide arrays consisting of 60 to 140 peptides and ranging in length from 5-mer to 12-mer were synthesized on cellulose membrane. Peptide arrays were designed based on the lead peptide sequences NGR or p160. A direct peptide array-whole cell binding assay using fluorescent labelling of the cells with CyQUANT dye allowed identification of several new peptides that showed higher affinity for the MDA-MB-435 and MCF-7 cancer cells compared to the wild type p160. These peptides did not recognize the normal endothelial HUVEC cells. Three p160 peptide analogues, namely, **11**, **18**, and **40**, that displayed highest affinity for the cancer cells were synthesized and labelled with FITC. The cancer cell binding ability of these selected peptides was

confirmed using fluorescence imaging and flow cytometry. FITC-**11** and FITC-**18** displayed high affinity for the cancer cells compared to the FITC-p160 peptide. In a competition experiment, the fluorescence for FITC-**18** was eliminated in the presence of excess of unlabeled **18**. On the other hand, the fluorescence for FITC-**11** was only 3% reduced in the presence of unlabeled **11** and was reduced to half (48%) in the presence of excess of unlabeled RGDfK, suggesting multiple binding sites for **11**. These results suggest the presence of a specific receptor on cancer cells and can help in the identification of a specific biomarker for cancer. The peptide array-cell binding assay established in this study is not only useful for the identification of cancer targeting peptides, but it can also be used for the generation of diagnostic tools for cancer.

2.4 Experimental Procedures

2.4.1 Materials and Methods

Solvents and Reagents

Wang resin (1.1mmol/g), benzotriazol-1-yloxy-tris(dimethylamino)-phosphonium hexafluorophosphate (BOP), 1-hydroxybenzotriazole (HOBt), 2-chlorotrityl chloride resin (1.4 mmol/g) and the Fmoc-amino acids were purchased from NovaBiochem (San Diego, CA, USA). The side chains of the amino acids used in the synthesis were protected as follows: Boc (Lys, Trp), Pbf (Arg), t-Bu (Thr), OtBut (Asp, Glu), and Trt (Asn, Cys, Gln, His). Dichloromethane (DCM), methanol, isopropyl alcohol (IPA), acetonitrile (ACN), diethyl ether, pyridine, and piperidine were purchased from Caledon Laboratories LTD (Canada). CyQUANT dye was obtained from Invitrogen (Eugene, Oregon, USA) and 5-FITC (Fluorescein-5-isothiocyanate) was from Anaspec (Fremont, CA). N,N-Disopropylcarbodiimide (DIC), (DMF), N-methyl morpholine (NMM), N-methyl-2-pyrrolidone (NMP), [3-(4,5-dimethylthiazol-2-yl)-2,5-diphenyl] tetrazolium bromide (MTT) (Sigma), tetrahydrofuran (THF), dichlorobenzoyl chloride (DCB), trifluoroacetic acid (TFA), triisopropyl silane (TIPS), and all other reagents were purchased from Sigma-Aldrich. All commercial reagents and solvents were used as received with no further purification. The absence of amines in DMF and NMP was detected using bromophenol (BPB).

Cell Lines

All cell lines were cultivated at 37 ºC in a 5% CO_2 incubator. The human cancer cell lines MDA-MB-435, MDA-MB-231, HT-1080, and Hey cells were obtained from American Type Culture Collection (ATCC) (Manassas, USA) and cultured in RPMI 1640 with 1% L-glutamine, and 10% FCS (Invitrogen, Karlsruhe, Germany), 100 IU/mL penicillin, and 100 IU/mL streptomycin. The human breast cancer cell line MCF-7 (ATCC, Manassas, USA) was cultured in DMEM 1% with 1% L-glutamine, 100 IU/mL penicillin, and 100 IU/mL and 10% FCS (Invitrogen). Human umbilical vein endothelial cells (HUVEC), kind gift from the laboratory of Sandra Davidge, University of Alberta, were cultivated using Endothelial Cell Growth medium (EGM, LONZA) containing 20% FCS, 2 mmol/L glutamine, 100 IU/mL penicillin, 100 IU/mL streptomycin, and 2 ng/mL basic fibroblast growth factor (Roche Diagnostics, Mannheim, Germany). APN/CD13 mAb (WM15) was obtained from (BD Bioscience, San Diego, CA).

Equipment

Peptide array was made using a semiautomatic robot Auto-Spot ASP 222 (Intavis AG, Germany). Solid phase synthesis of peptides on Wang resin was done using manual synthesis. Peptide syntheses were performed in plastic columns with plastic sinters at their base for solvent removal under suction. HPLC purification and analysis were carried out on a Varian Prostar HPLC system (Walkersville, MD, USA) using Vydac C18 semi-preparative (1 x 25 cm, 5 μm) and analytical (0.46 x 25 cm, 5 μm) columns. Peptides were detected by UV absorption at 220 nm. Mass spectra were recorded on a matrix-assisted laser

desorption ionization time-of-flight (MALDI-TOF) Voyager spectrometer (Applied Biosystems) or Waters micromass ZQ. Imaging experiments were done using Kodak imager 4000M (USA), Carl Zeiss microscope (Göttingen, Germany), and confocal laser scanning microscopy using Zeiss 510 LSMNLO confocal microscope (Carl Zeiss Microscope systems, Jena, Germany). FACS experiments were performed on Becton-Dickinson Facsort and analyzed by DakoCytomation Summit software. ELISpot scanning was done using Bioreader 3000 (Dr. Kevin Kane Lab, Dept. of Medical Microbiology & Immunology, University of Alberta).

2.4.2 Synthesis of NGR Peptide Array on Cleavable Membrane

The Spot method was used for simultaneous multiple peptide synthesis on separate sites on a homogeneous membrane. Preactivated amino acid derivatives were spotted onto the porous cellulose membrane. The spots formed resemble individual reaction compartments for chemical reaction in solid phase synthesis. The spots were arranged in a defined format for the synthesis. The number of spots per area and the spot size were determined by membrane porosity and volume of the drops. Using this strategy, six peptides based on the sequence of NGR peptide (CVLNGRXC) were synthesized by a robotic peptide synthesizer (Autospot) on a β-alanine derivatized cellulose membrane. The peptides were synthesized using the default 12 x 8 format. The synthesis of peptides on cellulose membrane was performed following sequential steps as described in the Appendix.

Cleavage of NGR peptides from the cellulose membrane

After the cleavage of the side-chain protecting groups, the peptides attached to the cellulose membrane were placed over a saturated solution of ammonia in THF. A saturated solution of ammonia was prepared by bubbling ammonia gas into a -78 °C THF for ~20 min. The saturated solution of ammonia in THF was placed in a desiccator and the membrane was placed on the top. Desiccator was closed and a partial vacuum was applied to remove any air and was left for overnight at room temperature.[27] The spots were punched out using 96 well puncher and each spot placed in eppendroff tube and then eluted with 30% ACN/water (150μL) sonicated for 30 min. The resulting peptide solutions were characterized using MALDI –TOF and analytical HPLC for purity.

Characterization of NGR soluble peptide

Peptides **1-6** were analyzed by MALDI-TOF mass spectrometry using a α-cyano-4-hydroxy-cinnamic acid as a matrix. The $[M+H]^+$ calculated and found is shown in **Figure 2.3**. Purity of peptide **2** was also tested using analytical reversed-phase HPLC on Vydac C18 column (250 x 4.6 mm) using flow rate 0.6 mL/min, monitored at 220 nm. Gradient of 1-5% ACN in 0.05% aqueous TFA over a period of 30 min was used.

2.4.3 Synthesis of NGR Peptide Array on Non-Cleavable Membrane

Thirty different peptides based on the sequence of NGR peptide (CVLNGRMEC) were synthesized on cellulose membrane following the same

procedure as described in Section 2.4.2. The array format of this library is shown in **Figure 2.4**. Peptide arrays were synthesized on an amino-PEG500 cellulose membrane-UC540 (Intavis, Germany). The surface of the membrane was derivatized with 10 unit polyethylene glycol (PEG) linker with a free amino terminal group. The Spot synthesis method was used to build the peptide arrays using standard Fmoc SPPS.[26] The C-terminal end of the peptide was anchored to the surface of the amino-PEG500 cellulose membrane through a β-alanine spacer. At the end, all peptides were N-terminally acetylated. The final removal of side chain protection was performed with TFA as described in the Appendix. After extensive washing with DCM, DMF, and ethanol, the membrane was dried with cold air. The dried membrane was stored in a sealed bag at -20 °C until use.

Cyclization of peptides containing cysteine was performed on the cellulose membrane to form disulfide bond as follow. The membrane was incubated with 0.1 M Tris-buffer (pH 8.5) at 4 °C overnight, followed by 10% DMSO in the same buffer for 8 h at 4 °C, and finally, with 20% DMSO overnight at room temperature. Subsequently, the membrane was washed with ethanol (3 x 3 min) and dried.[48]

2.4.4 APN/CD13 Expression Level using FACS Analysis

Fluorescence activated cell sorting (FACS) was performed to quantify the level of expression of APN/CD13 on the surface of both MDA-MB-231 and HT-1080 cell lines. Briefly, a million cells were suspended in 100 μL FACS buffer (PBS with 5% FCS, and 0.09% sodium azide) and incubated with 20 μL of FITC

labeled CD13 antibody (WM-15) for 30 min at 4 °C. The cells were washed twice with FACS buffer, and the APN/CD13 expression level was measured using flow cytometry. The data was analyzed using CELL Quest software (Becton Dickinson).

2.4.5 Screening Peptide Array for Cell Binding using MTT Reagent

The cellulose membrane with the peptide array was soaked in ethanol for 30 seconds to prevent precipitation of hydrophobic peptides, followed by incubation in sterile PBS (pH 7.4) for 30 min. The membrane was blocked with blocking solution (TBS with 2% Skim milk powder, 0.2% v/v Tween 20) for 2 h at room temperature on side to side shaker. Afterwards, the membrane was washed with TBS-T (TBS, pH 7.6 and 0.2% (v/v) Tween 20) three times for 5 min each. The membrane was then scanned with Kodak imager or Elispot. The membrane was washed with RPMI-1640 serum free media, and incubated with cell suspension (1 x 10^5 cells) for 36 h. All the above steps were done at room temperature.

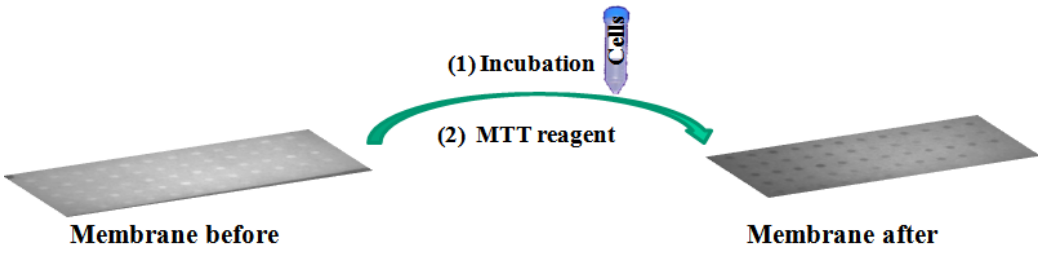

Figure 2.23. Schematic representation of cell binding and MTT–detection after 36 h incubation of NGR peptide array with HT-1080 cell lines.

Unbounded and non-specifically bound cells were removed by washing with PBS (3 x 25 mL, 5min) on side to side shaker. MTT reagent (25 mL, 5 mg/mL) in PBS was added to the membrane bound cells and incubated for 3 h, and the membrane was washed with PBS. The membrane was imaged again with either the Kodak imager or using the Elispot. After scanning, the membrane was regenerated as follows. The bound cells were removed by first washing with ethanol (3 x 25 mL, 5 min), followed by treatment with 0.1 N HCl (2 x 25 mL, 20 min). Finally, the peptide array membrane was washed with DMF (4 x 25 mL, 20 min), ethanol (3 x 25 mL, 3 min), and dried in air. Each cell-binding experiment was repeated twice.

2.4.6 Synthesis of P160 Library

P160 peptide library was synthesized on PEG-cellulose membrane. Seventy peptide sequences in duplicates ranging in length from 9 to 12 amino acids were synthesized in an array format on a cellulose membrane using an AutoSpot robot. The peptide array was synthesized following the same procedure as described in Section 2.4.3.

2.4.7 Screening Peptide Array for Cell Binding using Fluorescence

The cellulose membrane with the peptide array was soaked in ethanol for 30 seconds followed by incubation in sterile PBS (pH 7.4) for 30 min. The cells were seeded directly on culture dish (75×10^3 /mL) containing the peptide array membrane for 4 h in serum free media, in order to prevent the proteolytic effect of serum on the peptides. After washing the non-bound cells, the membrane was frozen at -80 ^{o}C for 2 h. The membrane was thawed at room temperature followed

by incubation with the CyQuant dye for 30 min following the manufacturer protocol. It was washed three times with PBS, each for 5 min by shaking on automatic shaker. The membrane was scanned using Kodak imager at 465 nm excitation and 535 nm emission and the net fluorescence intensity of each peptide spot was quantified using Kodak Molecular Imaging Software Version 4.0. The binding affinity of the cells for each peptide (spot) was determined by subtracting the net fluorescent intensity of the peptide itself. An external standard (set of peptides) was used to calibrate the fluorescence intensity between scans done on the same day and on different days. After each cell-binding experiment, the membrane was regenerated as described before (Section 2.4.5). Each cell-binding experiment was repeated twice. The results are presented as average fluorescence intensity (± standard deviation) of two duplicate peptide spots, two scans, and two different experiments. The relative cell adhesion ratio for each peptide analogue was calculated as the ratio of the fluorescence of the peptide analogue divided by that of the p160 peptide.

Synthesis of FITC-labeled Peptides

The peptides p160 (VPWXEPAYQRFL), β-Ala-p160 (β-Ala-VPWXEPAYQRFL), β-Ala-11 (β-Ala -RGDPAYQGRFL), β-Ala-18 (β-Ala-WXEAAYQRFL), and β-Ala-40 (β-Ala-WXEPAYQRKL) were obtained by solid phase peptide synthesis using Fmoc coupling protocols (**Scheme 2.1**). The peptide synthesis was performed manually in a polyethylene peptide synthesis vessel with a frit at the bottom and screw cap with a septum at the top for addition of reagents. Solvents and soluble reagents were removed by suction. Washing

between deprotection and coupling was carried out with DMF (4 x 1min), DCM (4 x 1min) and IPA (4 X 1min). Fmoc group was removed by treatment with 20% piperidine/DMF (2 x 7min). In a solid phase reactor, Wang resin (90 mg, 0.1 mmol) was weighed and washed with DMF, DCM and IPA and swelled for 1

Scheme 2.1. Solid phase peptide synthesis of (FITC-β-Ala-18)

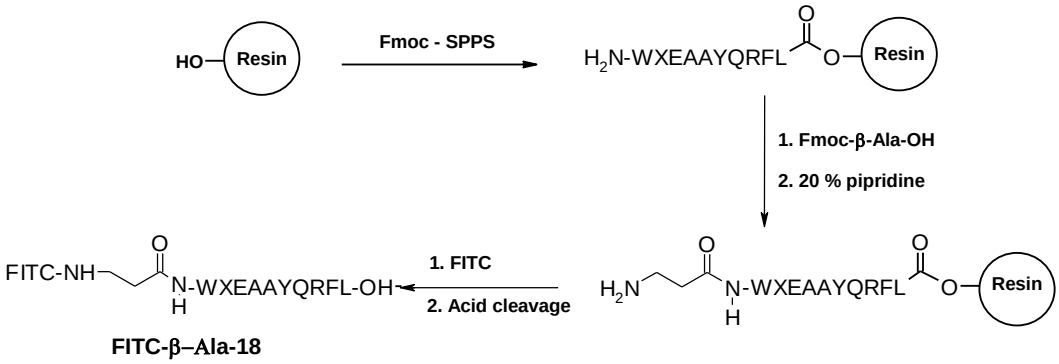

FITC-β–Ala-18

h in DCM. Next, the first amino acid, N- α-Fmoc-Leu (234 mg, 4 equiv), DCB (57 μL, 4 equiv), pyridine (54 μL, 6 equiv) was activated for 5 min and then added to the swelled resin. The reaction was mixed for overnight. The Fmoc protecting group of the first amino acid was removed with a solution of piperidine–DMF (1:4) and the linear peptide was assembled using standard Fmoc procedures by consecutive addition of the protected amino acid (2 equiv), BOP (86 mg, 1.95 equiv), HOBt (27 mg, 2 equiv), and NMM (50 uL, 4.5 equiv) in DMF for 1 to 2 h. After addition of the last amino acid, the N-terminal Fmoc group was then removed with 20% piperidine in DMF (2 X 10 min). Fmoc-β-alanine (spacer) was conjugated to the N-terminal amino group followed by coupling with 5-FITC. 5-FITC (0.3 mmol) and DIPEA (0.15 mmol) in anhydrous DMF (1 mL) were added to the peptide resin, followed by stirring for 20 h at

room temperature in the dark. The resin was washed using DMF and IPA. FITC-labeled peptide was cleaved from the resin by TFA-TIPS-H_2O (95:2.5:2.5, 7.5 mL). The resulting mixture was agitated for 2 h before washing with TFA:CH_2Cl_2 (1:9, 7 mL). The acid washings were concentrated to approximately 1 mL and precipitated by cooled diethyl ether. The precipitate was collected by centrifugation and washed with ice-cooled dry diethyl ether (4× 30 mL) to give orange powder. The precipitate was isolated and dried in a stream of nitrogen and freeze-dried using lyophilization. The crude product was purified by preparative HPLC. The mass of the products was determined by MALDI-TOF mass spectrometry.

Synthesis of c-RGDfK peptide

Cyclized RGD peptide, c-RGDfK, was synthesized following the previously described procedure.[49] Briefly, a solution of Fmoc-Asp-OAll (119 mg, 3 equiv) and DIPEA (210 μL, 12 equiv) in dry CH_2Cl_2 were added to 2-chlorotrityl resin (0.1 mmol, 70 mg). The resin was capped and the Fmoc protecting group was removed and the linear pentapeptide was assembled using standard Fmoc procedures. After addition of the last amino acid, the C-terminal allyl ester was removed by treatment with $Pd(PPh_3)_4$ (0.16 equiv) and $PhSiH_3$ (16 equiv) in DCM/DMF for 2 h. The reaction mixture was washed with diethyldithiocarbamic acid sodium salt. The N-terminal Fmoc group was then removed with piperidine–DMF (1:4) before addition of BOP (1.95 equiv, 86 mg), HOBt (27 mg, 2 equiv), and NMM (50 uL, 4.5 equiv) in DMF for 2 h to allow on-resin cyclization and give cyclized peptide. It was treated with TFA:CH_2Cl_2 (1:1,

8 mL) for 2 h and washed with TFA:CH_2Cl_2 (1:9). The acid washings were concentrated to approximately 1 mL and precipitated by cooled diethyl ether to obtain c-RGDfK in 70% yield and more than 95% purity as confirmed by HPLC and mass spectrometry.

2.4.8 In Vitro Cell Binding Using Fluorescence and Confocal Microscopy

MDA-MB-435 cells (50,000) were cultured on the top of cover slip at 37 ºC for 24 h. The medium was removed and replaced with fresh serum free medium (1 mL) containing FITC-labeled peptides at a concentration of 10^{-5} mol/L. The cells were incubated with the peptides for 30 min at 37 ºC. After incubation, the medium was removed and the cells were washed with serum free medium (3 x 2 mL). The cells were fixed on ice with 2% formaldehyde for 20 min. The formaldehyde was removed by washing with medium (3 x 2 mL). The cover slips were put on slides containing one drop of DAPI-Antifade (Molecular Probes) to stain the nucleus. The cells were imaged under the fluorescence microscope (Zeiss) using green and blue filters with 20x magnification.

The samples prepared for fluorescence microscopy were also visualized by confocal microscopy. Confocal laser scanning microscopy was performed with a Carl Zeiss LSM 510 inverted confocal microscope (Carl Zeiss Microscope systems, Jena, Germany) with a 100x oil immersion lens. Confocal stacks were processed using the Carl Zeiss LSM 5 Image software, which also operates the confocal microscope. For the competitive binding, the same experiment was carried out in the presence of unlabeled p160 peptide (10^{-4} mol/L) as a competitor.

The cells were incubated with unlabeled p160 and FITC-labeled peptide analogues (10^{-5} mol/L or 10^{-6} mol/L). Confocal imaging was done on an inverted microscope as described above.

2.4.9 In Vitro Cell Binding Using FACS Analysis

Fluorescence-activated cell-sorting (FACS) analysis was used to evaluate the binding of the FITC-labeled peptides to the cancer MDA-MB-435 and the normal HUVEC cells. The MDA-MB-435 and HUVEC cells were placed into 6-well plates at a density of 10^6 and 3 x 10^5, respectively, in 3 mL of culture medium at 37 ºC for 24 h. The culture medium was replaced by 1 mL of fresh serum-free medium, containing FITC-labeled peptides, FITC-p160, FITC-**11**, FITC-**18,** and FITC-**40** at concentration of 10^{-5} mol/L. Cells were incubated with the peptides for 30 min at 37 ºC. The media was then removed and the cells were washed 3 times with ice-cold phosphate-buffered saline (PBS) to remove the unbound peptide. The cells were then scrapped from the wells using manual scrapper. The cells were transferred to centrifuge tubes and centrifuged at 1,000 rpm for 7 min. The pellet was resuspended in FACS buffer (PBS with 5% FCS, and 0.09% sodium azide), washed once more and then resuspended again in FACS buffer. Untreated cells were subjected to similar steps without any peptide treatment to detect autofluorescence of the cells. The samples were then subjected to the FACS instrument, Becton-Dickinson Facsort to acquire data. The data was analyzed by DakoCytomation Summit software.

Competition binding assays were performed using the MDA-MB-435 cancer cell line with FITC-**11** in the presence of a 100-fold excess unlabeled

peptide **11** or c-RGDfK. After incubation for 30 min at 37 ºC, the cells were washed with ice-cold PBS. Thereafter, FACS analysis was performed as described above. Similar experiment was repeated for FITC-**18** in the presence of excess unlabeled peptide **18**. All the experiments for binding assay were repeated 2-4 times.

2.5 References

(1) Aina, O. H. S., T. C.; Chen, M. L.; Lam, K. S. *Biopolymers* **2002**, *66*, 184-99.

(2) Li, Z., Zhao, R., Wu, X., Sun, Y., Yao, M., Li, J., Xu, Y., Gu, J. *Faseb J* **2005**, *19*, 1978-85.

(3) Wong, S. C., Wakefield, D., Klein, J., Monahan, S. D., Rozema, D. B.;,Lewis, D. L., Higgs, L., Ludtke, J., Sokoloff, A. V., Wolff, J. A. *Mol Pharm* **2006**, *3*, 386-97.

(4) Zhang, J. S., H.; Schwab, M., *Cancer Lett* **2001**, *171*, 153-64.

(5) Arap, W., Pasqualini, R., Ruoslahti, E. *Science* **1998**, *279*, 377-80.

(6) Pierschbacher, M. D., Ruoslahti, E. *Nature* **1984**, *309*, 30-3.

(7) Zitzmann, S., Ehemann, V., Schwab, M. *Cancer Res* **2002**, *62*, 5139-43.

(8) Colombo, G., Curnis, F., De Mori, G. M., Gasparri, A., Longoni, C., Sacchi, A., Longhi, R., Corti, A. *J Biol Chem* **2002**, *277*, 47891-7.

(9) Pasqualini, R. K., E.; Kain, R.; Lahdenranta, J.; Sakamoto, M.; Stryhn, A.; Ashmun, R. A.; Shapiro, L. H.; Arap, W.; Ruoslahti, E. *Cancer Res* **2000**, *60*, 722-7.

(10) Corti, A., Curnis, F., Arap, W., Pasqualini, R. *Blood* **2008**, *112*, 2628-35.

(11) Curnis, F., Arrigoni, G., Sacchi, A., Fischetti, L., Arap, W., Pasqualini, R., Corti, A. *Cancer Res* **2002**, *62*, 867-74.

(12) Curnis, F., Sacchi, A., Borgna, L., Magni, F., Gasparri, A., Corti, A. *Nature Biotechnology* **2000**, *18*, 1185-6.

(13) van Laarhoven, H., Gambarota, G., Heerschap, A., Lok, J., Verhagen, I., Corti, A., Toma, S., Gallo Stampino, C., van der Kogel, A., Punt, CJ. *Invest New Drugs* **2006**, *24*, 27-36.

(14) Ellerby, H. M., Arap, W., Ellerby, L. M., Kain, R., Andrusiak, R., Rio, G. D., Krajewski, S., Lombardo, C. R., Rao, R., Ruoslahti, E., Bredesen, D. E., Pasqualini, R. *Nature Medicine* **1999**, *5*, 1032-9.

(15) Askoxylakis, V., Mier, W., Zitzmann, S., Ehemann, V., Zhang, J., Kramer, S., Beck, C., Schwab, M., Eisenhut, M., Haberkorn, U *J Nucl Med* **2006**, *47*, 981-8.

(16) Askoxylakis, V., Zitzmann, S., Mier, W., Graham, K., Kramer, S., von Wegner, F., Fink, R. H., Schwab, M., Eisenhut, M., Haberkorn, U *Clin Cancer Res* **2005**, *11*, 6705-12.

(17) Carrico, Z., Romanini, DW., Mehl, RA., Francis, MB. *Chem Commun* **2008**, *14*, 1205-7.

(18) Dechantsreiter, M. A., Planker, E., Matha, B., Lohof, E., Holzemann, G., Jonczyk, A., Goodman, S. L., Kessler, H *J Med Chem* **1999**, *42*, 3033-40.

(19) Kramer, A., Schuster, A., Reineke, U., Malin, R., Volkmer Engert, R., Landgrat, C. Schneider Mergener,J. *Methods* **1994**, *6*, 388-95.

(20) Rudiger, S., Germeroth, L., Schneider Mergener ,J., and Buckau, B *EMBO.J* **1997**, *16*, 1501-7.

(21) Kramer, A., Vakalopoulou, E., Schleuning, W. D.,Schneider Mergener, J. *Mol Immunol* **1995**, *32*, 459 - 65.

(22) Stigler, R., Ruker, F., Katinger, D., Elliot, G., Hohne, W., Henklein, P.. Ho, J. X., Kramer, A., Nugel, E., Porstmann, T., and Schneider Mergener, J *Protein Eng* **1995**, *8*, 471-9.

(23) Volkmer Engert, R., Ehrhard, B., Hohne, W., Kramer, A., Hellwig, J., and Schneider Mergener, J *Let. Pept Sci* **1994**, *1*, 24 -53.

(24) Weiergraber, O., Schneider Mergener,J.,Grotzinger,J.,Wollllllcr.A.,Kiister,A., Exner, M., and Heinrich, P. C *FEBS Lett.* **1996**, *379*, 122 - 6.

(25) Tegge, W., Frank, R., Hofmann, F. & Dostmann, W.R *Biochemistry* **1995**, *34*, 10569-77.

(26) Frank, R. *J Immunol Methods* **2002**, *267*, 13-26.

(27) Andrew, M., Bray, N., Joe Maeji, Akhil, G., Jhingran, Robert, M. *Tetrahdron lett* **1991**, *32*, 6163-66.

(28) Reineke, U., Sabat, R., Kramer, A., Stigler, R. D., Seifert, M., Michel, T., Volk, D., and Schneider Mergener, J *Mol Diversity* **1995**, *1*, 141-8.

(29) Moffatt, S., Wiehle, S., Cristiano, R. J. *Hum Gene Ther* **2005**, *16*, 57-67.

(30) Terauchi, M., Kajiyama, H., Shibata, K., Ino, K., Nawa, A., Mizutani, S., Kikkawa, F. *BMC Cancer* **2007**, *7*, 140.

(31) Mosmann, T. *J Immunol Methods* **1983**, *16*, 55-63.

(32) Okochi, M., Nomura, S., Kaga, C., Honda, H *Biochem Biophys Res Commun* **2008**, *371*, 85-9.

(33) Shield, K., Riley, C., Quinn, M. A., Rice, G. E., Ackland, M. L., Ahmed, N. *Journal of Carcinogenesis* **2007**, *6*, 11-5.

(34) Morini, M., Mottolese, M., Ferrari, N., Ghiorzo, F., Buglioni, S., Mortarini, R., Noonan, D. M., Natali, P. G., Albini, A. *Int J Cancer* **2000**, *87*, 336-42.

(35) Meiklejohn, D., Karlsson, RK., Karlsson, AC., Chapman, JM., Nixon, DF., Schweighardt, B. *J Immunol Methods* **2004**, *288*, 135-47.

(36) Karlsson, R., Jennes, W., Page-Shafer, K., Nixon, DF., Shacklett, BL. *J Immunol Methods* **2004**, *285*, 89-92

(37) Jones, L. J., Gray, M., Yue, S. T., Haugland, R. P., Singer, V. L. *J Immunol Methods* **2001**, *254*, 85-98.

(38) Frank, R. W. *Tetrahdron* **1992**, *48*, 9217-32.

(39) Baillie, G. S., Adams, D. R., Bhari, N., Houslay, T. M., Vadrevu, S., Meng, D., Li, X., Dunlop, A., Milligan, G., Bolger, G. B., Klussmann, E., Houslay, M. D. *Biochem J* **2007**, *404*, 71-80.

(40) Bluschke, B., Eckey, V., Kunert, B., Berendt, S., Landmesser, H., Portwich, M., Volkmer, R., Schneider, E. *J Mol Biol* **2007**, *369*, 386-99.

(41) Guo, J. P.; Petric, M.; Campbell, W.; McGeer, P. L. *Virology* **2004**, *324*, 251-6.

(42) Lentze, N., Narberhaus, F. *Biochem Biophys Res Commun* **2004**, *325*, 401-7.

(43) Chambers, A. F. *Cancer Res* **2009**, *69*, 5292-3.

(44) Frasor, J., Weaver, A., Pradhan, M., Dai, Y., Miller, L. D., Lin, C. Y., Stanculescu, A. *Cancer Res* **2009**, *69*, 8918-25.

(45) Shangguan, D., Meng, L., Cao, Z. C., Xiao, Z., Fang, X., Li, Y., Cardona, D., Witek, R. P., Liu, C., Tan, W. *Anal Chem* **2008**, *80*, 721-8.

(46) Tang, Z., Shangguan, D., Wang, K., Shi, H., Sefah, K., Mallikratchy, P., Chen, H. W., Li, Y., Tan, W. *Anal Chem* **2007**, *79*, 4900-7

(47) Lyakhov, I., Zielinski, R., Kuban, M., Kramer-Marek, G., Fisher, R., Chertov, O., Bindu, L., Capala, *J Chembiochem*, *11*, 345-50.

(48) Hilpert, K., Hansen, G., Wessner, H., Volkmer-Engert, R., Höhne, W. *J Biochem* **2005**, *138*, 383-90.

(49) McCusker, C. F., Kocienski, P. J., Boyle, F. T., Schatzlein, A. G. *Bioorg Med Chem Lett* **2002**, *12*, 547-9.

CHAPTER 3 Novel Peptidomimetic β-Peptides from L-Aspartic Acid and β-Amino-L-Alanine

3.1 Introduction

The use of peptides as drugs is limited due to their susceptibility to proteolytic degradation, poor absorption from the gut, rapid excretion though the kidneys, and consequently low bioavailability. Moreover, the high flexibility of short and medium linear peptide sequences decreases the activity and selectivity. Therefore, manipulation of the peptide structure could improve pharmacological properties of peptides.[1-3] Peptidomimetics has emerged over the years to overcome the limitations of natural α-peptides, and help identify drug-like molecules.

As described in Chapter 1 (Section 1.2.1), different classes of peptidomimetic molecules have been developed through the structural modification of the peptide backbone. Among the known peptidomimetics, β-peptides have gained recognition as their parallel synthesis, solution conformation, and pharmacokinetics have been well studied.[4-6] A number of biologically active β-peptides have been reported in the past five years.[7] β^2- and β^3-peptides are synthesized from the corresponding β^2- and β^3-amino acid monomers (**Figure 3.1**). When we set out to synthesize β-peptides, we realized that only few β^3-amino acids are commercially available and are extremely expensive. For instance, Fmoc-β-hArg(Pmc)-OH and Fmoc-β-hGlu(Otbu)-OH cost around USD 380/g and USD 220/g, respectively. The other β^3-amino acids as well as all β^2-amino acids need to be synthesized from known procedures.

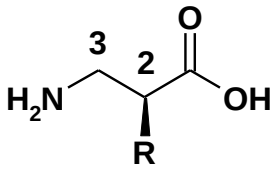

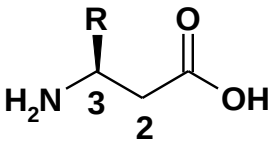

β^2-amino acid
(**β^2**h-amino acid)

β^3-amino acid
(**β^3**h-amino acid)

Figure 3.1. Chemical strucures of β^2- and β^3-amino acid monomers.

With respect to the synthesis of β^2-amino acids, most reported routes (Section 1.2.2) involve chiral auxiliaries,[8,9] the removal of which requires basic or acidic conditions. Epimerization at the α-position can arise under basic conditions making isolation of a pure isomer more difficult. The synthesis of protected β^3-amino acid monomers is also non trivial (Section 1.2.2) and allows access to only a limited number of Fmoc- β-amino acids. In addition, to synthesize β-peptide mimics of biologically active α-peptides, we needed large quantities of Fmoc-β-amino acids. Novel methods for easy access of these oligomers with a wide variety of side chains are therefore highly sought for.

We hypothesized that new families of β^3- and β^2-peptides can be synthesized from L-aspartic acid and β-amino-L-alanine monomers (L-diaminopropionic acid, L-Dap), respectively (**Figure 3.2**). This approach is similar to that of Farrera-Sinfreu et al., which they applied for the synthesis of γ-peptides based on *cis*-γ-amino-L-proline.[10] L-Asp and L-Dap monomers can allow synthesis of β-peptides with a wide variety of side chains.

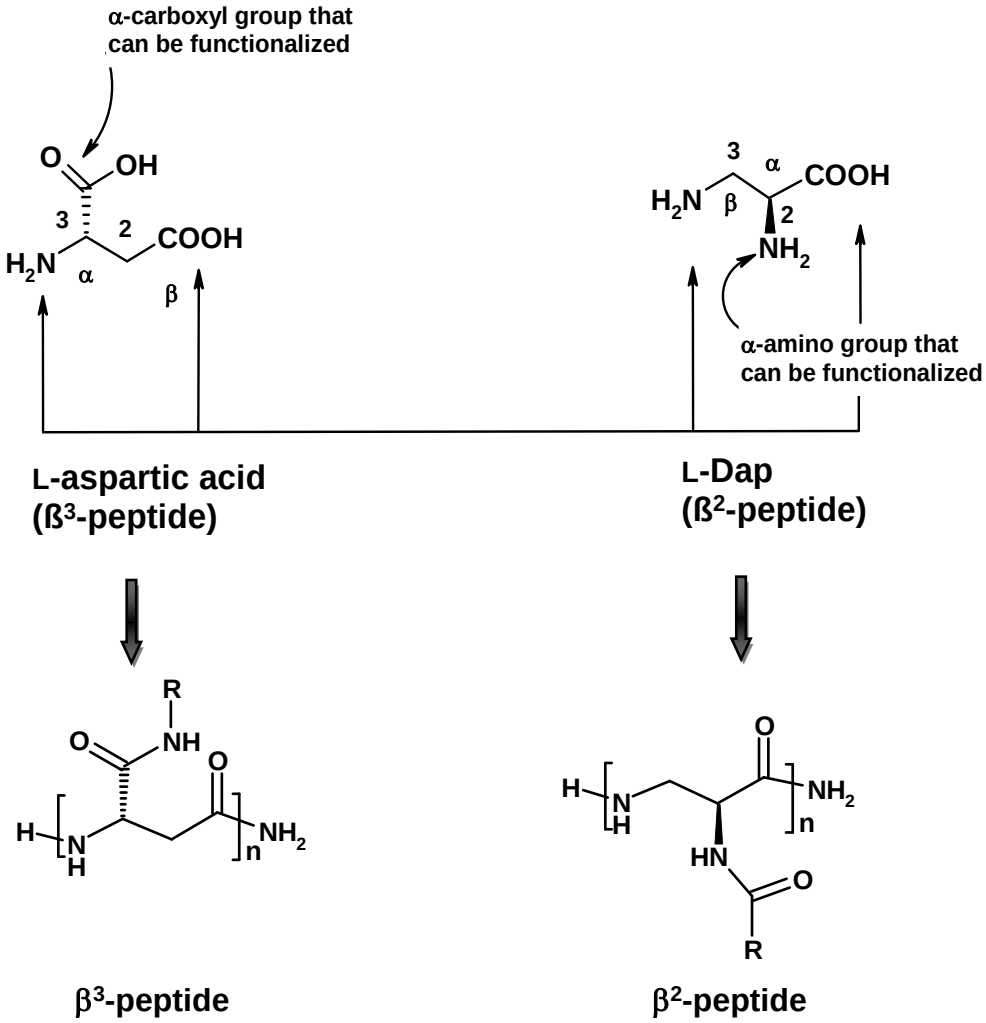

Figure 3.2. β^3- and β^2-peptides (bottom) derived from L-Aspartic acid (left) and β-amino-L-alanine (right) monomers (top), respectively.

The β-amino acids derived from L-Asp or L-Dap will be referred to as β-amido (β-am) amino acids due to the presence of extra amide bond in the side chain, whereas, β-amino acids synthesized from α-amino acids are denoted as β-homo (β-h) amino acids (**Figure 3.3**).

β3am-residue β3h-residue

Figure 3.3. Comparison of the chemical structures of β^3am-residues derived from L-Asp with the β^3h-residues derived by homologation of α-amino acids.

The objective of this study was to develop solid phase syntheses for β^3- and β^2-peptides from Fmoc-protected L-Asp and L-Dap monomers, respectively. As the β-peptides from these monomers have an additional amide in the side chain, the solution conformation of these *novel* peptides was evaluated using circular dichroim and NMR methods. Proteolytic stability of representative β^3- and β^2-peptides, as well as, a mixed α/β-peptide was also studied.

The above objectives were achieved by performing the following specific aims which are described in this chapter:

(i) Design, synthesis, and characterization of novel β-peptides (β^3 and β^2) from L-Asp and L-Dap monomers respectively,

(ii) Evaluation of solution conformation of β-peptides in TFE and water using circular dichroism and 2D NMR spectroscopy,

(iii) Design and synthesis of β^3-peptides for enhanced conformational stability. The conformation was studied using circular dichroism and 2D NMR spectroscopy,

(iv) Evaluation of proteolytic stability of β-peptides (β^2 and β^3) and a mixed α/β-peptide against proteolytic enzymes (pronase, trypsin, and elastase) and human serum, and

(v) Evaluation of cellular toxicity of representative β^3 and - β^2-peptides.

3.2 Results and Discussion

3.2.1 Design of β^3 and β^2- peptides from L-Aspartic acid and β- amino-L-Alanine monomers

As mentioned above, easily available L-aspartic acid monomers will be used for the stepwise synthesis of β^3-peptides with a wide variety of side chains (**Figure 3.4**, Top).[11] The α-carboxy group of L-aspartic acid is left free for the introduction of different substituents (to obtain heterooligomer) during the synthesis, whereas, the amino and β-carboxy groups are used for building the peptide backbone. The synthesis of mono-substituted β^2-peptides will be done similarly using β-amino L-alanine monomers (**Figure 3.4**, Bottom). Using this strategy, we designed representative β-peptides from both classes, namely, two heterooligomer β^3-hexapeptides (**1**, and **2**, **Figure 3.5**) with different side chain substitutions and three different β^2-hexapeptides, two heterooligomer with different side chain substitutions (**3**, and **4**) and a homooligomer **5**. In heterooligomeric β^3-peptides **1**, and **2** and β^2-peptides **3** and **4**, the different side chains were introduced after coupling of each monomer and deallylation of the side chain amino group in case of β^2- and carboxy group in case of β^3-peptide.

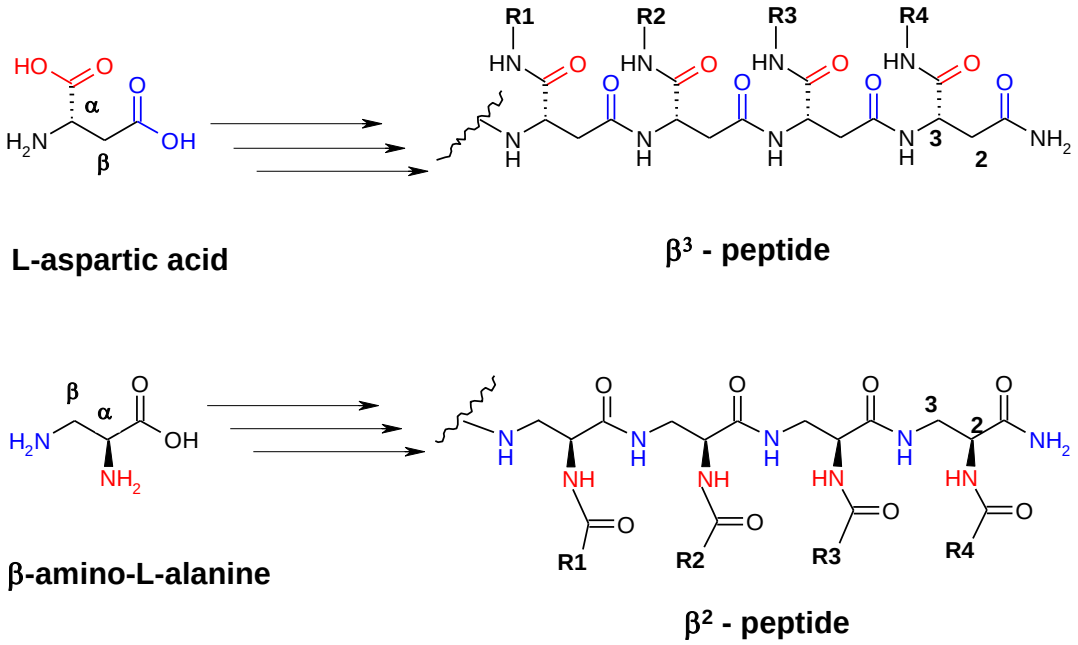

Figure 3.4. Stepwise addition L-aspartic acid and β-amino L-alanine to obtain mono-substituted ß^3-peptides (top) or ß^2-peptides (bottom), respectively.

In peptides **1**-**4,** one or two of the side chains were chosen to be charged to keep a balance between both the hydrophobic and the charged groups, to enhance solubility in an aqueous medium. β^3-peptides **1** and **2** are quite similar except residue 5 in **1** is lysine mimic (β^3-amK) whereas, it is a glutamic mimic (β^3-amE) in **2**. β^3-peptides **2** was synthesized to study the effect of intramolecular charge-charge interaction toward conformational stability. β^2-peptides **3** and **4** are also similar except residue 2. In peptide **4**, aromatic side chain was introduced at residue 2 instead of a charged side chain, to provide a convenient probe for determining the concentration of the peptide. β^2-Peptide **5** is homooligomer where the backbone was synthesized first, and all the side chain allyl protections were removed at the end, to study the effect of side chain amidic bonds on the conformational stability.

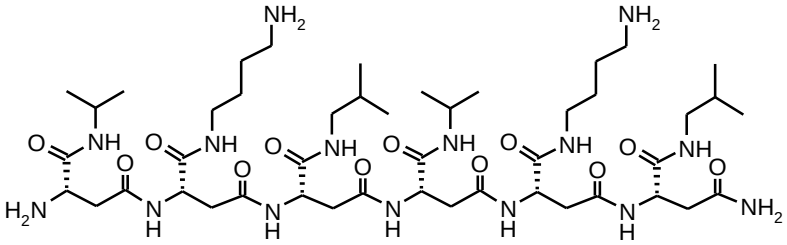

1

(1) NH_3-β³amV-β³amK-β³amL-β³amV-β³amK-β³amL-$CONH_2$

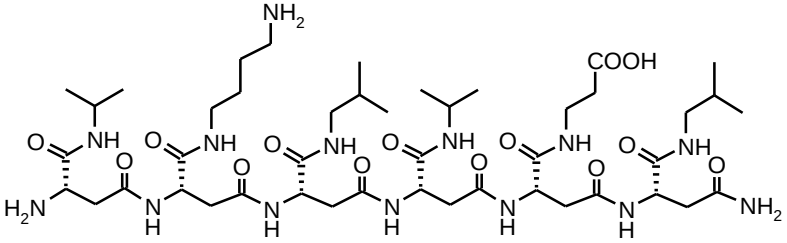

2

(2) NH_3-β³amV-β³amK-β³amL-β³amV-β³amE-β³amL-$CONH_2$

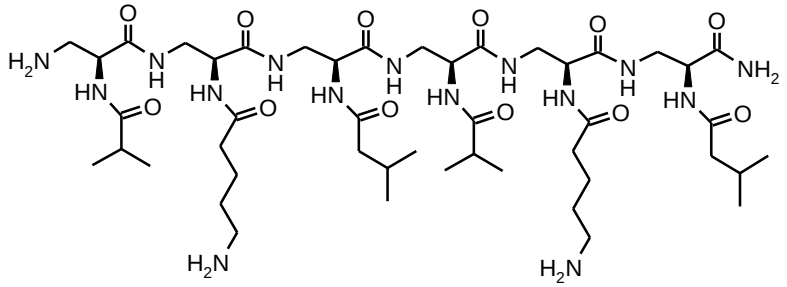

3

(3) NH_3-β²amV-β²amK-β²amL-β²amV-β²amK-β²amL-$CONH_2$

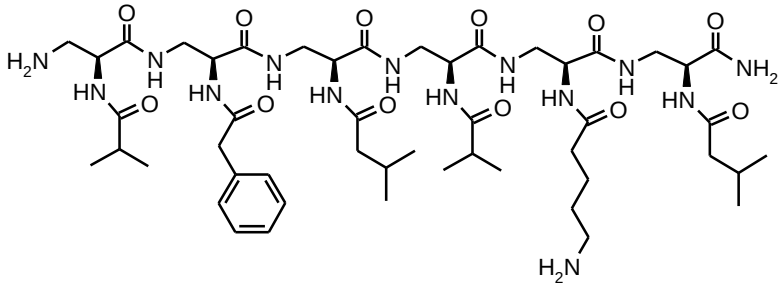

4

(4) NH_3-β²amV-β²amF-β²amL-β²amV-β²amK-β²amL-$CONH_2$

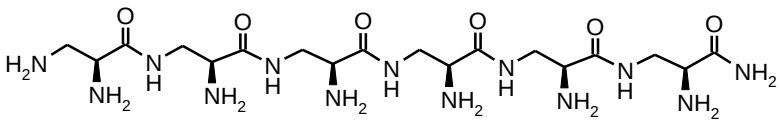

5

Figure 3.5. Chemical structure of β³- (**1**-**2**) and β²-hexapeptides (**3**-**5**).

3.2.2 Synthesis of Novel β^3 and β^2-peptides (1-5)

Synthesis of β^3-peptides

The backbone of β^3-peptides **1** (prepared previously by my lab-mate Reem Beleid)[12] and **2** was prepared from orthogonally protected L-aspartic acid, N^{α}-Fmoc-L-aspartic acid α-allyl ester, using BOP with HOBt as coupling agents on rink amide MBHA resin (**Scheme 3.1**). The reaction was monitored by the ninhydrin test. The side chain was deallylated by treatment with 0.08 equiv of $Pd(PPh_3)_4$ and 8 equiv of $PhSiH_3$ for 35 min three times followed by the introduction of the corresponding amine side chain using the same coupling reagents as mentioned above.

Scheme 3.1. General pathway of solid-phase synthesis of amino-substituted β^3-peptides.

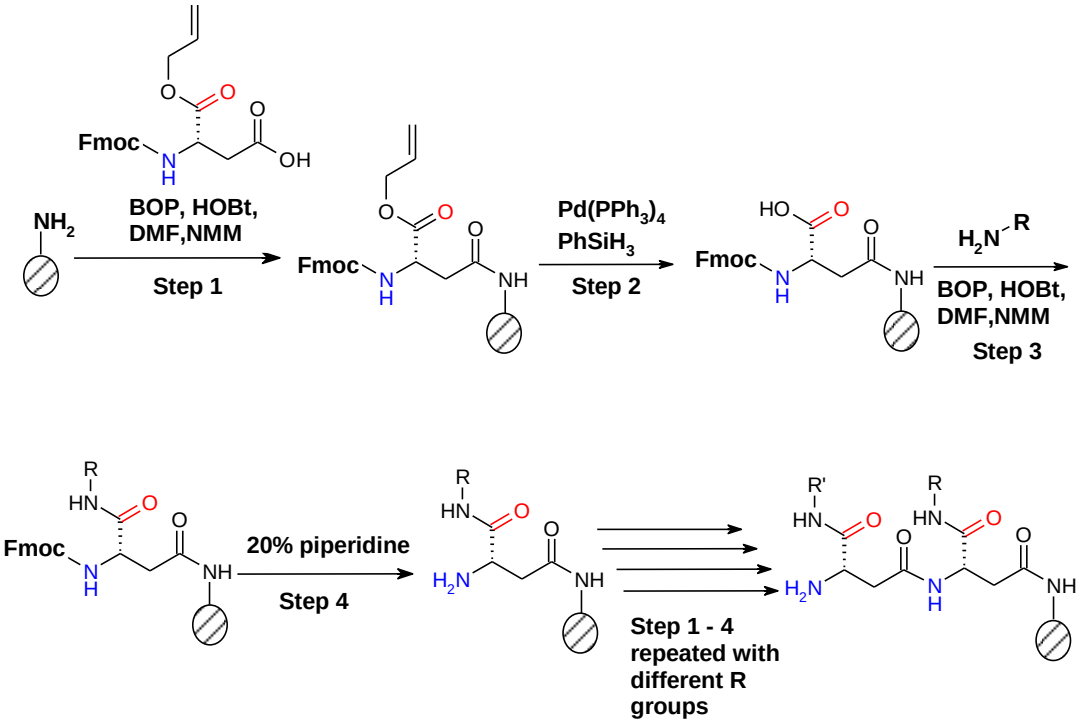

The four steps (**Scheme 3.1**), namely, coupling monomer, deallylation, coupling side chain amine, and Fmoc-deprotection, were repeated six times to obtain hexapeptide **2**. At the end of the synthesis, and after the removal of the terminal Fmoc group, β^3-peptide **2** was cleaved from the resin by treatment with TFA/H_2O/silane for 2 h at room temperature. Crude peptide was purified using analytical reversed-phase HPLC with an overall yield of 39%. The HPLC purification of **2** was difficult as the elution was sensitive to pH change and polarity of the solvent. Different gradient methods were tried for its separation. The best method found to purify **2** was using 15-27 % CH_3CN/H_2O for 50 min utilizing analytical HPLC column at flow rate 0.9 mL/min. Three peaks that eluted at 28.5-29.5, 30.4-31, and 31-31.8 minutes (**Figure 3.6**) were collected. Fraction 2 and 3 showed the correct mass, while highest purity of peptide **2** was found to be in fraction 3. The mass was found to be 1027.23 $[M+H]^+$, (calcd ($[M+H]^+$ 1027.00), as determined by MALDI-TOF mass spectrometry using α-cyano-4-hydroxycinnamic acid as a matrix (**Figure 3.7**). Peptide **2** was also present in fraction 1 as determined by mass spectrometry. However, fraction 1 contained mainly truncated peptide with mass of 741 m/z. This mass corresponds to the structure of a pentapeptide as shown in **Figure 3.8** . This impurity was expected as coupling of glutamic mimic side chain (H-βAla-OtBu) to carboxyl was found to be difficult. In contrast, coupling of several other amines, such as, isopropyl, isobutyl, and mono-trityl 1,4-diaminobutane acetic acid salt, occurred easily.

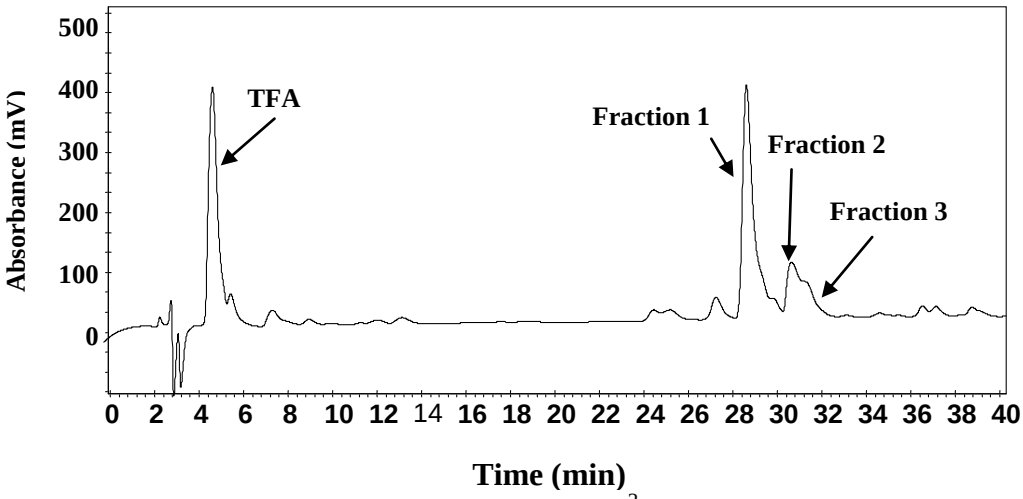

Figure 3.6. RP-HPLC chromatogram of crude β^3-hexapeptide **2** showing fractions 2 and 3 that contain peptide **2**.

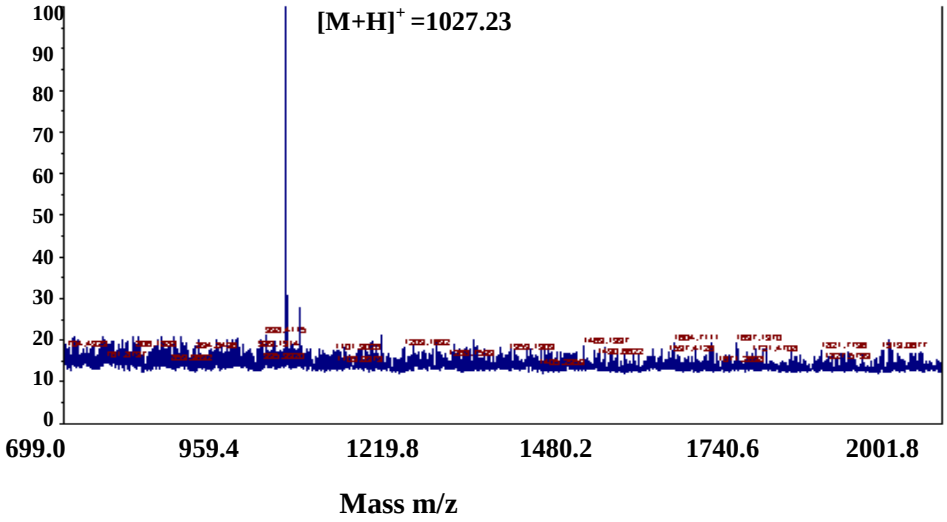

Figure 3.7. MALDI-TOF mass spectrum of pure β^3-hexapeptide **2**.

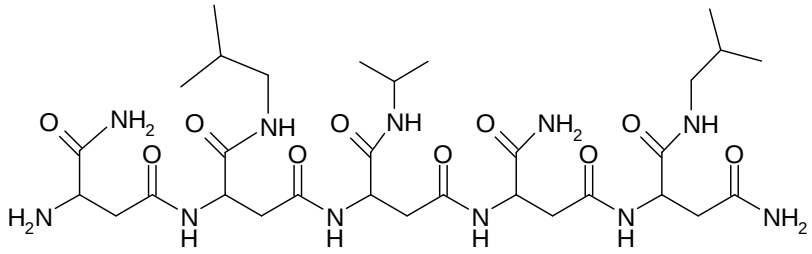

Figure 3.8. Truncated peptide obtained during synthesis of β^3-hexapeptide **2**.

Synthesis of β^3-amino acid monomers

Coupling of some amines to the side chain of the peptide was found to be difficult, during the stepwise addition of L-Asp monomers for β^3-peptide synthesis. Therefore, we decided to prepare β^3-monomers with different side chains (**Schemes 3.2** and **3.3**). These monomers can then directly couple to the growing peptide on the resin. To do so we developed two strategies to synthesize Fmoc β^3-amidoamino acids (**6**), (i) solution synthesis starting from α-Fmoc-L-aspartic acid-(OtBu), and (ii) solid phase synthesis using α-Fmoc-L-aspartic acid α-allyl ester. Solution phase synthesis was done by coupling appropriate amine to α-carboxyl of α-Fmoc-L-aspartic acid-(OtBu) in presence of BOP, HOBt and NMM (**Scheme 3.2**). The mixture was stirred at room temperature for 24 h, followed by cleavage of the tBu protection using TFA/H_2O/TIPS to give **6.** This method was found to be effective for synthesizing Fmoc β^3-amido amino acids which do not have acid sensitive side chain protections, such as, Fmoc β^3-amV (**7)**, and Fmoc β^3-amL (**8**) (**Figure 3.9**). The compounds prepared by this method were found to be pure as characterized by mass spectrometry, NMR and HPLC. The overall yield was 80-81%, and the products were used without further purification.

For the solid phase synthesis of Fmoc β^3-amido amino acids, α-Fmoc-L-aspartic acid α-allyl ester was first coupled to trityl resin in the presence of DIPEA for 2 h followed by deallylation using $Pd(PPh_3)_4$ and $PhSiH_3$ (3 x 35 mins) (**Scheme 3.3**). Subsequently side chain amine was coupled in the presence of BOP, HOBt and NMM for 5 h (once or sometimes twice) followed by

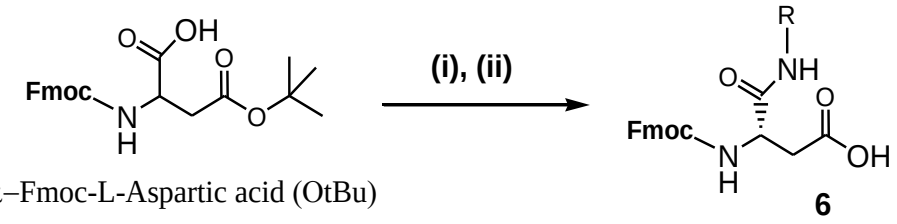

α–Fmoc-L-Aspartic acid (OtBu)

6

Scheme 3.2. Solution synthesis of Fmoc β^3-amido amino acids starting from α-Fmoc-L-aspartic acid-(OtBu).

Steps and Reagents: (i) Coupling of side chain amine in presence of BOP, HOBt and NMM stirring at room temperature for 24 h (ii) Cleavage of the tBu protection using TFA/H_2O/TIPS for 2 h**.**

cleavage of the monomer from the resin. The cleavage from resin was achieved using 50%TFA/DCM for 30 min for Fmoc β^3-amV (**7)**, and Fmoc β^3-amL (**8**). The overall yield for both was ~65%. For the cleavage of amino acids that had acid sensitive side chain protection, such as, Fmoc β^3-amE (**9**), and Fmoc β^3-amK amino acids (**10**) (**Figure 3.9**), TFE/DCM (20/80%) for 45 min was used. The overall yield was ~53% (**Scheme 3.3**). This method also provided highly pure monomers as revealed by the HPLC (**Figure 3.10**). The low yield could be due to the low loading efficiency of the Fmoc-L-aspartic acid α-allyl ester on the trityl resin.

Scheme 3.3. Solid Phase Synthesis of Fmoc β^3-amido amino acids starting from α-Fmoc-L-aspartic acid α-allyl ester.

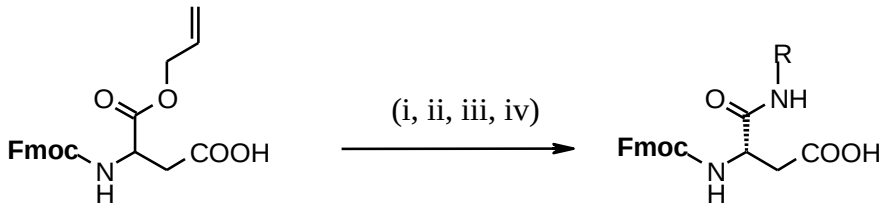

α-Fmoc-Aspartic acid -α-allyl ester

6

Steps and Reagents: (i) Coupling to trityl resin in presence of DIPEA for 2 h, (ii) Deallylation using $Pd(PPh_3)_4$ and $PhSiH_3$ (3 x 35 mins) (iii) Coupling of side chain amine in presence of BOP, HOBt and NMM for 5 h (iv) Cleavage of the monomer from the resin with 50 % TFA or (20/80 %)TFE/DCM.

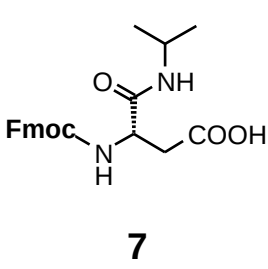

7

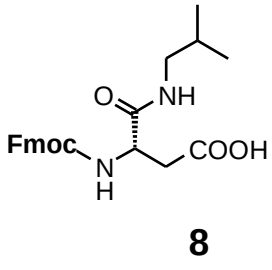

8

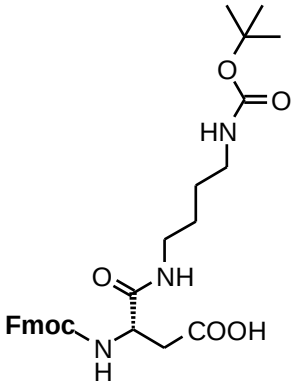

9

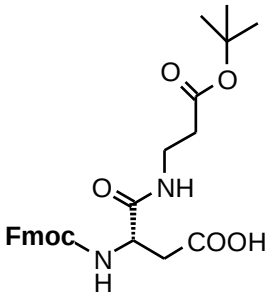

10

Figure 3.9. Structures of β^3-amino acid monomers **7-10**.

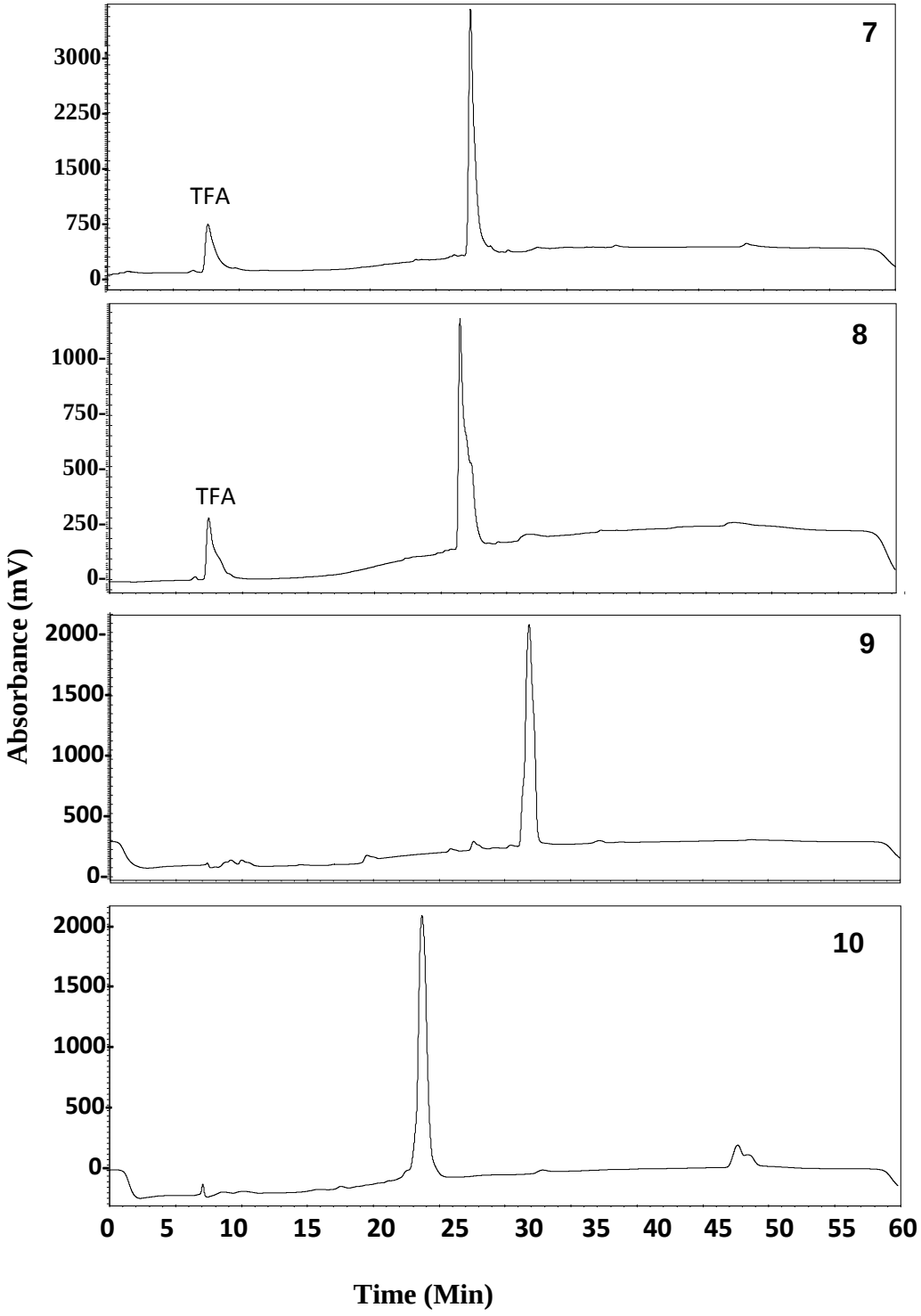

Figure 3.10. RP-HPLC traces of crude β^3-amido amino acid monomers **7-10** using 30-100% IPA/H_2O in 35 min with flow rate, 2 mL/min.

Synthesis of β^2-peptides 3-5

β^2-peptides **3-5** were synthesized utilizing Fmoc/allyl combined solid-phase strategy using the N^{α}-Alloc-N^{β}-Fmoc-L-diaminopropionic acid **(16)**. Monomer **16**, however, was not commercially available. The synthesis of **16** was done using commercially available Boc-L-Asn and is described in the next section. As with β^3-peptides, here also the Fmoc protection was used to build the backbone of the peptide and allyl protection was used to introduce the side chain functionalities.[11] The backbones of β^2-peptides **3** and **4** were prepared from orthogonally protected L-DAP **16** using BOP with HOBt as coupling agents on rink amide MBHA resin (**Scheme 3.4**). For heterooligomeric β^2-peptides **3** and **4**, the different side chains were introduced after coupling each monomer. The coupling reaction of the monomer was monitored by the ninhydrin test. After coupling of the monomer, deallylation of the side chain amino group was performed. To achieve complete deallylation of the side chain amine, the reaction was optimized by varying (i) the amount of palladium catalyst used, (ii) the length of the reaction time, and (iii) the number of times the reaction was repeated (**Table 3.1**) Treatment with 0.08 equiv of $Pd(PPh_3)_4$ and 8 equiv of $PhSiH_3$ for 35 min and repeating the reaction twice led to complete deallylation as confirmed by the analytical HPLC and electrospray mass spectrometry. It is evident from **Table 3.1** that both the concentration of the catalyst as well as the contact time play critical role in the deallylation step.

Scheme 3.4. General pathway of solid-phase synthesis of acyl-substituted β^2-peptides.

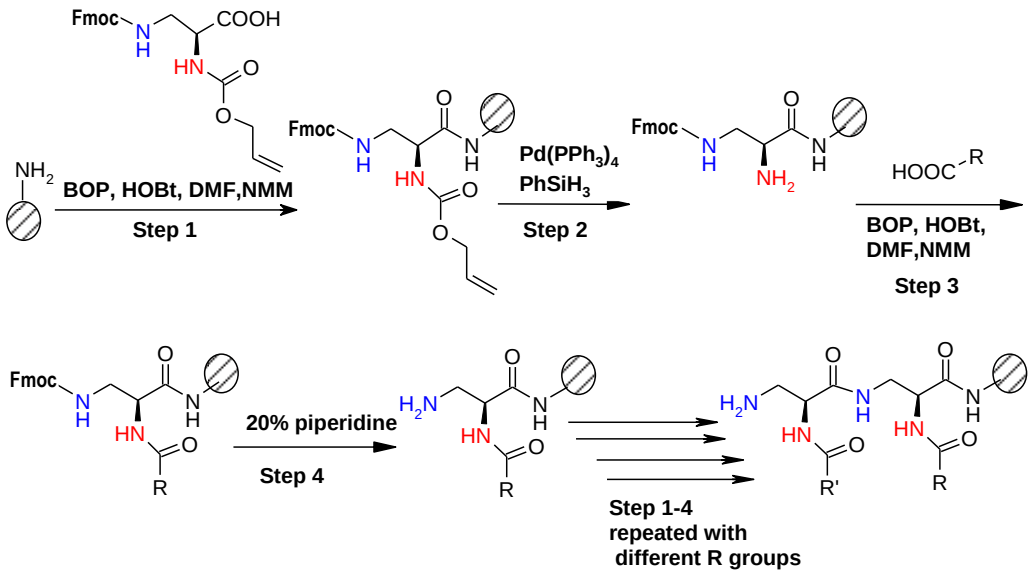

Table 3.1: Deallylation of the Alloc group from side chain amine.

Time (min) x the number of repeats	Equivalents of ($Pd(PPh_3)_4$	Deallylation (%)
15x3	0.08	28
15x3 &10x2	0.08, 0.16	88
20x3	0.16	47
20x4	0.16	70
30x3	0.16	89
32x1	0.16	26
32x2	0.16	65
32x3	0.16	94
35x3	0.16	>99
35x3	0.08	>99

Deallylation (%) was determined from the HPLC fraction collected using 20% ACN/water over 30 min flow rate, 1 mL/min.

Steps 1-4 were repeated to reach the desired peptide length (**Scheme 3.4)**. At the end of the synthesis, Fmoc group was removed using 20% piperidine in DMF (2 x 16 min), with no detection of any remaining Fmoc group. This is an

advantage for the β-amido peptides, as β-peptides synthesized from β-h-amino acid need longer Fmoc deprotection times, and usually require the use of expensive deprotection agents, such as, DBU at high temperature (60 °C).[13] Finally, peptide **5** was synthesized using the same strategy as **3** and **4** except the complete backbone was synthesized first and at the end all the alloc protections were removed simultaneously as shown in **Scheme 3.5**.

Scheme 3.5. Solid-phase synthesis of β^2-peptide **5**.

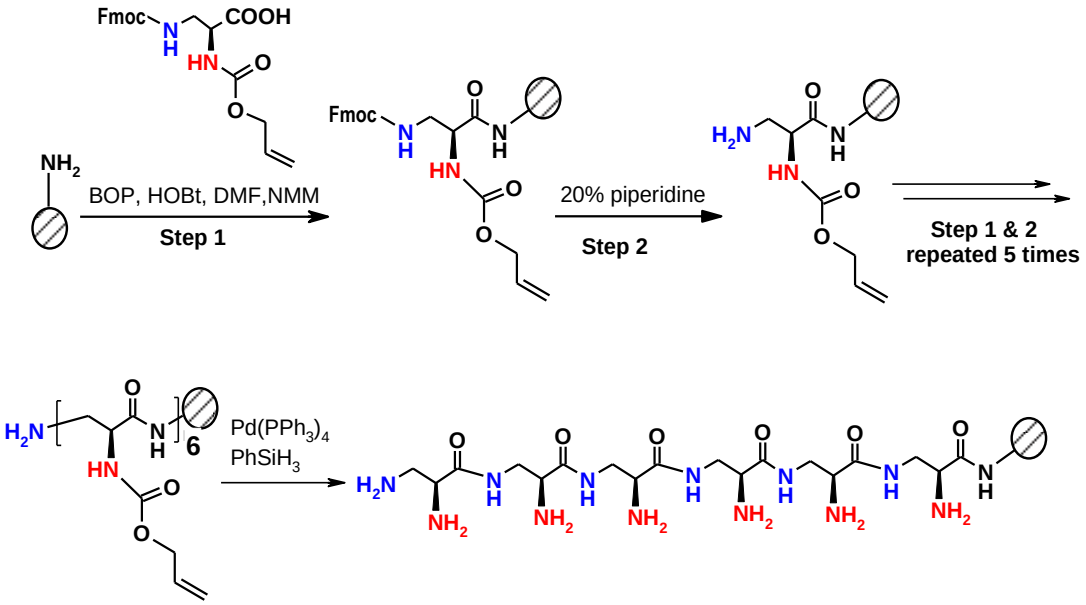

β^2-peptides **3-5** were cleaved from the resin by treatment with TFA/H_2O/TIPS for 2 hours. The crude peptides were reconstituted in 30% CH_3CN /water and purified using semi-preparative RP- HPLC to give pure peptides. The overall yields of peptides **3, 4,** and **5** were found to be 39%, 42% and 92%, respectively. The identity and purity of the peptides were assessed by

C_8 analytical HPLC (**Figure 3.11**) and mass spectrometry. In general, peptides were found to be >95% pure.

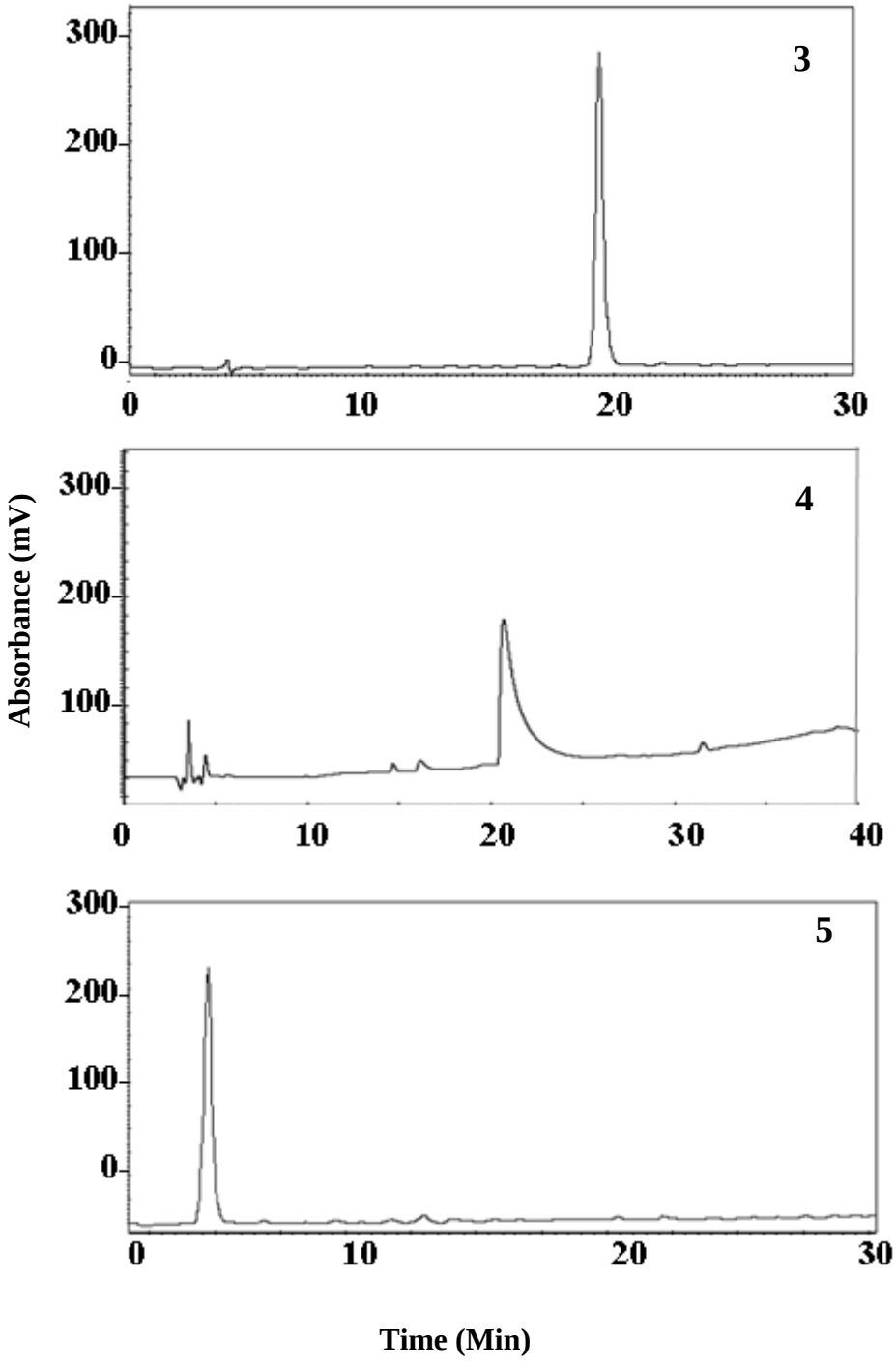

Figure 3.11. RP-HPLC chromatogram of β^2-hexapeptide **3**, **4**, and **5**.

Synthesis of another β^2-hexapeptide (**11**) was attempted; however, could not be completed. The main problem faced during the synthesis of this peptide was at the step of coupling methyl side chain using acetic anhydride. Several attempts to add methyl side chain were tried, such as, repeated coupling with acetic anhydride in the presence of 0.8 M LiCl in NMP yielded less than 10% dipeptide. Next, instead of acetic anhydride, acetic acid or acetyl chloride were used to introduce methyl side chain. However, no improvement in the coupling was detected.

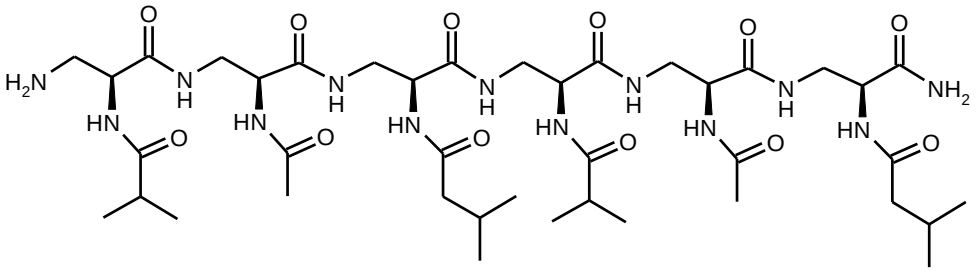

11

Synthesis of N^{α}-Alloc-N^{β}-Fmoc-L-diaminopropionic acid (16)

Most reported routes to β^2-amino acids involve chiral auxiliaries, the removal of which requires basic or acidic conditions. Epimerization at the α-position can arise under basic conditions. The acidic removal conditions preclude the use of acid-labile protecting groups for side-chain functionality, like Boc, which are convenient when Fmoc-based oligomer synthesis is planned. We present a new route to β^2-amino acids that offers significant advantages relative to the existing methods with the presence of orthogonal protection which enables the buildup of the peptides as well as the introduction of different side chain. Our approach is outlined in **Scheme 3.6.** As mentioned earlier, **16** was not commercially available. It was synthesized in four steps. The first 3 steps have

been reported previously,[14] starting with α-amino acid, Boc protected L-asparagine **12** as shown in **Scheme 3.6**. Boc-L-Asn (**12**) was subjected to rearrangement, in the presence of iodosobenzene, yielding N^{α}-Boc-2,3-diaminopropionic acid (**13**). Fmoc protection of the *β*-amino group was performed using Fmoc-Cl in presence of Na_2CO_3 and water /dioxane mixture for 1 h at 0 °C followed by another hour at room temperature to yield N^{α}-Boc-N^{β}-Fmoc-2,3-diaminopropionic acid (**14**). The Boc protection from the α-amino group was removed by treatment of **14** with TFA in presence of scavengers TIPS and water for 2 h to give N^{β}-Fmoc-2, 3-diaminopropionic acid (**15**).

Scheme 3.6. Solution-phase synthesis of orthogonally protected L-diamino propionic acid **16.**

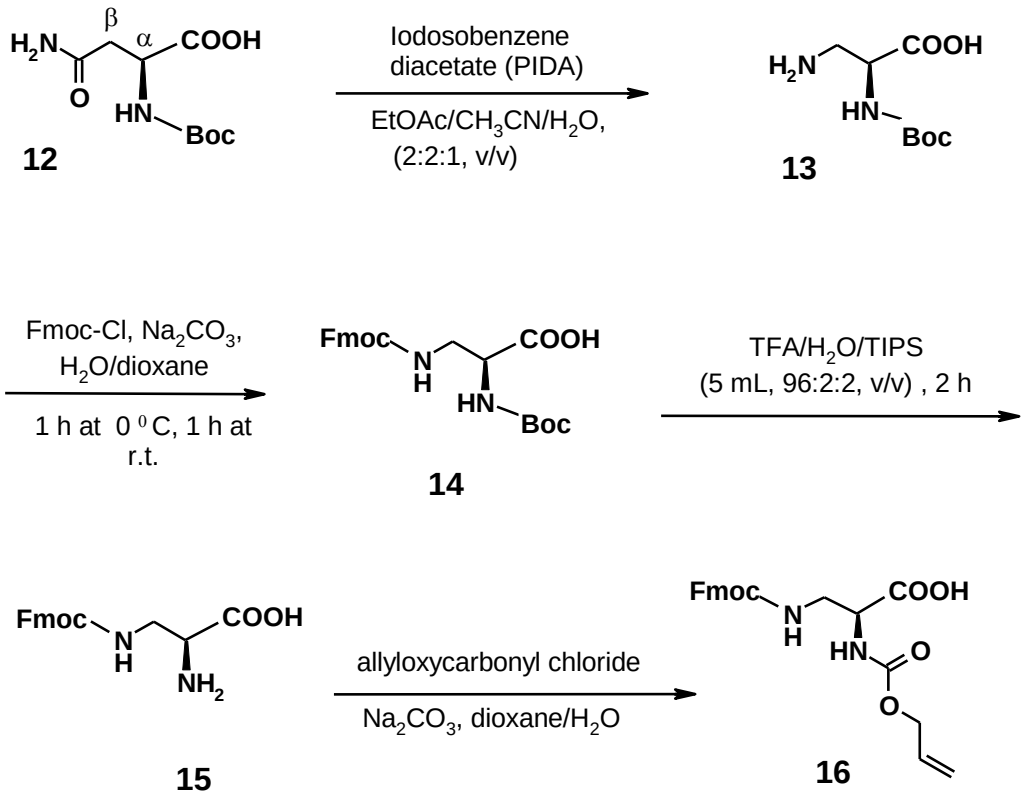

Finally, the α-amino group in **15** was protected using allyloxycarbonyl chloride to give the orthogonally protected **16** in overall 54% yield. The α-amino group protected with Alloc in **16** allows direct introduction of different side chains to obtain the Fmoc-β^2 amido amino acids. For instance, isobutyrl chloride or isovaleryl chloride was reacted with **15** to give β^2-amV and β^2-amL, respectively.

3.2.3 Solution Conformation of β-Peptides 2-5 using Circular Dichroism

The ability of β-peptides **1-5** to adopt an ordered secondary structure was evaluated by Circular Dichroism (CD) spectroscopy. CD is frequently used for analyzing α-peptidic structures. CD in the far-UV region (190-250 nm) is commonly employed to examine secondary structures of α-amino acid peptides and proteins.[15] The signal in this region arises largely from the backbone amide. Information obtained in this way is of low resolution, but structural conclusions can be drawn in the case of α-peptides as CD signals have been correlated with NMR structure. However, for β-peptides, the correlation between CD pattern and secondary structure is not yet fully established. For certain β-peptides, CD spectra have been correlated with secondary structures when used in combination with other spectroscopic techniques.

The CD spectroscopy for β^3-peptides **1-2** and β^2-peptides **3-5** was evaluated in different solvents, such as, TFE, methanol, water, and phosphate buffer (pH 7.4) (**Figures 3.12** and **3.13**). Peptides were studied at different concentrations (100-500 μM), and the CD spectra were found to be independent

of concentration, suggesting that no aggregation in this concentration range. The CD spectra of **1** display a marked difference in organic (TFE and methanol) and aqueous solvents (water and phosphate buffer). In TFE, there is a minimum at 214 nm (θ = -20 X 10^3) and a maximum at 204 nm (**Figure 3.12 A**). Similarly, in methanol there is a minimum at 214 nm; however, this peak is not present in aqueous solvents. Organic solvents such as TFE and methanol have been suggested to be conducive to secondary structure formation and the CD spectra of **1** suggest a gain of some structural feature in organic solvents. The CD spectra of monosubstituted β^3-peptides typically display a negative minimum at 214-220 nm and a positive maximum near 200 nm that have been ascribed to 14-helical structure.[16] β^3-Peptide **1** is different from the previous reported β-peptides as it contains an extra amide group in the side chain and the CD of this peptide measures the collective signal of all the amides, including those within the side chain making the spectrum difficult to interpret. In this context, it is of particular interest to note that Fernandez-Santin et al. observed a helical structure for a β^3-polypeptide, poly(α-isobutyl- L-aspartate), made by polymerization of α-isobutyl-L-aspartate based on X-ray diffraction and molecular modeling studies.[10] This also supports our conjecture regarding the helical nature of β^3-peptides from L-aspartic acid.

Surprisingly, peptide **2** in TFE displayed a big minimum ~207 nm which is shifted from the normal 14-helix around 214 nm (**Figure 3.12 B**). In water, the minimum was further shifted to ~202 nm. The CD results suggest that either peptide is folded by salt bridge interaction and pH in different solvent is giving

slight shift in the minima or this could be an indication of aggregation of the peptide. Clearly, CD is not able to interpret the solution conformation of peptide **2**. NMR spectroscopy will be used to elucidate secondary structure of **2**.

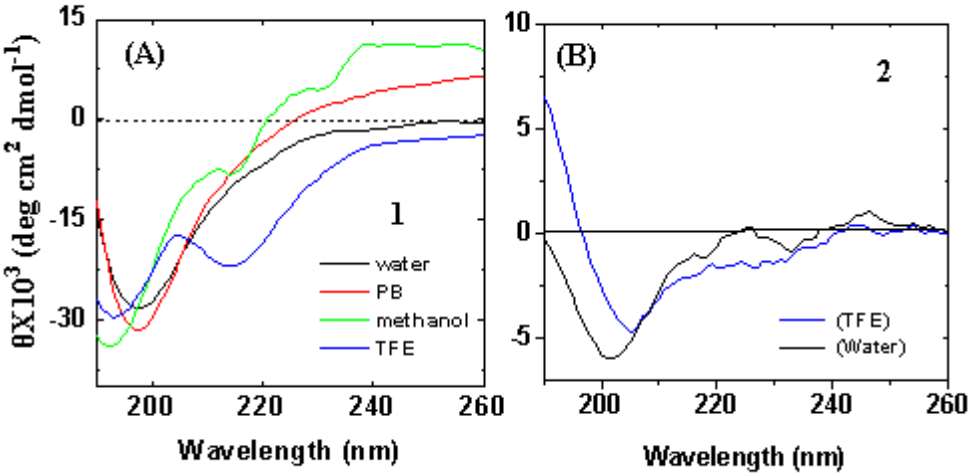

Figure 3.12. Circular dichroism spectra of (A) β^3-peptide **1** in water, phosphate buffer (1 mM, pH 7.4), methanol, and TFE, and (B) β^3-peptide **2** in water and TFE at 25 °C.

The CD spectrum of β^2-hexapeptides **3-5** was studied at different concentrations (100-1000 μM), and once again the CD spectra were found to be independent of concentration, suggesting that no changes in aggregation state. Typically, 14-helical β^2-peptides composed of acyclic amino acid residues display a common CD signature with a minimum around 220 nm, and the other extremum of opposite sign at 195 nm. The CD spectrum of β^2-hexapeptides **3** and **4** in TFE display a minimum around 224 nm and a maximum at 208 nm **(Figure 3.13**). For peptide **3 (Figure 3.13 A**) in methanol, the broad minimum at ~230 nm is much less intense; however, at 208 nm, a strong positive maximum is observed. The intensity of peaks in water and phosphate buffer is reduced substantially.[11]

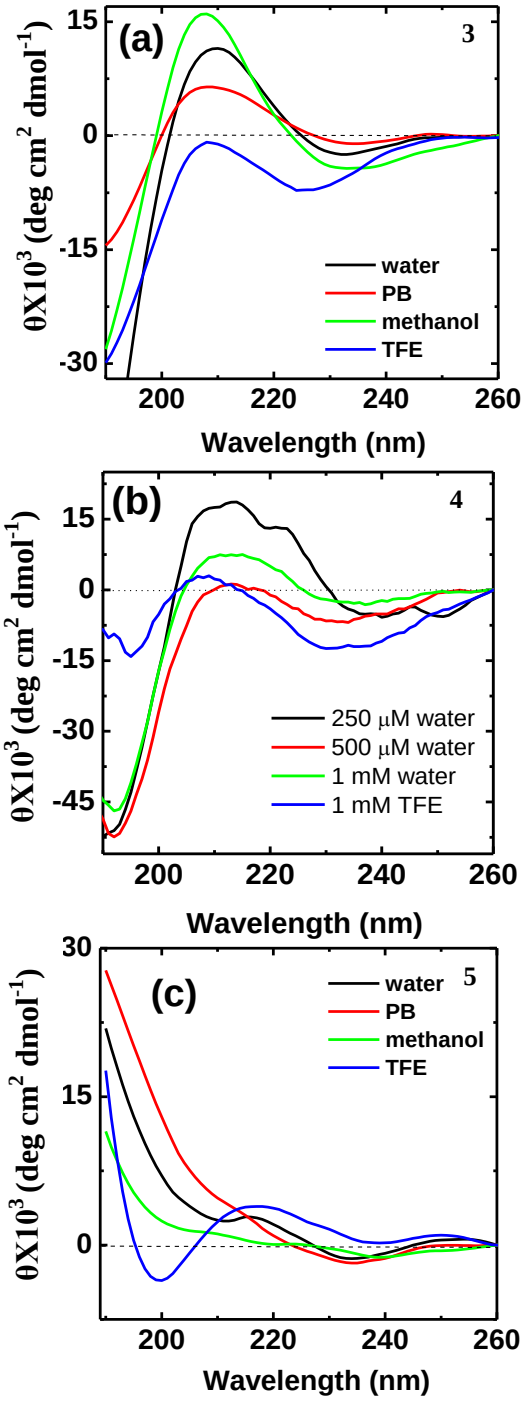

Figure 3.13. Circular dichroism spectra of β^2-peptides **3** (a), **4** (b), and **5** (c) in water, phosphate buffer (1 mM, pH 7.4), methanol, and TFE at 25 °C.

Based on the conformational studies of known β-peptides it has been found that, β^2-peptides form less stable helix as compared to β^3-peptides with the same side chains.[4,17,18] Lelais et al have shown that for β^2-peptides, in order to observe a 3_{14}-helical CD-pattern of comparable intensity to β^3-peptides, the MeOH solution of the β^2-hexapeptide had to be cooled to -20°C.[18] The difference in stability might be due to smaller steric hindrance between NH and a neighboring substituent (R) in β^3-residues, while big steric hindrance of CO and a neighboring R group in β^2-residues. This could lead to a weakening of the intramolecular H-bonds.[17, 19] The β^2-hexapeptide **5** with free amino groups in the side chain seems to be essentially unstructured in all the solvents as no minima are observed between 210 and 230 nm (**Figure 3.13 C**). This could be due to the interruption of the backbone hydrogen bonding by the side chain amino group and destabilization of the structure. The β^2-peptides described here are more polar than previously reported β-peptides with similar side chains due to the extra amide bond in the side chain. The CD spectra obtained here cannot be directly compared to β-peptides from β-h-amino acids due to the presence of an additional side chain amide bond in **3** and **4** that also contribute to the spectrum. Therefore, high-resolution structures will be required to fully interpret the CD results.

3.2.4 Solution Conformation of β-Peptides 2-5 using NMR Spectroscopy

Previous 1D and 2D NMR studies in our lab showed that β^3-hexapeptide **1** forms a helical structure in TFE and one major conformational isomer is present in solution.[23] The NOESY spectrum showed multiple long-range CαH(*i*)

CβH(*i*+3) NOEs which are a hallmark of 14-helical secondary structure.[20] A three-dimensional structure of **1** showed that **1** forms a right-handed 14-helical structure in TFE with a radius of 2.6 Å and 4.69 Å rise/turn.[12,23]

1D NMR of β^3-peptide **2** in TFE showed a big triplet in the amidic region which interfered with the elucidation of the compound's amidic protons (**Figure 3.14,** Top). It is suspected that peptide **2** may contain an impurity of low molecular weight that could not be detected by mass, and is of relative similar polarity which makes it elute with the peptide at the same retention time during HPLC purification.

1D NMR of β^2-peptides **3** and **4** allowed assignment of all the protons. However, the backbone and the side chain amide peaks were overlapping and could not be resolved by 1D NMR (**Figure 3.14,** Bottom). Because of the broad lines resulting from aggregation at concentrations necessary for NMR analysis, sequential assignments could not be obtained. All NMR experiments were done at McGill University (Quebec/Eastern Canada High Field NMR Centre, Montreal, Quebec) in collaboration with Dr. Tara Sprules.

For β^2-peptide **5,** complete assignments were obtained from the 1D NMR analysis. 2D NMR was used to elucidate any secondary structure information. **5** did not show any sign of folding which matched the CD data for this peptide. These results suggest that β^2-peptides with additional side chain amide does not help in stabilizing the secondary structure of β^2–peptides compared to β^2–peptides made from homo β^2-amino acids.[11]

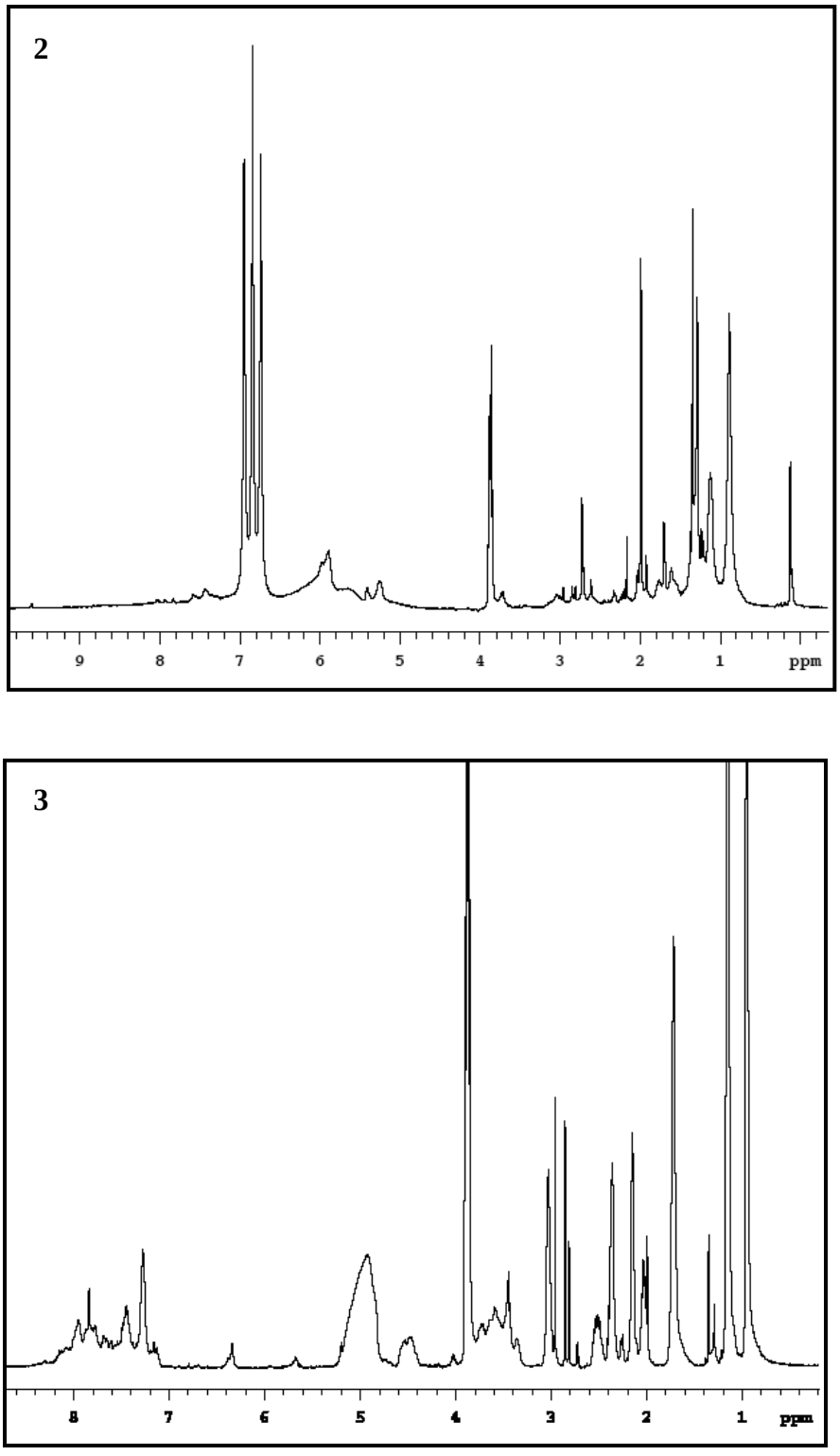

Figure 3.14. ^{1}H-NMR (500 MHz) spectrum of β^{3}-peptide **2** and β^{2}-peptide **3** in CF_3CD_2OH.

From our and previous studies, it seems that β^2-amino acid or small peptide fragments could be of great value when used in mixed peptides such as α/β^2-peptide. α/β^2 mixed peptides may be able to obtain specific conformation as was the case in somatostatin analogue.[4]

3.2.5 Enhancement of Helical Conformation in β^3-Peptides from L-Aspartic acid by Salt Bridge Effect

14-Helix of β-peptides is stabilized by the hydrogen bond between the protons at NH position i and the carbonyl group at i+2 (**Figure 1.17**). Examination of the top view of the helix indicates that the side chains of residues i and i+3 are located nearly on the top of each other (**Figure 1.18**). Several strategies to stabilize the 14-helical secondary structure of β-peptides in water have been developed. Some of these strategies include salt bridge or lactam formation between complementary charged i/i+3 side chains, as well as introduction of cyclic residues such as *trans*-2-aminocyclohexanecarboxylic acid. Presence of positively and negatively charged side-chains at positions *i* and *i+3* also help stabilize secondary structure especially in aqueous environment as well as ensure high water solubility.[21,22]

The new class of β^3-peptides fold to form 14-helical structure in TFE as mentioned earlier in Section 3.2.4.[11] A representative β^3-peptide **1** forms a right-handed 14-helical structure in TFE.[11,23] In contrast, the reported β^3-peptides formed from β^3-homoamino acids form left-handed 14-helices.[24] Right-handed 14-helix seems to be a better mimic of right-handed α-helix of α-peptides. Although we are starting to understand some of the factors influencing the folding

of these molecules, much work remains until we are able to correctly predict how such sequence of our new building blocks will fold, especially in aqueous media.

A number of analogues of **1,** (**18-21**), were designed and synthesized to stabilize the 14-helical conformation by introduction of salt bridge at positions i and i+3 (**Figure 3.15**). Also, a β^3-peptide **17** was synthesized from β^3-h amino acids with the same side chains as **1** (**Figure 3.15**). Peptide **17** was prepared to compare the 14-helical structures in **1** and **17**. Peptides **18**, **19**, and **20** are tetramer, pentamer, and hexamer with similar sequences. Peptides **19** and **20** have additional charged side chain for the formation of salt bridge. Further, for each of the sequence, the side chain with amine group was either a mimic of Lysine (analogues a) or Ornithine (analogues b). This was done to study the effect of side chain length in the formation of salt bridge. Finally, peptide **21** contains 4 residues with charged side chains to allow formation of two salt bridges. In all peptides, at least one side of the helix is covered by aliphatic side chains to allow for intramolecular hydrophobic interactions.

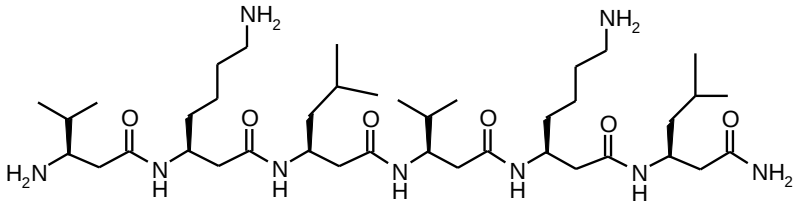

17

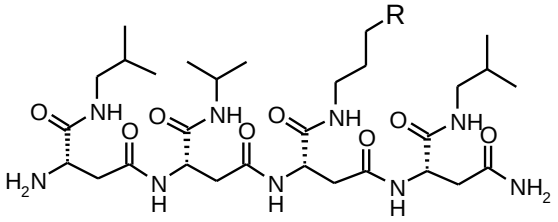

18

a) R = CH_2NH_2
b) R = NH_2

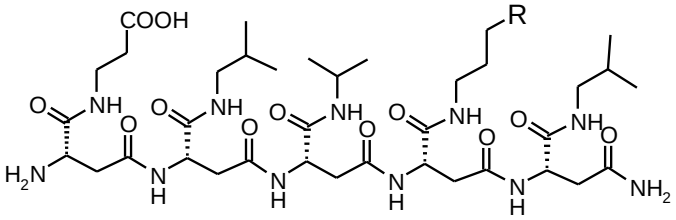

19

a) R= CH_2NH_2
b) R= NH_2

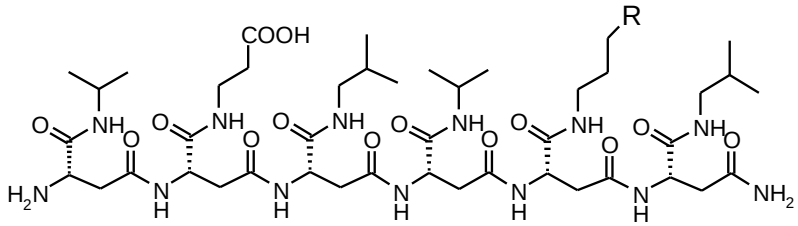

20

a) R =CH_2NH_2
b) R =NH_2

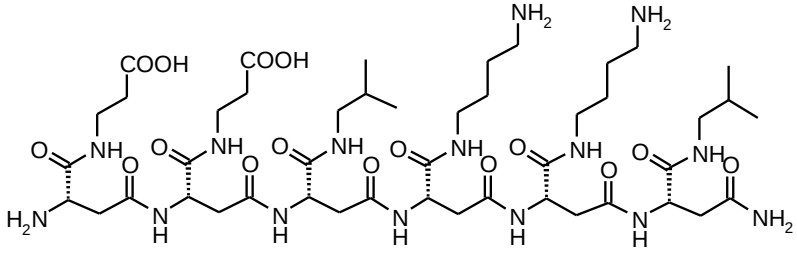

21

Figure 3.15. Structures of the β^3-peptides **17**, and **18-21** derived from β^3- homo and β^3-amido residues, respectively.

The side chain lengths can affect the stability of the salt bridge in helical conformations in aqueous environment.[21,25] In addition, the placement of a

negatively charged (side chain) amino acid at the N-terminus has been found to stabilize the peptide macrodipole.[25] Whereas, a negatively charged amino acid at the C-terminus does not stabilize the peptide macrodipole in case of α-peptide while the opposite is correct for β-peptide. In some other studies by Alana Schepartz and coworkers, they found that salt bridge formation is more stabilized by shorter side chain rather than longer one and the helical macrodipole play an important role in stabilizing β-peptide secondary structure in aqueous environment.[25] The new analogues (**18**-**21**) designed will hopefully shed some light with respect to the folding of these novel β^3-peptides in solution.

3.2.5.1 Solid Phase Synthesis of β^3-Peptide 17

Peptide **17** was synthesized following the standard Fmoc-SPPS using literature procedure.[5] Commercially available β^3-amino acids were coupled using BOP with HOBt on rink amide MBHA resin (**Scheme 3.7**). At the end of the synthesis, and after the removal of the terminal Fmoc group, β^3-peptide **17** was cleaved from the resin using TFA/H_2O/silane at room temperature for 2 h.

Crude peptide was purified using semipreparative RP-HPLC prior to characterization by mass spectrometry (**Table 3.2**) and analytical HPLC (**Figure 3.16 A**). A crude yield of 89% was obtained which contained both the peptide with and without the Fmoc group. Longer deprotection times for the final Fmoc group deprotection were required. Even after deprotection for three times (15 min each), about 50% of the peptide was protected with Fmoc.

Scheme 3.7. SPPS of β^3-peptide **17.**

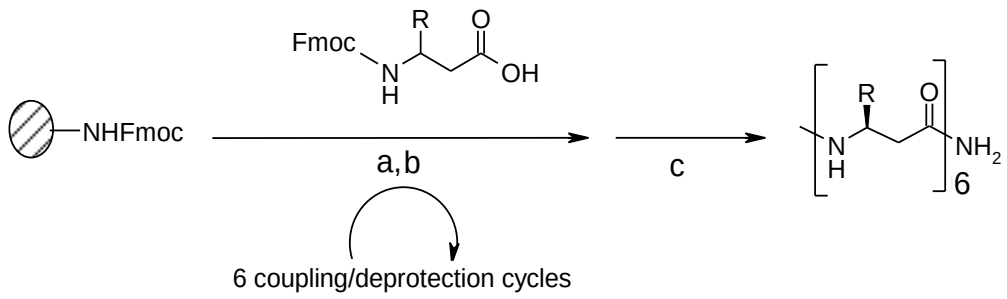

Steps and Reagents: (a) 20% piperidine/DMF (3x15 min); (b) Fmoc-β^3hX-OH (2 equiv), BOP (2 equiv), HOBt (2 equiv), NMM (4.5 equiv), DMF, 3.5 h; (c) TFA-TIPS-H_2O 96:2:2 (2 h).

3.2.5.2 Solid Phase Synthesis of β^3-Peptides 18-21

β^3-peptides **18-21** were prepared from orthogonally protected L-aspartic acid, N^{α}-Fmoc-L-aspartic acid α-allyl ester, using BOP with HOBt on rink amide MBHA resin as described before (Section 3.2.2).[11] Crude peptides were purified using semipreparative RP-HPLC prior to characterization by electrospray and/or MALDI-TOF mass spectrometry and analytical HPLC (**Table 3.2** and **Figure 3.16**). Peptides were obtained in relatively high yield due to the use of β^3-amido amino acid monomers instead of orthogonally protected L-aspartic acid.

Table 3.2: Characterization of β^3-peptides **17**-**21**.

Peptide #	Mass[M+H]$^+$ Observed (Calcd.)	HPLC Solvent purification	Elution time(min)	Flow rate (mL/min)	Crude yield (%)
17	782.88 (782.61)	20-65 % CH_3CN/H_2O in 25 min	16	2	89
18a	699.78 (699.44)	12-20 % CH_3CN/H_2O in 25 min	29.5	2	62
18b	685.30 (685.42)	12-20 % CH_3CN/H_2O in 25 min	30	2	53
19a	885.76 (885.50)	12-45 % CH_3CN/H_2O in 30 min	21	2	72
19b	871.77 (871.42)	19-28 % CH_3CN/H_2O in 23 min	22	2	54
20a	1041.6 (1041.20)	19-28 % IPA/H_2O in 30 min	23	1.5	81
20b	1027.85 (1027.58)	19-40 % CH_3CN/H_2O in 23 min	21.5	2	82
21	1100.41 (1100.58)	15-30 % IPA/H_2O in 30 min	16.7	1.5	90

HPLC column used was Vydac C18 semi-preparative (1 x 25 cm, 5 μm) column.

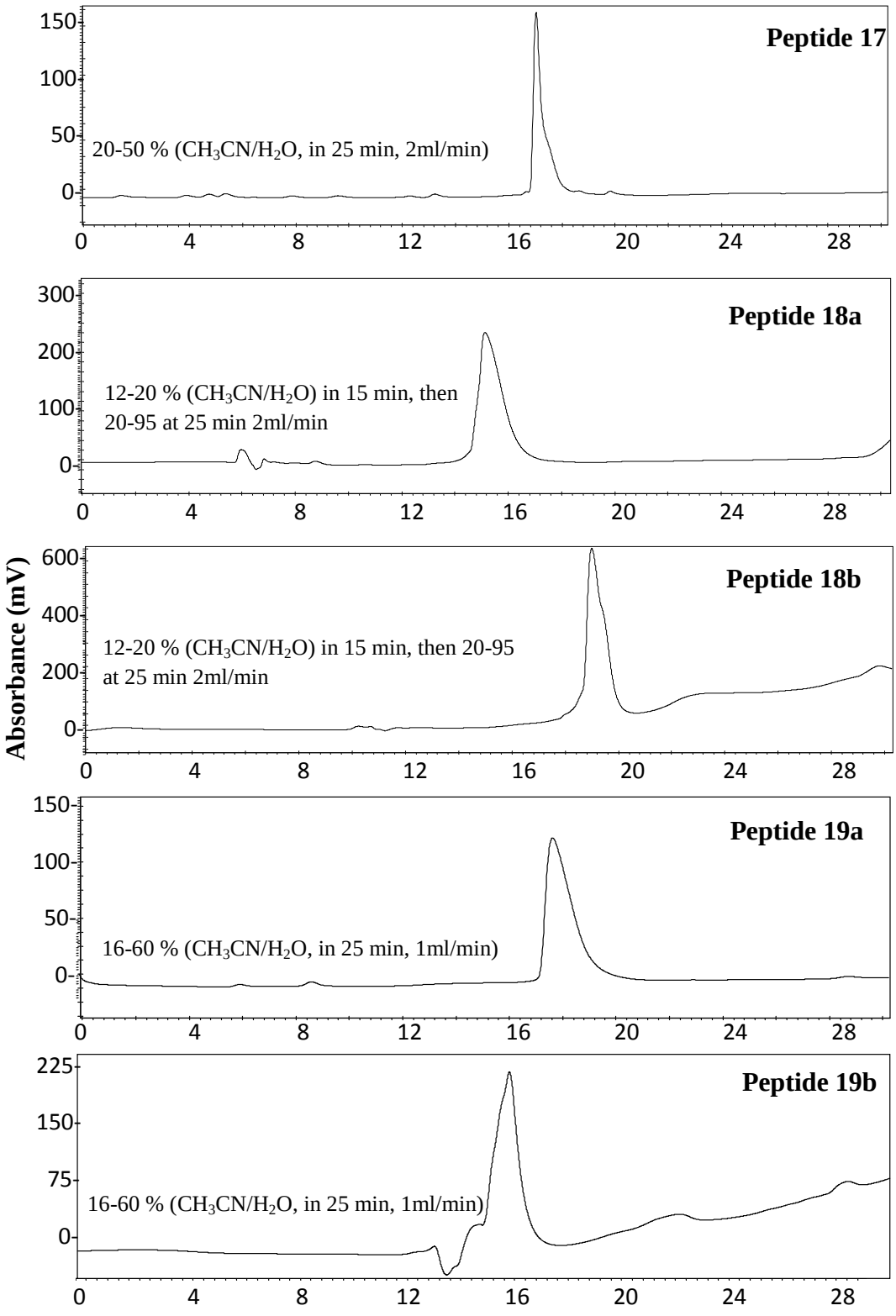
Peptide 17
20-50 % (CH_3CN/H_2O, in 25 min, 2ml/min)
Peptide 18a
12-20 % (CH_3CN/H_2O) in 15 min, then 20-95 at 25 min 2ml/min
Peptide 18b
12-20 % (CH_3CN/H_2O) in 15 min, then 20-95 at 25 min 2ml/min
Peptide 19a
16-60 % (CH_3CN/H_2O, in 25 min, 1ml/min)
Peptide 19b
16-60 % (CH_3CN/H_2O, in 25 min, 1ml/min)
Absorbance (mV)

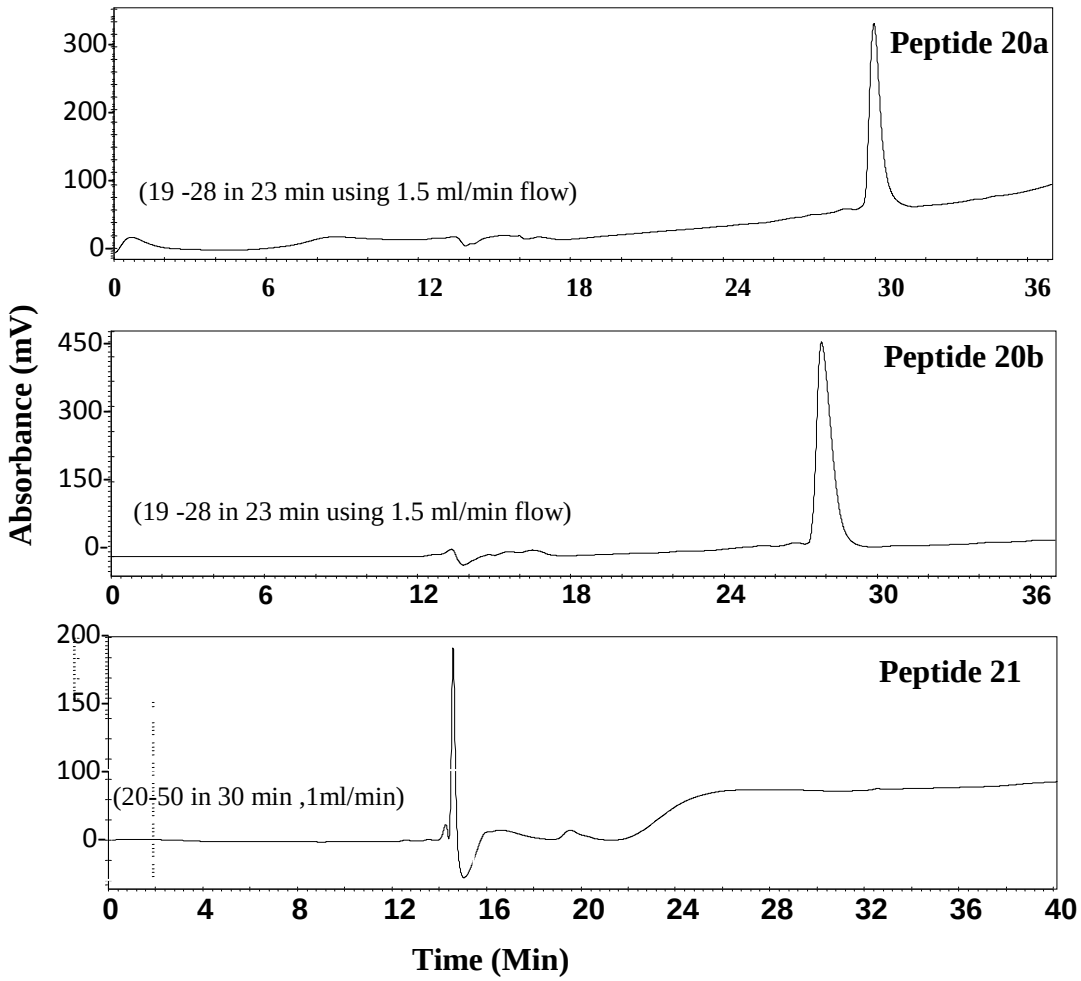

Figure 3.16. RP-HPLC chromatograms of pure β^3-peptides **17-21** obtained using analytical Vydac C18 analytical column (0.46 x 25 cm, 5 μm).

3.2.5.3 Circular Dichroism Spectroscopy of β^3-Peptides 17-21

The solution conformation of ß^3-peptides **17-21** was first evaluated in TFE and water using CD spectroscopy. CD spectra can provide good initial estimate of solution conformation in relatively short time.

Figure 3.17 a shows far-UV CD data for β^3-hexapeptides **1, 17, 20a, 20b** and **21** in TFE at 200 μM concentration. All five peptides show a minimum around 214 nm but with different intensity. This peak is indicative of 14-helical structure in β-peptides. Surprisingly, **1** shows the largest minima at 214 nm

(θ = -20 x 10^3) suggesting highest helical structure in TFE. Peptide **21** with the next largest minimum (θ = -16 x 10^3) is also helical. Peptide **20a** with lysine mimic side chain shows some helix and is more folded than the corresponding ornithine side chain peptide **20b**.

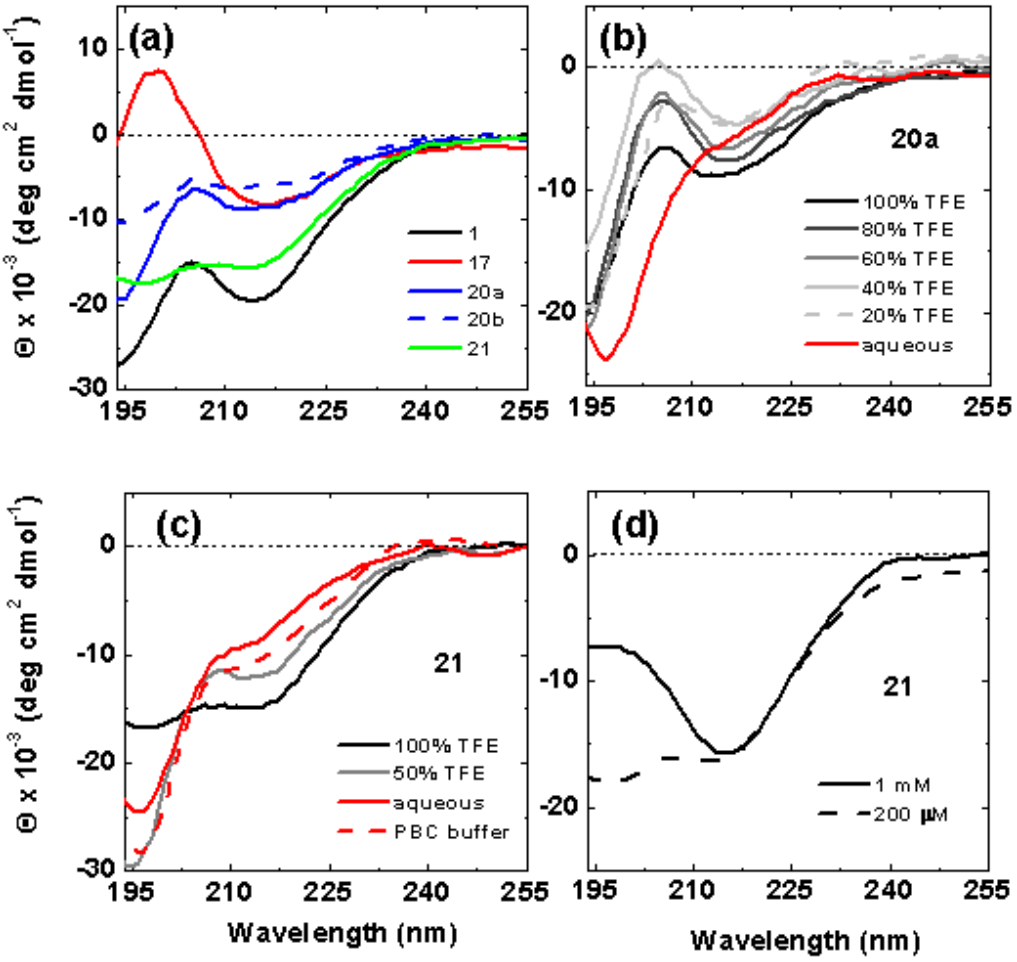

Figure 3.17. Circular Dichroism (CD) spectra for β^3-hexapeptides **1**,**17**-**21** at 25 °C: (a) β^3-hexapeptides **1**, **17**, **20a**, **20b,** and **21** in TFE, (b) **20a** in TFE, TFE/water, and in aqueous solution, (c) **21** in TFE, TFE/water, aqueous media and PBC buffer (pH 7.4), and (d) **21** in TFE at two concentrations, 200 µM and 1 mM.

Finally, the minima for **17** and **20a** are same suggesting same extent of helical conformation. However, the CD of **17** and **20a** may not be directly comparable as the two β-peptides have very different side chains.

Figure 3.17 b shows far-UV CD for peptide **20a** in TFE/water mixture with decreasing TFE concentration. A decrease in the minimum at 214 nm was observed with increasing water concentration suggesting loss of helical conformation. However, to our surprise, the 14-helix of the peptide was maintained even in 20% TFE (v/v). The CD shows no minimum in water suggesting disappearance of folding in water. Peptide **21** displayed similar behavior in TFE/water mixture as shown by peptide **20a** (**Figure 3.17 c**). CD of **21** in 100% and 50% TFE shows characteristic minima at -16 x 10^3 and -12 x 10^3, respectively. Peptide **21** in water and PBC buffer (pH 7.4, 1 mM) shows loss of folding due to the decrease in the minimum at 214 nm. In PBC buffer, the minima at 214 nm was -10.5 x 10^3 and only a small shoulder was observed in aqueous solution. The CD was performed in PBC buffer at pH 7.4 to ensure that all the amine side chain are protonated and the carboxylate are deprotanated in peptide **21** to enhancing salt bridge interaction. However, the peptide was definitely not as folded as in the presence of TFE.

Finally, CD of **21** was also studied at a higher concentration. As shown in **Figure 3.17 d**, the CD spectra of **21** at 200 μM and 1 mM show similar minima at 214 nm and were found to be independent of concentration, suggesting that no changes in aggregation state occur in this concentration range.

The folding of 4-mer, 5-mer, and 6-mer peptides **18**-**20** was also studied using CD spectroscopy (**Figure 3.18**). The CD spectra of the peptides were obtained at 200 μM concentration in TFE and PBC buffer (pH 7.4, 1mM). In general, peptides with lysine mimic side chain (**18**-**20a**) appeared to be more folded compared to peptides with ornithine mimic side chain (**18**-**20b**) as observed with the larger negative minima (**Figure 3.18 a** and **b** compared to **Figure 3.18 c** and **d**). Also it is observed that only peptide **20a** shows a clear

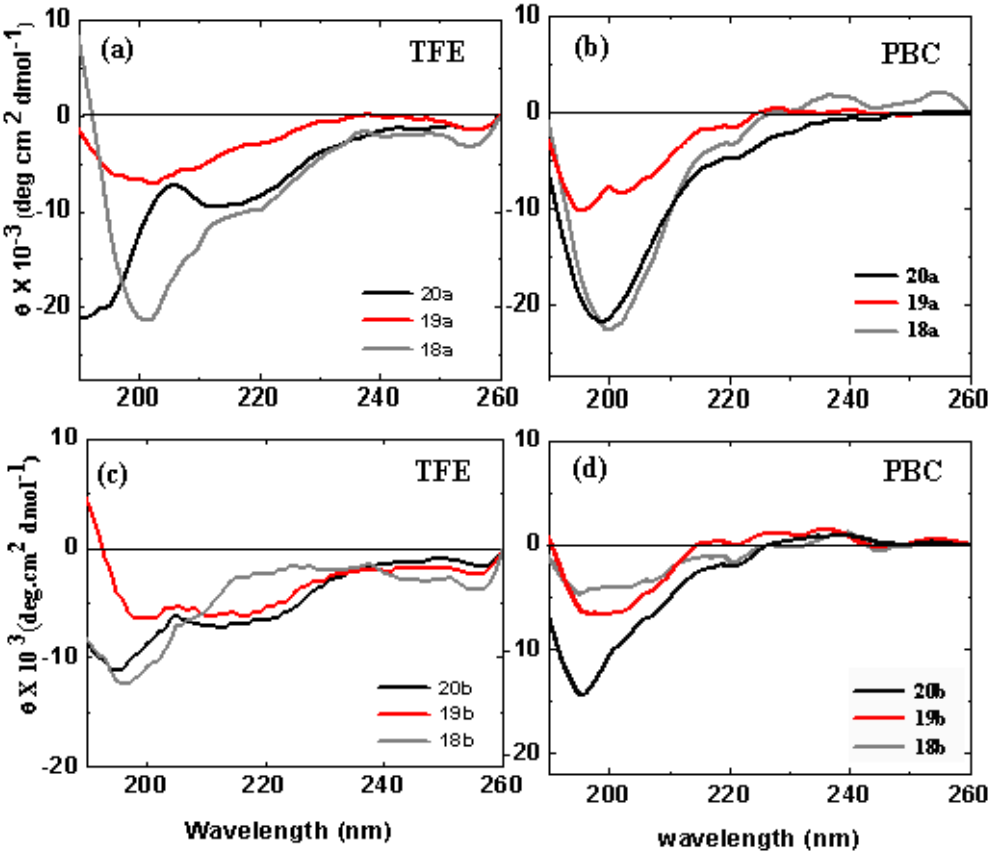

Figure 3.18. Circular Dichroism (CD) spectra of β^3-peptides **18**-**20** (200 μM) in TFE (a & c) and PBC buffer pH 7.4 (b& d).

minima (θ = -10 x 10^3) at 214 nm in TFE. Most other peptides in TFE and PBC buffer show a negative peak at around 200 nm. This minimum might indicate presence of a bundle rather than a monomeric unit in short sequences as shown previously.[26] The characteristic 14-helical minima around 214 nm was lost in PBC buffer for all the peptides indicating loss of secondary structure (**Figure 3.18, b** and **d**).

3.2.5.4 NMR solution structure studies of β^3-peptides

To probe the secondary structure of β^3-peptides **17-21** in solution, a detailed NMR spectroscopic investigation was carried out in collaboration with Dr. Tara Sprules. 1D NMR of all the eight peptides in TFE-d_2 (CF_3CD_2OH) were examined (see appendix **Figures A.15-Figure A.22**) and the presence of a regular secondary structure was indicated by a large dispersion of the chemical shifts. The well dispersed chemical shifts in the amide region allowed assignment of all the backbone and side chain protons. A two-dimensional (2D) NOESY experiment was also performed for all the peptides which allowed observation of NOEs between protons from residues that are not sequentially adjacent. The characteristics 14-helical peaks were observed only for peptides **17** and **21**. NOESY spectrum of β^3-hexapeptide **17** showed multiple (five out of six possible) long range $C_\beta H(i) \rightarrow C_\alpha H$ (i+3) (**Figure 3.19**). Whereas for peptide **21,** all the possible (six) long range $C_\beta H(i) \rightarrow C_\alpha H$ (i+3) NOEs were observed (**Figure 3.20**) suggesting helical conformation in both the peptides. These peaks are a hallmark of 14-helical secondary structure.[4, 21]

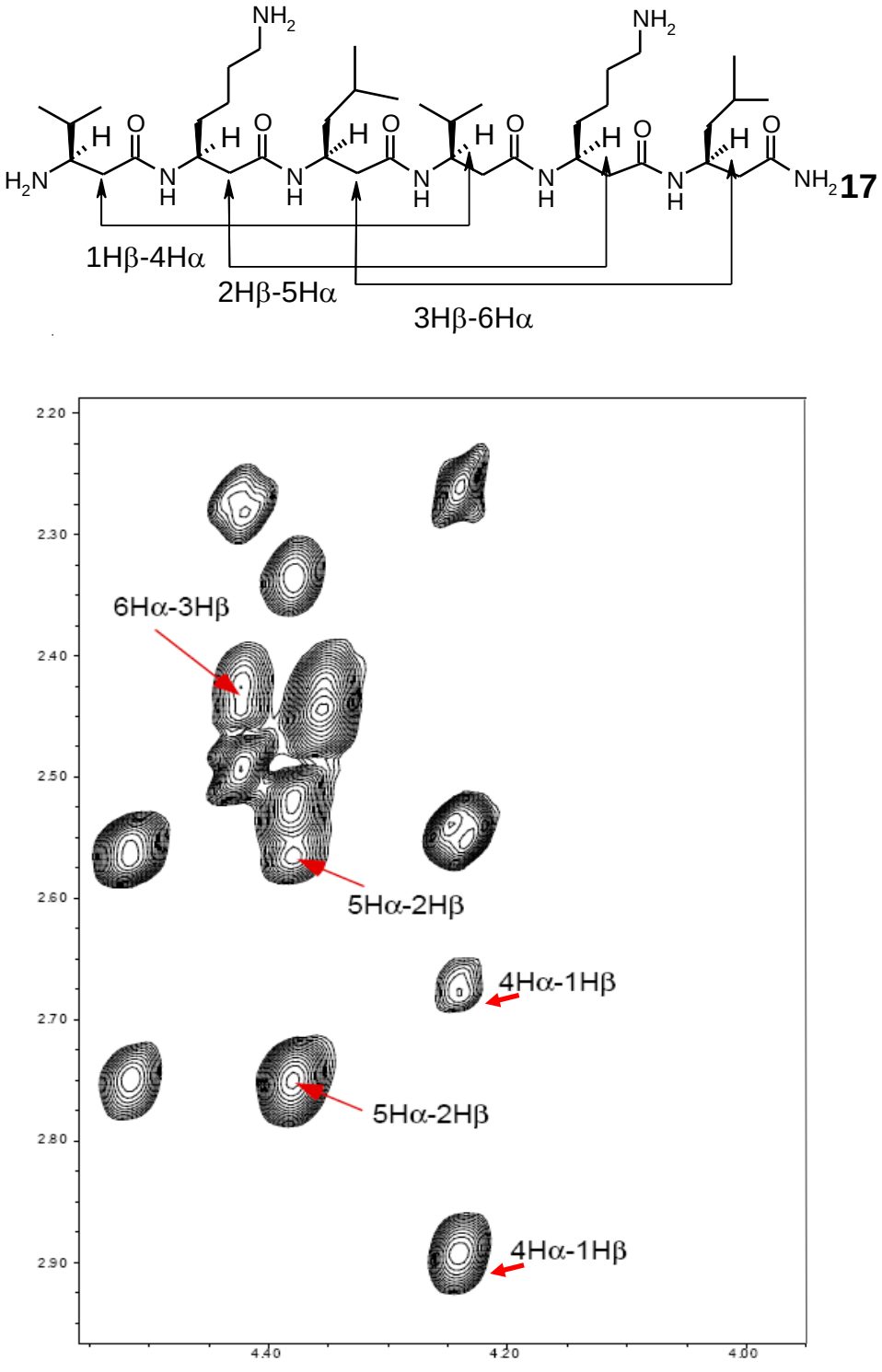

Figure 3.19. 2D NOESY of β^3-peptide 17 in TFE showing the long range NOEs, CβH(i)-CαH(i+3) characteristic of 14-helix conformation.

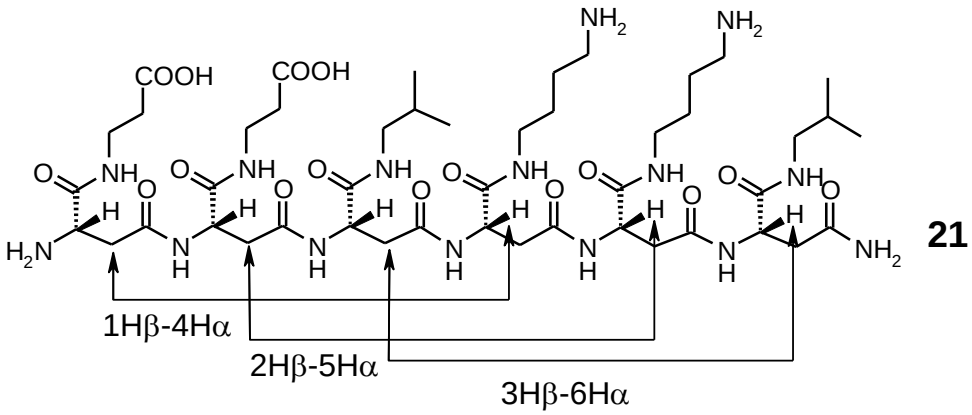

21

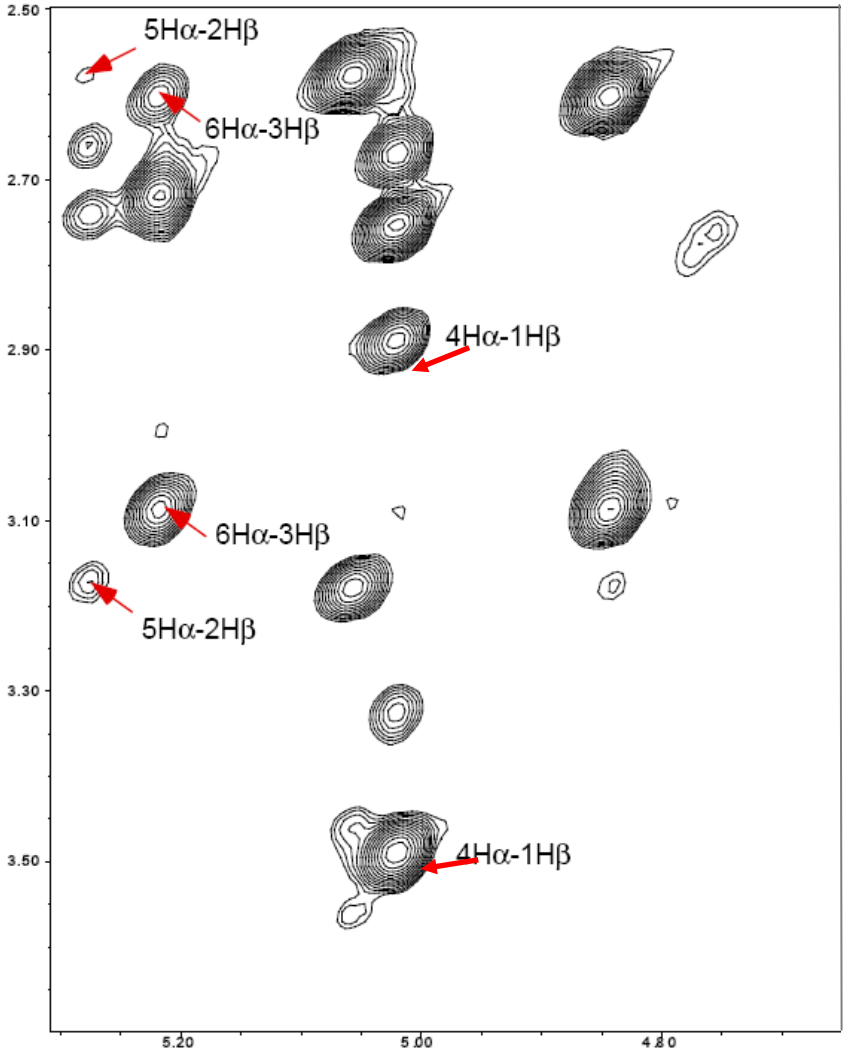

Figure 3.20. 2D NOESY of β^3-peptide **21** in TFE showing the long range NOEs, CβH(i)-CαH(i+3) characteristic of 14-helix conformation.

Further, the extent of helical folding in different β-peptides can be compared using NOE data. At least four NOE patterns involving backbone and side chain protons that are suggestive of 14-helix can be compared. These NOE patterns are NH(i)→Hα(i+3), NH(i)→Hα(i+2),Hβ(i)→Hα(i+3), and the side Hβ(i)→ HS (i+3). As shown in **Figure 3.21**, the direct comparison of these NOEs showed that peptides **1** and **21** have comparable helical conformation in solution. Peptide **20a** seems to be the least structured out of the four peptides as it showed only two of the $H_{\beta}(i) \rightarrow H_{\alpha}(i+3)$ NOEs.

On the other hand, these peptides behaved very differently in aqueous conditions. For instance, 2D NOESY and TOCSY spectra were recorded for **21** in phosphate buffer (25 mM) at pH 6.1 and 6.6. There was little chemical shift dispersion, therefore the hall mark long-range NOEs for 14-helix could not be identified. This lack of dispersion suggests that the peptide is not (stably) folded. All the backbone amides, and Hα and Hβ peaks were overlapped. The β-Leu and β-Lys side chain shifts were exactly overlapped. The two β-Glu side chain amides showed up separately, as well as the aliphatic protons were slightly different, this may be due to the fact that one of the β-Glu is the N-terminal residue.

These observations agreed with the CD results as the characteristic minima for 14-helix were not observed for the peptides in aqueous conditions. Further, the NMR data suggests that the peptides were not aggregated in water as the line widths were comparable to the spectra in TFE.

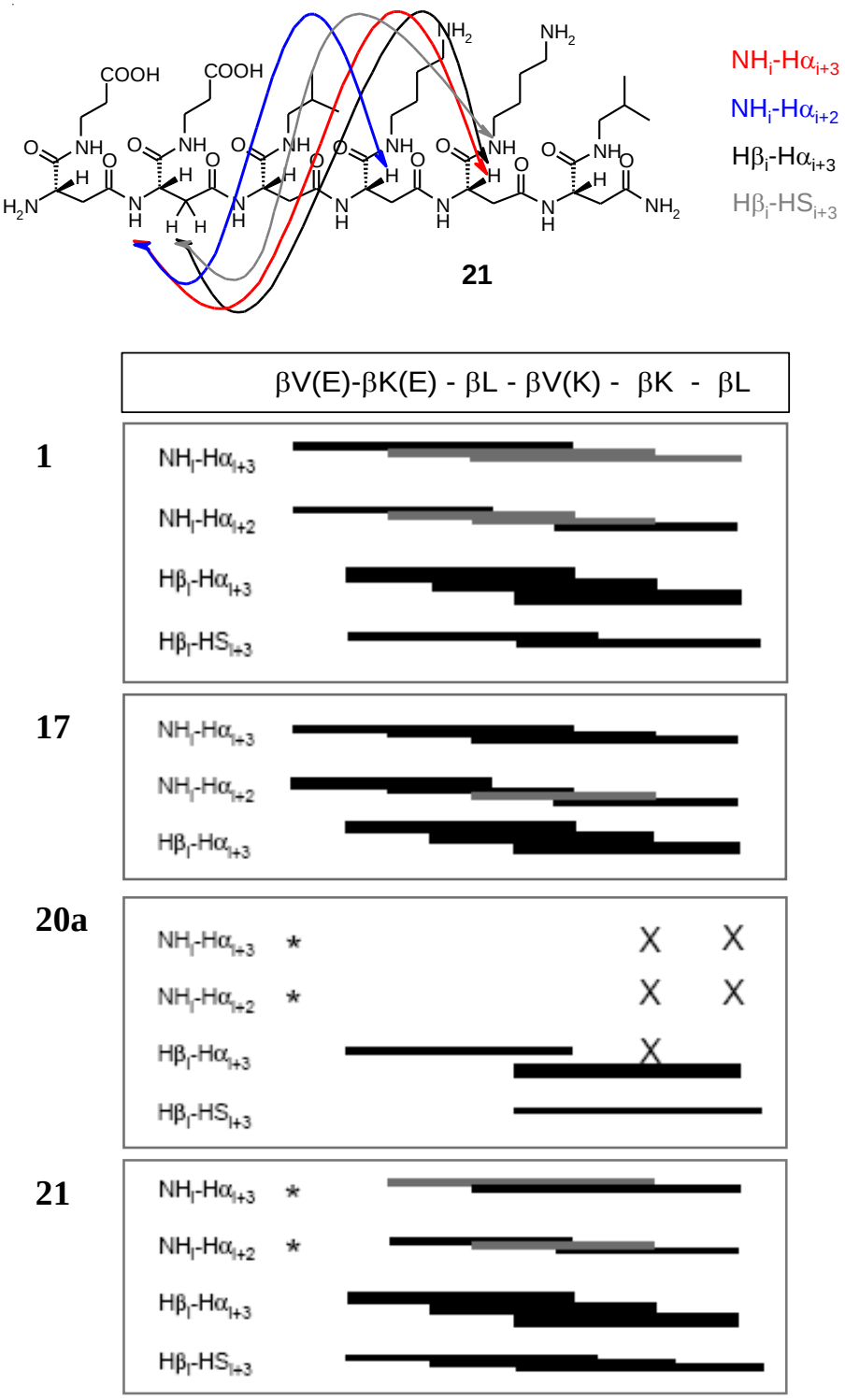

Figure 3.21. A comparison of the NOE of peptides **1, 17, 20a** and **21** are summarized. * denotes amide protons not observed due to exchange with solvent and X stands for Hα protons not observed due to overlap with solvent signal. Grey lines indicate ambiguous assignments.

The three-dimensional structures of **1** (done previously), **17** and **21** were obtained using the NOE data (see Appendix, **Table A.1**, and **Table A.2**) and the program CYANA program.[27] The input data and structure calculation statistics of peptides **17** and **21** are summarized in **Table 3.3** and **Table 3.4**. The pdb coordinates of the 20 structures obtained from CYANA program were averaged to obtain the final peptide structures in TFE (**Figure 3.22)**. β^3-hexapeptides **1** and **21** form a right-handed 14-helical structure with a radius of 2.6 Å and 4.69 Å rise/turn. In contrast, the β^3-hexapeptide **17** formed from βh-amino acids forms left-handed 14 helix (**Figure 3.23**). The difference in the conformation of the two helices (right-handed versus left-handed) could be due to the opposite stereochemistry at the β^3 carbon in the peptide backbone. The radius and the pitch for the two helices are found to be similar. The right-handed 14-helical conformation of **1** and **21** is a better mimic of right-handed α-helix of α-peptides (**Figure 3.23**).

Table 3.3: Structure calculation statistics for β^3-hexapeptide 17.

Structure calculation statistics for β^3-hexapeptide 17	
NOE upper distance limits	170
Intra-residue	68
Sequential	47
Medium range (I to i-2 or i+3)	53
Long range (I to i+4)	2
Final CYANA structures [a]	
CYANA target function	0.011±0.008
Average backbone RMSD	0.54±0.10 Å
Average heavy atom RMSD to mean	1.15±0.15 Å
Distance restraint violations	0

[a] 20 lowest energy structures of the 200 calculated.

Table 3.4: Structure calculation statistics for β^3-hexapeptide **21**

Structure calculation statistics for β^3-hexapeptide 21	
NOE upper distance limits	167
Intra-residue	71
Sequential	42
Medium range (I to i-2 or i+3)	53
Long range (I to i+4)	1
Final CYANA structures [a]	
CYANA target function	0.0298±0.0287
Average backbone RMSD	0.50±0.12 Å
Average heavy atom RMSD to mean	1.44±0.14 Å
Distance restraint violations	0

[a] 20 lowest energy structures of the 200 calculated.

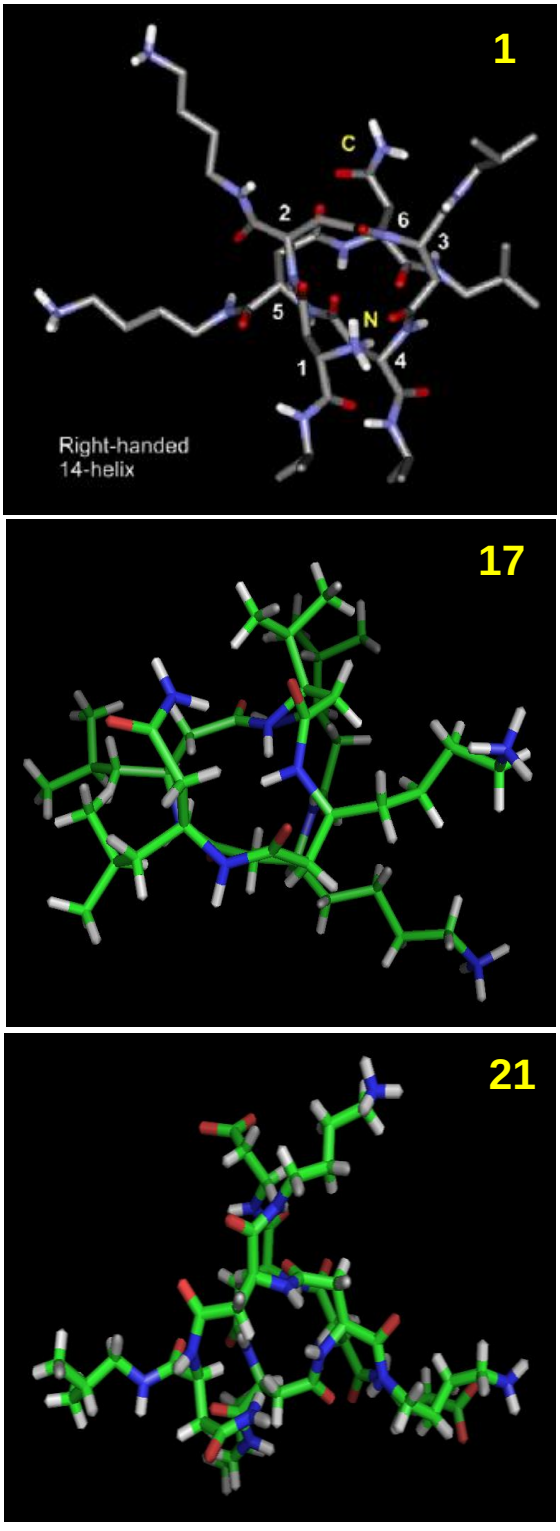

Figure 3.22. NMR solution structures of β^3-peptides **1**, **17** and **21** in TFE. Top views of the helices are shown using stick model.[23]

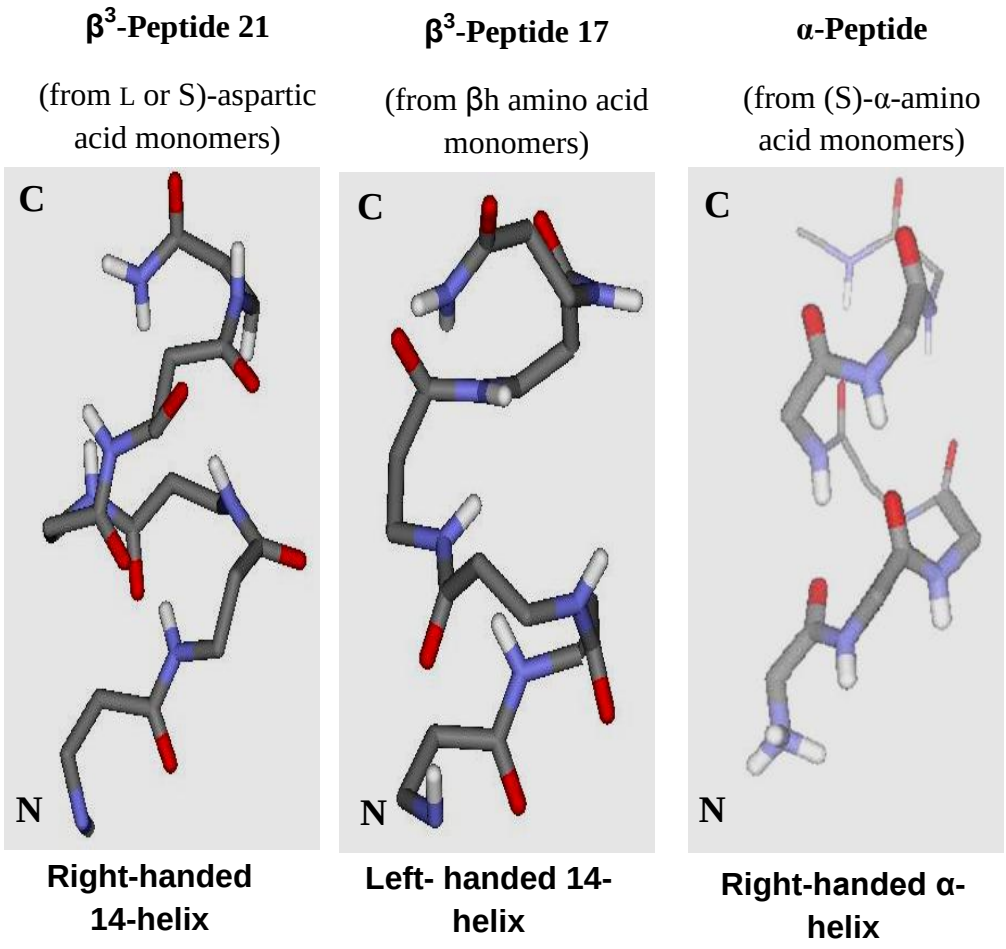

Figure 3.23. Solution structures of β^3-peptides right-handed and the left-handed helices, based on the amino acid composition.

Peptide **21** formed a well defined helix in TFE with two salt bridge interactions. However peptide **21** did not reveal any secondary structure in water as observed by NMR and CD. The loss of the secondary structure of peptide **21** in water could be due to the placement of the amino acid opposite to the macrodipole. β^3-Peptides are known to have macrodipole with negative charge near the N-terminal and positive charge near the C-terminal. This macrodipole can destabilize the secondary structure. However, secondary structure can be

stabilized by neutralizing the macrodipole by placing amino acids with negative charge side chain, such as, aspartic and glutamic acid near the C-terminal and amino acids with positive charge side chain, such as, lysine and ornthine near the N-terminal.[25]

In order to have correct macrodipole for the secondary structure stabilization, we decided to synthesize an 11-mer β^3-peptide **22**. Peptide **22** has negative charge near the C-terminal and positive near the N-terminal.

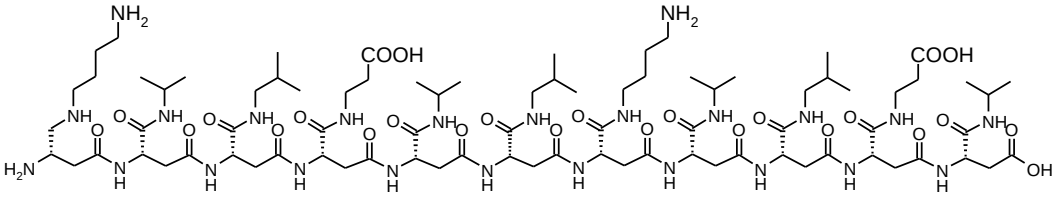

22

Peptide **22** was synthesized following the same procedure as before, except Wang resin was used instead of Rink amide resin. Coupling of amino acid monomer after 8 residues became difficult, and needed longer times, to proceed to 11 residues. Deallylation of the allyl side chain of the last amino acid (residue 11) revealed neither the product, nor the starting material. This suggests that optimization of the synthesis of longer β^3-peptides with multiple deallylations may be needed.

3.2.6 Design and Synthesis of Mixed α/β^3-Peptide 23

The synthesis of β-peptides with length greater than 10 residues has been found to be difficult.[13]As observed above, the synthesis of **22** could not be achieved successfully. However, mixed α/β-peptides are good alternative to long β-peptides. Mixed α/β-peptides have been found to fold to new types of helical secondary structures held together by hydrogen-bonded rings containing 9 through 15 atoms.[28-30]In mixed α/β-peptides, α- and β-amino acids can be arranged in numerous ways to form mixed peptides.[31] Peptide **23** was designed by replacement of some of the β-amino acids with the α-amino acids in peptide **22** in a specific manner. Amino acid was placed in an α-β-β pattern in the sequence. This pattern allowed replacement of four charged β^3-amino acids with α-amino acid to give mixed α/β peptide **23**. Peptide **23** was synthesized using Wang resin following the same synthetic strategy as used before. Peptide **23** was purified using HPLC to obtain pure **23** with an overall yield of 64%.

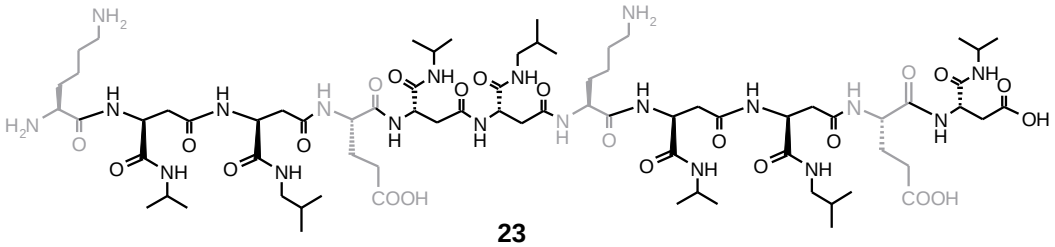

23

Solution conformation of peptide 23

Circular Dichroism was used to study the solution conformation of peptide **23.** The CD spectra displayed large minima around 203 nm in TFE and 201 nm

in the case of water (**Figure 3.24**). In both solvents, the minima is not around 214 nm which is the characteristic for 14-helix. However, a minima around 201-203 suggests the presence of secondary structure. Gellman and his group studied different analogues of α/β-peptides of alternative sequences, and found that this class of peptides gives minima around 204 nm in CD.[32] Their NMR studies revealed that these analogues represent 14/15-helical or 11-helical secondary structure. Recent work from Gellman and his group indicated that mixed α/β-peptides have specific type of secondary structure which has characteristic minima around 207 nm.[33] The authors explain that the structure of these mixed peptides displayed features that are unprecedented among all known helix bundles composed of either alpha-peptides or β-peptides. In order for us to gain more insight regarding the secondary structure of **23**, NMR study was attempted.

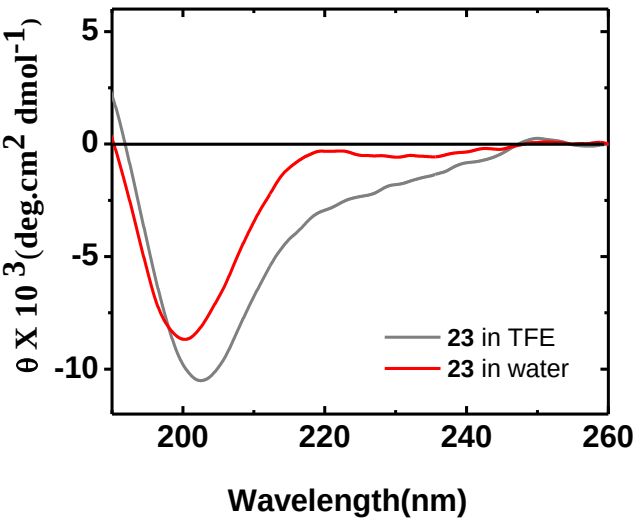

Figure 3.24. CD spectra of α/β^3-peptide **23** in TFE and water at a concentration of 250 μM.

Broad lines in NMR resulting from aggregation at concentrations necessary for NMR analysis precluded any sequential assignments.[34] DPC-micelle could be used in future to remove aggregation and promote helical structure. Also, analytical ultracentrifugation could be used to determine if the native state of a peptide is a monomer, dimer, or a higher order structure.

3.2.7 Proteolytic Stability of β-Peptides and a Mixed α/β-Peptide

Several strategies have been used to obtain appropriate balance between proteolytic stability, bioavailability and biological activity, such as the design of mixed peptides containing α- and β-amino acid residues or design of peptides where the backbone and the side chains together mimic the natural α-peptide.[6,35] Efforts to modify the electronic environment by the introduction of electron withdrawing groups adjacent to the backbone carbonyl of a β-peptide, such as introduction of one or two fluorine atoms or a hydroxyl group in the alpha-position of beta-homoalanine, failed to facilitate proteolytic degradation.[35] Designing β-peptides, such as N-(L)β^2hXaa-(L)β^3hXaa-C, that resemble α-peptide with respect to the position and configuration of the side chain groups also did not make it susceptible to proteolytic degradation.[6] It is speculated that the β-peptides from L-Asp and L-Dap monomers may be susceptible to enzymatic cleavage because of the presence of an additional amide bond in the side chain. In addition, β^3-peptide from L-Asp units contains an intrinsic L-α-amino acid (or α-linkage) in the sequence that may facilitate recognition and hydrolysis by peptidases. Finally, mixed α/β-peptides containing both α- and β-amino acid residues, where β-amino

acids are derived from L-Asp, within α peptide should allow achievement of a better balance between proteolytic stability and biological activity.[36,37,38]

In this context, the proteolytic stability of β-peptides **1**, **3**, and **4** derived from L-Asp monomers (β^3-hexapeptide **1**) and L-Dap monomers (β^2-hexapeptides **3** and **4**), as well as a mixed α/β^3-peptide **23** was compared with an α-hexapeptide **24** (**Figure 3.25**). The proteolytic stability of these representative peptides was tested against three enzymes, namely, pronase, trypsin and elastase, as well as, against human serum.

Peptides (**1, 3, 4,** and **23**) with different backbones, namely, β^3, β^2 or mixed α/β^3, and varying side chains mimicking hydrophobic (valine and leucine), aromatic (phenylalanine) and charged (lysine and aspartic acid) amino acids were chosen for evaluation of biological stability. The sequences (or side chains) of β^3-peptide **1** and β^2-peptides **3** and **4**, were kept very similar to the reported 'regular' β-peptides (β-peptides synthesized from homologated α-amino acids) to allow comparison of their biological stabilities.[39] Mixed α/β^3-undecamer peptide **23** was prepared to study the influence of a substituted α-amino acid in the β-peptide backbone, as in most cases the α-peptides with biological activity lose their activity due to the cleavage at certain cleavable site. An α-hexapeptide **24** with the same side chains as β-peptides **1** and **3** was synthesized as a standard (or positive control) using SPPS.

To monitor the proteolytic degradation, peptides were incubated with pronase, trypsin or elastase, and the stability of the peptides was monitored using RP-HPLC analysis. This procedure allowed isolation of the possible degradation

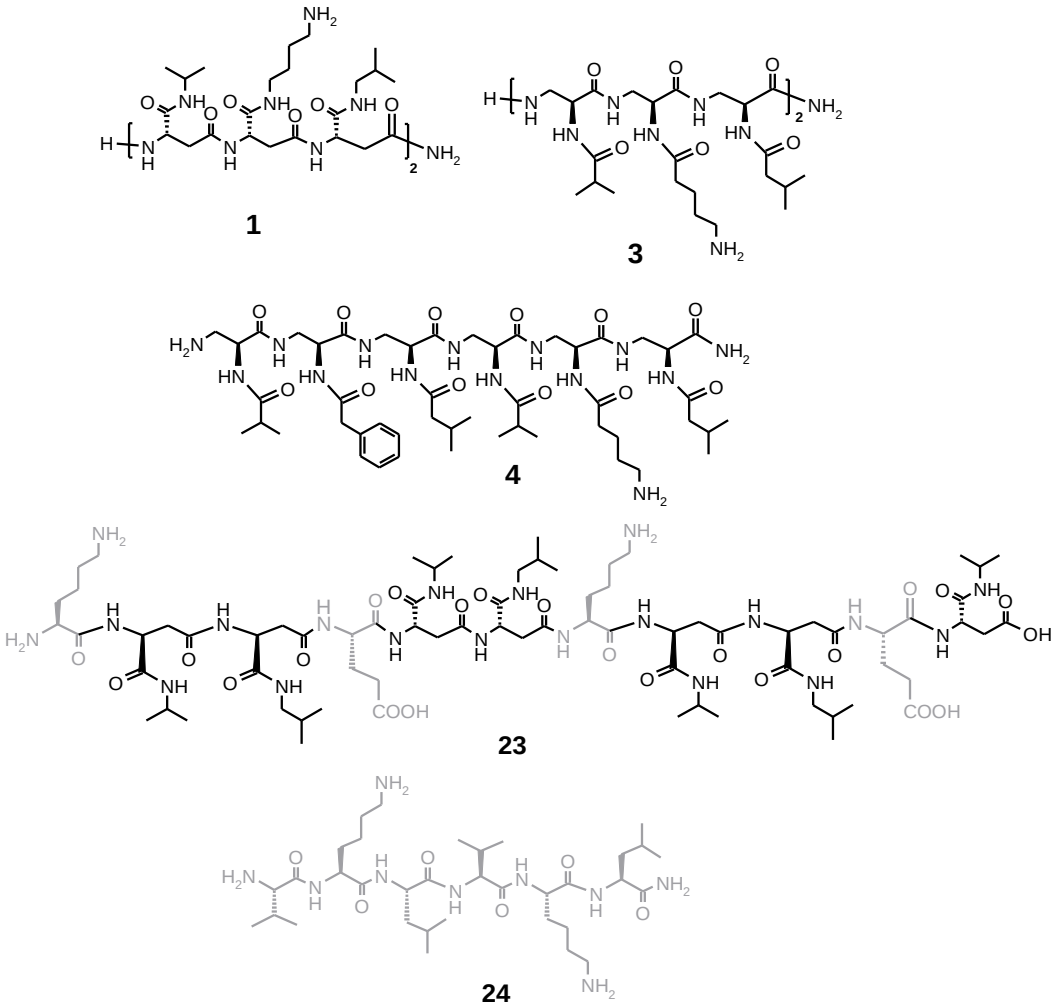

Figure 3.25. Chemical structures of peptides used for proteolytic stability study. α-amino acids are shown in grey.

products which could then be characterized by electrospray ionization mass spectrometry. All the enzymes were used in high specific concentrations allowing complete degradation of α-peptide **24** within an hour. As shown in **Figure 3.26**, and **Table 3.5**, β^3-peptide **1** and β^2-peptides **3** and **4** showed no sign of any degradation up to 4 days. After incubation with pronase, trypsin, or elastase, the HPLC peaks were collected and characterized by mass spectrometry. The collected peaks showed the same mass as the original peptides, suggesting that

Table 3.5: Treatment of peptides with three proteolytic enzymes or human serum.

Enzyme or Serum	Enzyme origin	**1** (β^3)	**3** (β^2)	**4** (β^2)	**23** (α/β^3)	**24** (α)
Pronase	*Streptomyces griseus*	−	−	−	+	+++
Trypsin	Porcine pancreas	−	−	−	+	+++
Elastase	Hog pancreas	−	−	−	−	+++
Human serum		−	−	n.t.	n.t.	+++

+, degradation; − no detectable degradation under the experimental conditions. n.t., not tested.

no cleavage occurred. β-peptides **1** and **3** also did not display any degradation in the presence of human serum when incubated with the serum for 5 days, while α-peptide **24** was completely degraded within 24 h under similar conditions.

Interestingly, the insertion of a single α-amino acid between four β-amino acid units rendered mixed α/β^3-undecamer peptide **23** susceptible to degradation. Mixed α/β^3-peptide **23** displayed variable degradation in the presence of pronase and trypsin, while retaining complete stability in the presence of elastase. As shown in **Table 3.6**, proteolytic degradation of mixed α/β^3-peptide **23** started within an hour and was fully degraded by pronase and trypsin in 24 h. After incubation with pronase for 2 h, the two additional peaks that eluted at 12 and 13 minutes, along with **23** eluting at 16 minutes, became more prominent (**Figure 3.27**). The mass $[M+H]^+$ of the peaks eluting at 12 and 13 minutes was found to be 630.23 and 1056.23, respectively. This corresponded to peptide bond cleavage

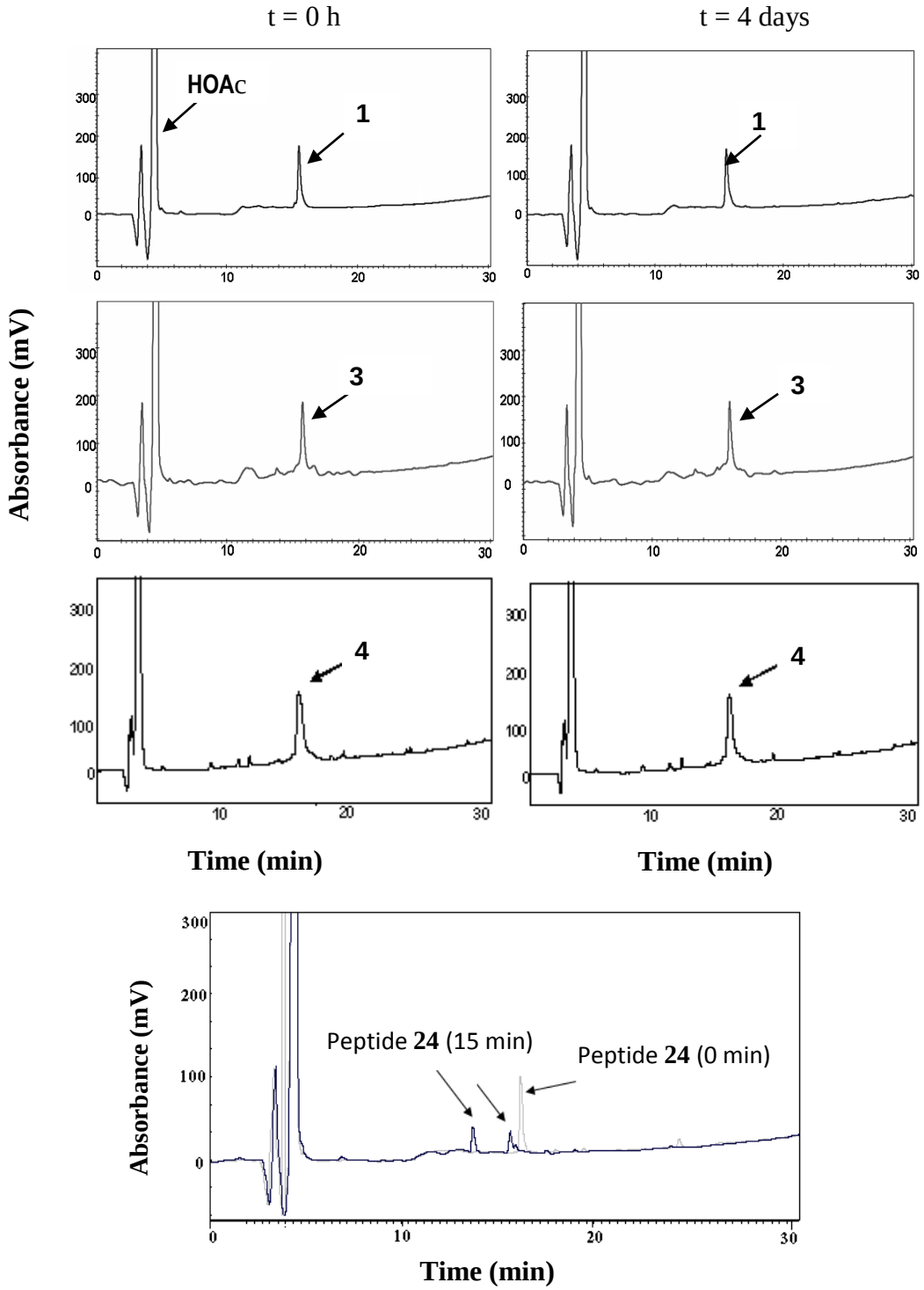

Figure 3.26. RP-HPLC chromatograms of peptides **1**, **3**, **4**, and **24** in the presence of pronase at different time intervals (0 hour and 4 days) illustrating the enzymatic stability.

between residues Lys7 and β^3amVal8 giving rise to heptapeptide **25** (calcd $[M+H]^+$, 1056.63) and tetrapeptide **26** (calcd $[M+H]^+$, 630.33). Further incubation with pronase led to complete loss of **23** with the appearance of multiple additional peaks at around 8 and 14 minutes. Mass spectrometric analysis of the two peaks that eluted at ~ 14 minutes showed $[M+H]^+$ of 1056.45 and 928.36. This suggested that the N-terminal fragment **25** was further hydrolyzed after Lys1 to give a hexapeptide **27** (calcd $[M+H]^+$, 928.53). In the presence of trypsin, mixed α/β^3-peptide **23** degraded to mainly two peaks eluting at 12 and 13 minutes. The mass of these peaks was found to be 629.80 and 1056.06, respectively, suggesting cleavage after Lys7. After 4 days of incubation, the parent peak for **23** was not observed, while peaks at 12 and 13 minutes corresponding to fragments **26** and **25**, respectively, were still present as shown in **Figure 3.27**.

Table 3.6: Degradation of mixed α/β-peptide **23** in the presence of three proteolytic enzymes.

Time(h)	% Intact Peptide		
	Pronase	Trypsin	Elastase
0	100	100	100
0.5	100	100	100
1	76	88	100
2	51	75	100
5	21	50	100
24	0	0	100
4 days	0	0	100

% intact peptide was calculated based on the area under the HPLC peak for the parent peptide.

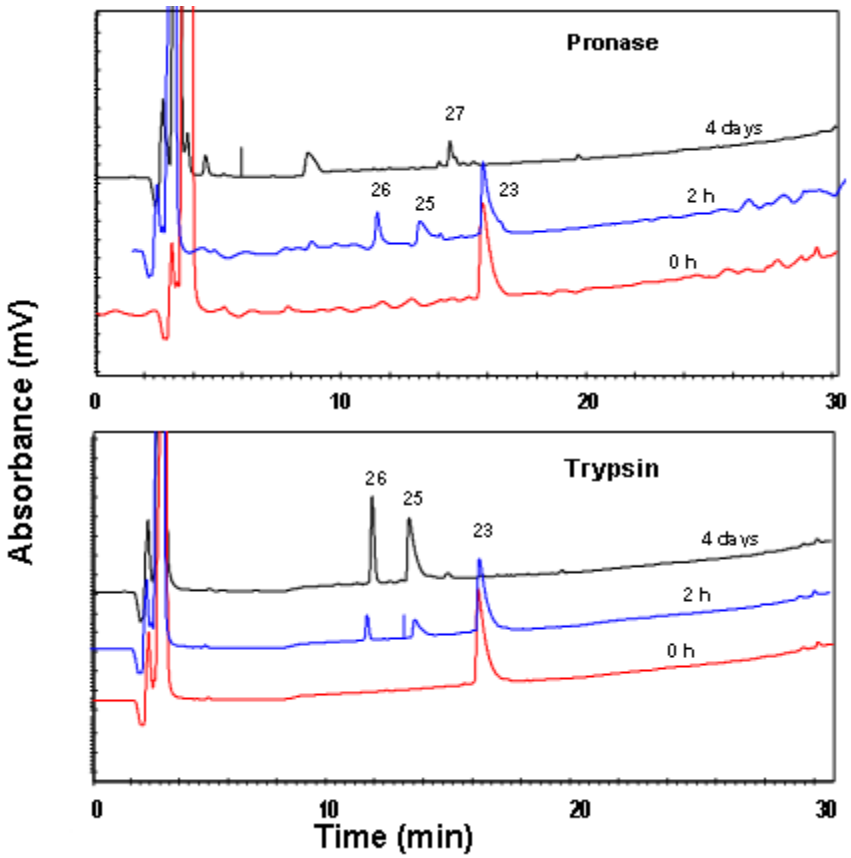

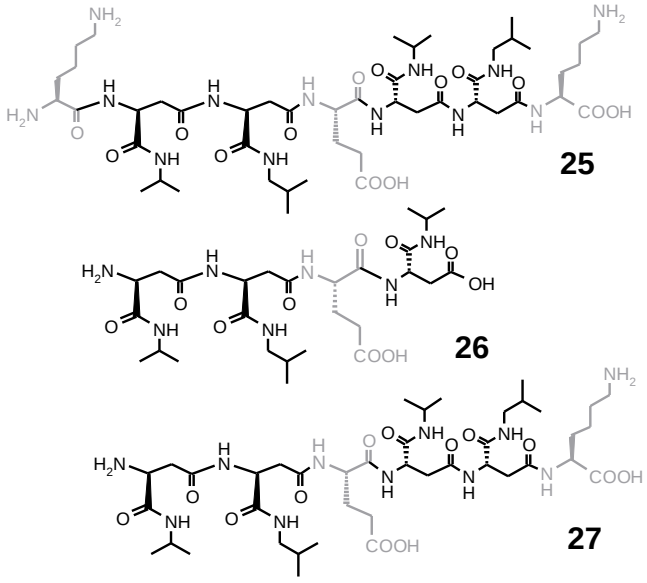

Figure 3.27. RP-HPLC chromatograms of mixed α/β-peptide **23** after incubation with pronase (top) and trypsin (bottom) for different time intervals, namely, 0 h, 2 h and 4 days. At the bottom are shown the molecular formulae of the final degradation product observed by mass spectrometry in the presence of pronase and trypsin.

The proteolytic susceptibility of the peptides discussed here was evaluated against three widely used proteases, namely, pronase, trypsin, and elastase from different biological sources. Trypsin and elastase are peptidases that cleave peptide bonds at specific residues.[40,41] Pronase, however, is a mixture of several exo and endopeptidases and was selected due to its high activity and broad substrate specificity.[42,43] The "pure" β-peptides **1, 3,** and **4** derived from L-Asp and L-Dap were resistant to cleavage by all the three enzymes (**Table 3.5**). In spite of possessing amide groups on the α-carboxylate (as shown in **Figure 3.28**) and α-amine of the aspartate and diaminopropionate residues, respectively, the side chain amides of β-peptides **1, 3,** and **4** were not cleaved on treatment with the three enzymes, a behavior consistent with the "regular" β-peptides (made from β-homo amino acids).

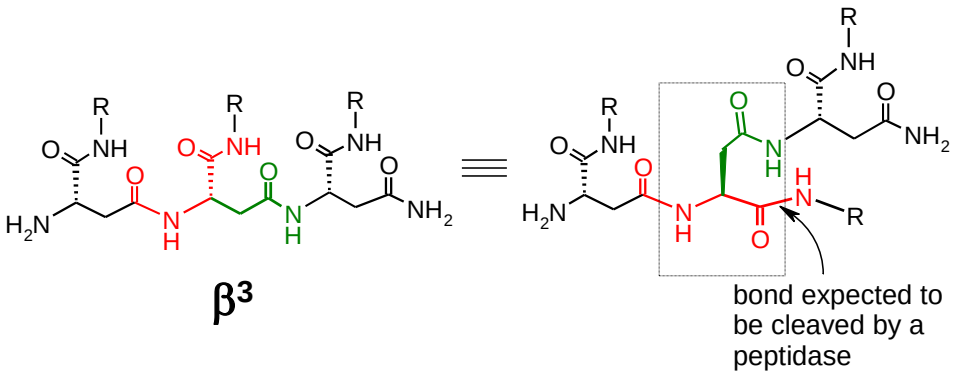

Figure 3.28. β^3-peptide prepared from L-aspartic acid monomers contain substituted L-α-amino acid (substituted L-asparagine) residues (highlighted in the dashed box).

Mixed α/β-peptide **23** was cleaved by two of the proteases (pronase and trypsin) at the amidic bonds followed by Lys residues as depicted in **Figure 3.29.**

Proteolysis of α/β-peptides has been observed previously, however, mainly by pronase.[44,6] After incubation with pronase, **23** lost its N-terminal Lys residue (as expected) and was also cleaved between residues 7 (Lys) and 8 (a β-Asp derived residue). This was an unexpected result because cleavage of a central α/β-peptide bond by proteases has been considered difficult.[44,6] Interestingly, the later bond between residues 7 and 8 was also cleaved by trypsin. Trypsin, a serine endopeptidase that cleaves peptide bonds adjacent to the basic residues (such as Arg or Lys), cleaved **23** after Lys7. This suggests that the Lys7/β^3-amVal8 bond may be susceptible to cleavage by pronase and trypsin as it represents an α/α-peptide bond with the correct absolute configuration. However, the rate of hydrolysis of this bond was significantly lower than that would be expected for an α/α-peptide bond in an α-peptide. Complete proteolysis of mixed α/β-peptide **23** occurred in 24 h (**Table 3.6**), whereas, α-peptide **24** was degraded by pronase in 15 minutes and by trypsin in 30 minutes under similar conditions. These results suggest that the use of L-Asp monomers to insert a β-peptide backbone in a biologically active peptide may have an additional advantage.

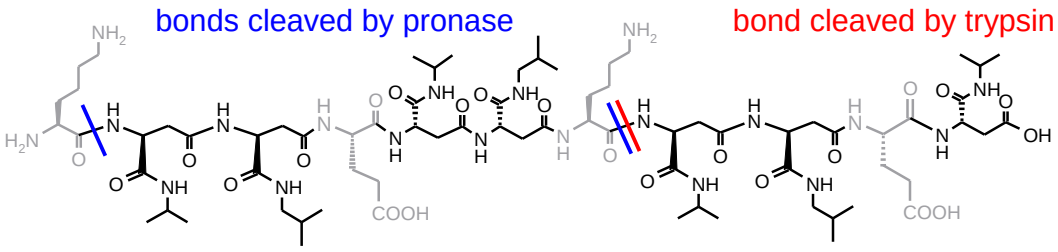

23

Figure 3.29. Degradation of mixed α/β^3-peptide **23** by protease. α-and β-amino acids are shown in grey and black, respectively.

3.2.8 Toxicity Studies of β-Peptides 1 and 3

In addition, to obtain a general view of the toxic profile displayed by the β-peptides discussed here, the cytotoxic properties of representative β-peptides **1** and **3** were assessed in Hela and COS-1 cells. The toxicities were determined by MTT assay and estimated to be lower than that of TAT peptide at the same concentration (**Figure 3.30**).[45] Cell penetrating peptide, (TAT^{47-57}), was used as a positive control for cell cytotoxicity assays because of the cytotoxic effects of TAT on several cell lines.[10]

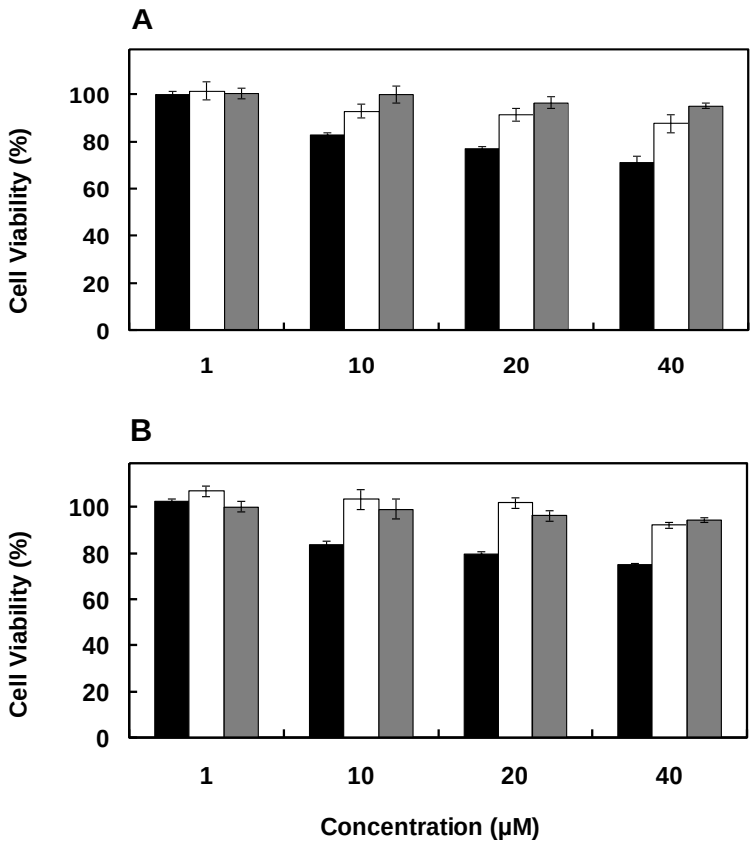

Figure 3.30. Cytotoxicity of β-peptide **1** (white) and β-peptide **3** (grey) compared to TAT (black) monitored in (A) HeLa and (B) COS-1 cell lines using MTT assay. Cells were incubated with different concentration of peptides for 24 h.

The viability of HeLa and COS-1 cells, after treatment with β^2-peptide 3 for 24 hours, was always higher than 95% at all the concentrations used (1-40 μM) as shown in **Figure 3.30**. β^3-Peptide 1 displayed slight cytotoxicity in Hela and COS-1 cells at the highest concentration used (40 μM), with a viability of 88 ± 2% and 92 ± 1%, respectively. At this concentration (40 μM), TAT peptide exhibited significant toxicity (71-76%) in both the cell lines.[34]

3.3. Conclusions

A method to synthesize two new classes of β-peptides, β^3- and β^2-peptides derived from L-Asp and L-Dap monomers, respectively has been developed. The methodology allowed independent buildup of the β-peptide backbone and the introduction of sequential side chain substitutions. Peptides ranging in length up to 6 residues were synthesized and characterized from both the classes. Secondary structures of representative peptides were studied using CD and NMR spectroscopy. β^3-peptides were more structured compared to the β^2-peptides in solution. Despite the presence of the additional amide bond in the side chain, β^3-peptides were well folded in organic solvent, as observed before for the β-peptide obtained from βhomo-amino acids. The β-peptides reported here form a right-handed 14-helix in TFE. β-peptides with additional sat bridge interactions introduced to enhance helical conformation in water, however, did not stabilize the helix in water.

Proteolytic stability studies of representative peptides convey that design of a peptidomimetic therapeutic agent based on β-peptides may require a combination of α and β-amino acid residues. β^3- (**1**), and β^2- (**3, 4**) peptides derived from L-Asp and L-Dap monomers were completely stable toward proteolytic enzymes. In contrast, mixed α/β^3-peptide **23** was susceptible to slow degradation by pronase and trypsin suggesting interaction with biological targets. Pronase cleaved the αLys/β^3haVal bond of **23** at two sites, N-terminal and a central peptide bond, suggesting the participation of both endo- and exopeptidases. Trypsin cleaved mixed peptide after the central Lys giving rise to two final degradation products, **25** and **26**. Toxicity studies of **1** and **3** towards Hela and COS-1 cell lines showed that the peptides are non toxic. Finally, it is shown that insertion of α-amino acid residues in a β-peptide derived from L-Asp monomers increases substrate-target recognition, retains the proteolytic degradation resistance, and imparts no cytotoxicity and also expands the potential application of such monomers in the design of biologically active peptides. As a result, such compounds can be used as candidates for new drugs and as tools to gain further insight into protein folding and molecular recognition processes.

3.4 Experimental Procedures

3.4.1 Methods and Materials

Solvents and Reagents

Rink amide methylbenzhydrylamine (MBHA) resin (0.58 mmol/g), 2-chlorotrityl chloride resin (1.4 mmol/g), N-α-Fmoc-L-aspartic acid α-allyl ester,

Fmoc-Asp(OtBu)-OH, Boc-L-asparagine, Fmoc-β^3hLeu-OH, Fmoc-β^3hLys(Boc)-OH, Fmoc-β^3hVal-OH, mono-trityl 1,4-diaminobutane acetic acid salt, mono-trityl 1,3-diamino propane acetic acid salt, β-alanine t-butyl ester hydrochloride, 1-hydroxybenzotriazole (HOBt), and benzotriazol-1-yl-oxy-tris-(dimethylamino)-phosphonium hexafluorophosphate (BOP) were purchased from NovaBiochem (San Diego, CA). Isobutylamine, isopropylamine, isobutaric acid, isovaleric acid were purchased from Aldrich. Boc-5-Ava-OH was obtained from Fluka. Dimethylformamide (DMF), N-methyl morpholine (NMM), dichlorobenzoyl chloride (DCB), pyridine, and trifluoroacetic acid (TFA) were from Aldrich, while piperidine, NaOH pellets and fuming HCl 37% were purchased from Caledon. All other reagents were purchased from Sigma-Aldrich (St Louis, MO, USA). All commercial reagents and solvents were used as received. Double distilled water was autoclaved before preparing buffers.

Silica gel for column chromatography was obtained from Rose Scientific Ltd. Column chromatography was performed under slight positive air pressure using silica gel 60 (70-230 mesh). Thin layer chromatography (TLC) was performed using silica-plates (Machery-Nagel Layer: 0.20 mm silica gel 60 with fluorescent indicator UV_{254}).

Trypsin from porcine pancreas (EC 232-650-8) lyophilized powder, (1,000-2,000 BAEE units/mg solid), Pronase E from *Streptomyces griseus* (EC 237-909-5) lyophilized powder with ~6 units/mg, and Elastase from hog pancreas (EC 254-453-6) were purchased from Sigma-Aldrich. HeLa cells were provided by the Campbell Laboratory (Department of Chemistry, University of

Alberta), while COS-1 cells were obtained from the Suresh Laboratory (Faculty of Pharmacy and Pharmaceutical Sciences, University of Alberta). TAT47–57 (YGRKKRRQRRR) peptide was purchased from GenScript Corp. (Piscataway, NJ, USA).

Equipment

RP-HPLC purification and analysis were carried out on a Waters (625 LC system) HPLC system using auto-injector mode or Varian Prostar HPLC system (Walkersville, MD, USA) using manual injector. Vydac C18 semi-preparative (1 x 25 cm, 5 μm) and analytical (0.46 x 25 cm, 5 μm) columns were used. Peptides were detected by UV absorption at 220 nm.

Mass spectra were recorded on a matrix-assisted laser desorption ionization time-of-flight (MALDI-TOF) Voyager spectrometer (Voyager^{TM} Elite) (Department of Chemistry) or Waters micromass ZQ (Waters Corp., Milford, MA, USA) mass spectrometer (Faculty of Pharmacy and Pharmaceutical Sciences, University of Alberta).

CD measurements were made on an olis CD spectrometer (Georgia, USA) at 25 °C in a thermally controlled quartz cell (Hellma, Plainview, NY) in the Department of Chemistry, University of Alberta. NMR experiments were recorded on a Bruker AM-300 spectrometer at the Faculty of Pharmacy and Pharmaceutical Sciences (University of Alberta), or on a Varian INOVA 500 MHz NMR spectrometer equipped with a triple-resonance HCN Cold Probe with z-axis pulsed field gradients, at the Quebec/Eastern Canada High Field NMR Centre, McGill University, Montreal, Quebec.

MTT assay measurement was done on VERSA max microplate reader (Molecular Device, Sunnyvale, CA, USA). For shaking plates, water bath YB-521 (Ultra-Tech) was used. All the procedures related to the cell culture maintenance, peptides solution preparation and treatments of cells were carried out in a NUNR BSC class II type A/B3 hood. Peptide solutions were sterilized by filtration through sterile filters (0.22 μm). pH measurements for all buffer solutions were done at 25 °C with a digital SB20 Symphony VWR pH meter using a calibration buffer set (Fluka).

3.4.2 General Solid Phase Synthesis of β^3-Peptides

Synthesis of β^3-peptides was performed manually in a polypropylene peptide synthesis vessel with a frit at the bottom and screw cap with a septum at the top for addition of reagents. Solvents and soluble reagents were removed by suction. At the start of the synthesis, the resin was washed with DCM, DMF, and IPA twice each prior to swelling in DMF for 30 min at room temperature. Washing between deprotection and coupling was carried out with DMF (4 x 1 min) and DCM (4 x 1 min) using 4 mL of solvent/0.05 mmol of resin each time. Fmoc group was removed by treatment with 20% piperidine/DMF (1 x 5 mins, 2 x 10 mins). Deprotection of the allyl from carboxyl group (All) was carried out with $Pd(PPh_3)_4$ (0.08 equiv) and $PhSiH_3$ (8 equiv) in DCM/DMF (3 x 35 mins) under nitrogen. Greater than 99% deallylation was achieved by carrying out the reaction with 0.08 equiv $Pd(PPh_3)_4$ and repeating the process twice. The reaction was monitored by test cleavage followed by analytical reverse-phased HPLC and mass spectrometric analysis.

Fmoc/allyl combined solid-phase strategy was used to carry out the synthesis of β^3-peptides on Fmoc-protected Rink amide resin (0.05 mmol). After removal of the Fmoc protection of the rink amide resin by treatment with 20% piperidine for 7 and 30 min, the resin was washed extensively with DMF, DCM and IPA. N-α-Fmoc-L-aspartic acid α-allyl ester (2 equiv) was coupled in the presence of BOP (1.96 equiv), HOBt (2 equiv) and NMM (4.5 equiv) in DMF for 2 h at room temperature. After coupling, the resin was washed with DMF and DCM. Coupling was monitored with the Kaiser test. Palladium catalyzed deprotection of the side chain allyl (All) from carboxyl group was done under nitrogen. $PhSiH_3$ (8 equiv) in NMP (1 mL) was added to pre-weighed $Pd(PPh_3)_4$ (0.08 equiv) in a vial, and the solution was flushed with nitrogen. Palladium solution was transferred to the resin using a steel canulla, and the resulting resin suspension was stirred under nitrogen for 35 min. The resin was washed and the deallylation step was repeated two more times. Following deallylation of the side chain carboxyl, coupling was carried out using corresponding amine (RNH_2, 5 equiv), using the same activating agent (BOP, HOBt, NMM) for 5 h once or twice at room temperature. The resin was washed with DMF and DCM followed by removal of the N^{α}-Fmoc group by treatment with 20% piperidine, and the sequence of reactions was repeated to complete the peptide synthesis. β^3-Peptide was cleaved from the resin using cleavage reagent (5 ml, 96:2:2, TFA/H_2O/TIPS) at room temperature for 2 hours, followed by washing the resin with the cleavage reagent (2 x 2 min, 3 mL). The cleaved peptide was collected, combined with TFA washes, and concentrated by rotary evaporation. The residue was added to

cold Et_2O (40 mL, -78°C) and centrifuged at 3,500 rpm for 5 min. The Et_2O was decanted and the pellet was resuspended in cold Et_2O (40 mL, -78 °C) and centrifugation was repeated. Again the Et_2O was decanted and the pellet was dried with N_2 until cracks appeared on the surface to obtain the crude peptide. Crude peptide was dissolved in CH_3CN/water mixture and was purified using HPLC. Peptides **1** (synthesized previously by Reem)[12] **2**, **11**, **18-21** were essentially synthesized using the above procedure.

Synthesis of β^3-hexapeptide 2

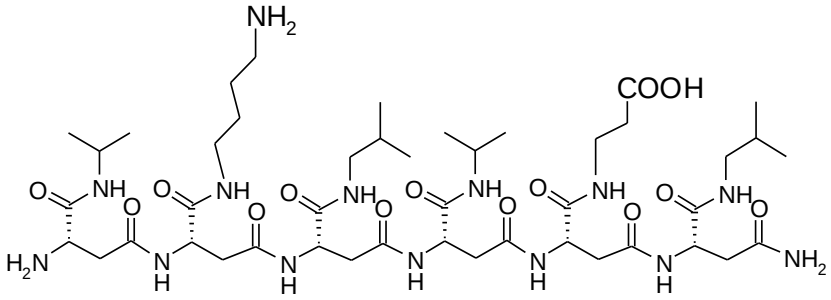

2

(NH_2-β^3amV- β^3amK- β^3amL- β^3amV- β^3amE- β^3amL-$CONH_2$**)**

Synthesis of β^3-hexapeptide **2** was achieved by following the general β^3-peptide synthesis procedure. Briefly, Fmoc-protected Rink amide resin (76.8 mg, 0.05 mmol) was used for building the peptide. N-α-Fmoc-L-aspartic acid α-allyl ester (39.4 mg, 2 equiv) was coupled in the presence of BOP (44 mg, 1.96 equiv), HOBt (13.5mg, 2 equiv) and NMM (25 μL, 4.5 equiv) in DMF for 2 h at room temperature. After coupling of the first amino acid, side chain allyl was removed by reacting with $Pd(PPh_3)_4$ (4.6 mg, 0.08 mmol) and $PhSiH_3$ (50 μL, 8 mmol) in NMP (1 mL) under nitrogen for 35 min. The resin was washed and the

deprotection step was repeated two more times. Following deallylation, side chain carboxyl was coupled to corresponding amine (RNH_2, 5 equiv), using the same activating agents for 5 h at room temperature. Side chain amines 4 and 5 were coupled twice. The resin was washed with DMF and DCM followed by removal of the N^{α}-Fmoc group, and the sequence of reactions was repeated to obtain peptide **2**. After cleavage from the resin using cleavage reagent (5 mL, 96:2:2, TFA/H_2O/TIPS) and trituration with cold ether for 2 mins, the peptide was collected upon centrifugation and decantation of the ether. The crude β^3-peptide **2** was dissolved in H_2O/CH_3CN (2:1), and purified on HPLC using analytical RP-HPLC column (15-27% CH_3CN/water in 50 min, flow rate 0.9 ml/min) to give pure **2** with an overall yield of 20%. **MALDI-TOF:** Calcd for $C_{45}H_{80}N_{14}O_{14}$, $[M + H]^+$ 1027.00; found $[M + H]^+$ 1027.23 as shown in **Figure 3.7**.

3.4.3 General Solid Phase Synthesis of β^2-Peptides

β^2-Peptides were synthesized essentially following the same procedure as described for β^3-peptides. Once again, Fmoc/allyl combined solid-phase strategy was used to carry out the synthesis of β^2-peptides on MBHA (Rink amide) resin. N^{α}-Alloc-N^{β}-Fmoc-L-diaminopropionic acid (2 equiv) was coupled to MBHA resin (0.05 mmol) in the presence of BOP (1.95 equiv), HOBt (2 equiv), and NMM (4.5 equiv) in DMF for 2-3 h at room temperature. The deallylation reaction for the removal of side chain Alloc from the amine group was optimized by varying the reaction conditions (**Table 3.1**). Greater than 99% deallylation was achieved by carrying out the reaction with $Pd(PPh_3)_4$ (0.08 equiv) and $PhSiH_3$

(8 equiv) in DCM/DMF for 35 minutes, and repeating the process twice. The reaction was monitored by test cleavage followed by analytical reverse-phased HPLC and mass spectrometric analysis.

Following deallylation of the Alloc, coupling of side chain amino group was carried out using RCOOH (2 equiv), BOP (1.95 equiv), HOBt (2 equiv), and NMM (4.5 equiv) in DMF for 3 h at 25 °C. After washing and removal of the Fmoc group, the reaction sequence was repeated to obtain the final peptide. Both the backbone elongation and the side chain coupling were monitored by the Kaiser test as well as test cleavage. After cleavage from the resin, the crude β^2-peptide was reconstituted in CH_3CN/H_2O and was purified using RP-HPLC. β^2-Peptides **3**, **4**, and **5** were essentially made by this procedure.

Synthesis of β^2-hexapeptide 3

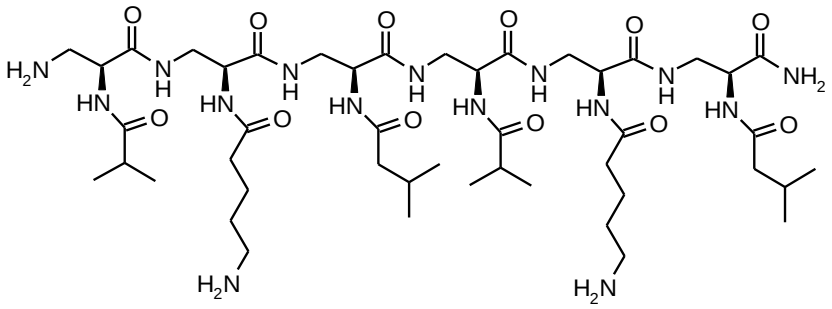

3

(NH_2-β^2amV- β^2amK- β^2amL- β^2amV- β^2amK- β^2amL-$CONH_2$**)**

Synthesis of β^2-hexapeptide **3** was achieved by following the general β^2-peptide synthesis procedure. Briefly, Fmoc-protected MBHA resin (86 mg, 0.05 mmol) was treated with 20% piperidine in NMP (3 mL) for 30 min. The resin was washed with DCM twice, drained for 5 min, followed by extensive washing

with DCM, DMF, and IPA (twice each). Resin was swelled in DMF for 10 min. N^{α}-Alloc-N^{β}-Fmoc-L-diaminopropionic acid (41 mg, 2 equiv) was coupled to the resin in the presence of BOP (43.1 mg, 1.95 equiv), HOBt (13.5 mg, 2 equiv), and NMM (25 ul, 4.5 equiv) in DMF for 2.5 h at room temperature. Following deallylation (3 x 35 min) of the Alloc, the side chain amine was couple to corresponding RCOOH (2 equiv) with BOP (43 mg, 1.95 equiv), HOBt (13.5 mg, 2 equiv), and NMM (25 uL, 4.5 equiv) in DMF for 3 h at 25 °C. After washing and removal of the Fmoc group, the reaction sequence was repeated to obtain **3**. After cleavage from the resin, the crude peptide was reconstituted in 30% CH_3CN and purified on a semipreparative Vydac C18 HPLC column (10 x 250 mm, flowrate = 2 mL/min, monitored at 220 nm) using a gradient of 10-35% CH_3CN in 0.05% aqueous TFA over a period of 1 h. Pure **3** was obtained with an overall yield of 39%. The identity and purity of the β^2-hexapeptide **3** was assessed by analytical HPLC as shown in **Figure 3.11**.

^{1}H NMR [CF_3CD_2OH, 500 MHz, 10°C] δ (ppm): 0.85-0.1 (m, 12H, isovaleric methyls), 1.05-1.2 (m, 12H, isopropyl methyls), 1.62-1.7 (m, 8H, two side chain CH_2 linkages to amine, $CH_2CH_2\mathit{CH_2CH_2}NH_2$), 2.02-2.1 (m, 2H, two isovaleric *CH*), 2.11-2.2 (m, 4H, two isovaleric $\mathit{CH_2}$), 2.31-2.40 (m, 4H, two side chain methylenes $\mathit{CH_2}CH_2CH_2CH_2NH_2$), 2.5-2.59 (m, 2H, two isopropyl *CH*), 3.0-3.09 (m, 4H, two side chain methylenes $CH_2CH_2CH_2\mathit{CH_2}NH_2$), 3.4- 3.8 (m, 12H, backbone $\mathit{CH_2}$), 4.4-4.9 (m, 6H, backbone *CH*), 7.15-7.98 (m, 12H, backbone and side chain amides, overlapping peaks could not be resolved in 1D NMR).

MALDI-TOF: Calcd for $C_{46}H_{85}N_{15}O_{12}$, $[M + H]^+$ 1040.00; found $[M + H]^+$ 1040.20 and $[M + Na]^+$ 1060.00 found $[M + Na]^+$ 1060.20.

Synthesis of β²-Peptide 4

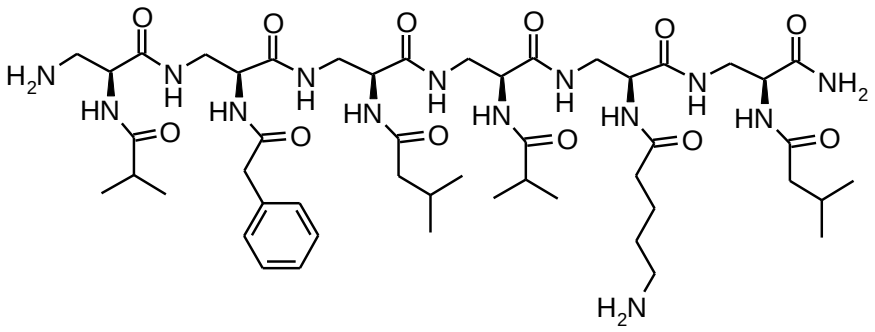

4

(NH_2-β^2amV- β^2amF- β^2amL- β^2amV- β^2amK- β^2amL-$CONH_2$**)**

Synthesis of β^2-peptide **4** was achieved following the same procedure as described for peptide **3** except that amino acids number 3 (β^2-amL) and 4 (β^2-amV) were added as monomers. After cleavage from the resin, the crude peptide was reconstituted in 30% CH_3CN and purified on a semipreparative Vydac C18 HPLC column (10 x 250 mm, flow rate = 2 mL/min, monitored at 220 nm) using a gradient of 10–35% CH_3CN in 0.05% aqueous TFA over a period of 1 h with an overall yield 42%. The identity and purity of the β^2-hexapeptide **4** was assessed by analytical HPLC as shown in **Figure 3.11**.

^{1}H NMR [CF_3CD_2OH, 500 MHz]: δ (ppm): 0.96 (m, 12 H, isovaleric methyls), 1.16 (m, 12 H, isopropyl methyls), 1.72 (m, 4H, side chain methylenes, $CH_2CH_2CH_2CH_2NH_3$), 2.06 (m, 2H, isovaleric *CH*), 2.16 (m, 4H, isovaleric CH_2), 2.38 (m, 2H, side chain methylenes, $CH_2CH_2CH_2CH_2NH_3$), 2.51 (m, 2H, isopropyl *CH*), 3.02 (m, 2H, side chain methylenes, $CH_2CH_2CH_2CH_2NH_3$), 3.27–

3.82 (m, 12H, backbone CH_2), 4.40–4.72 (m, 6H, backbone *CH*), 7.31 (side chain amine), 7.28, 7.33, 7.38 (phenyl ring), 7.36–8.16 (backbone and side chain amides). Because of broad lines resulting from aggregation at concentrations necessary for NMR analysis, sequential assignments could not be obtained. **MALDI-TOF**: Calcd for $C_{49}H_{82}N_{14}O_{12}$, $[M+H]^+$ 1059.62; found $[M+H]^+$ 1059.54 and $[M + Na]^+$ found 1081.51.

Synthesis of β^2-peptide 5 (homooligomer)

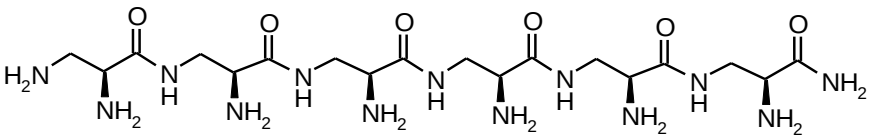

5

Synthesis of β^2-peptide **5** was carried out on MBHA resin (86 mg, 0.05 mmol) as mentioned above. N^{α}-Alloc-N^{β}-Fmoc-L diaminopropionic acid (41 mg, 2 equiv) was coupled to the resin in the presence of BOP (43.1 mg, 1.95 equiv), HOBt (13.5 mg), and NMM (25 uL, 4.5 equiv) in DMF for 2.5 h at room temperature. This was followed by Fmoc deprotection and the procedure was repeated six times. After stepwise coupling of the amino acids, deallylation was carried out in the presence of $Pd(PPh_3)_4$ (0.48 equiv, 0.08 equiv for each allyl group) and $PhSiH_3$ (48 equiv) in DCM/DMF (4 x 35 mins) under nitrogen to obtain **5**. After cleavage from the resin, the crude peptide was reconstituted in 10% CH_3CN and purified on a semipreparative Vydac C18 HPLC column (1 x 25 cm, flow rate = 2 mL/min, monitored at 220 nm) using a gradient of 8-40% CH_3CN in 0.05% aqueous TFA over a period of 1 h with an overall yield 92%.

The identity and purity of the β^2-hexapeptide **5** was assessed by analytical HPLC as shown in **Figure 3.11**.

^{1}H NMR [CF_3CD_2OH, 500 MHz]: δ= 3.35-3.8 (m, 12H, backbone CH_2), 4.02-4.31 (m, 6H, backbone CH), 7.5-7.7 (m, 2H, carboxamide), 8.3-8.85 (m, 5H backbone amides). **ES-MS**: Calcd for $C1_8H_{39}N_{13}O_6$, $[M + H]^+$ 534.00; found $[M + H]^+$ 534.05 and $[M + Na]^+$ 556.00; found $[M + Na]^+$ 556.23.

3.4.4 Synthesis of Fmoc-β^3-Amido-Amino Acid Monomers

β^3-amido amino acid monomers were synthesized in four steps as shown **Scheme 3.3**. In a solid phase reactor, chlorotrityl resin (74 mg, 0.1 mmol) was suspended in DCM (4 mL) for swelling for 30 min. The swelled resin was reacted with a solution of Fmoc-L-aspartic acid α-allyl ester (118.62 mg, 3 equiv) and DIPEA (210 μL, 12 equiv) in dry CH_2Cl_2 for 2 h. The resin was capped by washing with a solution of dry CH_2Cl_2–MeOH–DIPEA (17:2:1). The resin was washed with DMF (4 x 1 min), DCM (4 x 1 min) and IPA. Deallylation was carried out in the presence of $(Pd(PPh_3)_4$ (0.08 equiv) and $PhSiH_3$ (8 equiv) in DCM (3 x 35 mins) under nitrogen to remove the side chain allyl protection. Subsequently, the side chain amine (2.5 equiv) was coupled using BOP (110 mg, 2.45 equiv) HOBt (33 mg, 2.5 equiv), and NMM (75 uL, 4.5 equiv) in DMF for 5 h. Cleavage of the monomer from the resin was done either by 50% TFA/DCM for 30 min, or with TFE/DCM (20/80%) for 45 min at room temperature.

Solid phase synthesis of N^{β}-Fmoc-β^3amV (7)

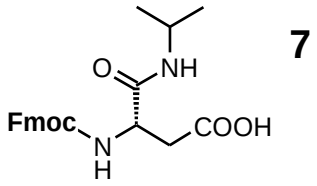

7

N^{β}-Fmoc-β^3amV (**7**) was synthesized using the same procedure as described above. β^3-amido amino acid **7** was cleaved from the resin using 50% TFA/DCM for 30 min. The cleaved monomer was collected, combined with TFA washes, and concentrated by rotary evaporation. The residue was added to cold Et_2O (40 mL, -78 °C) and centrifuged at 3,500 rpm for 5 min. The Et_2O was decanted and the pellet was resuspended in cold Et_2O (40 mL, -78°C) and centrifugation was repeated. Again the Et_2O was decanted and the pellet was dried with N_2 until cracks appeared on the surface to obtain **7** with an overall yield 65%. The purity of **7** was assessed by analytical HPLC as shown in **Figure 3.10.**

^{1}H NMR (300 MHz, CD_3OD): δ= 1.06 (d, J= 6.7, 6H, *$(CH_3)_2$*CH), 2.6 (m, 2H, *CH_2*COOH), 3.94 (m, 1H, $(CH_3)_2$*CH*), 4.25 (m, 1H, *CH*CH_2O), 4.6 (t, 1H, *CH*CH_2COOH), 4.7 (m, 2H, CH*CH_2*O), 7.2-7.8 (m, 8H, aryl H). **^{13}C NMR** (300 MHz, DMSO-d_6, CD_3OD): δ= 19.93, 40.67, 40.76, 46.51, 50.68, 65.50, 119.76, 124.99, 126.80, 127.35, 140.52, 143.57, 155.56, 168.8, 172.87, and **ES-MS**: Calcd for $C_{22}H_{24}N_2O_5$, $[M + H]^+$ 397.47; found $[M + H]^+$ 397.06.

Solid phase synthesis of N^{β}-Fmoc-β^3amL (8)

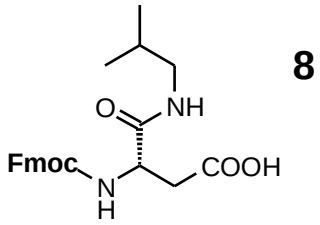

8

N^{β}-Fmoc-β^3amL (**8**) was synthesized using the same procedure as described above. β^3-amido amino acid **8** was cleaved from the resin, using 50% TFA/DCM for 30 min, with an overall yield of 63%. The purity of **8** was assessed by analytical HPLC as shown in **Figure 3.10**. The monomer was characterized as follow.

^{1}H NMR (300 MHz, $CDCl_3$): δ= 0.96 (d, J=6.6, 6H, *$(CH_3)_2$*CH), 1.85 (m, 1H, $(CH_3)_2$*CH*), 2.8 (m, 1H, *CH_2*COOH), 2.9 (m, 1H, *CH_2*COOH), 3.2 (m, 2H, $(CH_3)_2$ CH*CH_2*NH), 4.2 (m, 1H, *CH*CH_2O), 4.45 (m, 2H, CH*CH_2*O, *CH*CH_2COOH), 7.2-7.8 (m, 8H, arylH). **^{13}C NMR** (300 MHz, $CDCl_3$): δ= 19.93, 27.9, 36.9, 46.06, 46.51, 50.68, 65.60, 119.76, 124.99, 126.8, 127.35, 140.52, 143.57, 155.56, 168.87, 172.8, and HR- **ES-MS:** Calcd for $C_{23}H_{26}N_2O_5$, $[M + H]^+$ 411.47; found $[M + H]^+$ =411.00.

Solid phase synthesis of N^{β}-Fmoc-β^3amK (Boc)-OH (9)

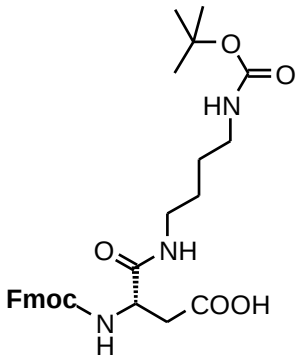

9

N^{β}-Fmoc-β^3amK (Boc)-OH (**9**) was synthesized using the same procedure as described above. β^3-amido amino acid **9** was cleaved from the resin, using TFE/DCM (20/80%) for 45 min, to obtain the monomer with an overall of yield 52%. The purity of **9** was assessed by analytical HPLC as shown in **Figure** 3.10. The monomer was characterized as follow.

^{1}H NMR (300 MHz, $CDCl_3$): δ=1.3 (m, 13H, *$(CH_3)_3$* CH *$(CH_2)_2$)*, 2.2-2.4 (m, 2H, *CH_2*COOH), 2.7- 3.1 (m, 4H, (NH)*CH_2* CH_2 CH_2 *CH_2*NH), 3.7 (m, 4H, *CH*CH_2O, 2H, CH*CH_2*O, *CH*CH_2COOH), 7.2-7.8 (m, 8H, aryl H). **^{13}C NMR** (300 MHz, CD_3OD): δ = 26.34, 26.83, 28.26, 40.69, 40.98, 51.04, 77.30, 119.98, 121.10, 122.17, 123.88, 127.68, 128.88, 129.43, 135.33, 137.36, 139.34, 142.50, 155.52, 170.93. **ES-MS**: Calcd $C_{28}H_{35}N_3O_7$, $[M - H]^-$ 524.25; found $[M - H]^-$ 524.

Solid phase synthesis of N^{β}-Fmoc-β^3amE(tBu)-OH (10)

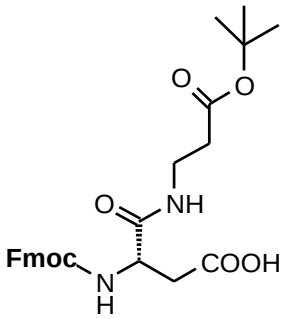

10

N^{β}-Fmoc-β^3amE(tBu)-OH (**10**) was synthesized using the same procedure as described above. β^3-amido amino acid **10** was cleaved from the resin, using TFE/DCM (20/80%) for 45 min, to obtain the monomer with an overall of yield 50%. The purity of **10** was assessed by analytical HPLC as shown in **Figure** 3.10. The monomer was characterized as follow.

^{1}H NMR (300 MHz, d-DMSO): δ= 1.4 (s, 9H, *$(CH_3)_3$*C), 2.5-2.8 (m, 4H, *CH_2*COOH, *CH_2*CH_2NHCO), 3.6 (m, 2H, CH_2*CH_2*NHCO*)*, 4.25-4.4 (m, 4H, *CH*CH_2O, CH*CH_2*O, *CH*CH_2COOH), 7.3-7.8 (m, 8H, aryl H). **^{13}C NMR** (300 MHz, d-DMSO): δ=27, 34.88, 34.98, 40.34, 46.64, 50.53, 65.77, 79.99, 120.14, 125.28, 127.13, 127.42, 127.68, 140.7, 143.80, 155.82, 170.76, 171.69, 173.04. **ES-MS:**: Calcd for $C_{26}H_{30}N_2O_7$, $[M - H]^-$ 481.54; found $[M - H]^-$ 481.20.

Solution phase synthesis of β^3-am-V (7) and β^3-am-L (8)

β^3-amido amino acids **7** and **8** were also synthesized using solution phase synthesis as illustrated in **Scheme 3.2**. Fmoc-Asp(OtBu)OH (411.50 mg, 1 mmol), BOP (442.3 mg, 1.95 equiv) , HOBt (135.1 mg, 2 equiv) and NMM (200

μL, 4.5 equiv) were weighted into a round bottom flask, and dissolved in DMF/DCM (4 mL). The mixture was stirred for 5 min to activate the carboxyl group, following which the amine side chain ($R\text{-}NH_2$, 5 equiv) was added and the reaction mixture was stirred for 24 h at room temperature. The completion of reaction was monitored by TLC. The reaction mixture was evaporated to give oil as the residue. The residue was dissolved in EtOAc (10 mL). The EtOAc was washed with 5% $NaHCO_3$ three times followed by washing (3x) with brine (0.9% NaCl solution). The organic layer was then dried (Na_2SO_4), filtered, concentrated, and lyophilized. The product was characterized using mass spectrometry. After confirmation of the mass, the precipitate was treated with TFA:TIPS:H_2O (96:2:2) cocktail mixture with stirring for 2 h. The reaction mixture was then evaporated under vacuum and the product was washed many times with diethyl ether. The precipitate obtained was further characterized with mass spectrometry, HPLC, and NMR spectroscopy. The overall yield was 80.5%. The product was used without further purification.

3.4.5 Solution Phase Synthesis of N^{α}-Alloc-N^{β}-Fmoc-L-DAP (16)

Orthogonally protected L-DAP (**16**) was synthesized in the four steps (**Scheme 3.6**) starting from Boc-L-Asn as described below.

N^{α}-Boc-2,3-diaminopropionic acid (13)

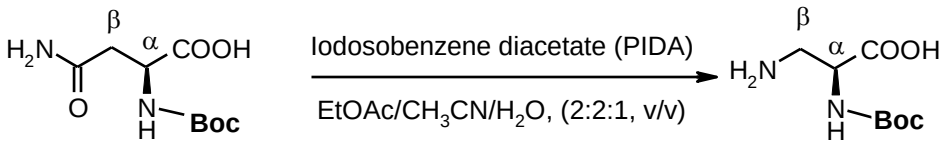

12 **13**

Boc-L-Asn **12** (3.75 g, 16.1 mmol) was reacted with iodobenzene diacetate (PIDA) (4.16 g, 19.4 mmol) in a mixture of solvents (45 mL, EtOAc:MeCN:H_2O, 2:2:1, v/v) at 0 °C. After 30 minutes, the reaction mixture was warmed to room temperature and stirring was continued for 4 h. At this point, the reaction mixture was cooled again to 0 °C and the precipitate was collected by filtration and washed with EtOAc (10 mL). The precipitate was dissolved in water and washed with ether (3 x 7 mL). The aqueous layer was evaporated to dryness to yield 2.52 g (76.6%) of **2** as white powder (m.p. 209-211°C). **^{1}H NMR** [D_2O, 300 MHz]: δ 1.4 (s, 9H, $C(CH_3)_3$), 3.15 (m, 1H, NH_2CH_2CH), 3.4 (m, 1H, NH_2CH_2CH), 4.2 (m, 1H, NH_2CH_2CH). **ES-MS**: Calcd for $C_8H_{16}N_2O_4$, $[M + H]^+$ 205.23; found $[M + H]^+$ 204.92, $[M + Na]^+$ 226.92.

N^{α}-Boc-N^{β}-Fmoc-2,3-diaminopropionic acid (14)

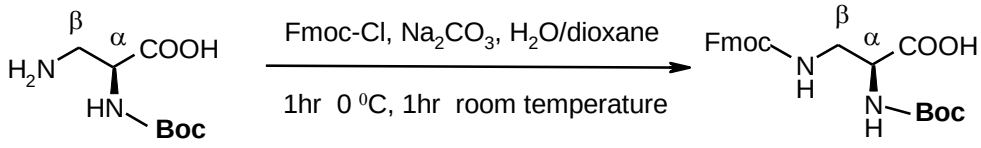

13 **14**

N^{α}-Boc-2,3-diaminopropionic acid **13** (260 mg, 1.3 mmol) was dissolved

in 10% aqueous Na_2CO_3 (3 mL) at 0 °C. To this solution, Fmoc-Cl (550 mg, 2.1 mmol) in dioxane (5 mL) was added dropwise and stirred at 0 °C for 1 h followed by stirring for another 1 h at room temperature. The reaction was quenched with water (50 mL), pH adjusted to 1 using conc. HCl, and extracted with EtOAc (3 x 25 mL) rapidly to give the crude product. Pure N^{α}-Boc-N^{β}-Fmoc-2,3-diaminopropionic acid **14** (535 mg, 96.6%) was obtained after column chromatography using EtOAc/hexane. **^{1}H NMR** [$CDCl_3$, 300 MHz]: δ 1.43 (s, 9H, $C(CH_3)_3$), 3.62 (m, 2H, $CHCH_2NH$) 4.2-4.4 (m, 4H, $CHCH_2O$, $CHCH_2O$, $CHCH_2NH$), 5.5 (br s, 1H, NH) and, 5.7 (br s, 1H, NH), 7.2-7.8 (m, 8H, aryl H). **ES-MS**: Calcd for $C_{23}H_{26}N_2O_6$, $[M + H]^+$ 427.47; found $[M + H]^+$ 426.92.

N^{β}-Fmoc-2,3-diaminopropionic acid (15)

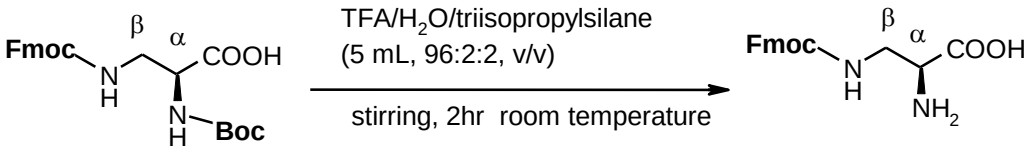

14 **15**

N^{α}-Boc-N^{β}-Fmoc-2,3-diaminopropionic acid **14** was treated with TFA/H_2O/triisopropylsilane (5 mL, 96:2:2, v/v) at room temperature for 2 h to give N^{β}-Fmoc-2,3-diaminopropionic acid **15**. The residue was added to cold Et_2O (40 ml, -78°C) and centrifuged at 3,500 rpm for 5 min. The Et_2O was decanted and the pellet was resuspended in cold Et_2O (40 mL, -78 °C) and centrifugation was repeated. Et_2O was decanted again and the pellet was dried with N_2 until cracks appeared on the surface to yield crude **15** in 80% yield. **^{1}H NMR** [DMSO,

300 MHz]: δ 3.3-3.62 (br m, 2H, CH*CH*$_2$NH), 4.1 (m, 1H, *CH*CH$_2$NH), 4.2-4.4 (m, 3H, CH*CH*$_2$O, *CH*CH$_2$O), 7.2-7.8 (m, 8H, aryl H). **ES-MS:** Calcd for $C_{18}H_{18}N_2O_4$, $[M + H]^+$ 327.00; found $[M + H]^+$ 326.98, $[M + Na]^+$ 349.98.

N$^{\alpha}$-Alloc-N$^{\beta}$-Fmoc-L-diaminopropionic acid (16)

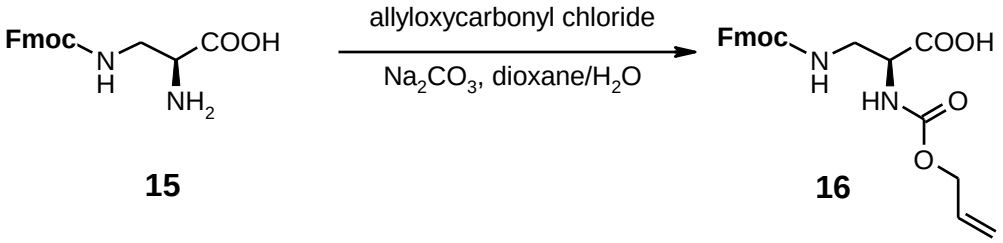

15 **16**

Alloc protection of the free amino group in N$^{\beta}$-Fmoc-2,3-diaminopropionic acid **15** was carried out by dropwise addition of allyloxycarbonyl chloride (17.6 μL, 1.5 equiv) to a mixture of **15** (36.2 mg, 1 equiv) and $NaHCO_3$ (44.8 mg) in dioxane/water (1:1, 7 mL) at 0 °C. The reaction mixture was stirred at 0 °C for 40 min followed by acidification (10% HCl) and extraction with DCM. The crude product was purified using column chromatography to give pure **16** (40 mg, 88% yield). The purity of **16** was assessed using semi-preparative RP-HPLC using 50% CH_3CN/water with flow rate of 2 mL/min. The compound eluted as a single peak around 12.5 min. **^{1}H NMR** [CD_3OD, 300 MHz]: δ 3.4-3.65 (m, 2H, CH*CH*$_2$NH), 4.2 (m, 1H, *CH*CH$_2$O), 4.25-4.4 (m, 3H, CH*CH*$_2$O & CH$_2$C*H*CO), 4.5 (d, 2H, CH*CH*$_2$O), 5.15 (d, J = 10.3 Hz, 1H, *cis* C*H*$_2$=CH), 5.3 (d, J = 17 Hz, 1H, *trans* C*H*$_2$=CH), 5.8-6.0 (m, 1H, CH$_2$=*CH*), 7.2-7.8 (m, 8H, *arylH*). 13C NMR [CD3OD,75 MHz]: δ 43.1, 48.4, 55.7, 66.9, 68.0, 117.6, 120.8, 126.2, 128.1, 128.7, 134.1, 142.4,

145.2, 158.3, 159.0, 173.5. **ES-MS:** Calcd for $C_{22}H_{22}N_2O_6$, $[M + H]^+$ 411.43; found $[M + H]^+$ 410.92, $[M + Na]^+$ 432.92.

Synthesis of N^{α}-isobuturyl-N^{β}-Fmoc-L-diaminopropionic acid (β^2-am-V)

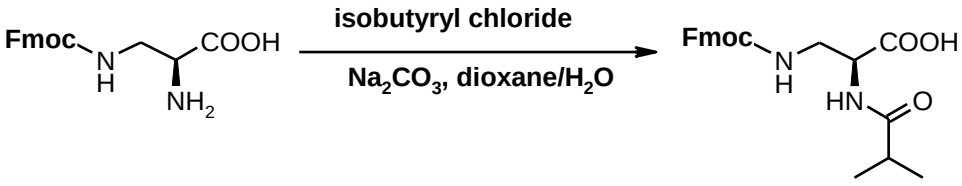

15 **β^2-amV**

β^2-amV was synthesized from **15** following the same procedure as used for the synthesis of **16**. Isobutyryl chloride was added dropwise (2.5 equiv) to a mixture of **15** (1 equiv) and $NaHCO_3$ (44.8 mg) in dioxane/water (1:1, 7 mL) at 0 °C. The reaction mixture was stirred at 0 °C for 40 min, followed by stirring at room temperature for 72 h. After that, the mixture was acidified with 10% HCl and extracted with DCM. The crude product was purified using column chromatography to give pure product with 98% yield. The purity of the product was assessed using semipreperative RP-HPLC using 20% CH_3CN/water with flow rate of 2 mL/min. The compound eluted as a single peak around 15.5 min. **^{1}H NMR** [CD_3OD, 300 MHz]: δ 1 (d, 6H, $(CH_3)_2CH$), 2.5(m, 1H, $(CH_3)_2CH$) 3.5 (m, 2H, $CHCH_2NH$), 4.2.4.4 (m, 1H, $CHCH_2O$), 4.5 (m, 2H, $CHCH_2O$), 7.2-7.8 (m, 8H, arylH). **ES-MS:** Calcd for $C_{22}H_{24}N_2O_5$, $[M + H]^+$ 397.17; found $[M + H]^+$ 397.12, $[M + Na]^+$ 419.07.

Synthesis of N^{α}-isovaleryl-$N^{ß}$Fmoc-2,3-diaminopropionic acid (β^2-am-L)

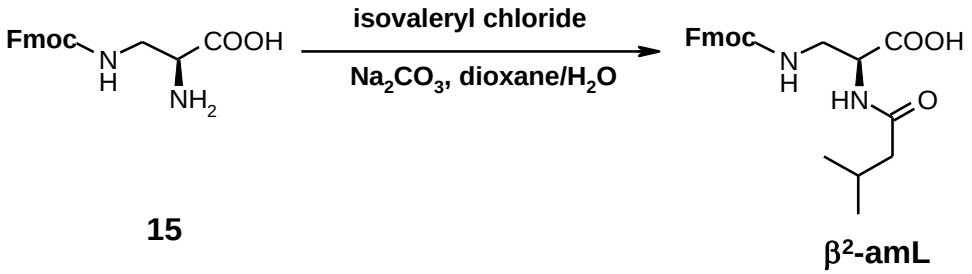

15 **β²-amL**

Following the same procedure as for the isobutyryl derivative, isovaleryl chloride was added dropwise (5 equiv) to a mixture of **15** (1 equiv) and $NaHCO_3$ (44.8 mg) in dioxane/water (1:1, 7 mL) at 0 °C. The reaction mixture was stirred at 0 °C for 40 min, followed by stirring at room temperature for 120 h. After acidification and extraction, the crude product was purified using column chromatography (using DCM: Methanol: HOAc, 180:8:2) to give pure product (95% yield). The purity of the product was assessed using semipreperative RP-HPLC using 25% CH_3CN/H_2O with flow rate of 2 mL/min. The compound eluted as a single peak around 11.7 min. **^{1}H NMR** [CD_3OD, 300 MHz]: δ 1 (d, 6H, $(CH_3)_2CH$), 2.1 (m, 1H, $(CH_3)_2CH$), 2.3 (d, 2H, $CHCH_2CO$), 3.5 (m, 2H, $CHCH_2NH$), 4.2-4.4 (m, 1H, $CHCH_2O$), 4.5 (m, 2H, $CHCH_2O$), 7.2-7.8 (m, 8H, arylH). **ES-MS:** Calcd for $C_{23}H_{26}N_2O_6$, $[M + H]^+$ 411.18; found $[M + H]^+$ 411.14, $[M + Na]^+$ 433.11.

3.4.6 Solid Phase Synthesis of β^3-Peptide 17

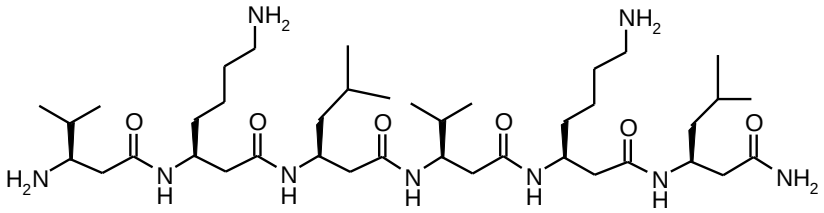

17

β^3-Peptide **17** was synthesized following the general Fmoc-solid phase synthesis procedure. Briefly, Fmoc-protected Rink amide resin (78.6 mg, 0.05 mmol) was treated with 20% piperidine/DMF twice (7 and 30 min), and washed with DMF, IPA, and CH_2Cl_2 (3x 5 mL, 5 min each). The resin was then agitated with Fmoc-β^3hLeu-OH (2 equiv), BOP (2 equiv), HOBt (2 equiv) and NMM (4.5 equiv) in DMF (1.5 mL) for 3.5 h, and washed with DMF, IPA, and CH_2Cl_2 (3 x 5 mL, 5 min each). The Fmoc-deprotection and amino acid coupling steps were repeated to complete the sequence. Coupling efficiencies were checked by the Kaiser test. Residual free amino groups were capped with 20% Ac_2O in CH_2Cl_2 (3 mL) (2 x 3 mL, 20 min each). The terminal Fmoc group was removed with 20% piperidine-DMF (3 x 15 min). Longer deprotection time was required to remove the N-terminal Fmoc protection, and the usual washing procedure was applied. The crude peptide was cleaved from the support with the cleavage reagent (5 mL, 96:2:2, TFA/H_2O/TIPS) at room temperature for 2 hours. The resin was washed with the cleavage reagent (2 x 2 mins, 3 mL each). The cleaved peptide was collected, combined with TFA washes, and concentrated by rotary evaporation. The residue was subjected to cold Et_2O (40 mL, -78 °C) twice as described before to obtain crude peptide **17**. The crude peptide was dissolved in CH_3CN/H_2O (2:1)

and either purified immediately or lyophilized and stored at -20 °C. The overall yield of **17** was 54%. **ES-MS:** Calcd for $C_{40}H_{79}N_9O_6$, $[M + H]^+$ 782.61; found $[M + H]^+$ 782.88.

Table 3.7: ^{1}H NMR chemical shift assignments for β^3-peptide **17** in CF_3CD_2OH (500 MHz).

Residue	Backbone shifts (δ)	Side chain shifts(δ)
1	7.39 (1H, $\underline{H_3N^+}$), 3.57(1H,NH$\underline{CH}$$CH_2$), 2.89,2.68(2H,NHCH$\underline{CH_2}$)	2.09(1H,$(CH_3)_2\underline{CH}$), 1.09(6H,($\underline{CH_3}$)$_2$CH)
2	8.34(d,J=9.4Hz,$\underline{HN}$), 4.52(1H,NH$\underline{CH}$$CH_2$), 2.75,2.57(2H,NHCH$\underline{CH_2}$),	7.29(3H,$\underline{NH_3^+}$$CH_2CH_2CH_2CH_2$), 3.03,2.97(2H,$NH_3\underline{CH_2}CH_2CH_2CH_2$), 1.79,1.68(2H,$NH_3CH_2\underline{CH_2}CH_2CH_2$), 1.58(2H,$NH_3CH_2CH_2CH_2\underline{CH_2}$), 1.45,1.42(2H,$NH_3CH_2CH_2\underline{CH_2}CH_2$)
3	8.27(d,J=9.2Hz,$\underline{HN}$), 4.36(1H,NH$\underline{CH}$$CH_2$), 2.46(2H,NHCH$\underline{CH_2}$)	1.52(1H,$(CH_3)_2\underline{CH}CH_2$), 1.45, 1.28(2H,$(CH_3)_2CH\underline{CH_2}$), 0.94,0.89(6H,($\underline{CH_3}$)$_2$CH CH_2)
4	7.47(d,J=9.4Hz,$\underline{HN}$), 4.24(1H,NH$\underline{CH}$$CH_2$), 2.57,2.26(2H,NHCH$\underline{CH_2}$),	1.73(1H,$(CH_3)_2\underline{CH}$), 0.91(6H,($\underline{CH_3}$)$_2$CH)
5	6.76 (d, J=8.9 Hz,$\underline{HN}$), 4.38(1H,NH$\underline{CH}$$CH_2$), 2.53,2.34(2H,NHCH$\underline{CH_2}$),	7.31(3H,$\underline{NH_3^+}$$CH_2CH_2CH_2CH_2$), 2.97(2H,$NH_3\underline{CH_2}CH_2CH_2CH_2$), 1.68(2H,$NH_3CH_2\underline{CH_2}CH_2CH_2$), 1.58,1.45(2H,$NH_3CH_2CH_2CH_2\underline{CH_2}$), 1.38(2H,$NH_3CH_2CH_2\underline{CH_2}CH_2$)
6	6.54(d,J=9.5Hz,$\underline{HN}$), 4.45(1H,NH$\underline{CH}$$CH_2$), 2.50,2.30(2H,NHCH$\underline{CH_2}$),	1.58(1H,$(CH_3)_2\underline{CH}CH_2$), 1.42, 1.31(2H,$(CH_3)_2CH\underline{CH_2}$), 0.94(6H,($\underline{CH_3}$)$_2$CH CH_2)
C-terminus	6.85, 5.82 (NH_2)	

The final conc. of **17** in TFE-d2 was 5 mM. The chemical shifts were referenced to the TFE methylene protons at 3.88 ppm and recorded at 15 ºC.

3.4.7 Solid Phase Synthesis of β^3-Peptides 18-21

β^3-Peptides **18-21** were essentially synthesized following general synthesis of β^3-peptides (Section 3.4.2), except, at certain steps β^3-amido amino acid monomers were added.

β^3-peptide 18a

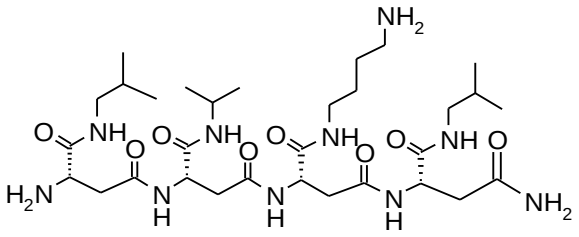

18a

β^3-Peptide **18a** was synthesized following general synthesis of β^3-peptides (Section 3.4.2). The overall yield of **18a** was 51%. **ES-MS:** Calcd for $C_{31}H_{58}N_{10}O_8$, $[M + H]^+$ 699.44; found $[M + H]^+$ 699.78.

Table 3.8: ^{1}H NMR chemical shift assignments for β^3-peptide **18a** in CF_3CD_2OH (500 MHz).

Residue	Backbone shifts (δ)	Side chain shifts (δ)
1	7.77 (NH_3^+-terminal), 4.28 (1H,NH<u>*CH*</u>CH_2), 3.08, 2.88 (2H,NHCH<u>*CH_2*</u>),	7.57 (1H, NH). 3.04 , 3.18 (2H, $(CH_3)_2$CHC<u>*H_2*</u>), 1.78 (1H, $(CH_3)_2$<u>*CH*</u>), 0.90(6H, <u>*$(CH_3)_2$*</u>$CHCH_2$),
2	8.21 (1H, <u>*HN*</u>), 4.88 (1H,NH<u>*CH*</u>CH_2), 2.75, 2.64(2H,NHCH<u>*CH_2*</u>)	7.02 (1H, <u>*NH*</u>) 3.96 (1H, $(CH_3)_2$<u>*CH*</u>), 1.15 (6H, <u>*$(CH_3)_2$*</u>CH),
3	7.63 (1H, <u>*HN*</u>), 4.79(1H,NH<u>*CH*</u>CH_2), 2.80, 2.66(2H,NHCH<u>*CH_2*</u>),	7.29 (1H, <u>*NH*</u>), 7.20 (3H, NH_3^+) 3.25 (2H,$NH_3CH_2CH_2CH_2$<u>*CH_2*</u>), 3.00(2H,NH_3<u>*CH_2*</u>$CH_2CH_2CH_2$), 1.66 (2H,NH_3CH_2<u>*CH_2*</u>CH_2CH_2), 1.57 (2H,$NH_3CH_2CH_2$<u>*CH_2*</u>CH_2),
4	7.54 (1H, <u>*HN*</u>), 4.93 (1H,NH<u>*CH*</u>CH_2), 2.77,2.67(2H,NHCH<u>*CH_2*</u>),	7.68 (1H, NH), 3.12 (1H $(CH_3)_2$CH C<u>*H_2*</u>), 3.00 (1H, $(CH_3)_2$CH C<u>*H_2*</u>), 1.80 (1H,$(CH_3)_2$<u>*CH*</u>), 0.92 (6H, <u>*$(CH_3)_2$*</u>$CHCH_2$),
C- terminus	6.85, 6.52 (NH_2)	

The final conc. of β^3-peptide **18a** in TFE-d2 was 0.5 mg/250 μL. The chemical shifts were referenced to the TFE methylene protons at 3.88 ppm. The N-terminal NH_3^+ was not completely assigned due to exchange with the solvent.

β^3-peptide 18b

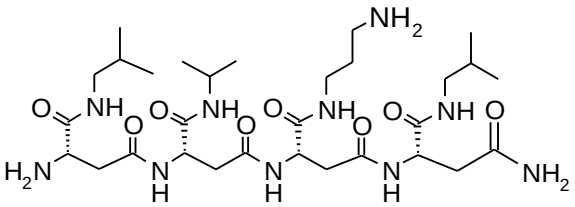

18b

β^3-Peptide **18b** was synthesized following general synthesis of β^3-peptides (Section 3.4.2). The overall yield of **18b** was 43%. **ES-MS:** Calcd for $C_{30}H_{56}N_{10}O_8$, $[M + H]^+$ 685.42; found $[M + H]^+$ 685.30.

Table 3.9: ^{1}H NMR chemical shift assignments for β^3-peptide **18b** in CF_3CD_2OH (500 MHz).

Residue	Backbone shifts (δ)	Side chain shifts (δ)
1	7.71 (NH_3^+-terminal), 4.27 (1H,NH*CH*CH_2), 3.20, 2.99 (2H,NHCH*CH_2*),	7.57 (1H, NH). 3.20, 2.99 (2H $(CH_3)_2$CH*CH_2*), 1.8 (1H, $(CH_3)_2$*CH*), 0.91 (6H, *$(CH_3)_2$*$CHCH_2$),
2	8.17 (1H, *HN*), 4.88 (1H,NH*CH*CH_2), 2.93(2H,NHCH*CH_2*)	7.03 (1H, *NH*) 4.02 (1H, $(CH_3)_2$*CH*), 1.16 (6H, *$(CH_3)_2$*CH)
3	7.61 (1H, *HN*), 4.82(1H,NH*CH*CH_2), 2.89 (2H,NHCH*CH_2*)	 3.45- 3.33(2H,$NH_3CH_2CH_2$*CH_2*), 2.60-2.77 (4H,NH_3*CH_2CH_2*CH_2)
4	7.57 (1H, *HN*), 4.93 (1H,NH*CH*CH_2), 2.77, 2.60(1H,NHCH*CH_2*)	7.69 (1H, NH) 2.60-2.77 (2H $(CH_3)_2$CH*CH_2*), 1.80 (1H,$(CH_3)_2$*CH*), 0.91 (6H, *$(CH_3)_2$*$CHCH_2$),
C-terminus	6.86, 6.48 (NH_2)	

The final conc. of peptide **18b** in TFE-d2 was 0.5 mg/250 μL. The N-terminal NH_3^+ was not completely assigned due to exchange with the solvent.

β^3-peptide 19a

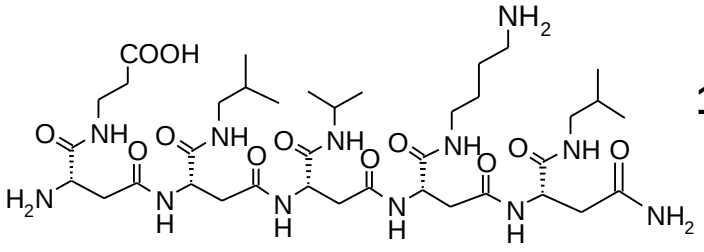

19a

β^3-Peptide **19a** was synthesized following general synthesis of β^3-peptides (Section 3.4.2). The overall yield of **18b** was 55.3% **ES-MS:** Calcd for $C_{38}H_{68}N_{12}O_{12}$, $[M + H]^+$ 885.50; found $[M + H]^+$ 885.76.

Table 3.10: ^{1}H NMR chemical shift assignments for β^3-peptide **19a** in CF_3CD_2OH (500 MHz).

Residue	Backbone shifts (δ)	Side chain shifts (δ)
1	4.27 (1H,NHC*H*CH_2), 2.64-3.14 (2H,NHCH*CH_2*)	7.79(NH), 3.72(1H,COOHCH$_2$*CH_2*NH) 3.64(1H,COOHCH$_2$*CH_2*NH), 2.54 (2H COOH*CH_2*CH_2NH)
2	8.57(1H, *HN*), 4.80 (1H,NH*CH*CH_2), 2.64-3.14 (2H,NHCH*CH_2*),	7.24 (1H, *NH*), 3.44(2H,$(CH_3)_2$CH*CH_2*), 1.80 (1H, $(CH_3)_2$*CH*), 0.91 (6H, *(CH_3)$_2$*CH)
3	8.57 (1H, *HN*), 5.00 (1H,NH*CH*CH_2), 2.64-3.14 (2H,NHCH*CH_2*)	6.74 (1H, *NH*) 4.02 (1H, $(CH_3)_2$*CH*), 1.14 (6H, *(CH_3)$_2$*CH)
4	7.31 (1H, *HN*), 5.05 (1H,NH*CH*CH_2), 2.64-3.14 (2H,NHCH*CH_2*)	7.96 (1H, *NH*), 7.20 (3H, NH_3^+) 3.47 (2H,$NH_3CH_2CH_2CH_2$*CH_2*), 1.68-1.84 (2H,NH_3CH_2*CH_2*CH_2CH_2)
5	7.29 (1H, *HN*), 4.27 (1H,NH*CH*CH_2), 2.56 (2H,NHCH*CH_2*)	8.34 (1H, *NH*), 3.32(2H,$(CH_3)_2$CH*CH_2*), 1.78(1H, $(CH_3)_2$*CH*), 0.91 (6H, *(CH_3)$_2$*CH)
C-terminus	6.76, 6.58 (NH_2)	

The final conc. of β^3-peptide **19a** in TFE-d2 was 0.6 mg/250 μL. The N-terminal NH_3^+ was not observed due to exchange with the solvent. One of the CH_2 protons of residue 4 were not assigned from the NMR due to broadness of the peaks.

β^3-peptide 19b

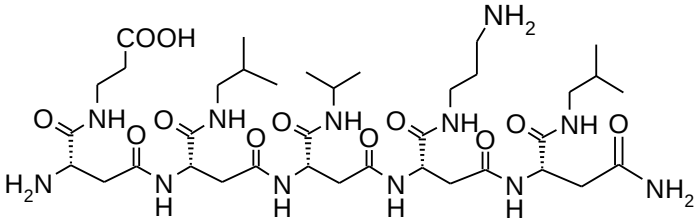

19b

β^3-Peptide **19b** was synthesized following general synthesis of β^3-peptides (Section 3.4.2). The overall yield of **19b** was 40.4 % yield. **ES-MS:** Calcd for $C_{37}H_{66}N_{12}O_{12}$, $[M + H]^+$ 871.42; found $[M + H]^+$ 871.77.

Table 3.11: ^{1}H NMR chemical shift assignments for β^3-peptide **19b** in CF_3CD_2OH (500 MHz).

Residue	Backbone shifts (δ)	Side chain shifts (δ)
1	4.26 (1H,NH*CH*CH_2), 3.36,2.84 (2H,NHCH*CH_2*)	7.78(NH),3.63(1H,COOHCH$_2$*CH_2*NH) 3.47(1H,COOHCH$_2$*CH_2*NH), 2.54 (2H COOH*CH_2*CH_2NH)
2	8.50 (1H, *HN*), 4.80 (1H,NH*CH*CH_2), 2.71,2.61 (2H,NHCH*CH_2*)	7.27 (1H, *NH*), 3.05(2H,$(CH_3)_2$CH*CH_2*), 1.77(1H, $(CH_3)_2$*CH*), 0.89 (6H, *$(CH_3)_2$*CH CH_2)
3	8.50 (1H,*HN*), 5.00 (1H,NH*CH*CH_2), 2.90,2.64 (2H,NHCH*CH_2*)	6.75 (1H, *NH*) 3.96 (1H, $(CH_3)_2$*CH*), 1.13 (6H, *$(CH_3)_2$*CH)
4	7.44 (1H,*HN*), 5.03 (1H,NH*CH*CH_2), 2.78,2.68 (2H,NHCH*CH_2*)	8.12 (1H, *NH*), 7.20 (3H, NH_3^+) 3.38 (2H,$NH_3CH_2CH_2$*CH_2*), 3.03 (2H,NH_3*CH_2*CH_2CH_2), 1.95 (2H,NH_3CH_2*CH_2*CH_2),
5	7.28 (1H, *NH*), 4.26 (1H,NH*CH*CH_2), 2.72-2.64 (2H,NHCH*CH_2*)	8.25 (1H, *NH*), 3.11, 2.96(2H,$(CH_3)_2$CH*CH_2*), 1.81(1H, $(CH_3)_2$*CH*), 0.91 (6H, *$(CH_3)_2$*CH)
C-terminus	6.76, 6.56 (NH_2)	

The final conc. of β^3-peptide **19b** in TFE-d2 was 0.6 mg/250 μL. The N-terminal NH_3^+ was not observed due to exchange with the solvent.

β^3-peptide 20a

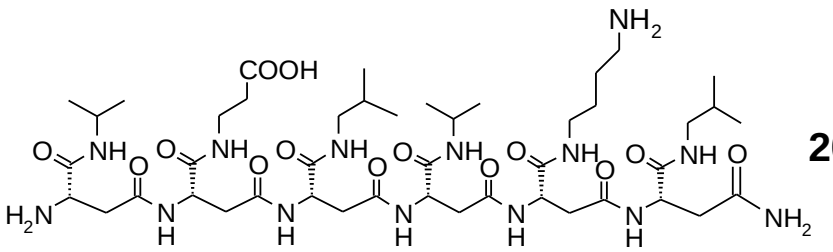

20a

β^3-Peptide **20a** was synthesized essentially following general synthesis of β^3-peptides (Section 3.4.2), except that the last amino acid β^3-amV was coupled to the peptide resin as a monomer using the coupling agents for 3.5 h. The overall yield of **20a** was 63.3%. **ES-MS:** Calcd for $C_{45}H_{80}N_{14}O_{14}$, $[M + H]^+$ 1041.20; found $[M + H]^+$ 1041.60.

Table 3.12: ^{1}H NMR chemical shift assignments for β^3-peptide **20a** in CF_3CD_2OH (500 MHz).

Residue	Backbone shifts (δ)	Side chain shifts (δ)
1	5.15 (1H,NH*CH*CH_2), 2.93,2.70 (2H,NHCH*CH_2*)	7.01 (1H, *NH*) 4.02 (1H, $(CH_3)_2$*CH*), 1.14 (6H, *$(CH_3)_2$*CH)
2	8.89 (1H, (*HN*-terminal), 5.00 (1H,NH*CH*CH_2), 3.16,2.57 (2H,NHCH*CH_2*)	7.56(NH), 3.52,3.44 (1H,COOHCH$_2$*CH_2*NH) 2.50 (2H COOH*CH_2*CH_2NH)
3	9.11 (1H, *HN*), 4.79 (1H,NH*CH*CH_2), 3.06,2.57 (2H,NHCH*CH_2*)	6.93 (1H, *NH*), 3.06, 3.02(2H,$(CH_3)_2$CH*CH_2*), 1.77(1H, $(CH_3)_2$*CH* CH_2), 0.87 (6H, *$(CH_3)_2$*CH CH_2)
4	8.50 (1H, *HN*), 5.08 (1H,NH*CH*CH_2), 2.64,2.47 (2H,NHCH*CH_2*)	7.75 (1H, *NH*) 4.00 (1H, $(CH_3)_2$*CH*), 1.20 (6H, *$(CH_3)_2$*CH)
5	7.30 (1H, *HN*), 5.30 (1H,NH*CH*CH_2), 2.68 (2H,NHCH*CH_2*)	8.43 (1H, *NH*), 3.44,3.06(2H,$NH_3CH_2CH_2CH_2$*CH_2*) 3.02(2H,NH_3 *CH_2*$CH_2CH_2CH_2$), 1.63(2H,$NH_3CH_2CH_2$*CH_2*CH_2), 1.70(2H,NH_3CH_2*CH_2*CH_2 CH_2)
6	7.19 (1H, *HN*) 5.22 (1H,NH*CH*CH_2), 2.70 (2H,NHCH*CH_2*)	8.20 (1H, *NH*), 3.06, 3.02(2H,$(CH_3)_2$CH*CH_2*), 1.80(1H, $(CH_3)_2$*CH*CH_2), 0.89 (6H, *$(CH_3)_2$*CH CH_2)
C-terminus	6.88, 6.73 (NH_2)	

The final conc. of β^3-peptide **20a** in TFE-d2 was 0.2 mg/250 μL. The N-terminal and side chain NH_3^+ were not observed due to exchange with the solvent.

β^3-peptide 20b

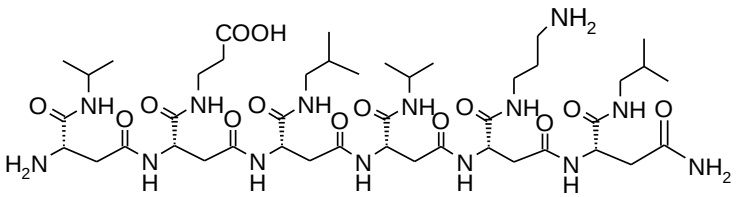

20b

β^3-Peptide **20b** was synthesized following general synthesis of β^3-peptides (Section 3.4.2), except that the last amino acid β^3-amV was coupled to the peptide resin as a monomer using the coupling agents for 3.5 h. The overall yield of **20b** was 61.5 % yield. **ES-MS:** Calcd for $C_{44}H_{79}N_{14}O_{14}$, $[M + H]^+$ 1027.58; found $[M + H]^+$ 1027.85.

Table 3.13: ^{1}H NMR chemical shift assignments for β^3-peptide **20b** in CF_3CD_2OH (500 MHz).

Residue	Backbone shifts (δ)	Side chain shifts (δ)
1	2.93, 2.71 (2H,NHCH<u>*CH*$_2$</u>)	7.03 (1H, <u>*NH*</u>), 4.05 (1H, $(CH_3)_2$<u>*CH*</u>),1.15 (6H, <u>*(CH*$_3$*)*$_2$</u>CH)
2	8.81 (1H, (<u>*HN*</u>-terminal), 5.03 (1H,NH<u>*CH*</u>CH_2), 3.09, 2.60 (2H,NHCH<u>*CH*$_2$</u>)	7.62(NH), 2.53(2H COOH<u>*CH*$_2$</u>CH_2NH) 3.55,3.47(2H COOHCH_2<u>*CH*$_2$</u>NH)
3	9.01 (1H, <u>*HN*</u>), 4.81 (1H,NH<u>*CH*</u>CH_2), 3.08, 2.60 (2H,NHCH<u>*CH*$_2$</u>)	6.97 (1H, <u>*NH*</u>),3.07, 3.04(2H, $(CH_3)_2$CH <u>*CH*$_2$</u>), 1.78(1H, $(CH_3)_2$<u>*CH*</u> CH_2), 0.90 (6H, <u>*(CH*$_3$*)*$_2$</u>CH CH_2)
4	8.47 (1H, <u>*HN*</u>), 5.11 (1H,NH<u>*CH*</u>CH_2), 2.65, 2.53 (2H,NHCH<u>*CH*$_2$</u>)	7.74 (1H, <u>*NH*</u>)1.18 (6H, <u>*(CH*$_3$*)*$_2$</u>CH) 4.05 (1H, $(CH_3)_2$<u>*CH*</u>),
5	7.46 (1H, <u>*HN*</u>), 2.71 (2H,NHCH<u>*CH*$_2$</u>)	8.52 (1H, <u>*NH*</u>), 3.46, 3.30 (2H,$NH_3CH_2CH_2$<u>*CH*$_2$</u>) 3.03 (2H,NH_3<u>*CH*$_2$</u>CH_2CH_2) 1.96 (2H,NH_3CH_2<u>*CH*$_2$</u>CH_2)
6	7.25 (1H, <u>*HN*</u>) 5.22 (1H,NH<u>*CH*</u>CH_2), 2.72 (2H,NHCH<u>*CH*$_2$</u>)	8.16(1H,<u>*NH*</u>),3.07,2.99 (2H,$(CH_3)_2$CH<u>*CH*$_2$</u>)1.80(1H,$(CH_3)_2$ <u>*CH*</u>CH_2),0.90 (6H, <u>*(CH*$_3$*)*$_2$</u>CH CH_2)
C- terminus	6.85, 6.76 (NH_2)	

The final conc. of β^3-peptide **20b** in TFE-d2 was 0.6 mg/250 μL. The N-terminal and side chain NH_3^+ were not observed due to exchange with the solvent.

β^3-peptide 21

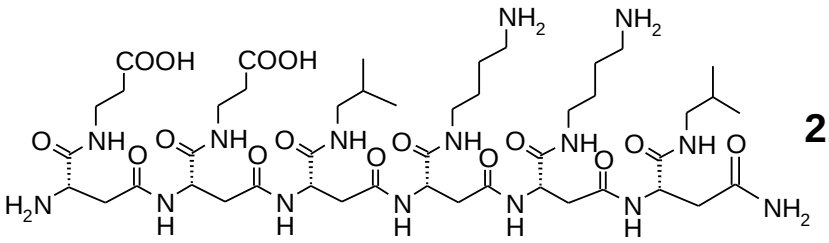

21

β^3-Peptide **21** was synthesized following general synthesis of β^3-peptides (Section 3.4.2), except that β^3-amL at position 3 and β^3-amK at position 4 were coupled to the peptide resin as monomers using the coupling agents for 3.5-4 h. Also the last amino acid, β^3-amE at position 1, was coupled as a monomer for 5 h. The overall yield of **21** was 77%. **ES-MS:** Calcd for $C_{46}H_{81}N_{15}O_{15}$, $[M + H]^+$ 1100.58.; found $[M + H]^+$ 1100.41.

Table 3.14: ^{1}H NMR chemical shift assignments for β^{3}-peptide **21** in CF_3CD_2OH (500 MHz).

Residue	Backbone shifts (δ)	Side chain shifts (δ)
1	4.34 (1H,NHC*H*CH$_2$), 3.49,2.89(2H,NHCHC*H$_2$*)	7.79(NH), 3.66(1H,COOHCH$_2$*CH$_2$*NH) 3.49(1H,COOHCH$_2$*CH$_2$*NH), 2.58 (2H COOH*CH$_2$*CH$_2$NH)
2	8.67(d, J=9.0Hz, *HN*), 5.06 (1H,NHC*H*CH$_2$), 3.182.58(2H,NHCHC*H$_2$*)	7.57(NH), 3.56,(1H,COOHCH$_2$*CH$_2$*NH) 3.45(1H,COOHCH$_2$*CH$_2$*NH), 2.56 (2H COOH*CH$_2$*CH$_2$NH)
3	9.08(d, J-8Hz, *HN*), 4.85 (1H,NHC*H*CH$_2$), 3.09,2.60(2H,NHCHC*H$_2$*)	6.94 (1H, *NH*), 3.07(2H,(CH$_3$)$_2$CH*CH$_2$*), 1.77(1H, (CH$_3$)$_2$*CH*), 0.89 (6H, *(CH$_3$)$_2$*CH)
4	8.52(d, J=7.9 Hz, *HN*), 5.03 (1H,NHC*H*CH$_2$), 2.75,2.67(2H,NHCHC*H$_2$*)	8.08(1H, *NH*),7.30(3H,NH_3^+) 3.33(2H,NH$_3$CH$_2$CH$_2$CH$_2$*CH$_2$*), 3.03(2H,NH$_3$*CH$_2$*CH$_2$CH$_2$CH$_2$), 1.73(2H,NH$_3$CH$_2$*CH$_2$*CH$_2$CH$_2$), 1.64 (2H,NH$_3$CH$_2$CH$_2$*CH$_2$*CH$_2$)
5	7.28 (1H, *HN*), 5.28(1H,NHC*H*CH$_2$), 2.74,2.67(2H,NHCHC*H$_2$*)	8.39 (1H, *NH*),7.24(3H,NH_3^+) 3.33(2H,NH$_3$CH$_2$CH$_2$CH$_2$*CH$_2$*), 3.03(2H,NH$_3$*CH$_2$*CH$_2$CH$_2$CH$_2$), 1.72(2H,NH$_3$CH$_2$*CH$_2$*CH$_2$CH$_2$), 1.64 (2H,NH$_3$CH$_2$CH$_2$*CH$_2$*CH$_2$),
6	7.22(1H, *HN*), 5.23 (1H,NHC*H*CH$_2$), 2.77(2H, NHCH*CH$_2$*).	8.23 (1H, NH) 3.07, 2.99(2H (CH$_3$)$_2$CH *CH$_2$*), 1.82 (1H, (CH$_3$)$_2$*CH*), 0.91 (6H, *(CH$_3$)$_2$*CHCH$_2$),
C-terminus	6.78, 6.72 (NH_2)	

The final conc. of β^{3}-peptide **21** in TFE-d2 was 1.5 mg/250 μL. The N-terminal NH_3^+ was not observed due to exchange with the solvent.

3.4.8 Circular Dichroism of β^{3}-peptides

CD measurements were made on an Olis CD spectrometer at 25 °C in 2 mm path length thermally controlled quartz cell, over 190-260 nm. All samples were prepared in the appropriate solvents immediately prior to recording the

spectra (TFE, H_2O, or PBC). Spectra represent the average of five scans, and were background-corrected and smoothed. Each peptide was analyzed at concentrations of 100, 200, 250, and 500 μM. Peptide concentrations were determined using dry weight of the lyophilized material. Spectra were normalized to mean residue ellipticity (deg cm^2 $dmol^{-1}$) using the formula A*M*3298/ (L*C), where C is concentration in g/L, M is average molecular weight (g/mol), L is path length of the cell.[3]

3.4.9 2D NMR and Structure Elucidation of β^3-Peptides 17 and 21

Two-dimensional NMR measurements and structure elucidation was done in collaboration with Dr. Tara Sprules (Quebec/Eastern Canada High Field NMR Centre, McGill University, Montreal, Quebec). A 1.5 mM sample of **17** and **21** in 100% TFE-d2 (CF_3CD_2OH) (Cambridge Isotope Laboratories, Inc.) was prepared for 2D NMR experiments. Sequence specific assignments were established by following the procedures used for β-amino acid peptides.[46] 2D TOCSY (60 ms mixing time), COSY and NOESY (mixing time 300 ms) spectra were recorded at 10°C on a Varian INOVA 500 MHz spectrometer. The upper distance restraints for **17** (see appendix, **Table A.1**) and **21** (see appendix, **Table A.2**) for structure calculations were obtained from a 300 ms mixing time 2D-NOESY recorded at 10 °C on a Varian INOVA 800 MHz NMR spectrometer, equipped with an HCN cold probe and pulsed-field gradients. Calculation of the complete three-dimensional structure was performed with the program CYANA v2. The structure calculation statistics for **17** and **21** are summarized in **Table** 3.3 and

Table 3.4, respectively. The final calculations were started with 200 randomized conformers all of which converged to the helical conformation (average backbone RMSD to mean for 200 structures: 0.54 ± 0.10 Å for **17** and 0.50 ± 0.12 Å for **21**). A bundle of the 20 lowest energy CYANA conformers were used to represent the NMR structures of **17** and **21** (**Figures 3.22** and **23**).

3.4.10 Synthesis of Mixed α/β^3-Peptide 23

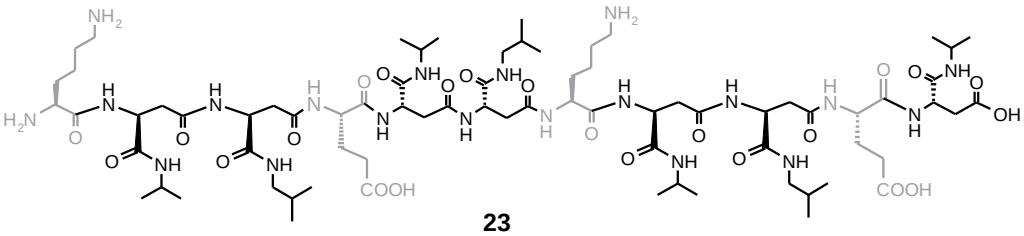

23

Solid-phase synthesis was used to carry out the synthesis of mixed α/β^3-peptide **23** on Wang resin (0.1 mmol). Fmoc/allyl combined solid-phase strategy was used to add β^3-amino acids to the resin as described before (Section 3.4.2), whereas, Fmoc-α-amino acids were coupled to the resin in single steps. The crude peptide obtained was reconstituted in 30% CH_3CN and purified on a semipreparative Vydac C18 HPLC column (1 x 25 cm, flow rate = 2 mL / min, monitored at 220 nm) using a gradient of 10–40% CH_3CN in 0.05% aqueous TFA over a period of 50 min. Peptide **23** was obtained with an overall yield of 64% The identity and purity of α/β^3-undecamer peptide **23** were assessed by analytical HPLC and MALDI-TOF mass spectrometry.

^{1}H NMR [CF_3CD_2OH, 500 MHz]: δ= 0.93 (m, 18H, isovaleric methyls), 1.16 (m, 24H, isopropyl methyls), 1.59 (m, 4H, side chain methylenes, $CH_2\mathit{CH_2}CH_2CH_2NH_3$), 1.80 (m, 3H, isovaleric CH), 1.80 (m, 4H, side chain methylenes, $CH_2CH_2\mathit{CH_2}CH_2NH_3$), 2.03 (m, 4H, side chain methylenes, $\mathit{CH_2}CH_2CH_2CH_2NH_3$), 2.15–2.27 (m, 4H, glutamic acid $\mathit{CH_2}CH_2COOH$), 2.56 (m, 4H, glutamic acid $CH_2\mathit{CH_2}COOH$), 3.07 (m, 6H, isovaleric CH_2), 3.08 (m, 4H, side chain methylenes, $CH_2CH_2CH_2\mathit{CH_2}NH_3$), 2.80–2.90 (m,14H, backbone $\mathit{CH_2}$), 4.01 (m, 4H, isopropyl *CH*), 4.10 (m, 2H, lysine *CH*), 4.36 (m, 2H, glutamic acid *CH*), 4.74 (m, 7H, backbone *CH*), 7.0–7.6 (side chain amides and lysine amine), 8.1–8.7 (m, 10H, backbone amides). Because of broad lines resulting from aggregation at concentrations necessary for NMR analysis sequential assignments could not be obtained. **MALDI-TOF:** Calcd for $C_{74}H_{130}N_{20}O_{23}$, $[M+H]^+$ 1667.00, found 1667.37 and calcd. $[M + Na]^+$ 1689.00 found 1689.36.

3.4.11 Synthesis of α-Peptide 24

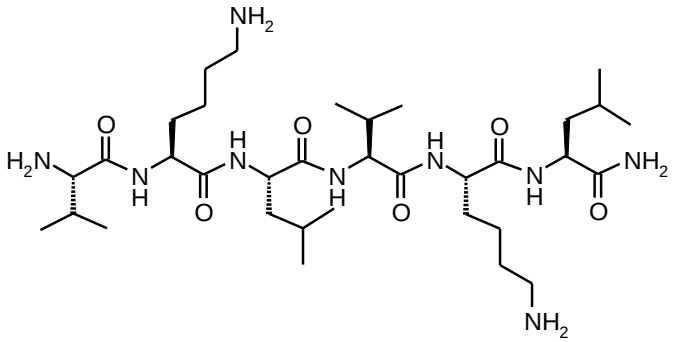

24

α-hexapeptide **24** (H-Val-Lys-Leu-Val-Lys-Leu-NH_2) was synthesized on MBHA resin using standard Fmoc-solid phase synthesis. The crude peptide was purified using semipreparative Vydac C18 HPLC column (1 x 25 cm, flow rate =

2 mL / min) using a gradient of 10–40% CH_3CN in 0.05% aqueous TFA over a period of 50 min to obtain pure **24** with an overall yield of 83%. The identity and purity of **24** were assessed by analytical HPLC and MALDI-TOF mass spectrometry. **MALDI-TOF:** Calcd for $C_{34}H_{67}N_9O_6$, $[M+H]^+$ 698, found 698.2 and calcd. $[M + Na]^+$ 720.02, and found 720.20.

3.4.12 Enzyme Stability Studies

Enzymatic degradation of β-peptides **1, 3, 4,** and **23** using three enzymes, namely, pronase (*Streptomyces griseus*), trypsin (porcine pancreas) and elastase (hog pancreas) was carried out by incubation of peptides with the enzyme at 37 °C. α-peptide **24** was used as a positive control.

Proteolysis degradation buffers

The following reaction buffers were used to assay the selected peptides in this study: 10 mM PBS at pH 7.5 for trypsin and elastase; 10 mM PBS at pH 7.8 for pronase. All the peptides employed in the degradation study were prepared as stock solution of 1 mM in PBS (10 mM, pH 7.5). Peptides were diluted with the select buffer before incubation with the enzyme.

Proteolytic stability assay

Enzymatic degradation was carried out by incubation of peptide (900 μL, 350 μM) with the enzyme (150 μL, 60 μM) at 37 °C for 5 days. The enzyme concentrations of the stock solutions were selected such that the α-hexapeptide **24** was totally degraded after a maximum of 1 h. The enzyme concentrations used

completely degraded **24** by pronase in 15 min, trypsin in 30 min and elastase in 1 h. Aliquots (70 μL) were periodically taken at 0 h to 5 days, 5 μL of 25% AcOH (v⁄v) was added and the degradation was monitored by RP-HPLC.

Serum stability studies

Enzymatic degradation using human serum (Gemini Bio-Products, West Sacramento, CA, USA) was carried out by incubating peptides at 37 °C with the serum at peptide-serum ratio 8:1 in PBS, using 100 μM final peptide concentration. Aliquots (95 μL) were periodically taken at 0, 5 and 24 h, poured into 100 μL of methanol to precipitate the proteins and cooled on ice for 30 min. The sample was centrifuged and the supernatant was analyzed by RP-HPLC.

3.4.13 Cytotoxicity Study (MTT assay)

HeLa and COS-1 cells were maintained in RPMI-1640 (with L-glutamine and $NaHCO_3$) culture medium (Sigma) containing 10% fetal calf serum, 50 μg ⁄ mL penicillin and 0.05 g ⁄ mL streptomycin in a humidified atmosphere (5% CO_2). Growing cells were detached from the culture flasks using a trypsin 0.25% EDTA solution and the cell suspension were seeded on Corning 96-well plates (Corning Inc, Lowell, MA, USA). Cells were incubated with the peptides in RPMI-1640 medium at 37 °C in CO_2 atmosphere. Cytotoxicity of β^3-peptide **1** and β^2-peptide **3** was determined by measuring the inhibition of cell growth using the 3-(4,5-dimethylthiazol-2yl)- 2,5-diphenyltetrazolium bromide (MTT) assay.[45] Cells were seeded in 96-well plates at a concentration of 1.0 x 10^4 cells ⁄ well per 100 μL in complete media and incubated at 37 °C in 5% CO_2 atmosphere. After

24 h, the culture medium was discarded and replaced with a new medium containing peptides at a final concentration of 1, 10, 20 and 40 μM for incubation with HeLa and COS-1 cell lines. All the assays were performed in two independent sets of quadruplicate including positive control (TAT peptide) and negative control (media only) groups. After exposure of the cells to the peptides for 24 h, the culture medium was discarded and MTT (0.5 mg⁄mL) was added to each well. Cells were incubated with MTT for 3 h. Following incubation, the medium was removed and the purple formazan product precipitated in each well was solublized in DMSO (200 μL). After gentle mixing for 5 min at room temperature, absorbance was measured at 570 nm using a VERSA max microplate reader (Molecular Devices) with a reference wavelength of 650 nm to subtract background. The percentage cell viability was expressed as the absorbance ratio of cells treated with peptides to untreated cells. Untreated cell were used as a negative control and wells with culture media but without the cells served as a blank control

3.5 References

(1) Ronald, N., Kerr,J., Kent, S., Moos, W. *J Am Chem Soc* **1991**, *114*, 10646–47.

(2) Appella, D. H., Christianson,L.A., Karle, I.L., Powell, D.R., Gellman, S.H. *J Am Chem Soc* **1999**, *121*, 6206–12.

(3) McMahon, B., Mays, D., Lipsky, J., Stewart, JA., Fauq, A., Richelson, E. *Antisense Nucleic Acid Drug Dev* **2002**, *12*, 65-70.

(4) Seebach, D., Beck, A., and Bierbaum, K. *Chem & Biodiversity* **2004**, *1*, 1111-1239.

(5) Gademann, K., Kimmerlin, T., Hoyer, D., Seebach, D. *J Med Chem* **2001**, *44*, 2460-68.

(6) Hook, D. F., Bindschadler, P., Mahajan, Y.R., Sebesta, R., Kast, P.,Seebach, D. *Chem Biodivers* **2005**, *2*, 591–632.

(7) Seebach, D., Beck, A. K., Bierbaum, D. J. *Chem Biodivers* **2004**, *1*, 1111-239.

(8) Hintermann, T. S., D. *Helv Chim Acta* **1998**, *81*, 2093–126.

(9) Seebach, D., Schaeffer, L., Gessier, F., Bindscha¨dler, P., Ja¨ger, C., Josien, D., Kopp, S., Lelais, G., Mahayan, Y. R.; Micuch, P.; Sebesta, R., Schweizer, B. W. *Helv Chim Acta* **2003**, *86*, 1852-1861.

(10) Farrera-Sinfreu, J., Zaccaro, L., Vidal, D., Salvatella, X., Giralt, E., Pons, M., Albericio, F., Royo, M. *J Am Chem Soc* **2004**, *126*, 6048-57.

(11) Ahmed, S., Beleid, R., Sprules, T., Kaur, K. *Org Lett* **2007**, *9*, 25-28.

(12) Beleid, R., M.Sc. Thesis, *University of Alberta* **2008**.

(13) Raguse, T., Porter, EA. Weisblum,B., Gellman,SH. *J Am Chem Soc* **2002**, *124*, 12774-85.

(14) Delaet, N. G., Robinson, L. A., Wilson, D. M., Sullivan, R. W., Bradley, E. K., Dankwardt, S. M., Martin, R. L., Van Wart, H. E., Walker, K. A. *Bioorg Med Chem Lett* **2003**, *13*, 2101-4.

(15) Jaenicke, R., Creighton, T. E. *Curr Biol* **1993**, *3*, 234-5.

(16) Gademann, K., Hintermann, T., Schreiber,J.V. *Curr Med Chem* **1999**, *6*, 905–25.

(17) Seebach, D., Abele, S., Gademann, K., Guichard, G., Hintermann,, T., Jaun, B., Mathews, J. L., Schreiber, J. V. *Helv Chim Acta* **1998**, *81*, 932-82.

(18) Lelais, G. S., D. *Biopolymers* **2004**, *76*, 206-43.

(19) Guichard, G. A., S.; Seebach, D. *Helv Chim Acta* **1998**, *81*, 187-206.

(20) Lee, M. R., Raguse, T.L., Schinnerl, M.,Pomerantz, W.C., Wang, X., Wipf, P. , Gellman, S.H. *Org Lett* **2007**, *9*, 1801-04.

(21) Kritzer, J. A., Tirado-Rives, J., Hart, S.A., Lear,J.D.,Jorgensen, W.L. , Schepartz,A. *J Am Chem Soc* **2005**, *127*, 167-178.

(22) Marqusee, S., Baldwin, RL. *Proc Natl Acad Sci U S A* **1987**, *84*, 8898-902.

(23) Kaur, K., Sprules, T., Soliman, W., Beleid, R., Ahmed, S. *Biochim Biophys Acta* **2008**, *1784*, 658–665.

(24) Cheng, R. P., Gellman,S.H.,DeGradoW,F. *Chem Rev* **2001**, *101*, 3219-32.

(25) Hart, S. A., Bahadoor, A. B., Matthews, E. E., Qiu, X. J., Schepartz, A. *J Am Chem Soc* **2003**, *125*, 4022-3.

(26) Pomerantz, W. C., Grygiel, T. L., Lai, J. R., Gellman, S. H. *Org Lett* **2008**, *10*, 1799-802.

(27) Güntert, P. *Meth. Mol Biol* **2004**, *278*, 353–78.

(28) Sharma, G. V., Nagendar, P., Jayaprakash, P., Radha Krishna, P., Ramakrishna, K. V., Kunwar, A. C. *Angew Chem Int Ed Engl* **2005**, *44*, 5878-82.

(29) De Pol, S., Zorn, C., Klein, C. D., Zerbe, O., Reiser, O. *Angew Chem Int Ed Engl* **2004**, *43*, 511-4.

(30) Hayen, A., Schmitt, M. A., Ngassa, F. N., Thomasson, K. A., Gellman, S. H. *Angew Chem Int Ed Engl* **2004**, *43*, 505-10.

(31) Seebach, D., Jaun, B., Sebesta, R., Mathad, R., Floegel, O., Limbach, M., Sellner, H., Cottens, S., *Helv Chim Acta* **2006**, *89*, 1801-25.

(32) Sadowsky, J. D., Fairlie, W. D., Hadley, E. B., Lee, H. S., Umezawa, N., Nikolovska-Coleska, Z., Wang, S., Huang, D. C., Tomita, Y., Gellman, S. H. *J Am Chem Soc* **2007**, *129*, 139-54.

(33) Giuliano, M., Horne, WS., Gellman, SH. *J Am Chem Soc.* **2009**, *131*, 9860-1.

(34) Ahmed, S., Kaur, K. *Chem Biol Drug Des* **2009**, *73*, 545-52.

(35) Hook, D. F., Gessier, F., Noti, C., Kast, P., Seebach, D. *Chembiochem* **2004**, *5*, 691–706.

(36) Horne, W. S., Gellman, S.H. *Acc Chem Res* **2008**, *41*, 1399–1408.

(37) Heck, T., Limbach, M., Geueke, B., Zacharias, M., Gardiner, J., Kohler, H. P., Seebach, D. *Chem Biodivers* **2006**, *3*, 1325-48.

(38) Hiraishi, T., Kajiyama, M., Yamato, I., Doi, Y. *Macromol Biosci* **2004**, *4*, 330-9.

(39) Wiegand, H., Wirz,B., Schweitzer, A., Camenisch,G.P., Rodriguez, M.I. ; Perez, G. G., R.Woessner, R. Voges, P.I. Arvidsson, J. Frackenpohl, D.; Seebach *Biopharm Drug Dispos* **2002**, *23*, 251–62.

(40) Corey, D. R., Willett, W. S., Coombs, G. S., Craik, C. S. *Biochemistry* **1995**, *34*, 11521-7.

(41) Largman, C., Brodrick, J. W., Geokas, M. C. *Biochemistry* **1976**, *15*, 2491-500.

(42) Narahashi, Y., Yanagita, M. *J Biochem* **1967**, *62*, 633-41.

(43) Narahashi, Y., Shibuya, K., Yanagita, M. *J Biochem* **1968**, *64*, 427-37.

(44) Schmitt, M. A., Weisblum, B., Gellman, S.H. *J Am Chem Soc* **2007**, *129*, 417–28.

(45) Mosmann, T. *J Immunol Methods* **1983**, *65*, 55-63.

(46) Wuthrich, K. *Wiley, New York* **1986,** 77-80.

Chapter 4 : Conclusions and Future Directions

4.1 General Conclusions

Current cancer therapies have low specificity for tumor cells and have serious toxic side effects. These side effects result from the non specific delivery of the cytotoxic drugs to both normal and cancer cells. Targeting drugs to the cancer cells can help improve the outcome of existing cancer therapies.[1] This can be achieved by using targeting agents. However, a prerequisite for the use of an agent as targeting vehicle is a selective binding to the tissue of interest and limited uptake by healthy tissues. Antibodies are commonly used as targeting agent, but there are some limitations for their use such as large size, poor stability and non specific uptake of the antibodies by reticuloendothelial cells, such as liver and spleen. Recently, several peptides have been identified by peptide phage display for targeting different tumors and cell types either by targeting the cell surface, such as, p160 peptide or the tumor vasculature, for instance, NGR peptide.[2-4] Peptides identified from the phage display for targeting cancer cells can be further improved for specific binding and metabolic stability by chemical manipulation of their structures. With respect to the former, which is improving the specific binding of peptides, we were able to develop a new method to screen peptides for specific recognition by cancer cells. First, we used NGR peptide as our model peptide and we were able to use the MTT reagent as a colorimetric detection reagent for cell binding using Kodak imager and the ELISpot method. The use of fluorescent CyQUANT dye, however dramatically improved the signal for detection. The peptide bound cells could be detected as low as 1000 cell bound per peptide spot on the array. Seventy peptides based on the a lead 12-mer p160

peptide sequence were synthesized on a cellulose membrane in an array format using SPOT synthesis and a direct method to study the peptide-whole cell interaction was developed using CyQUANT. The relative binding affinity of the cells for different peptides was evaluated by measuring the net fluorescent intensity of the fluorescently labelled cells. The use of CyQUANT as fluorescent dye was very helpful to improve the signal to noise ratio (S/N), as well as the peptide arrays were very effective way to do a comparative study of different peptide sequences at the same time. The method developed allowed us to screen large number of peptides against different cell lines which was facilitated by the regeneration of the membrane for reuse. Screening allowed identification of at least five new peptides that displayed higher affinity for MDA-MB-435 and MCF-7 human cancer cells compared to the p160 peptide. These peptides showed very little binding to the normal human umbilical vein endothelial cells. The in vitro cell binding studies using FITC-labelled peptides confirmed the high and specific affinity of an 11-mer peptide **11** and 10-mer peptide **18** for the cancer cells. The peptide array-whole cell binding assay reported here is a complementary method to phage display for further screening and optimization of cancer targeting peptides. These peptide arrays can also be developed for screening cell types, such as, identification of cancer cells from a given tissue sample for use as diagnostics.

Despite the advances in developing peptides as cancer targeting agents, the use of peptides as pharmaceutical agents is limited due to their susceptibility to proteolytic degradation and their poor absorption from the gut, rapid excretion

though the kidneys and therefore low bioavailability. Moreover, the high flexibility of short and medium linear peptide sequences decreases the activity and selectivity. For example, p160 peptide which is proven to be a good candidate as cancer targeting agent was found to decompose in the human serum after 5 min of incubation.[2,3] Over the years, numerous efforts have been made to develop synthetic mimetic of biologically active peptides that maintain a significant activity of the parent compound as well as produce improved pharmacological properties such as metabolic stability, bioavailability. Peptidomimetics have emerged as an avenue to overcome these problems as well as identify drug-like molecules having a secondary structure as well as other structural features analogous to that of the original peptide.

In this context, we report here a method to synthesize two new classes of β-peptides, β^2-, and β^3-peptides derived from L-Dap and L-Asp monomers, respectively. Our strategy allowed the synthesis of the two classes from orthogonally protected amino acids. This synthetic strategy permits build up of the peptide as well as allows introduction of different side chains, which could be similar or different from natural amino acids.[5] β^3-peptides were able to adopt stable helical secondary structure in organic solvents, as well as give right handed helical structure which is a good mimic of α-helical peptides.[6] β^2- and β^3-peptides studied here were found to be completely stable to different proteolytic enzymes as well as human serum, which might indicate less interaction of these peptides with the proteolytic enzymes. The mixed α/β^3-peptide **23,** however, exhibited proteolysis in the presence of trypsin and pronase but not elastase. The rate of

degradation of the mixed peptide **23** was slower than that of the α-peptide **24**. Pronase cleaved the α/β peptide **23** between residue 7 (αLys) and 8 (β^3haVal) as well as removed the N-terminal Lys residue. Trypsin cleaved the mixed peptide after the central Lys giving rise to two final degradation products. Toxicity studies of **1** and **3** towards Hela and COS-1 cell lines confirmed that the peptides are non toxic. These results expand the potential application of β-peptides in the design of biologically active peptides. As a result, these compounds represent good candidates for new drugs.[7]

4.2 Future Directions

The promising results obtained from the p160 peptide array library (Chapter 2) and the stable helical secondary structure of β-peptides (Chapter 3) will allow further refinement of p160 analogues in order to develop potent cancer targeting agents. These peptides will be developed for conjugation to micelles for targeted drug delivery (in collaboration with Dr. Afsaneh Lavasanifar, Faculty of Pharmacy, U of Alberta).

Five new analogues (10-mer peptides) of p160 were identified with good binding properties to cancer cells. New β^3-amino acids derived from L-asp will be introduced in these sequences to enhance proteolytic stability. Askoxylakis and coworker have shown that p160 peptide (VPWMEPAYQRFL) is rapidly degraded by serum proteases and the cleavable sites were identified to be between the amino acids ^{10}Arg-^{11}Phe, ^{9}Gln-^{10}Arg, and ^{4}Met-^{5}Glu. The degradation

products of p160 start to be detected only after 5 min of incubation with serum. These cleavable sites at the p160 sequence can be substituted with β-amino acids.

Table 4.1: Expected modification of p160 based peptides with β^3-amino acids to increase the proteolytic stability. Underlined amino acids will be replaced with β-amino acids.

Peptide analogue #	Amino acid sequence
1 (p160)	VPWMEPAYQRFL
11	**RGD**PAY**QGR**FL
18	WXE**A**AYQRFL
40	WXEPAYQR**K**L
47	WXEPAYQRF**K**
60	XEPAYQR**K**L

Following the synthesis of these analogues, they will be fluorescently labelled with FITC. Their proteolytic stability will be conducted in the presence of pronase and trypsin. The proteolytically stable peptides will be labelled with FITC to study cell uptake by MDA-MB-435 and MCF-7 cells using flow cytometry.

Further, the peptide-whole cell binding assay developed here can be used to develop a highly reliable method to profile fresh cancer cells derived from patient specimens against a number of cancer targeting peptides. Such binding profile may one day enable us to choose appropriate peptide from a cocktail of "off-the-shelf" targeting peptides to treat a specific cancer.

Based on the results presented in chapter 3, the new class of β^3-peptides can be applied to different antibacterial peptides to improve their proteolytic stability. For instance, Leucocin A, a potent antimicrobial peptide can be designed into a α/β mixed peptide. Leucocin A (LeuA), from *Leuconostoc gelidum* is a 37 residue IIa bacteriocin with nanomole activity against *Listeria monocytogenes.* whose sequence was reported (**Figure 4.1**).[8] The middle part of LeuA from residues 19-31 is helical and is important for antibacterial activity. LeuA is helical only in membrane mimicking solvents and is unstructured in water. β^3-Peptides from L-Asp are capable of forming stable secondary structure in membrane mimicking solvents like TFE.[6] Replacement of the middle helical part of LeuA with β^3-amino acids may result in improved peptide stability as well as antimicrobial activity.

Figure 4.1. Amino acid sequence of LeuA (Top). NMR solution structure of LeuA in TFE displaying disulfide bridge and α-helical portion (Bottom)**.**

4.3 References

(1) Yamamoto, Y., Tsutsumi, Y., Mayumi, T. *Curr Drug Targets* **2002**, *3*, 123-30.

(2) Askoxylakis, V., Zitzmann, S., Mier, W., Graham, K., Kramer, S., von Wegner, F., Fink, R. H., Schwab, M., Eisenhut, M., Haberkorn, U. *Clin Cancer Res* **2005**, *11*, 6705-12.

(3) Askoxylakis, V., Mier, W., Zitzmann, S., Ehemann, V., Zhang, J., Kramer, S., Beck, C., Schwab, M., Eisenhut, M., Haberkorn, U. *J Nucl Med* **2006**, *47*, 981-8.

(4) Buehler, A., van Zandvoort, MA., Stelt, BJ. *Arterioscler Thromb Vasc Biol.* **2006**, *26*, 2681–7.

(5) Ahmed, S., Beleid, R., Sprules, T., Kaur, K. *Org. Lett* **2007**, *9*, 25-28.

(6) Kaur, K., Sprules, T., Soliman, W., Beleid, R., Ahmed, S. *Biochim Biophys Acta* **2008**, *1784*, 658–665.

(7) Ahmed, S., Kaur, K. *Chem Biol Drug Des* **2009**, *73*, 545-52.

(8) Kaur, K., Andrew, L. C., Wishart, D. S., Vederas, J. C. *Biochemistry* **2004**, *43*, 9009-20.

Appendix

Procedure for using AutoSpot Robot ASP 222 for peptide array synthesis.

Semiautomatic AutoSpot was used for the synthesis of peptide arrays. AutoSpot software (Peptide synthesis control software, INTAVIS AG, Version 1.5.03, Germany) was used to operate the instrument. Sequential steps were followed as described below:

1. Power up the Robot and the dilutor before turning on the computer.
2. Double click the Autospot icon. A small screen will come up asking for the password. Enter password.
3. Once the program opens, go to File menu and click on "New". In the new file click on "Edit" tool to define the sequences that will be synthesized as shown in **Figure A.1**.
4. **Define Sequences.** Editing sequences is the first step to define the sequence that will be synthesized. To edit the sequence, press file menu and select edit sequences. Each amino acid is defined with one letter symbol (correct sequence shows up in blue). There are different methods to enter the sequence, either each peptide entered individually or using analog sequences by putting * at the position to be replaced by different amino acids.

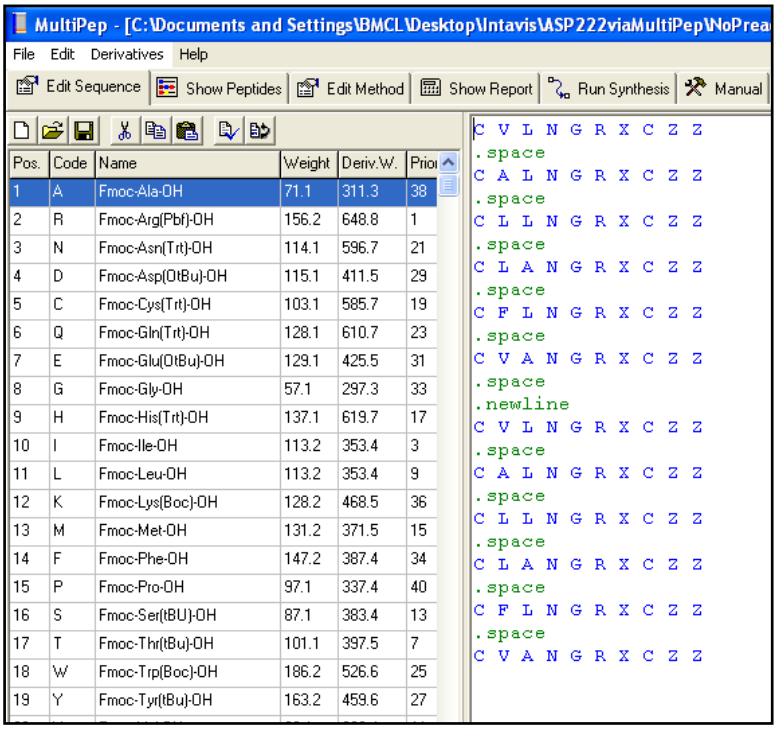

Figure A.1. Definition of peptide sequences using Edit tool.

5. After editing is finished, go to edit and press check file. Then clean file and the editing window will appear. Finally, click on Show peptides to see the peptides position on the membrane, their MW and sequences (**Figure A.2**).

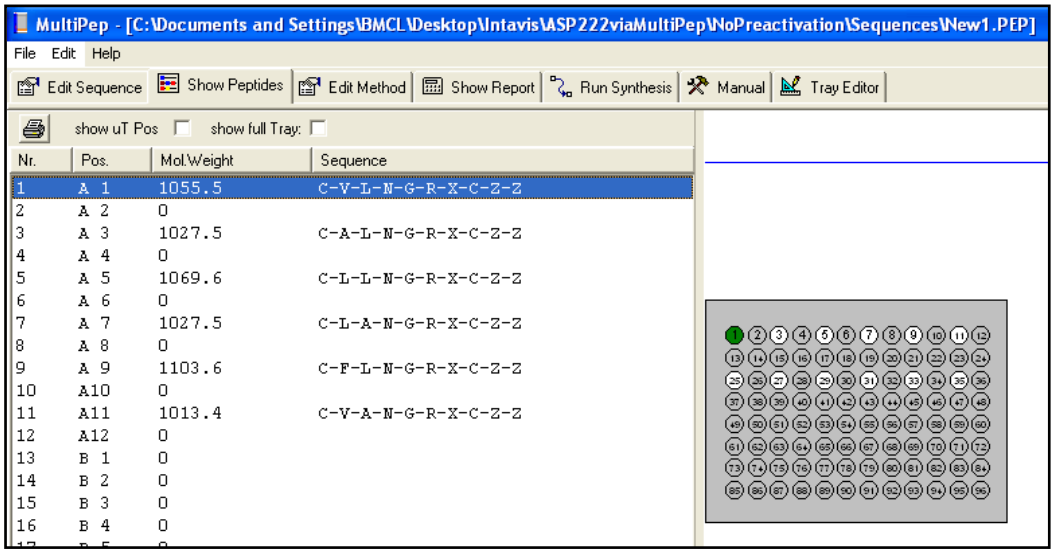

Figure A.2. Show Peptide tool, showing the position of each peptide.

6. **Peptide Reports.** After checking the position and the sequences, click on peptides reports to see how much of each amino acid need to be prepared, amount of activator needed, and the solvent and the number of coupling cycles for each amino acid.
7. **Edit Method.** Click on "Edit Method" in the tool bar to edit the method and determine the number, the length of coupling for each amino acid, and the amount of activated amino acid that will be delivered to each spot (**Figure A.3**). In this step, the number of coupling cycles per each round is determined as follow: two coupling for each amino acid for 20 min till the fourth amino acid and the time is increased to 35 min per one coupling cycle till the last amino acid.

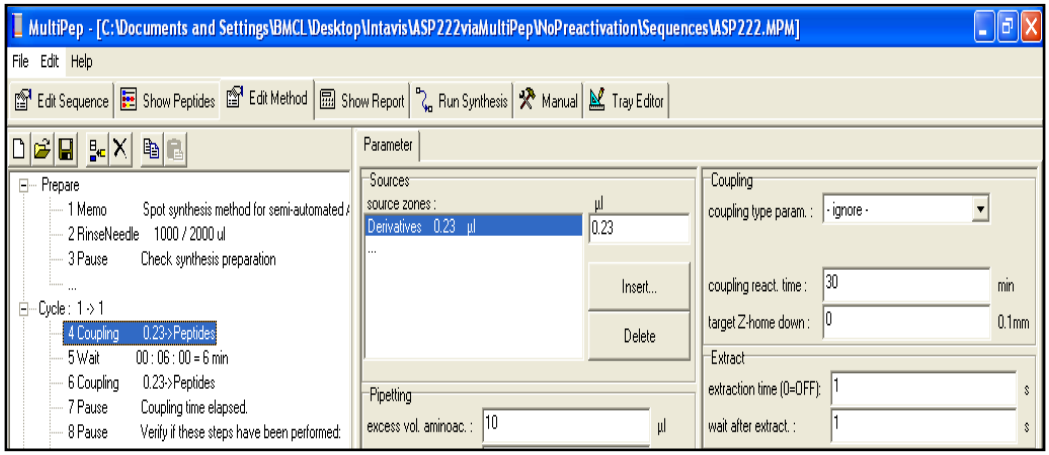

Figure A.3. Edit Method tool, showing the required field to build the synthesis method.

8. **Manual steps:** Before starting the synthesis, the manual steps include preparation of activated amino acids stock solutions (as described below) and ensuring there is enough DMF in the rinse solvent bottle.

Preparation of amino acid derivative stock solutions

1. To each cartridge of 0.5 mM amino acid, add 1.0 mL of (0.75 mmol/ml) HOBt in dry NMP. Add NMP to each cartridge to achieve a total volume of approximately 1.5 mL. Shake vigorously to dissolve amino acid derivatives. Store the solutions at 4°C till use. These can be stored for up to one week.
2. Prepare an activator stock solution of 1.1 mmol/mL DIC in NMP (0.4 mL DIC and 2.1 mL NMP). This solution is stable for a day.
3. To prepare activated amino acids, mix amino acid and the activator solution from 1 and 2 to obtain 0.25 mmol/mL of activated amino acid. For instance, transfer 150 μL amino acid stock into an eppedorf tube and add 50 μL activator stock solution to it.
4. Place the tubes in the amino acid rack.

9. **Run Synthesis.** After starting the Robot, first check pipetting accuracy and positioning of the needle. Then load the membrane(s) on the work area. To start the synthesis, click on "Run Synthesis" in the tool bar. In this window, select the cycle number and then press the start icon (**Figure A.4**).

10. **Manual steps:** After each coupling, capping and Fmoc cleavage has to be performed manually as described below. Take the membrane off the holder and perform the following steps manually.

a) **Capping:** Immerse the membrane for 30 sec in the capping solution, 20% acetic anhydride in DMF, decant and repeat for 2-5 min with fresh solution.

b) **DMF wash:** Wash the membrane with 15 mL DMF (1 x 30 sec and 2 x 2 min).

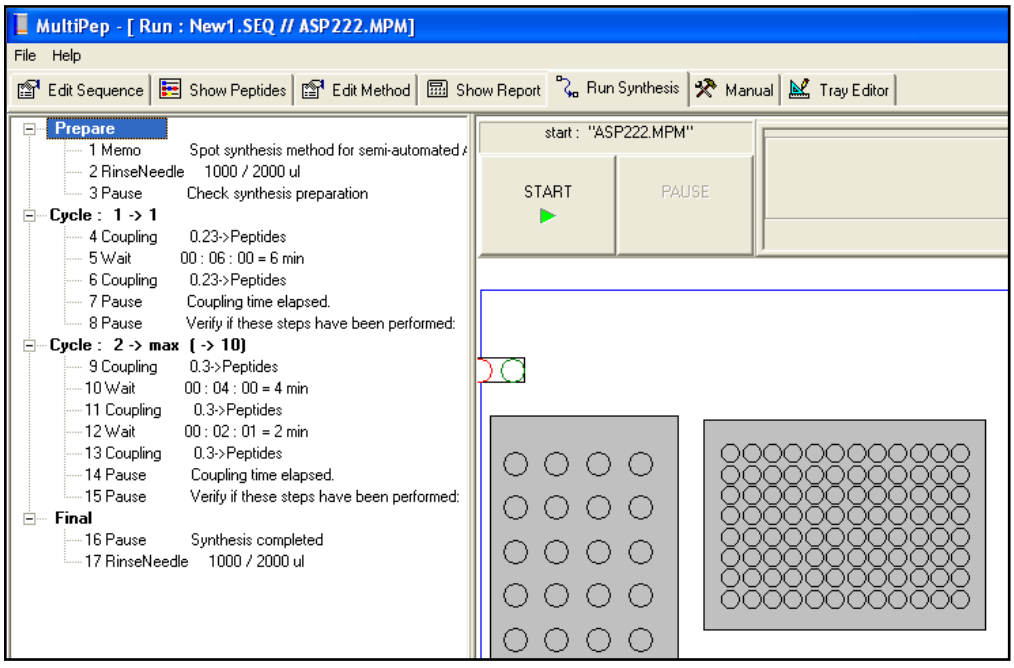

Figure A.4. Run Synthesis tool, showing the start icon and the number of cycles for the whole synthesis.

c) **Fmoc-deprotection:** Immerse the membrane for 8 min in 20% piperidine/ DMF (15 mL).

d) **DMF wash:** Wash with DMF (15 mL, 1 x 30 sec and 3-4 x 2 min).

e) **Ethanol wash:** Wash with ethanol (1 x 30 sec and 2 x 2 min).

f) **Drying:** Press the membranes between several layers of clean chromatography paper to remove excess liquid, then dry the membrane with a stream of cold air. The first synthesis cycle is completed. The procedure listed above is carried out for each synthesis cycle until the largest peptide of the series has been assembled.

Final Fmoc deprotection: Take the membrane from the holder and carry out Fmoc deprotection as described above.

Side chain deprotection: Prepare 10 mL of deprotection solution (15 mL TFA: 15 mL DCM: 900 μL TIPS: 600 μL water). Let the membrane react with this solution for about 3 h. The reaction is carried out in a polypropylene box with a lid. Wash of the membrane using DCM, DMF, and finally ethanol (4 x 20 mL, 2 min), then dry with cold air. Store the membrane in zip lock bag until use at -20 ^{o}C.

11. **Shut down Robot:** At the end of the synthesis, shut down the instrument and dispose left over chemicals properly.

FIGURES

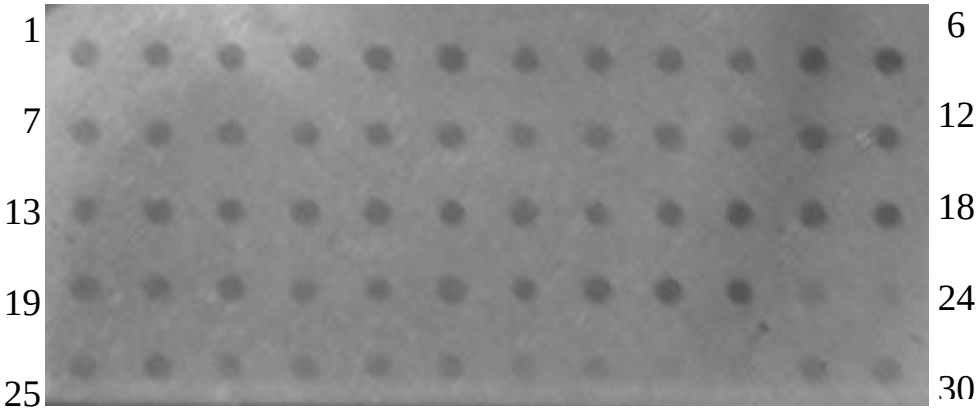

Figure A.5. Image of NGR peptide library after incubation with 75 x 10^3 cell /ml Hey cells for 18 h at 37 °C, followed by staining with MTT reagent.

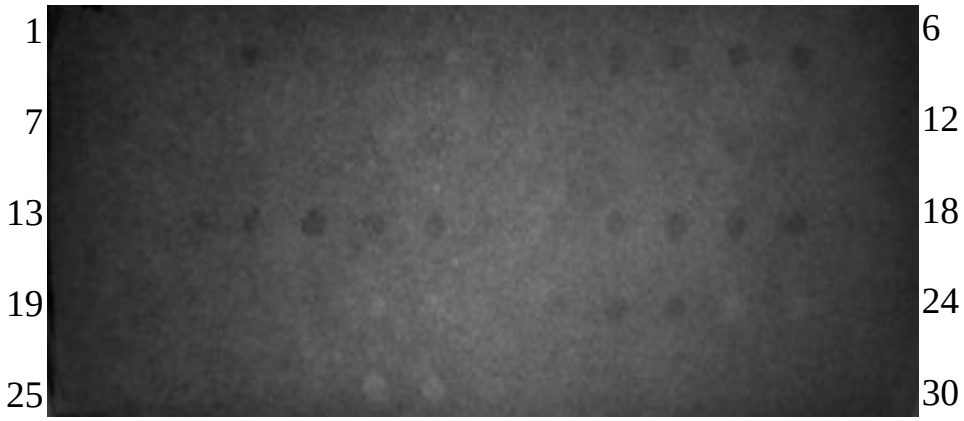

Figure A.6. Image of NGR peptide library after incubation with 75 x 10^3 cell /ml MDA-MB-231 cells for 18 h at 37 °C, followed by staining the cells with MTT reagent**.**

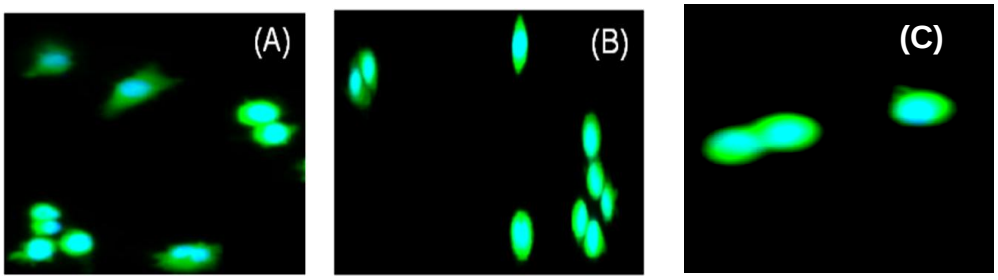

Figure A.7. Fluorescence microscopy images of MDA-MB-435 cells after incubation with FITC labeled peptide analogues **11** (A), **18** (B), and **40** (C) for 30 minutes at a peptide concentration of (10^{-5} mol/L). Cell nuclei were stained with DAPI (blue).

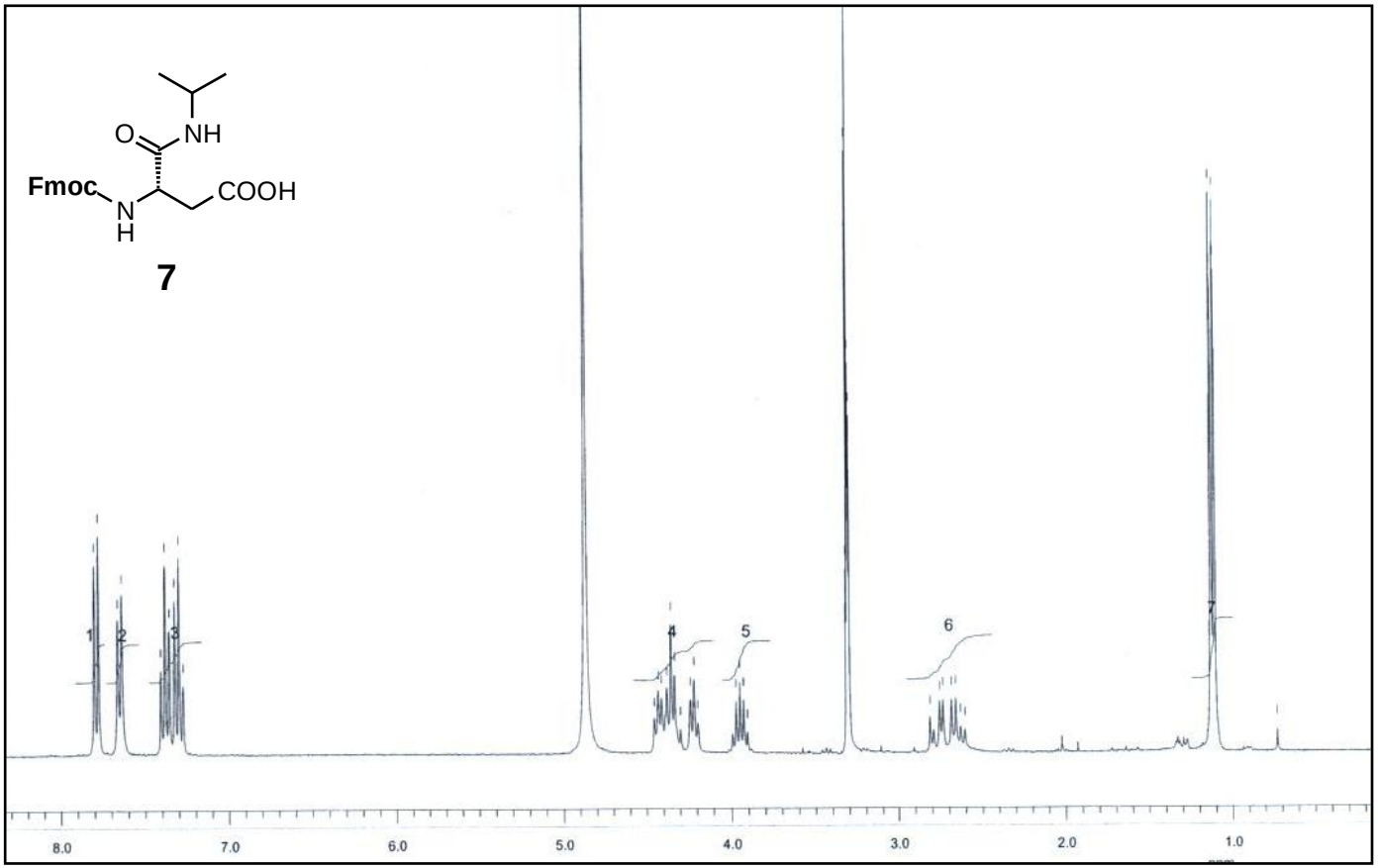

Figure A. 8. ^{1}H-NMR spectrum of N$^{\beta}$-Fmoc-**β^{3}am**V (**7**) in CD_3OD.

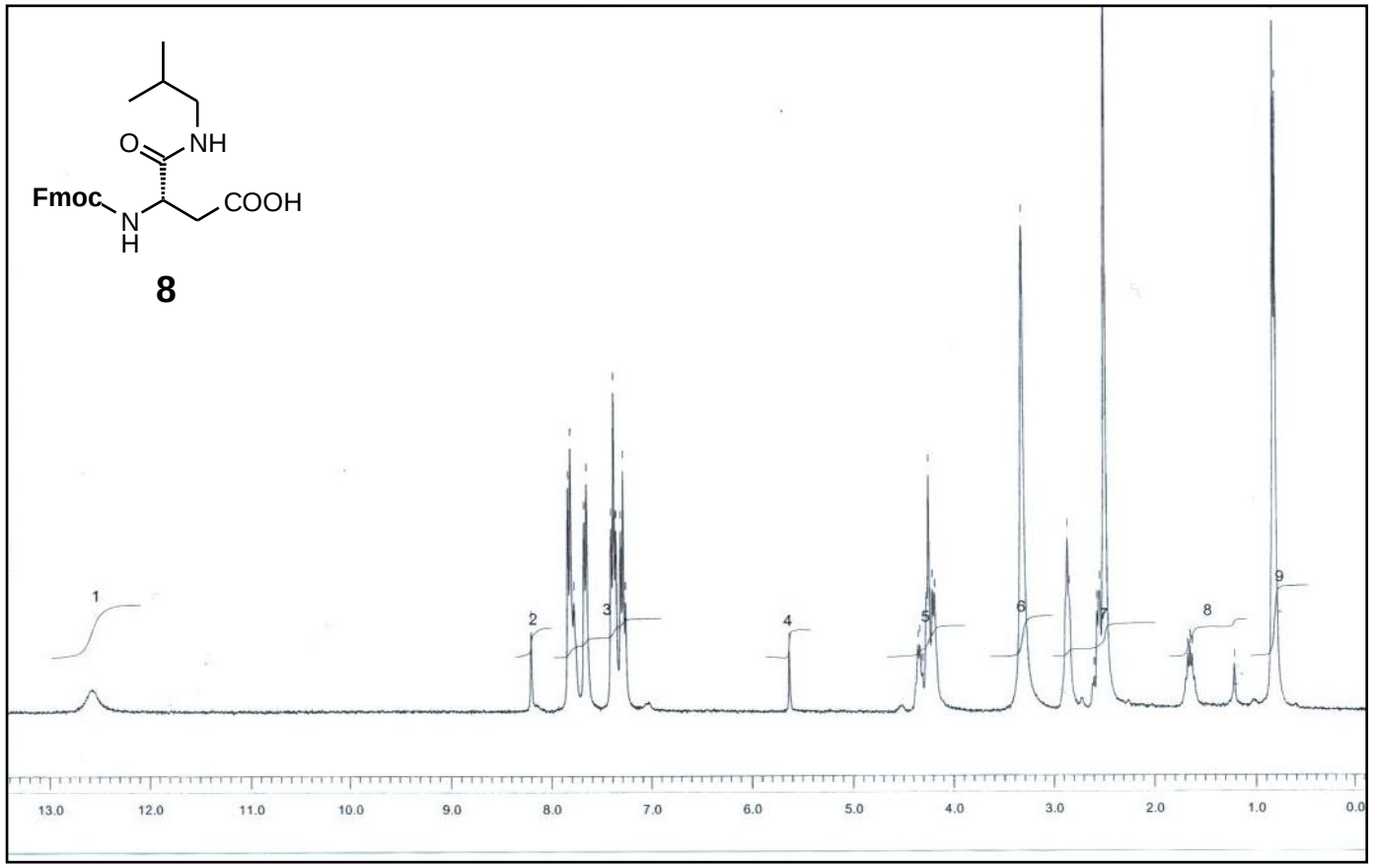

Figure A. 9. ^{1}H-NMR spectrum of N^{β}-Fmoc-**β^{3}am**L (**8**) in CD_3OD.

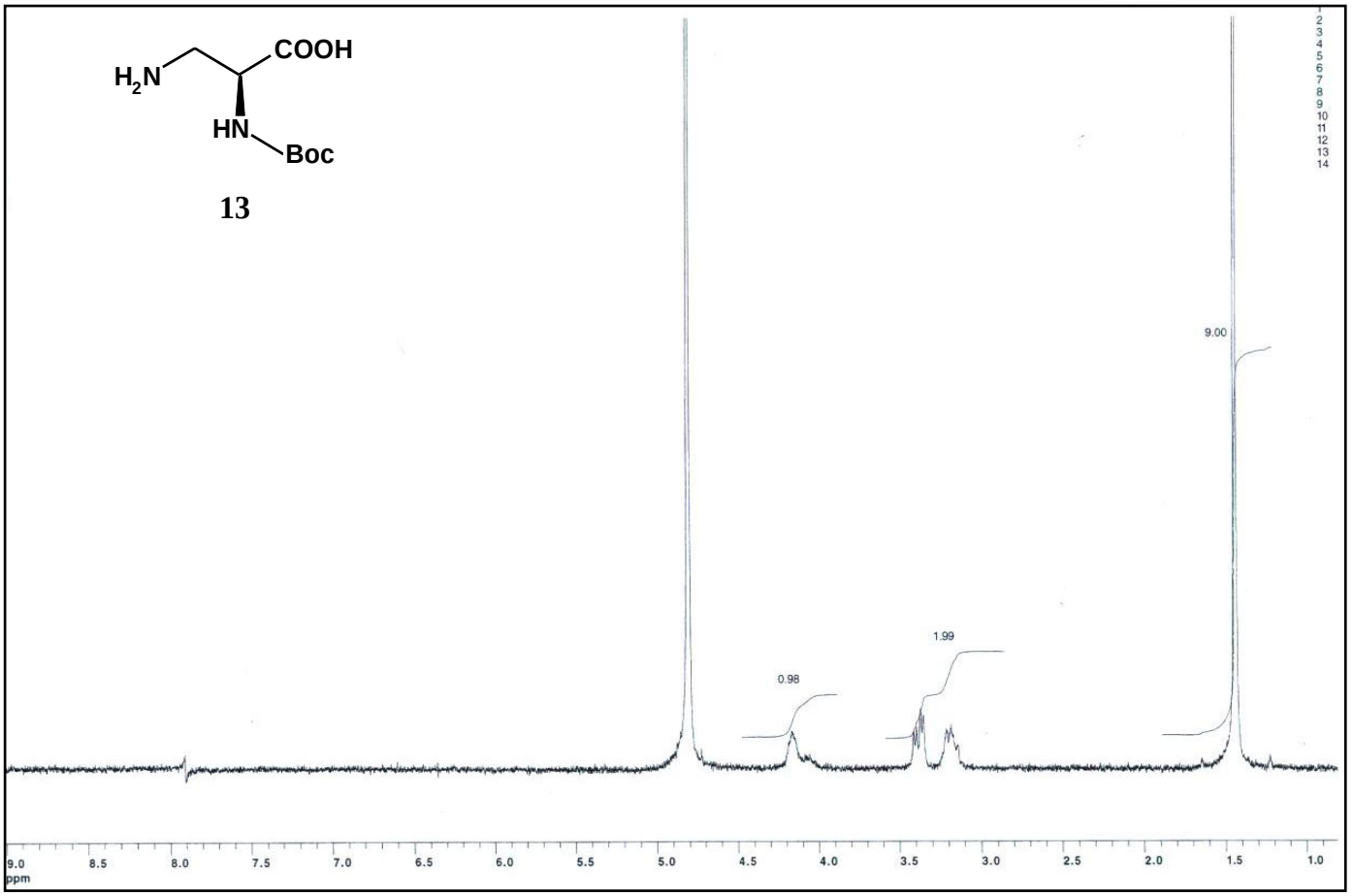

Figure A.10. ^{1}H-NMR spectrum of N^{α}-Boc-L-2,3-diaminopropionic acid (**13**) in CD_3OD.

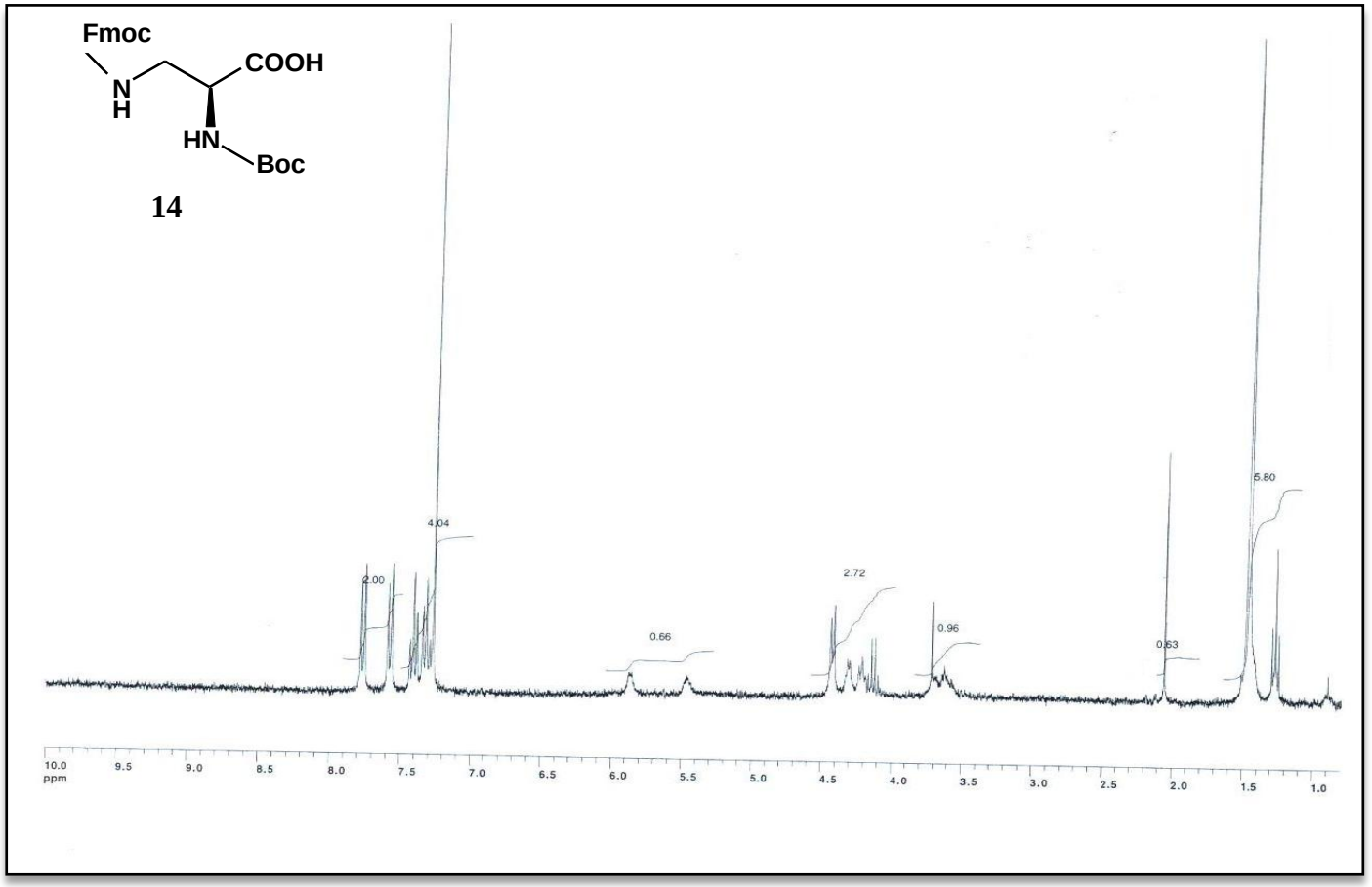

Figure A. 11. ^{1}H-NMR spectrum of N^{α}-Boc-N^{β}-Fmoc-L-2,3-diaminopropionic acid (**14**) in $CDCl_3$.

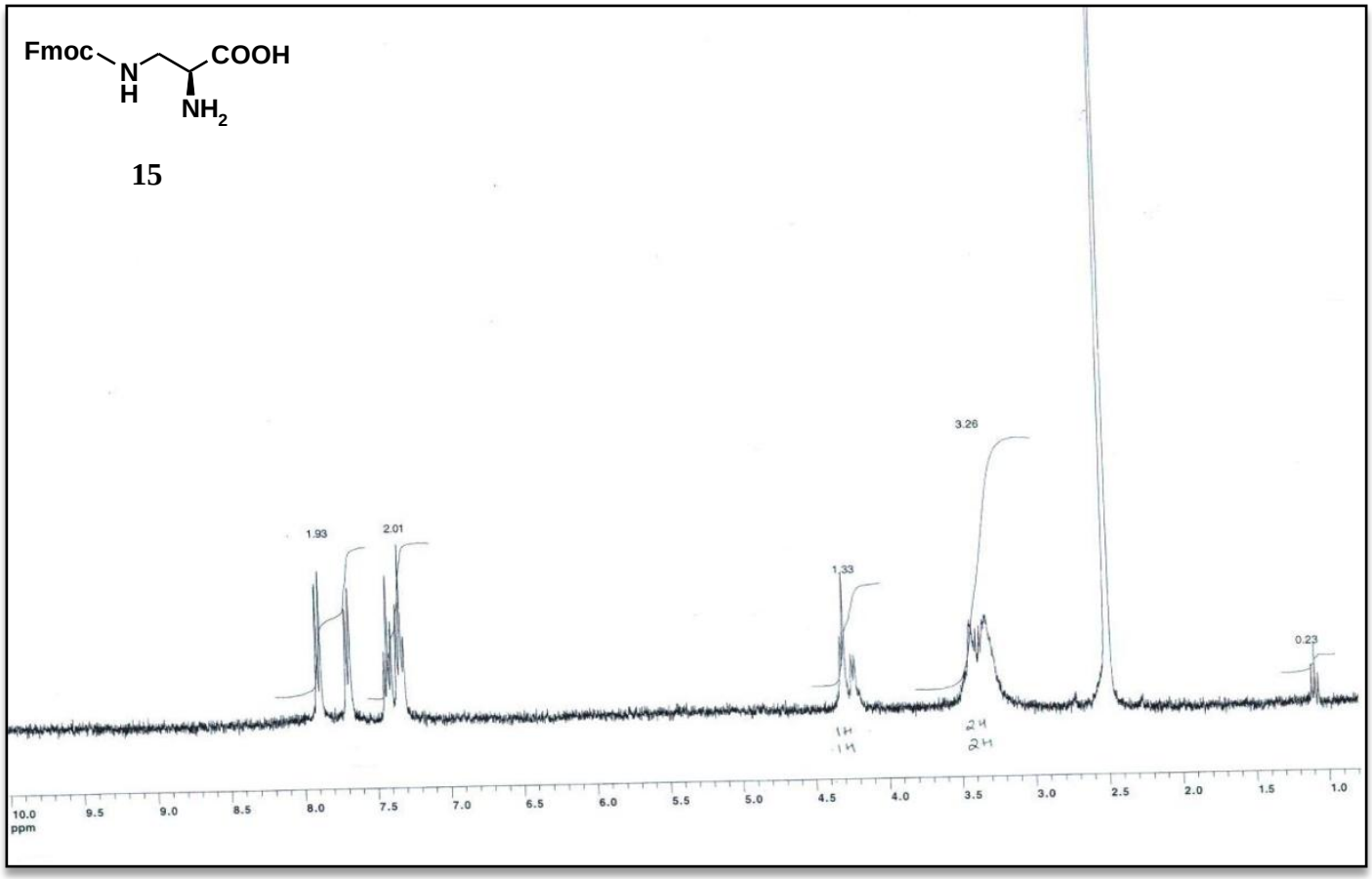

Figure A.12. ^{1}H-NMR spectrum of N^{β}-Fmoc-L-2,3-diaminopropionic acid (**15**) in DMSO-d_6

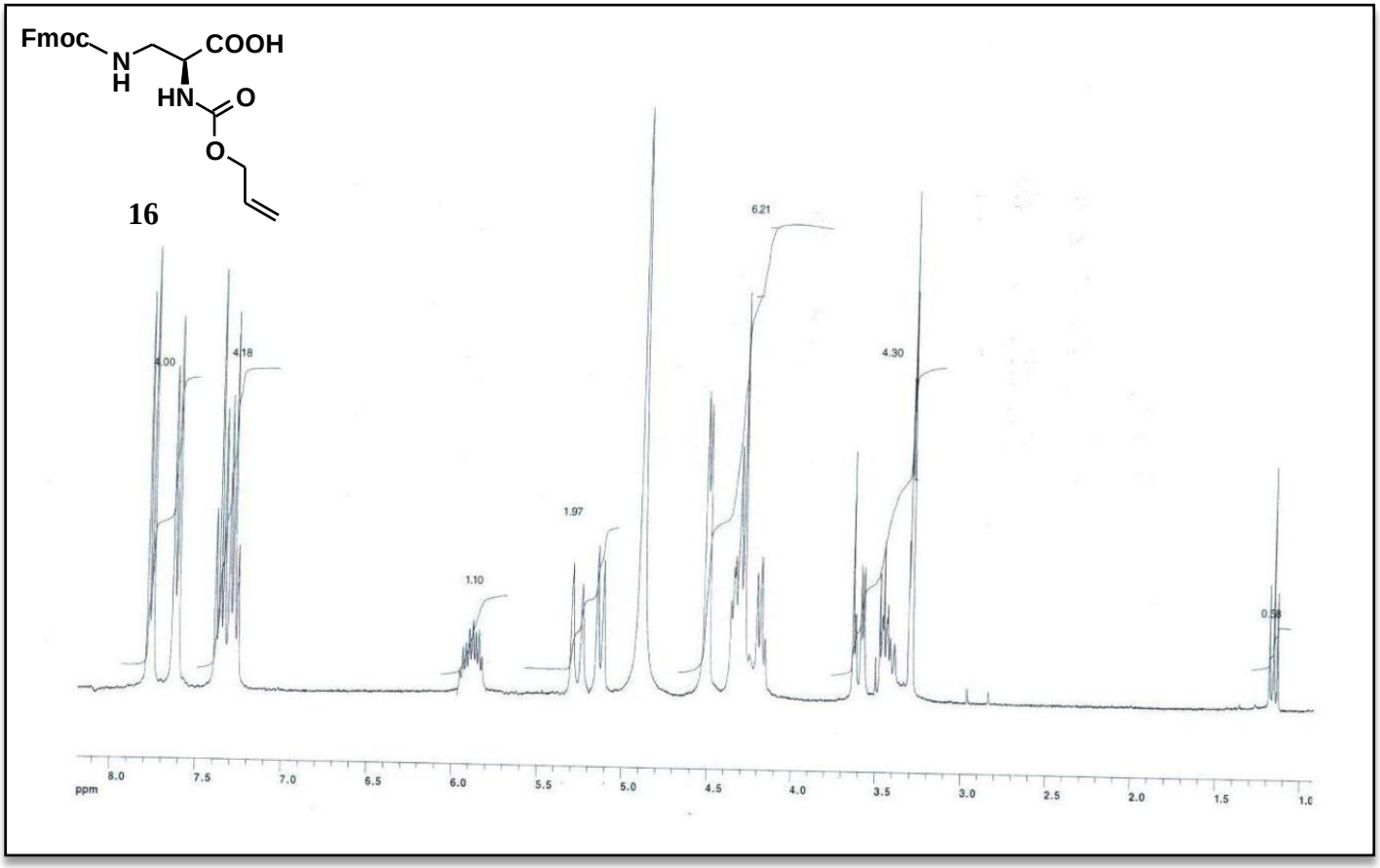

Figure A.13. ^{1}H-NMR spectrum of N^{β}-Alloc-N^{α}-Fmoc-L-2,3-diaminopropionic acid (**16)** in CD_3OD.

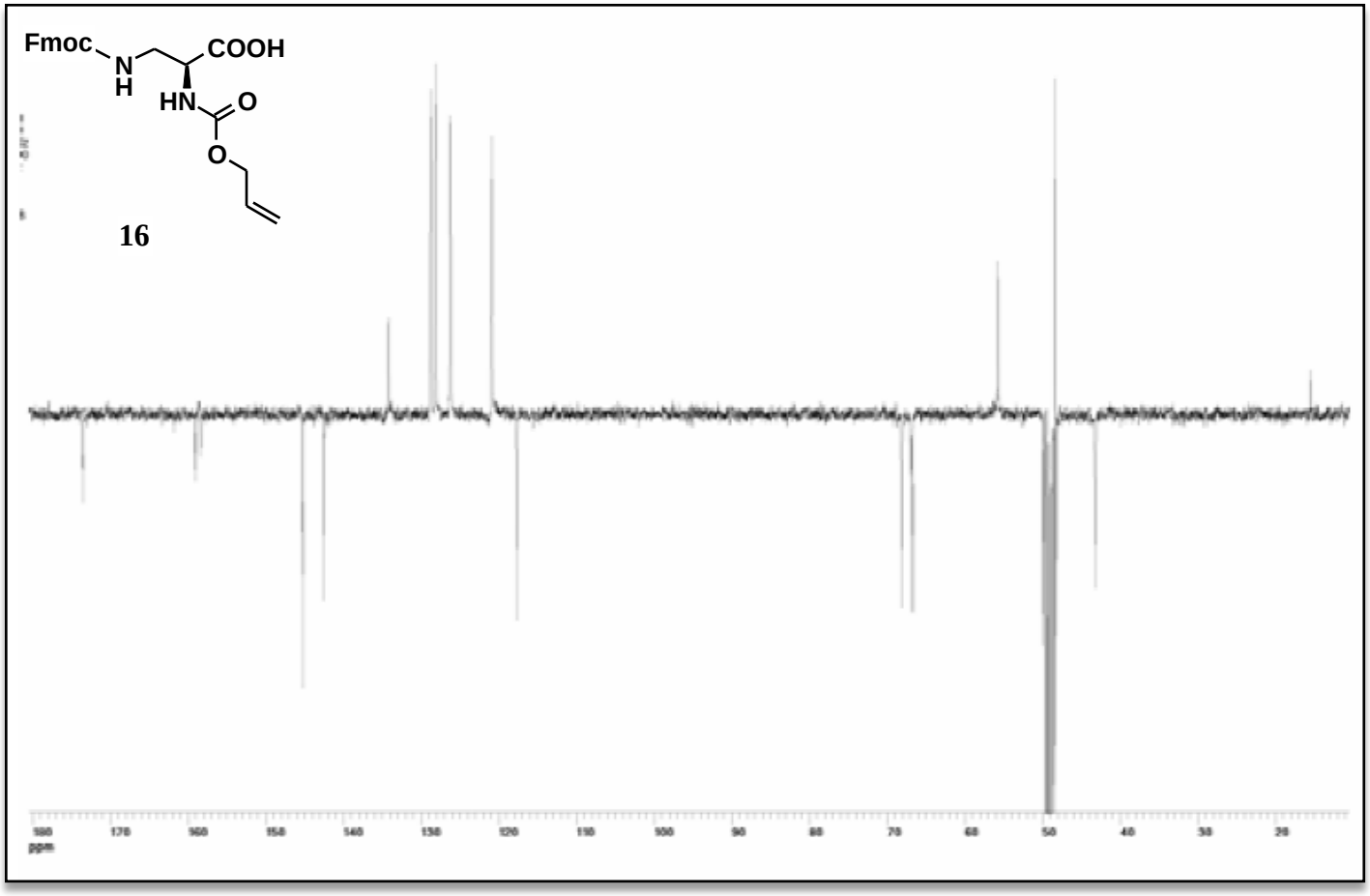

Figure A.14. ^{13}C-NMR spectrum of N^{β}-Alloc-N^{α}-Fmoc-L-2,3-diaminopropionic acid (**16**) in CD_3OD.

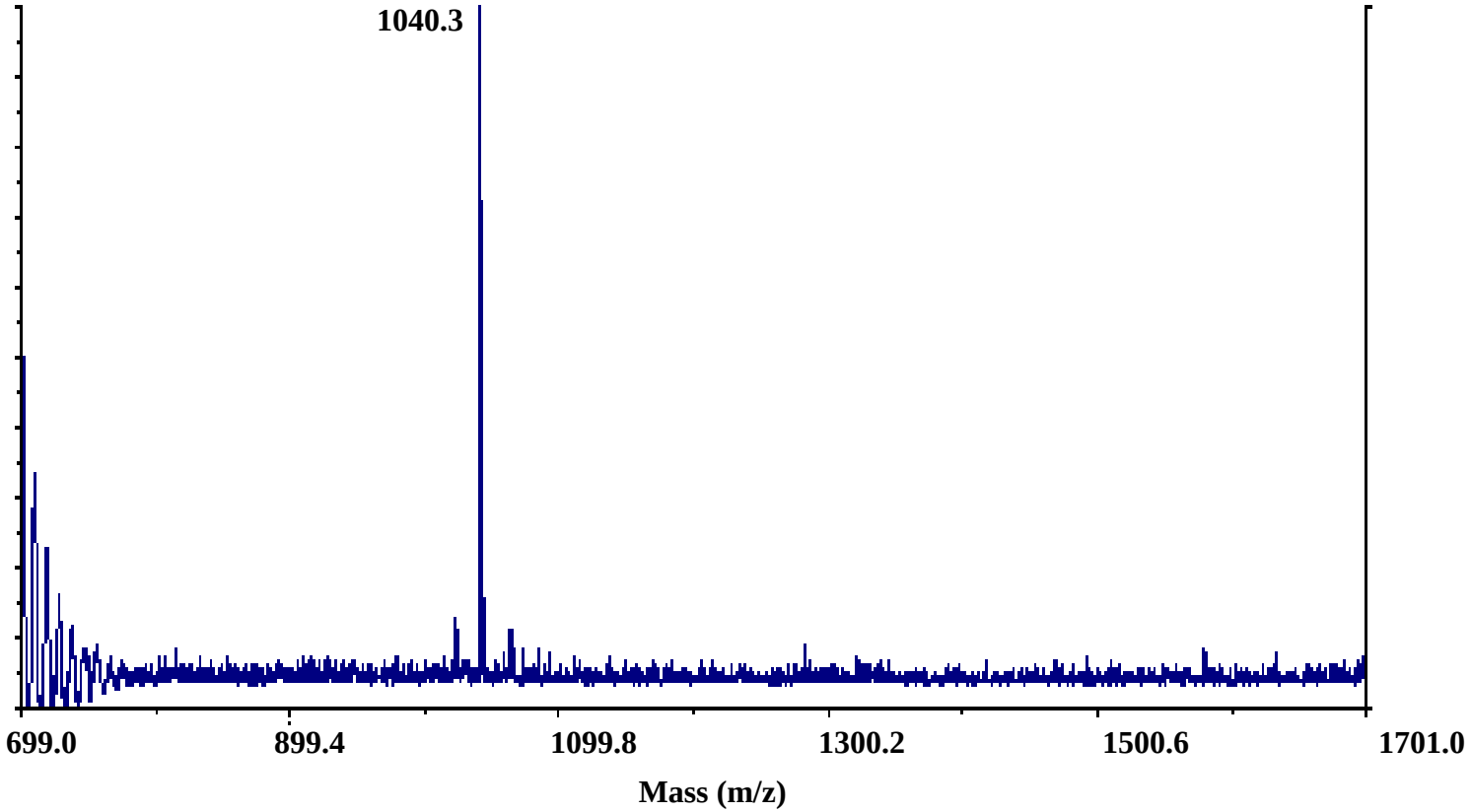

Figure A.15. Mass spectrum of pure ß^2-hexapeptide **3**.

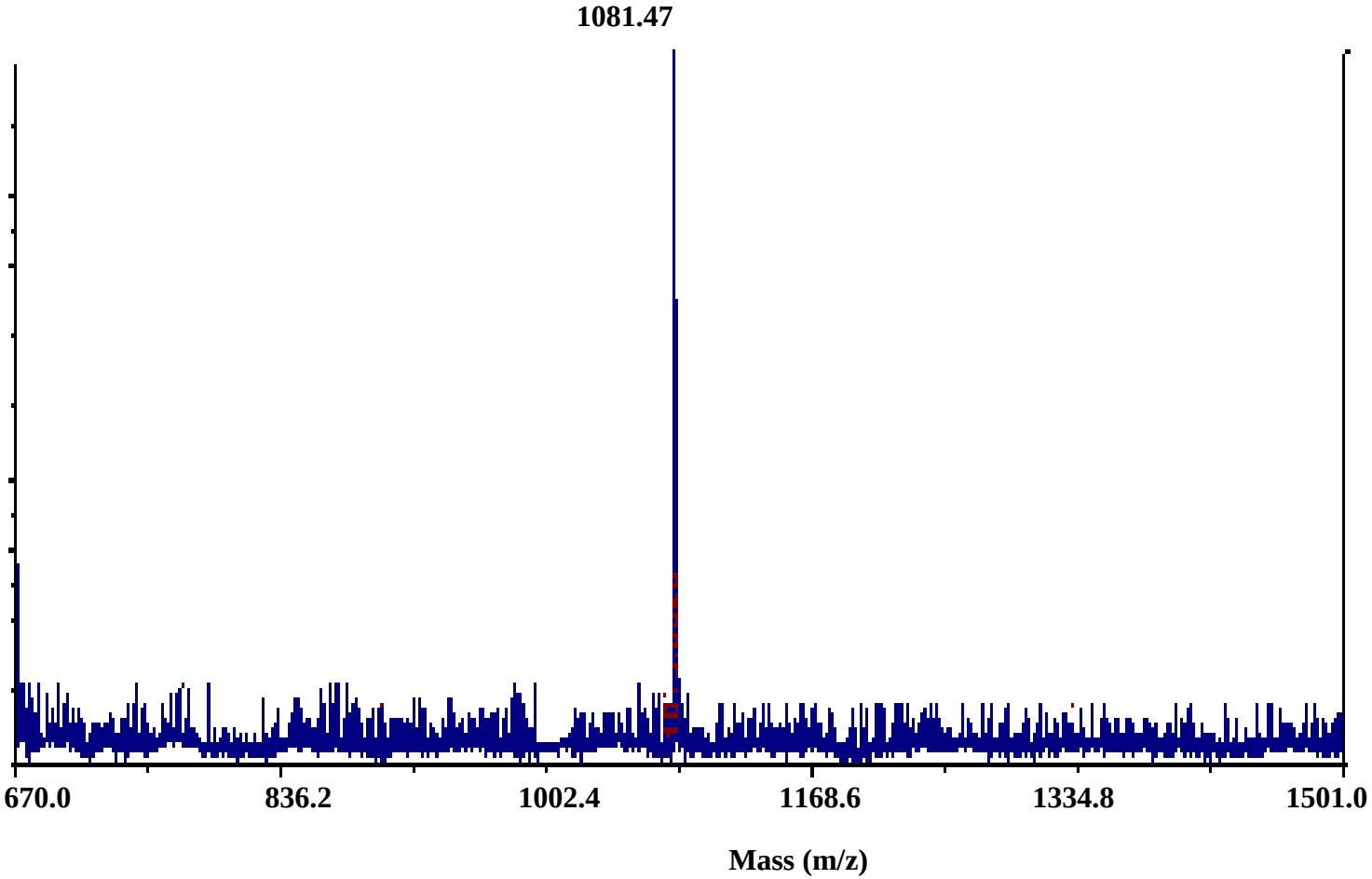

Figure A.16. Mass spectrum of pure ß^2-hexapeptide **4.**

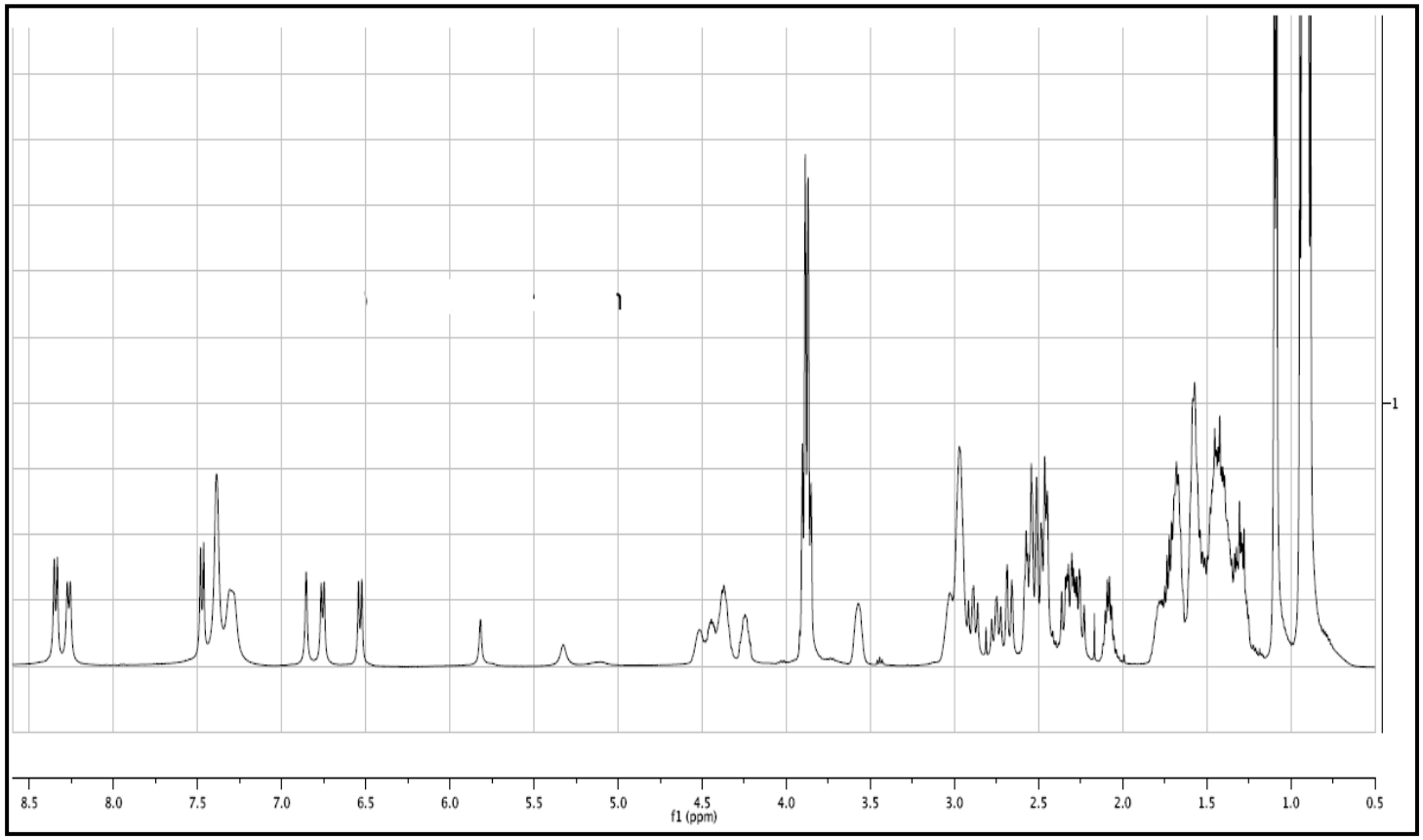

Figure A.17. ^{1}H-NMR spectrum of β^{3}-peptide **17** in CF_3CD_2OH (500 MHz).

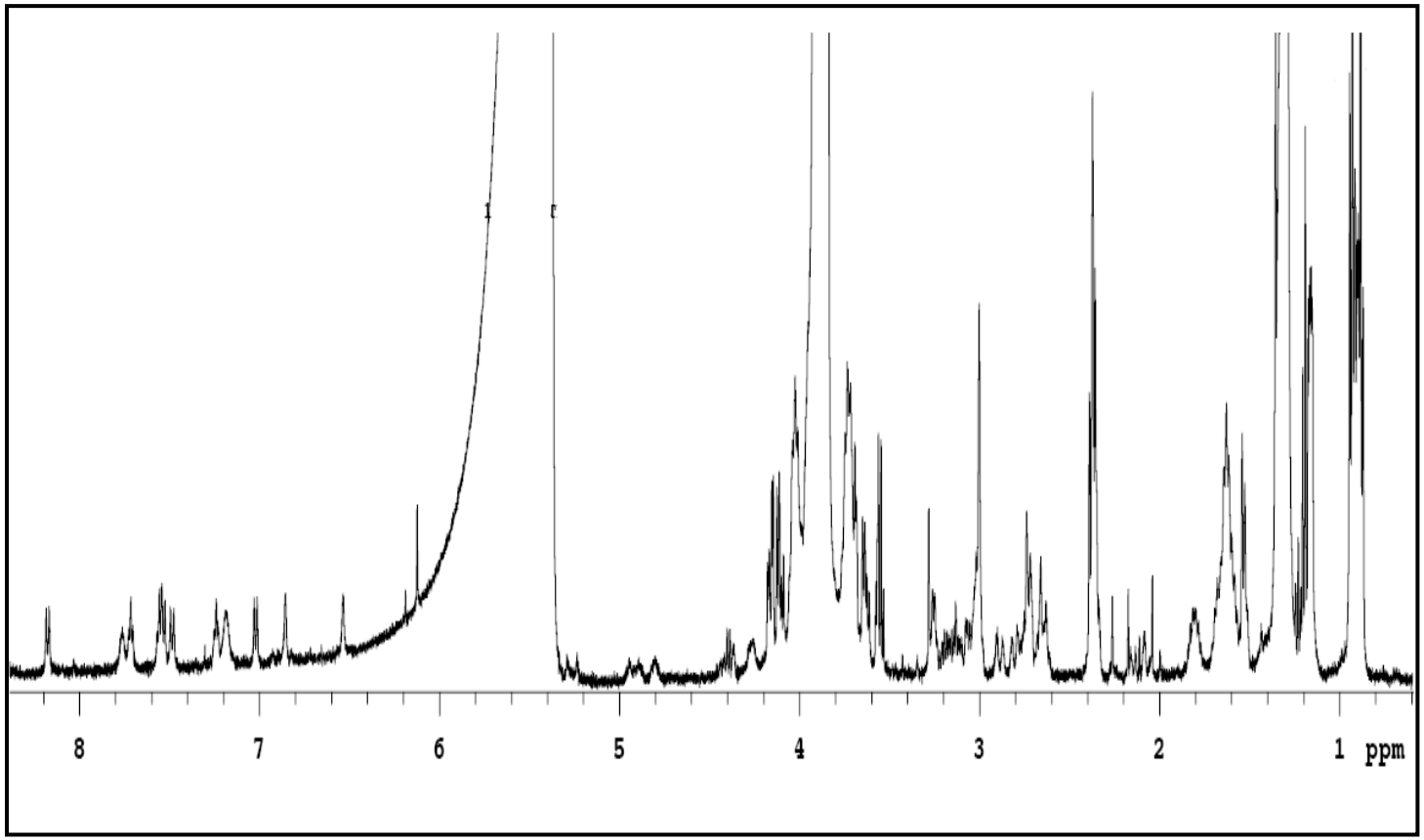

Figure A.18. ^{1}H-NMR spectrum of β^{3}-peptide **18a** in CF_3CD_2OH (500 MHz).

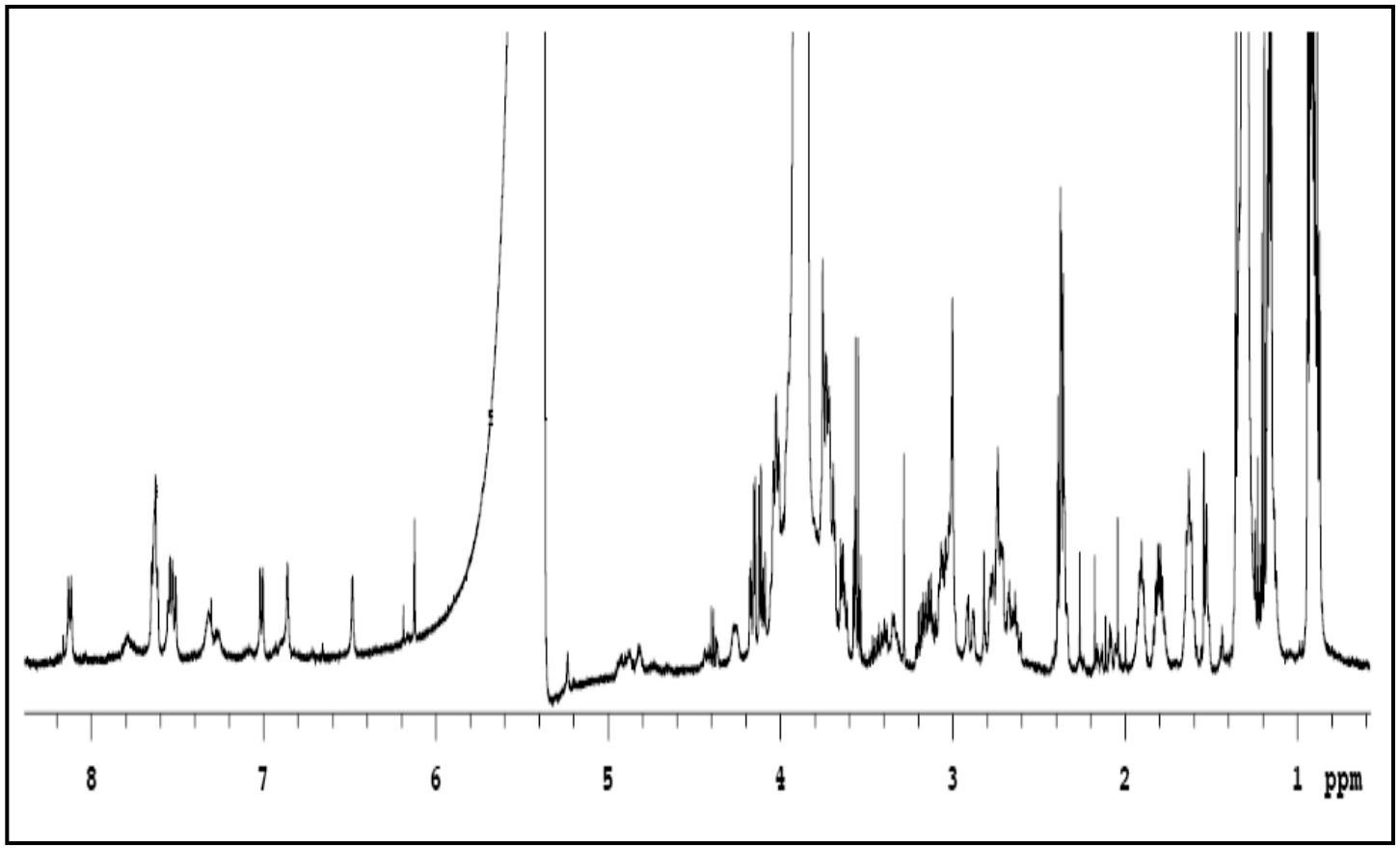

Figure A.19. ^{1}H-NMR spectrum of β^{3}-peptide **18b** in CF_3CD_2OH (500 MHz).

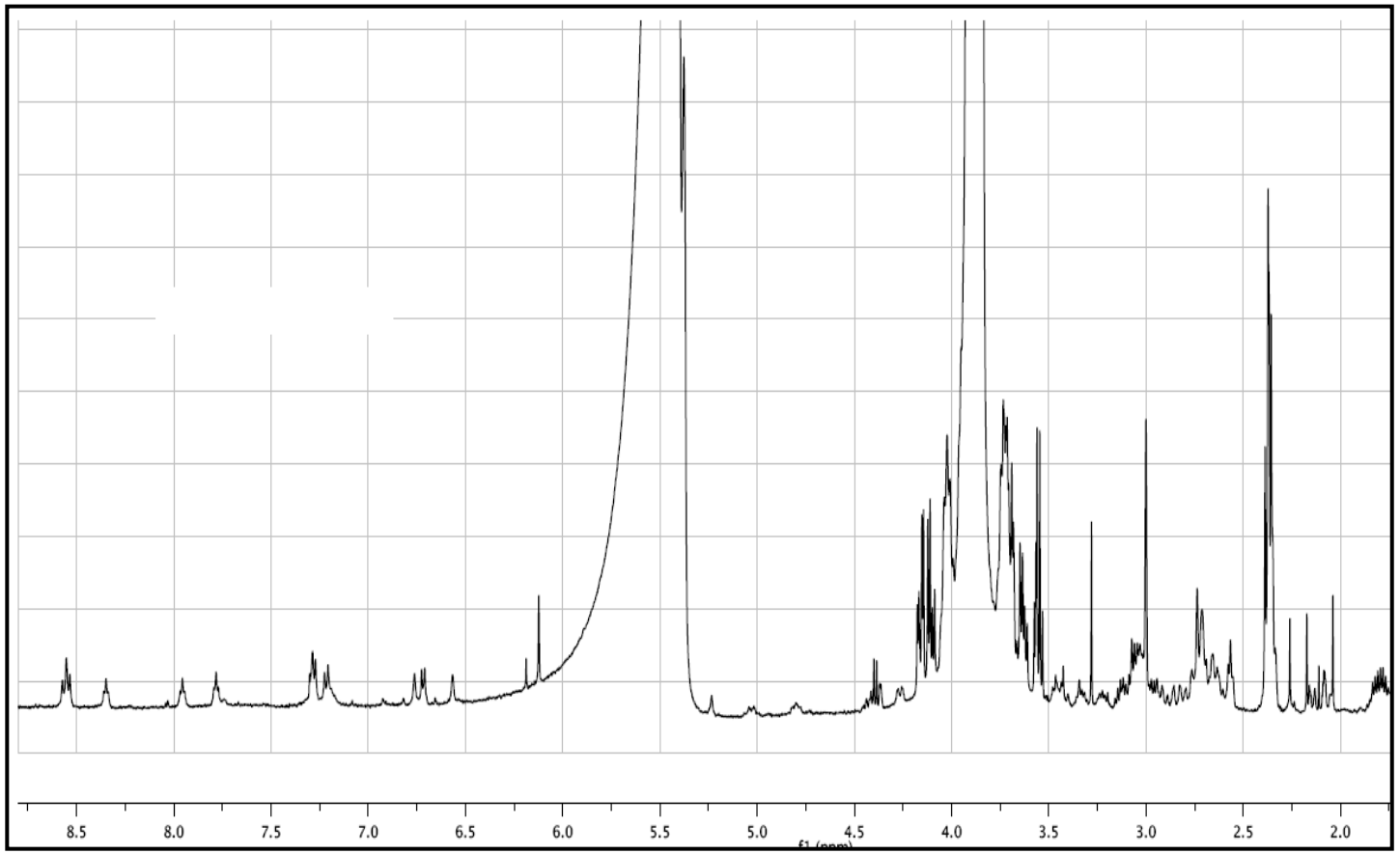

Figure A.20. ^{1}H-NMR spectrum of β^{3}-peptide **19a** in CF_3CD_2OH (500 MHz).

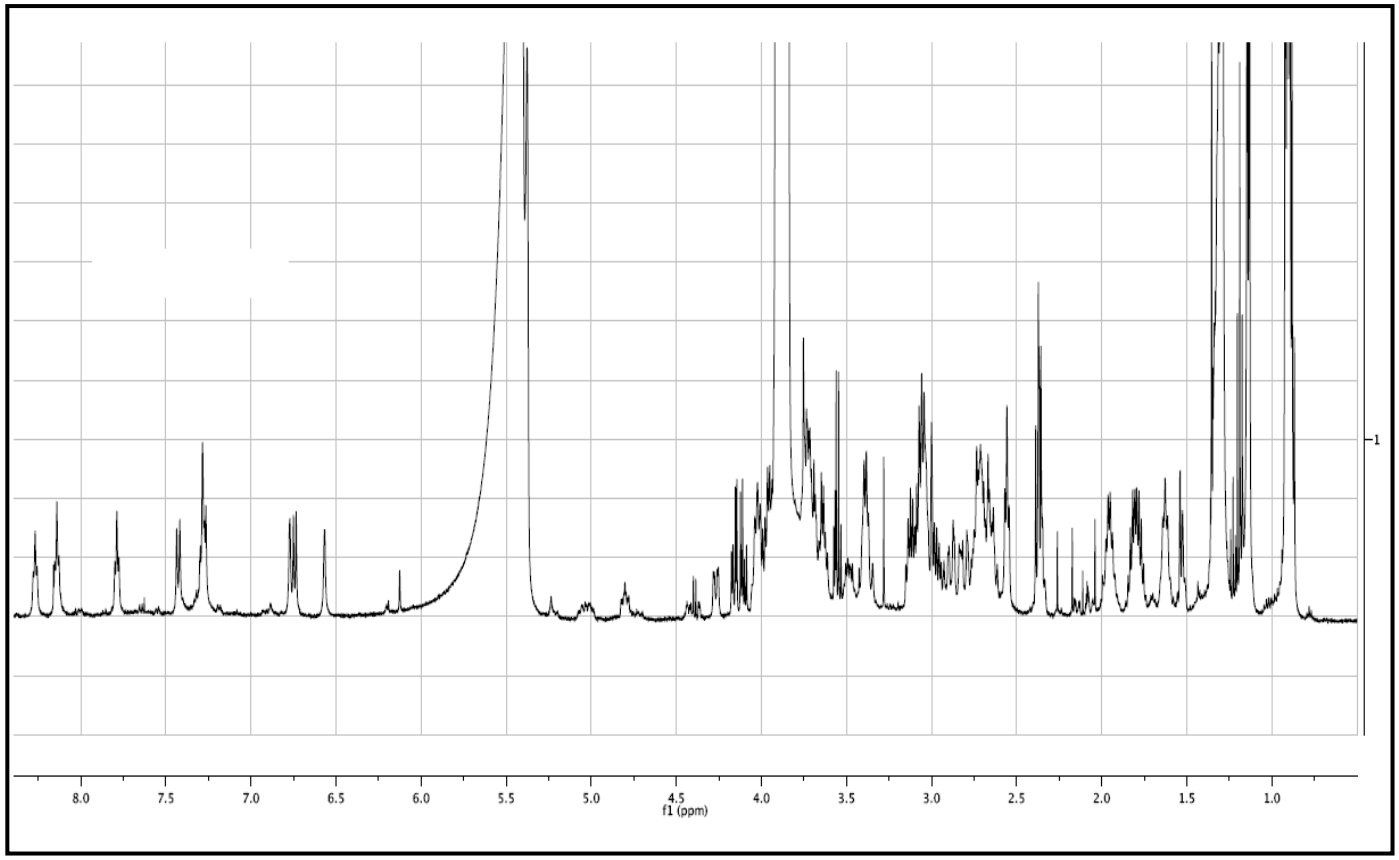

Figure A.21. ^{1}H-NMR spectrum of β^{3}-peptide **19b** in CF_3CD_2OH (500 MHz).

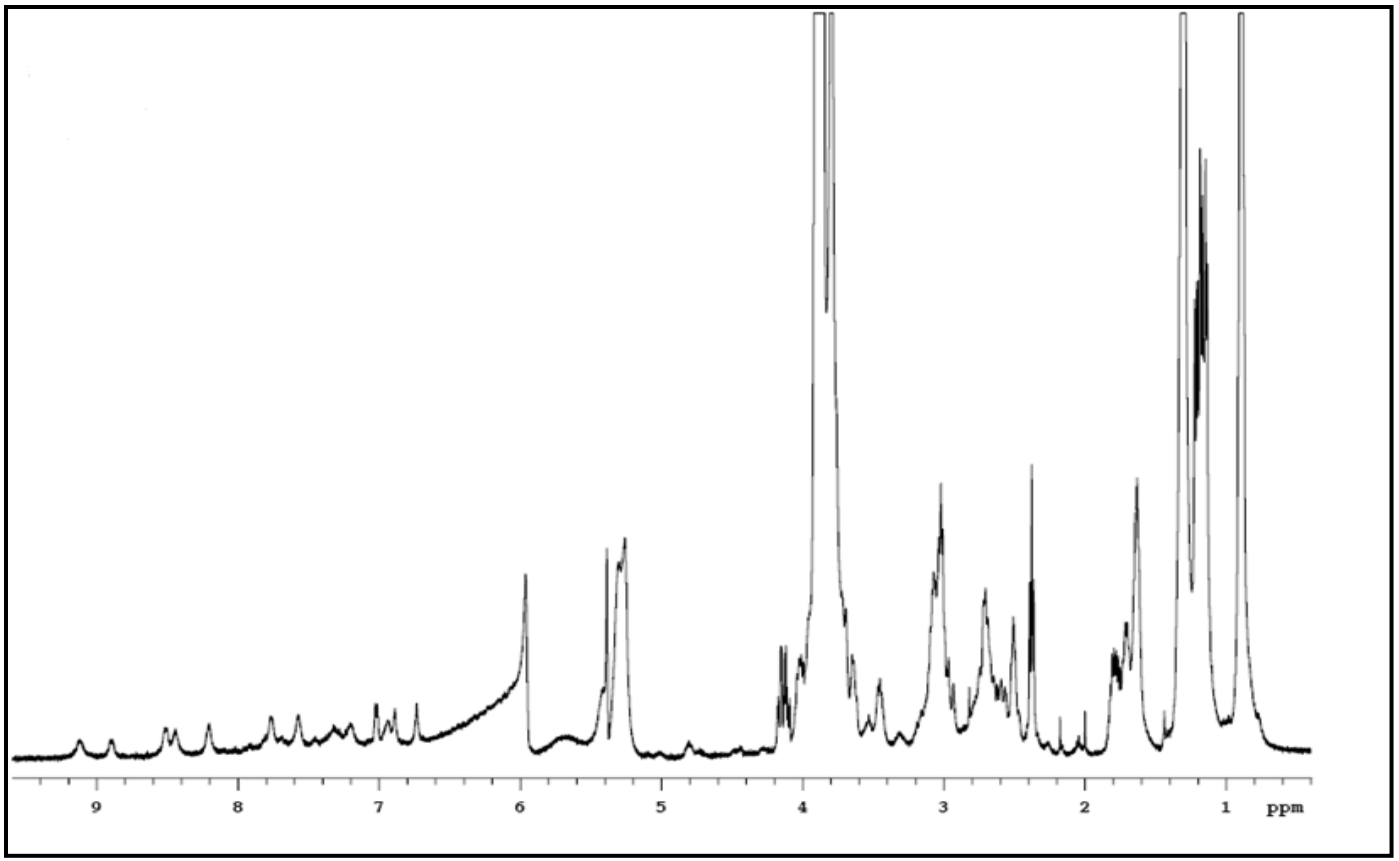

Figure A.22. ^{1}H-NMR spectrum of β^{3}-peptide **20a** in CF_3CD_2OH (500 MHz).

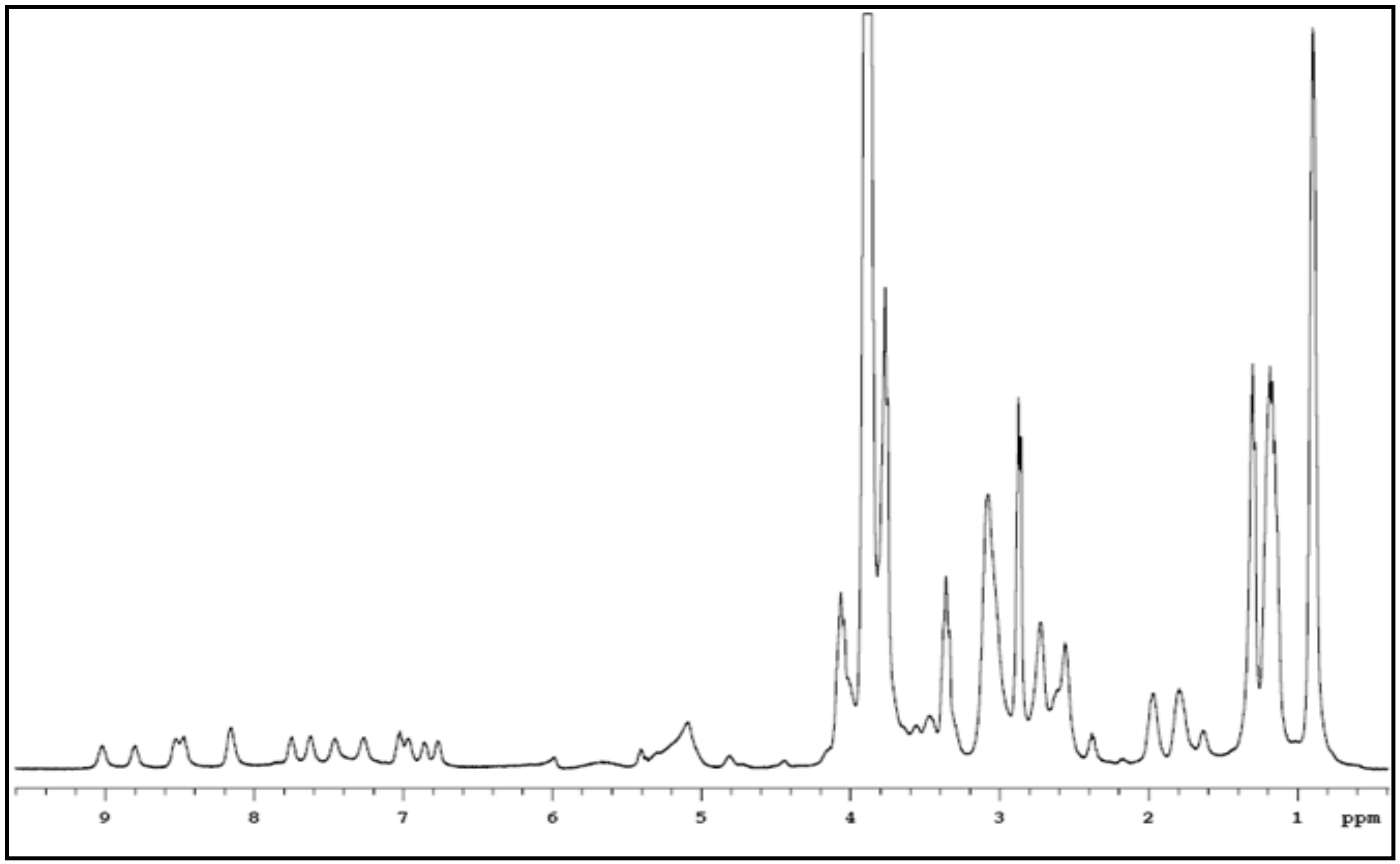

Figure A.23. ^{1}H-NMR spectrum of β^{3}-peptide **20b** in CF_3CD_2OH (500 MHz).

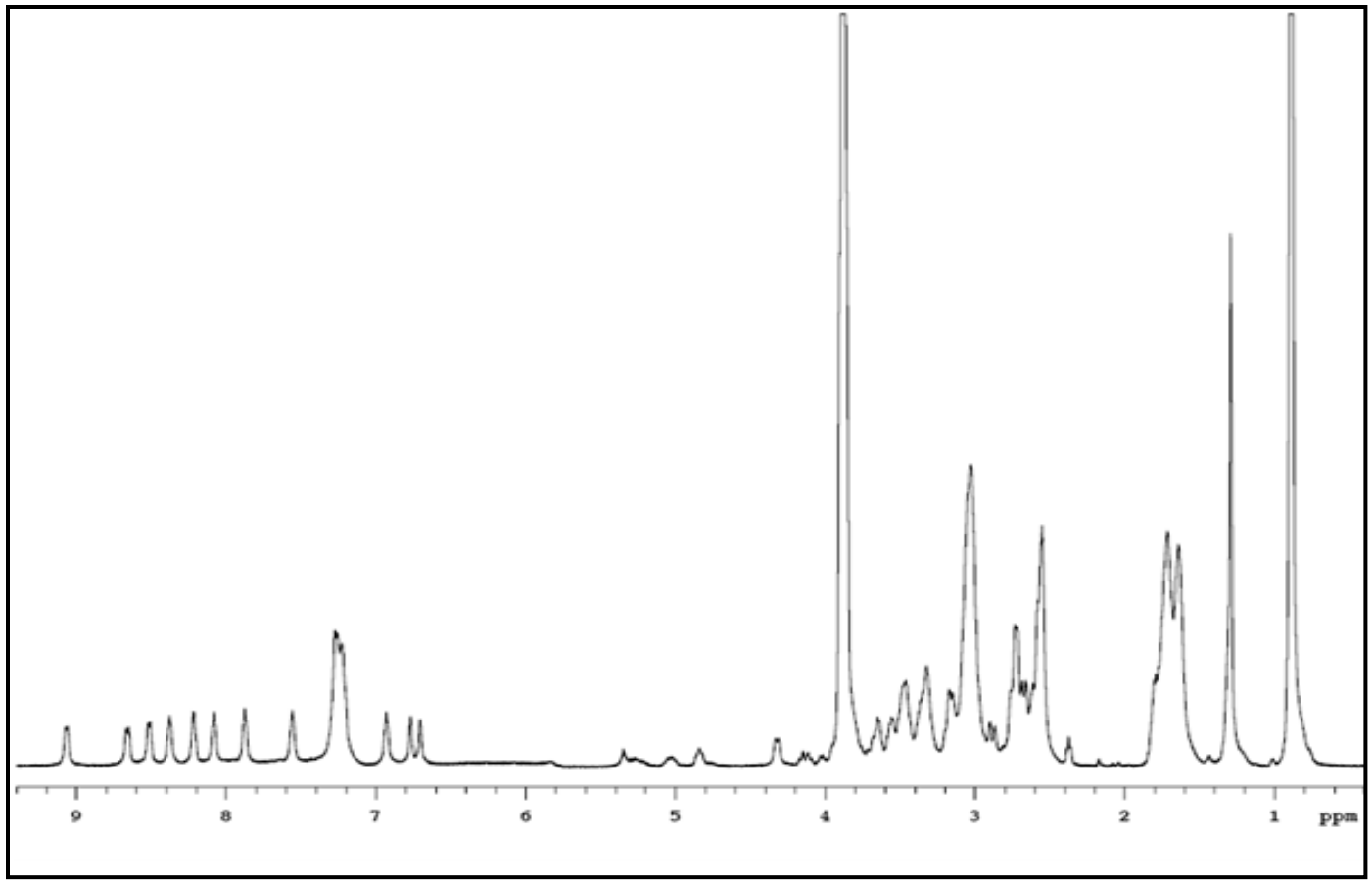

Figure A.24. ^{1}H-NMR spectrum of β^{3}-peptide **21** in CF_3CD_2OH (500 MHz).

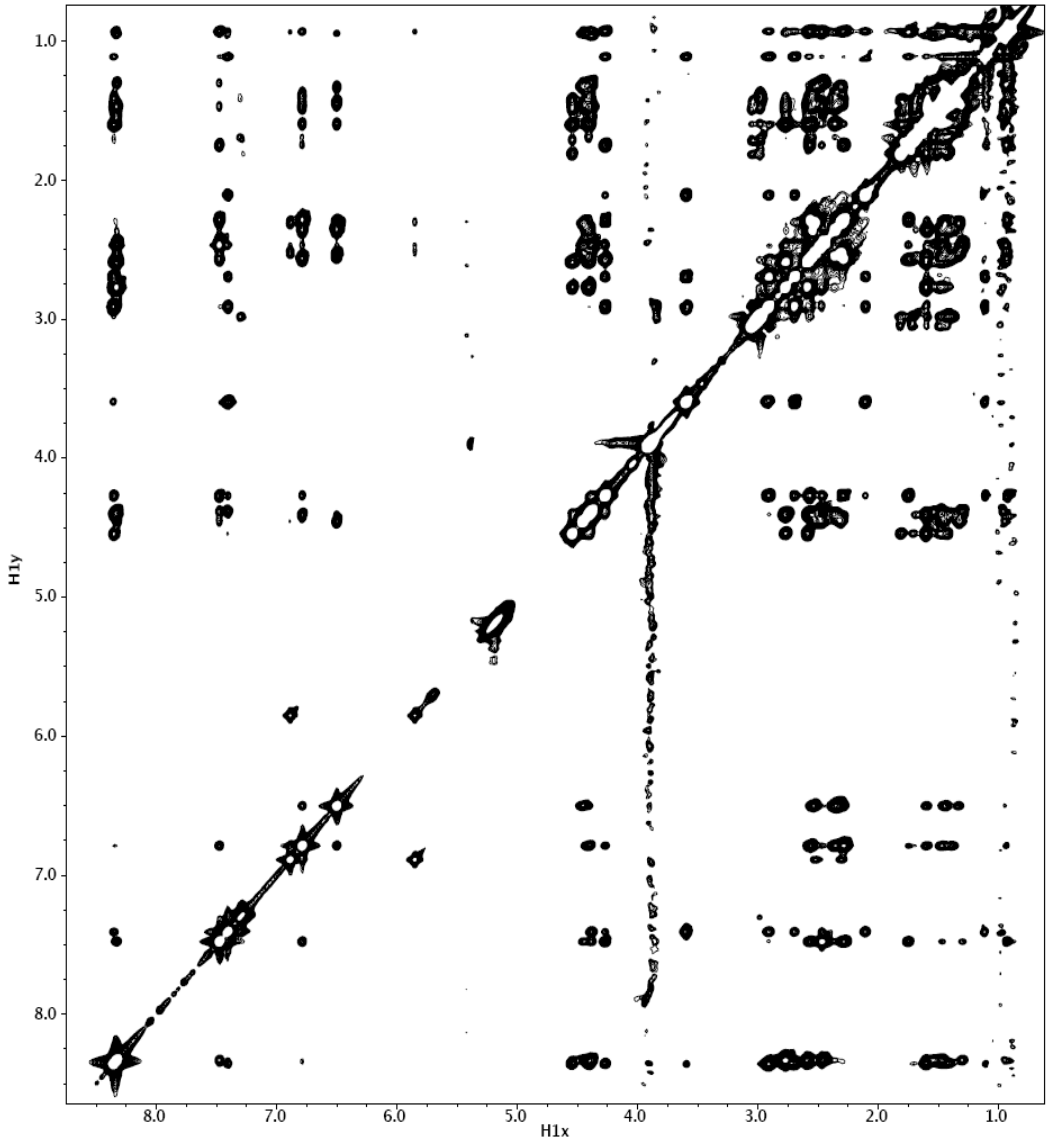

Figure A 25. 2D NOESY of β^3-hexapeptide **17** in TFE.

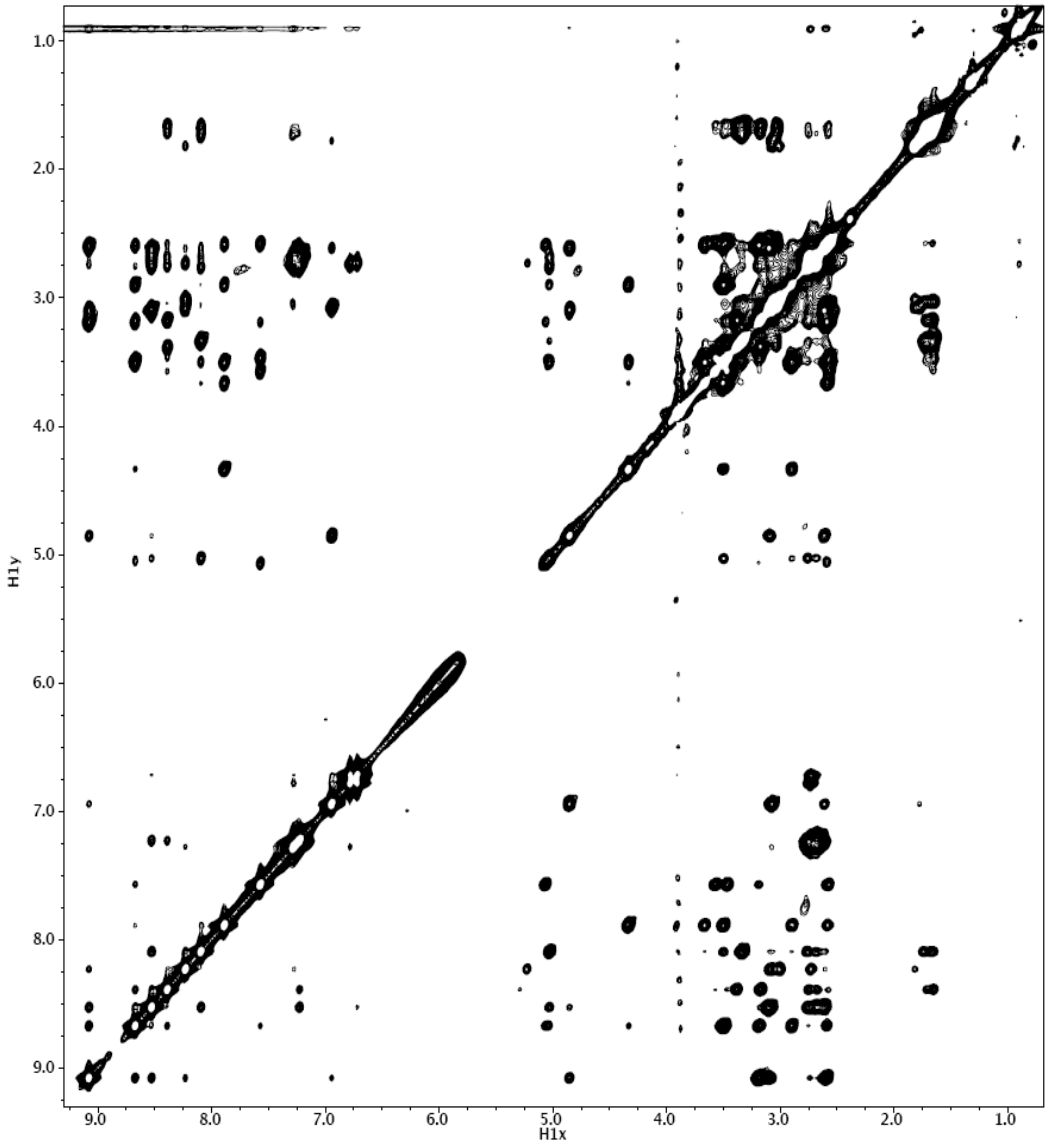

Figure A.26. 2D NOESY of β^3-hexapeptide **21** in TFE.

TABLES

Table A.1: NOE upper limit constraints for β^3-hexapeptide **17** used for structure calculation.

2	LYSB	H	5	LYSB	H	5.26			#SUP	0.68	#QF	0.68
1	VALB	H	2	LYSB	H	4.64	#peak	1	#SUP	0.94	#QF	0.94
3	LEUB	H	4	VALB	H	4.21	#peak	2	#SUP	0.81	#QF	0.81
4	VALB	H	6	GLNB	HT	25.50	#peak	3	#SUP	0.75	#QF	0.75
4	VALB	H	5	LYSB	H	3.88	#peak	4	#SUP	0.81	#QF	0.81
4	VALB	H	6	GLNB	H	5.50	#peak	5	#SUP	0.87	#QF	0.87
4	VALB	H	6	GLNB	HT3	5.50	#peak	6	#SUP	0.84	#QF	0.84
3	LEUB	H	6	GLNB	H	5.50	#peak	7	#SUP	0.93	#QF	0.93
6	GLNB	H	6	GLNB	H2	5.49	#peak	8	#SUP	0.89	#QF	0.89
5	LYSB	H	6	GLNB	H	4.17	#peak	9	#SUP	0.84	#QF	0.84
5	LYSB	H	6	GLNB	HT2	4.27	#peak	11	#SUP	0.67	#QF	0.67
1	VALB	HA	2	LYSB	H	4.68	#peak	12	#SUP	0.96	#QF	0.96
4	VALB	HA	5	LYSB	H	4.50	#peak	14	#SUP	0.85	#QF	0.85
6	GLNB	HA	6	GLNB	HT2	5.32	#peak	16	#SUP	0.71	#QF	0.71
3	LEUB	QB	6	GLNB	HT3	5.06	#peak	19	#SUP	0.68	#QF	0.68
4	VALB	QQE	6	GLNB	HT3	5.00	#peak	21	#SUP	0.72	#QF	0.61
6	GLNB	H	6	GLNB	QQZ	4.50	#peak	22	#SUP	0.76	#QF	0.76
4	VALB	QQE	5	LYSB	H	4.31	#peak	23	#SUP	0.80	#QF	0.74
5	LYSB	H	6	GLNB	QQZ	4.79	#peak	23	#SUP	0.80	#QF	0.74
4	VALB	QQE	6	GLNB	HT2	5.25	#peak	24	#SUP	0.89	#QF	0.55
6	GLNB	QQZ	6	GLNB	HT2	5.50	#peak	24	#SUP	0.89	#QF	0.55
5	LYSB	HB22	6	GLNB	H	3.37	#peak	29	#SUP	0.65	#QF	0.65
6	GLNB	H	6	GLNB	HE	4.00	#peak	30	#SUP	0.72	#QF	0.72
6	GLNB	H	6	GLNB	HD3	4.06	#peak	31	#SUP	0.77	#QF	0.77
6	GLNB	H	6	GLNB	HD2	4.06	#peak	32	#SUP	0.63	#QF	0.63
2	LYSB	QD	5	LYSB	H	4.71	#peak	35	#SUP	0.97	#QF	0.67
5	LYSB	H	5	LYSB	QZ	5.17	#peak	36	#SUP	0.83	#QF	0.83
4	VALB	HD	5	LYSB	H	5.20	#peak	37	#SUP	0.81	#QF	0.81
5	LYSB	HB21	6	GLNB	H	3.37	#peak	38	#SUP	0.63	#QF	0.63
4	VALB	HB22	5	LYSB	H	4.03	#peak	39	#SUP	0.76	#QF	0.76
3	LEUB	QB	5	LYSB	H	4.92	#peak	41	#SUP	0.85	#QF	0.85
4	VALB	HB21	5	LYSB	H	4.03	#peak	42	#SUP	0.72	#QF	0.44
1	VALB	H	2	LYSB	HA	5.32	#peak	43	#SUP	0.91	#QF	0.91
1	VALB	H	3	LEUB	HA	3.93	#peak	44	#SUP	0.70	#QF	0.70
1	VALB	H	4	VALB	HA	4.76	#peak	45	#SUP	0.77	#QF	0.77
3	LEUB	HA	4	VALB	H	4.72	#peak	47	#SUP	0.77	#QF	0.71
4	VALB	H	5	LYSB	HA	5.03	#peak	47	#SUP	0.77	#QF	0.71
4	VALB	H	6	GLNB	HA	4.63	#peak	48	#SUP	0.89	#QF	0.89
2	LYSB	H	4	VALB	HA	4.10	#peak	50	#SUP	0.84	#QF	0.84
5	LYSB	HA	6	GLNB	H	4.67	#peak	51	#SUP	0.91	#QF	0.91
3	LEUB	H	6	GLNB	HA	4.08	#peak	52	#SUP	0.66	#QF	0.66
2	LYSB	H	5	LYSB	HA	3.67	#peak	54	#SUP	0.71	#QF	0.71
1	VALB	HD	2	LYSB	H	5.44	#peak	55	#SUP	0.89	#QF	0.89
3	LEUB	H	3	LEUB	QB	3.03	#peak	57	#SUP	0.82	#QF	0.82
2	LYSB	HB22	3	LEUB	H	3.15	#peak	59	#SUP	0.47	#QF	0.47
1	VALB	HB22	2	LYSB	H	3.29	#peak	60	#SUP	0.76	#QF	0.76
2	LYSB	HB21	3	LEUB	H	3.15	#peak	61	#SUP	0.71	#QF	0.71
1	VALB	HB21	2	LYSB	H	3.29	#peak	62	#SUP	0.79	#QF	0.79
1	VALB	HB21	4	VALB	H	5.50	#peak	65	#SUP	0.83	#QF	0.83
1	VALB	HB22	4	VALB	H	5.50	#peak	68	#SUP	0.58	#QF	0.58
4	VALB	H	4	VALB	HB21	3.67	#peak	69	#SUP	0.88	#QF	0.88

```
3 LEUB QB   4 VALB H    2.64  #peak  71 #SUP  0.74  #QF  0.74
1 VALB H    3 LEUB QB   4.75  #peak    72 #SUP  0.88  #QF  0.88
1 VALB H    1 VALB HD   3.81  #peak    73 #SUP  0.79  #QF  0.79
4 VALB H    4 VALB HB22 3.67  #peak    74 #SUP  0.77  #QF  0.77
4 VALB H    4 VALB QQE  3.28  #peak    76 #SUP  0.77  #QF  0.77
1 VALB H    4 VALB QQE  4.74  #peak    77 #SUP  0.84  #QF  0.84
3 LEUB H    6 GLNB QQZ  4.30  #peak    80 #SUP  0.62  #QF  0.62
1 VALB QQE  2 LYSB H    4.65  #peak    81 #SUP  0.88  #QF  0.88
1 VALB QQE  4 VALB H    5.08  #peak    82 #SUP  0.93  #QF  0.93
1 VALB H    1 VALB QQE  3.69  #peak    83 #SUP  0.85  #QF  0.85
3 LEUB HD2  4 VALB H    5.50  #peak    84 #SUP  0.59  #QF  0.59
3 LEUB HD3  4 VALB H    5.50  #peak    85 #SUP  0.85  #QF  0.65
5 LYSB HE2  5 LYSB HI1  5.50  #peak    86 #SUP  0.67  #QF  0.44
5 LYSB HE3  5 LYSB HI1  5.50  #peak    86 #SUP  0.67  #QF  0.44
2 LYSB QD   2 LYSB HI1  5.50  #peak    88 #SUP  0.74  #QF  0.74
4 VALB H    4 VALB HD   3.69  #peak    92 #SUP  0.75  #QF  0.75
2 LYSB H    2 LYSB HZ3  5.50  #peak    93 #SUP  0.91  #QF  0.91
2 LYSB H    2 LYSB HZ2  5.50  #peak    94 #SUP  0.99  #QF  0.99
2 LYSB H    2 LYSB QD   3.17  #peak    95 #SUP  0.86  #QF  0.86
3 LEUB H    3 LEUB HD3  3.97  #peak    96 #SUP  0.65  #QF  0.65
3 LEUB H    3 LEUB HD2  3.97  #peak    97 #SUP  0.67  #QF  0.67
1 VALB HB21 4 VALB HA   4.21  #peak    99 #SUP  0.72  #QF  0.72
1 VALB HB22 4 VALB HA   4.21  #peak   104 #SUP  0.71  #QF  0.71
3 LEUB QB   4 VALB HA   4.47  #peak   106 #SUP  0.72  #QF  0.72
1 VALB HD   4 VALB HA   4.84  #peak   108 #SUP  0.69  #QF  0.69
2 LYSB QD   4 VALB HA   5.46  #peak   110 #SUP  0.69  #QF  0.69
4 VALB HA   5 LYSB HE2  5.50  #peak   112 #SUP  0.66  #QF  0.24
4 VALB HA   5 LYSB HE3  5.50  #peak   112 #SUP  0.66  #QF  0.24
1 VALB QQE  4 VALB HA   3.78  #peak   113 #SUP  0.76  #QF  0.76
4 VALB HA   4 VALB QQE  3.24  #peak   114 #SUP  0.80  #QF  0.80
1 VALB QQE  3 LEUB HA   5.44  #peak   115 #SUP  0.62  #QF  0.62
1 VALB HA   4 VALB QQE  5.45  #peak   116 #SUP  0.88  #QF  0.88
1 VALB HA   1 VALB QQE  3.68  #peak   117 #SUP  0.82  #QF  0.82
3 LEUB QB   4 VALB HD   4.80  #peak   133 #SUP  0.73  #QF  0.73
2 LYSB QD   2 LYSB HT3  4.99  #peak   140 #SUP  0.88  #QF  0.88
2 LYSB QD   2 LYSB HT2  4.99  #peak   141 #SUP  0.99  #QF  0.95
2 LYSB QD   2 LYSB HB21 3.17  #peak   142 #SUP  0.87  #QF  0.87
2 LYSB QD   2 LYSB HB22 3.17  #peak   149 #SUP  0.89  #QF  0.89
3 LEUB HD2  3 LEUB QB   3.34  #peak   150 #SUP  0.69  #QF  0.69
3 LEUB HD3  3 LEUB QB   3.34  #peak   153 #SUP  0.77  #QF  0.77
2 LYSB QD   3 LEUB QB   5.50  #peak   154 #SUP  0.59  #QF  0.23
3 LEUB QB   6 GLNB HE   5.50  #peak   154 #SUP  0.59  #QF  0.23
1 VALB QQE  1 VALB HB21 3.54  #peak   160 #SUP  0.79  #QF  0.79
1 VALB QQE  1 VALB HB22 3.54  #peak   161 #SUP  0.89  #QF  0.89
1 VALB QQE  4 VALB HD   4.30  #peak   168 #SUP  0.77  #QF  0.77
1 VALB HB21 4 VALB QQE  4.71  #peak   172 #SUP  0.81  #QF  0.81
1 VALB HB22 4 VALB QQE  4.71  #peak   174 #SUP  0.85  #QF  0.85
4 VALB QQE  4 VALB HB21 3.23  #peak   175 #SUP  0.82  #QF  0.82
3 LEUB QB   4 VALB QQE  4.07  #peak   176 #SUP  0.82  #QF  0.71
3 LEUB QB   6 GLNB QQZ  4.55  #peak   176 #SUP  0.82  #QF  0.71
4 VALB QQE  4 VALB HB22 3.23  #peak   177 #SUP  0.66  #QF  0.66
1 VALB HD   4 VALB QQE  4.44  #peak   178 #SUP  0.78  #QF  0.78
6 GLNB HD3  6 GLNB QQZ  3.82  #peak   183 #SUP  0.84  #QF  0.41
6 GLNB HD2  6 GLNB QQZ  3.82  #peak   184 #SUP  0.77  #QF  0.77
1 VALB QQE  4 VALB QQE  3.05  #peak   187 #SUP  0.81  #QF  0.81
3 LEUB HA   4 VALB QQE  5.13  #peak   190 #SUP  0.90  #QF  0.84
3 LEUB HA   6 GLNB QQZ  5.50  #peak   190 #SUP  0.90  #QF  0.84
```

```
6 GLNB HA   6 GLNB QQZ  3.63  #peak   191 #SUP  0.63  #QF  0.63
5 LYSB HA   5 LYSB QZ   4.68  #peak   199 #SUP  0.94  #QF  0.94
2 LYSB QD   5 LYSB HA   3.49  #peak   200 #SUP  0.90  #QF  0.59
3 LEUB QB   6 GLNB HA   3.62  #peak   210 #SUP  0.67  #QF  0.67
1 VALB H    1 VALB QB   3.57  #peak    64
1 VALB H    2 LYSB QB   5.33  #peak    70
1 VALB H    3 LEUB QQZ  4.87  #peak    78
1 VALB QQE  1 VALB QB   3.06  #peak   161
1 VALB QQE  2 LYSB QB   5.33  #peak   163
1 VALB QQE  4 VALB QB   5.33  #peak   163
1 VALB QB   2 LYSB H    2.76  #peak    62
1 VALB QB   2 LYSB HA   5.29  #peak   102
1 VALB QB   2 LYSB QB   4.26  #peak   122
1 VALB QB   3 LEUB QB   5.07  #peak   124
1 VALB QB   4 VALB H    4.80  #peak    65
1 VALB QB   4 VALB HA   3.42  #peak    99
1 VALB QB   4 VALB QQE  4.11  #peak   172
1 VALB QB   5 LYSB HA   5.24  #peak   103
2 LYSB H    2 LYSB QE   3.78  #peak    98
2 LYSB H    2 LYSB QZ   4.83  #peak    94
2 LYSB H    4 VALB QB   5.15  #peak    56
2 LYSB HA   2 LYSB QZ   3.84  #peak   197
2 LYSB QD   2 LYSB QZ   3.42  #peak   169
2 LYSB QD   4 VALB QB   5.33  #peak   159
2 LYSB QD   5 LYSB QB   4.13  #peak   138
2 LYSB QE   2 LYSB HI1  5.33  #peak    87
2 LYSB QE   2 LYSB QB   3.91  #peak   143
2 LYSB QE   5 LYSB HA   3.48  #peak   205
2 LYSB QZ   2 LYSB QB   5.08  #peak   139
2 LYSB QB   3 LEUB H    2.63  #peak    61
2 LYSB QB   3 LEUB QB   4.17  #peak   125
2 LYSB QB   4 VALB H    5.33  #peak    66
2 LYSB QB   5 LYSB H    5.32  #peak    28
2 LYSB QB   5 LYSB HA   3.30  #peak   101
2 LYSB QB   6 GLNB QQZ  4.66  #peak   173
3 LEUB H    3 LEUB QD   3.24  #peak    96
3 LEUB H    3 LEUB QQZ  4.53  #peak    79
3 LEUB H    5 LYSB QB   4.98  #peak    58
3 LEUB HA   3 LEUB QQZ  3.46  #peak   189
3 LEUB QD   3 LEUB QB   2.89  #peak   150
3 LEUB QD   4 VALB H    4.85  #peak    84
3 LEUB QQZ  3 LEUB QB   4.22  #peak   165
4 VALB H    4 VALB QB   3.17  #peak    74
4 VALB H    5 LYSB QD   5.33  #peak    85
4 VALB HA   5 LYSB QD   5.33  #peak   111
4 VALB HD   4 VALB QB   3.45  #peak   132
4 VALB QQE  4 VALB QB   2.80  #peak   175
4 VALB QB   5 LYSB H    3.24  #peak    39
4 VALB QB   5 LYSB QD   5.15  #peak   159
5 LYSB H    5 LYSB QD   3.53  #peak    34
5 LYSB H    5 LYSB QE   4.14  #peak    33
5 LYSB H    5 LYSB QB   3.20  #peak    40
5 LYSB QD   5 LYSB QT   5.10  #peak   141
5 LYSB QD   5 LYSB QB   3.10  #peak   152
5 LYSB QE   5 LYSB QT   3.56  #peak   144
5 LYSB QE   5 LYSB QB   4.68  #peak   158
5 LYSB QZ   5 LYSB QB   5.03  #peak   137
```

```
5 LYSB QB   6 GLNB H    2.77  #peak    38
6 GLNB H    6 GLNB QD   3.33  #peak    31
6 GLNB H    6 GLNB QB   3.10  #peak    75
6 GLNB QD   6 GLNB QB   2.99  #peak   151
6 GLNB QD   6 GLNB HT2  5.33  #peak    25
```

Table A.2: NOE upper limit constraints for β^3-hexapeptide **21** used for structure calculation.

```
3 BLEU H    3 BLEU HG2  4.87                #SUP  0.63  #QF  0.63
3 BLEU H    6 BGLN H    5.28  #peak    1 #SUP  0.47  #QF  0.47
2 BGLU HG2  3 BLEU H    4.87  #peak    2 #SUP  0.68  #QF  0.68
3 BLEU H    4 BLYS H    3.75  #peak    4 #SUP  0.62  #QF  0.62
2 BGLU H    3 BLEU H    3.77  #peak    5 #SUP  0.68  #QF  0.68
2 BGLU H    5 BLYS H    5.06  #peak    6 #SUP  0.98  #QF  0.98
2 BGLU H    2 BGLU HG2  4.32  #peak    7 #SUP  0.80  #QF  0.80
1 BGLU HG2  2 BGLU H    5.09  #peak    8 #SUP  0.73  #QF  0.73
2 BGLU H    4 BLYS HG2  5.50  #peak    9 #SUP  0.98  #QF  0.98
2 BGLU H    4 BLYS H    4.45  #peak   10 #SUP  0.84  #QF  0.84
4 BLYS H    5 BLYS H    3.69  #peak   12 #SUP  0.78  #QF  0.78
4 BLYS H    6 BGLN HT3  4.71  #peak   13 #SUP  0.52  #QF  0.52
4 BLYS H    6 BGLN HT2  4.29  #peak   14 #SUP  0.41  #QF  0.41
5 BLYS H    5 BLYS HG2  4.42  #peak   15 #SUP  0.98  #QF  0.98
6 BGLN H    6 BGLN HG2  4.22  #peak   16 #SUP  0.71  #QF  0.71
4 BLYS HG2  5 BLYS H    5.42  #peak   17 #SUP  1.00
6 BGLN H    6 BGLN HT3  4.09  #peak   18 #SUP  0.63  #QF  0.63
6 BGLN H    6 BGLN HT2  4.50  #peak   19 #SUP  0.59  #QF  0.59
5 BLYS H    6 BGLN HT2  4.77  #peak   20 #SUP  0.69  #QF  0.69
5 BLYS H    6 BGLN HT3  4.76  #peak   21 #SUP  0.50  #QF  0.50
3 BLEU H    3 BLEU QQZ  4.63  #peak   22 #SUP  0.66  #QF  0.66
6 BGLN HG2  6 BGLN QQZ  4.10  #peak   23 #SUP  0.53  #QF  0.53
3 BLEU HG2  3 BLEU QQZ  4.55  #peak   24 #SUP  0.65  #QF  0.65
5 BLYS QZ   5 BLYS QI   4.02  #peak   27 #SUP  0.98  #QF  0.98
5 BLYS QE   5 BLYS QI   4.40  #peak   28 #SUP  0.93  #QF  0.93
3 BLEU H    6 BGLN HA   4.10  #peak   29 #SUP  0.64  #QF  0.64
2 BGLU HA   3 BLEU H    4.34  #peak   30 #SUP  0.77  #QF  0.77
2 BGLU HB21 3 BLEU H    2.78  #peak   33 #SUP  0.65  #QF  0.65
3 BLEU H    3 BLEU HB22 3.13  #peak   34 #SUP  0.63  #QF  0.63
3 BLEU H    6 BGLN QB   5.50  #peak   35 #SUP  0.54  #QF  0.31
2 BGLU HB2 23 BLEU H    3.90  #peak   36 #SUP  0.80  #QF  0.70
2 BGLU H    2 BGLU HB22 3.90  #peak   37 #SUP  0.99  #QF  0.99
2 BGLU H    4 BLYS HB22 4.71  #peak   38 #SUP  0.91  #QF  0.91
2 BGLU H    4 BLYS HB21 4.71  #peak   39 #SUP  0.99  #QF  0.99
1 BGLU HB22 2 BGLU H    3.03  #peak   40 #SUP  0.95  #QF  0.95
2 BGLU H    2 BGLU HB21 3.26  #peak   41 #SUP  0.93  #QF  0.93
1 BGLU HB21 2 BGLU H    3.03  #peak   42 #SUP  0.89  #QF  0.89
1 BGLU HA   2 BGLU H    4.48  #peak   43 #SUP  0.91  #QF  0.91
2 BGLU H    3 BLEU HA   4.96  #peak   44 #SUP  0.97  #QF  0.97
4 BLYS H    6 BGLN HA   4.81  #peak   46 #SUP  0.71  #QF  0.71
3 BLEU HA   4 BLYS H    4.35  #peak   48 #SUP  0.75  #QF  0.75
4 BLYS H    4 BLYS QD   4.56  #peak   50 #SUP  0.64  #QF  0.64
3 BLEU HB22 4 BLYS H    2.78  #peak   51 #SUP  0.68  #QF  0.68
4 BLYS H    5 BLYS HB22 3.24  #peak   53 #SUP  0.51  #QF  0.51
3 BLEU HB21 4 BLYS H    3.49  #peak   54 #SUP  0.72  #QF  0.72
5 BLYS HG2  5 BLYS QE   3.28  #peak   55 #SUP  0.93  #QF  0.93
5 BLYS HG2  5 BLYS QZ   3.75  #peak   56 #SUP  0.95  #QF  0.95
```

```
2 BGLU QE   5 BLYS HG2  4.25   #peak   57 #SUP  0.88  #QF  0.88
4 BLYS HB22 5 BLYS HG2  3.93   #peak   58 #SUP  0.94  #QF  0.94
4 BLYS HB21 5 BLYS HG2  3.93   #peak   59 #SUP  0.86  #QF  0.86
5 BLYS HG2  5 BLYS QT   4.72   #peak   60 #SUP  0.95  #QF  0.95
2 BGLU HD3  5 BLYS HG2  4.54   #peak   63 #SUP  0.97  #QF  0.97
2 BGLU HD2  5 BLYS HG2  4.54   #peak   64 #SUP  0.97  #QF  0.97
6 BGLN HA   6 BGLN HG2  3.70   #peak   66 #SUP  0.97  #QF  0.97
6 BGLN HG2  6 BGLN QB   3.86   #peak   69 #SUP  0.99  #QF  0.99
6 BGLN HG2  6 BGLN HE   3.88   #peak   71 #SUP  0.84  #QF  0.84
4 BLYS HG2  4 BLYS HE3  3.76   #peak   72 #SUP  1.00
4 BLYS HG2  4 BLYS HE2  3.76   #peak   73 #SUP  0.99  #QF  0.99
4 BLYS HG2  4 BLYS QZ   3.44   #peak   74 #SUP  0.73  #QF  0.73
3 BLEU HB21 4 BLYS HG2  4.61   #peak   75 #SUP  0.80  #QF  0.80
4 BLYS HG2  4 BLYS QT   4.74   #peak   79 #SUP  0.98  #QF  0.98
3 BLEU HB22 4 BLYS HG2  4.63   #peak   80 #SUP  0.97  #QF  0.97
4 BLYS HG2  4 BLYS QD   2.77   #peak   81 #SUP  1.00
4 BLYS HA   4 BLYS HG2  2.98   #peak   84 #SUP  0.95  #QF  0.95
1 BGLU HG2  4 BLYS HA   5.02   #peak   85 #SUP  0.80  #QF  0.80
1 BGLU HA   1 BGLU HG2  3.12   #peak   86 #SUP  0.66  #QF  0.66
1 BGLU HG2  1 BGLU HB21 3.31   #peak   88 #SUP  0.82  #QF  0.76
1 BGLU HG2  1 BGLU HB22 3.31   #peak   89 #SUP  0.75  #QF  0.75
1 BGLU HG2  1 BGLU QE   3.51   #peak   90 #SUP  0.78  #QF  0.78
2 BGLU HG2  2 BGLU QE   3.12   #peak   91 #SUP  0.68  #QF  0.68
2 BGLU HG2  2 BGLU HB21 4.43   #peak   92 #SUP  0.80  #QF  0.80
2 BGLU HA   2 BGLU HG2  3.38   #peak   95 #SUP  0.71  #QF  0.71
4 BLYS HA   5 BLYS H    4.29   #peak   97 #SUP  0.96  #QF  0.96
5 BLYS H    5 BLYS HD3  5.50   #peak   98 #SUP  0.90  #QF  0.90
2 BGLU HB21 5 BLYS H    5.50   #peak   99 #SUP  0.80  #QF  0.47
5 BLYS H    5 BLYS HD2  5.50   #peak   99 #SUP  0.80  #QF  0.47
3 BLEU HB22 5 BLYS H    4.78   #peak   100 #SUP  0.86 #QF  0.86
5 BLYS HB22 6 BGLN H    3.11   #peak   104 #SUP  0.63 #QF  0.63
5 BLYS H    5 BLYS HB22 2.54   #peak   105 #SUP  0.63 #QF  0.63
5 BLYS H    5 BLYS HB21 3.81   #peak   106 #SUP  0.95 #QF  0.71
3 BLEU HG2  3 BLEU HB21 3.68   #peak   107 #SUP  0.70 #QF  0.70
3 BLEU HG2  3 BLEU QD   2.86   #peak   108 #SUP  0.72 #QF  0.72
3 BLEU HA   3 BLEU HG2  2.77   #peak   109 #SUP  0.64 #QF  0.64
6 BGLN QB   6 BGLN HT3  3.51   #peak   110 #SUP  0.67 #QF  0.67
6 BGLN QB   6 BGLN HT2  3.29   #peak   111 #SUP  0.63 #QF  0.63
3 BLEU HB22 6 BGLN HT2  4.96   #peak   112 #SUP  0.62 #QF  0.62
2 BGLU H    4 BLYS HA   3.74   #peak   113 #SUP  0.97 #QF  0.97
4 BLYS QZ   4 BLYS QI   3.86   #peak   114 #SUP  0.79 #QF  0.79
5 BLYS HB22 6 BGLN HT2  4.12   #peak   115 #SUP  0.44 #QF  0.44
3 BLEU HA   3 BLEU QQZ  4.89   #peak   116 #SUP  0.67 #QF  0.67
2 BGLU HB21 3 BLEU QQZ  5.28   #peak   117 #SUP  0.74 #QF  0.74
3 BLEU QD   3 BLEU QQZ  3.80   #peak   118 #SUP  0.93 #QF  0.84
6 BGLN QQZ  6 BGLN QB   4.19   #peak   120 #SUP  0.56 #QF  0.56
2 BGLU HB22 3 BLEU QQZ  5.22   #peak   121 #SUP  0.76 #QF  0.44
3 BLEU QQZ  3 BLEU HB21 5.50   #peak   121 #SUP  0.76 #QF  0.44
4 BLYS HA   5 BLYS QE   5.50   #peak   122 #SUP  0.24 #QF  0.24
4 BLYS HA   4 BLYS QZ   4.53   #peak   123 #SUP  0.88 #QF  0.88
1 BGLU HA   1 BGLU QE   4.64   #peak   124 #SUP  0.94 #QF  0.94
1 BGLU HA   4 BLYS HA   4.69   #peak   128 #SUP  0.95 #QF  0.95
2 BGLU QE   5 BLYS HA   5.50   #peak   129 #SUP  0.84 #QF  0.27
2 BGLU HB22 5 BLYS HA   5.50   #peak   129 #SUP  0.84 #QF  0.27
2 BGLU HB21 5 BLYS HA   4.28   #peak   132 #SUP  0.53 #QF  0.53
3 BLEU HB21 6 BGLN HA   4.51   #peak   133 #SUP  0.99 #QF  0.99
3 BLEU HB22 6 BGLN HA   3.51   #peak   136 #SUP  0.93 #QF  0.93
```

```
2 BGLU HB21 6 BGLN HA   5.05   #peak   137 #SUP  0.88 #QF  0.88
1 BGLU HB22 4 BLYS HA   3.51   #peak   141 #SUP  0.99 #QF  0.99
3 BLEU HB22 4 BLYS HA   4.66   #peak   142 #SUP  0.93 #QF  0.93
4 BLYS HA   4 BLYS QD   4.21   #peak   144 #SUP  0.99 #QF  0.99
1 BGLU HB21 4 BLYS HA   3.51   #peak   145 #SUP  0.73 #QF  0.73
2 BGLU HB21 3 BLEU HA   4.52   #peak   146 #SUP  0.91 #QF  0.91
1 BGLU HD2  4 BLYS QZ   4.73   #peak   152 #SUP  0.93 #QF  0.93
2 BGLU HD2  5 BLYS QE   4.14   #peak   154 #SUP  0.91 #QF  0.91
2 BGLU HD2  5 BLYS QZ   4.74   #peak   155 #SUP  0.94 #QF  0.94
1 BGLU HD3  4 BLYS QZ   4.73   #peak   156 #SUP  0.26 #QF  0.26
2 BGLU HD3  5 BLYS QZ   4.74   #peak   157 #SUP  0.83 #QF  0.83
2 BGLU HD3  5 BLYS QE   4.14   #peak   158 #SUP  0.90 #QF  0.90
4 BLYS QD   4 BLYS QZ   3.29   #peak   160 #SUP  0.92 #QF  0.92
5 BLYS QE   5 BLYS QT   3.59   #peak   162 #SUP  0.98 #QF  0.85
4 BLYS HB21 5 BLYS QZ   5.50   #peak   166 #SUP  0.71 #QF  0.71
4 BLYS HB21 5 BLYS QE   4.64   #peak   167 #SUP  0.81 #QF  0.81
4 BLYS HB22 5 BLYS QE   4.64   #peak   168 #SUP  0.91 #QF  0.91
4 BLYS HB22 5 BLYS QZ   5.50   #peak   169 #SUP  0.72 #QF  0.25
1 BGLU QE   4 BLYS QZ   4.61   #peak   170 #SUP  0.44 #QF  0.44
2 BGLU QE   5 BLYS QE   4.10   #peak   171 #SUP  0.84 #QF  0.84
2 BGLU HA   2 BGLU HD2  4.98   #peak   178 #SUP  0.94 #QF  0.94
2 BGLU HA   2 BGLU HD3  4.98   #peak   179 #SUP  0.80 #QF  0.80
5 BLYS HD2  5 BLYS QZ   3.55   #peak   182 #SUP  0.99 #QF  0.99
5 BLYS HD3  5 BLYS QZ   3.55   #peak   185 #SUP  0.98 #QF  0.98
2 BGLU QE   5 BLYS QZ   4.28   #peak   188 #SUP  0.39 #QF  0.39
3 BLEU HB22 6 BGLN QB   3.95   #peak   193 #SUP  0.80 #QF  0.80
2 BGLU H    5 BLYS HG2  4.68   #peak   200 #SUP  0.94 #QF  0.94
4 BLYS H    4 BLYS HG2  3.63   #peak   201 #SUP  0.66 #QF  0.66
5 BLYS HB21 6 BGLN H    3.57   #peak   202 #SUP  0.90 #QF  0.90
1 BGLU HA   1 BGLU QD   4.46   #peak   127
1 BGLU QD   1 BGLU QB   4.58   #peak   150
1 BGLU QD   4 BLYS HG2  4.20   #peak    83
1 BGLU QD   4 BLYS QD   4.57   #peak   191
1 BGLU QD   4 BLYS QE   4.51   #peak   153
1 BGLU QD   4 BLYS QZ   4.10   #peak   156
1 BGLU QD   4 BLYS QT   4.67   #peak   149
1 BGLU QE   1 BGLU QB   4.39   #peak   199
1 BGLU QB   2 BGLU H    2.62   #peak    42
1 BGLU QB   2 BGLU HA   4.79   #peak   180
1 BGLU QB   3 BLEU H    4.88   #peak    32
1 BGLU QB   4 BLYS H    4.80   #peak    49
1 BGLU QB   4 BLYS HA   2.96   #peak   145
1 BGLU QB   4 BLYS HG2  4.57   #peak    78
1 BGLU QB   4 BLYS QB   3.95   #peak   175
2 BGLU H    4 BLYS QB   4.06   #peak    39
2 BGLU HA   2 BGLU QD   4.35   #peak   179
2 BGLU QD   2 BGLU HB21 5.18   #peak   177
2 BGLU QD   5 BLYS HG2  3.92   #peak    64
2 BGLU QD   5 BLYS QD   5.15   #peak   177
2 BGLU QD   5 BLYS QZ   4.09   #peak   157
2 BGLU QD   5 BLYS QT   4.70   #peak   176
3 BLEU H    4 BLYS QB   5.19   #peak    35
4 BLYS H    4 BLYS QB   3.17   #peak    52
4 BLYS HA   4 BLYS QE   4.81   #peak   181
4 BLYS HG2  4 BLYS QE   3.25   #peak    73
4 BLYS HG2  4 BLYS QB   4.57   #peak    76
4 BLYS QE   4 BLYS QT   3.26   #peak   162
```

```
4 BLYS QE   4 BLYS QI   4.51   #peak    26
4 BLYS QZ   4 BLYS QB   5.33   #peak   169
4 BLYS QB   5 BLYS H    3.34   #peak   106
4 BLYS QB   5 BLYS HG2  3.38   #peak    59
4 BLYS QB   5 BLYS QE   4.04   #peak   167
6 BGLN HA   6 BGLN QD   4.51   #peak   135
```